Universidad de Navarra

Facultad de Ciencias

Dual targeting of histone methyltransferase G9a and DNMT1 for the treatment of experimental hepatocellular carcinoma

MARINA BÁRCENA VARELA

2018

Universidad de Navarra

Facultad de Ciencias

Dual targeting of histone methyltransferase G9a and DNMT1 for the treatment of experimental hepatocellular carcinoma

Memoria presentada por Dª Marina Bárcena Varela para asistir al grado de Doctor por la Universidad de Navarra.

El presente trabajo se ha realizado bajo mi dirección en el Departamento de Hepatología del Centro de Investigación Médica Aplicada y autorizo su presentación ante el Tribunal que lo ha de juzgar.

Pamplona, 5 de noviembre de 2018.

Dr. Matías Ávila Zaragozá

Dra. Maite García Fernández de Barrena

A mis padres y hermano.

A Joaquín.

AGRADECIMIENTOS

Dedicación y constancia.
Pero ante todo, pasión.

En primer lugar quiero agradecer al Ministerio de Economía y Competitividad del Gobierno de España por otorgarme la ayuda predoctoral del Programa de Formación del Personal Investigador (FPI) y por la financiación concedida para la realización de este proyecto. Agradecer también a la Universidad de Navarra y al Centro de Investigación Médica Aplicada (CIMA) la posibilidad de realizar la tesis doctoral y desarrollar el presente trabajo científico.

Mi más sincero agradecimiento a mis directores de tesis, Dr. Matías Ávila y Dra. Maite García, por hacer posible la realización de este trabajo y mi desarrollo profesional a lo largo de estos años.

Matías, gracias por tu confianza, paciencia y dedicación. Siempre he pensado que el buen maestro es aquél que te impulsa a razonar, que te fomenta la curiosidad y te da el apoyo y libertad necesarios para que puedas evolucionar. Tú has sido ese maestro para mí. Desde mi comienzo has ido asentando en mí las bases que necesitaba para aprender a desenvolverme e ir creciendo a lo largo de este periodo de formación tan importante para mi futuro profesional. Como tú mismo dirías, aún soy "pequeñita", pero hoy, gracias a ti, puedo decir que me siento más segura de mis capacidades y con la base necesaria para ir desarrollándome científicamente. Gracias, no solo por los momentos felices en que obteníamos los resultados del duro trabajo sino también por los difíciles, en los que siempre he encontrado tu puerta abierta. Tentando mis límites para hacerme un poco mejor, más válida, y sobre todo, más ambiciosa y perfeccionista he tenido que ir superando todos los retos que han ido apareciendo. Al final has tenido razón, y la perseverancia ha logrado sus frutos. Sé que vendrán más retos. Espero siga superándolos y creciendo de la forma en que tú me has enseñado a hacerlo.

Maite, eres la persona a la que más necesito dar las gracias. Quizá por eso me resulta lo más complicado de escribir. Directora de mi tesis, compañera, y me atrevería a decir amiga, GRACIAS. Eres una mentora excepcional. Por todo el esfuerzo que has dedicado

en mi formación. Todas las horas que has pasado conmigo; transmitiéndome tus conocimientos, haciéndome pensar, razonando juntas, debatiendo sobre resultados, resolviendo problemas, preparando charlas, escribiendo informes, escribiendo una tesis. Toda una suma de horas incontables en las que te has volcado para ayudarme y enseñarme cómo hacer las cosas paso a paso. Y sé lo difícil que es sacar tiempo y fuerza para hacer todo eso. Siempre amable, siempre agradecida, me has enseñado de primera mano a desenvolverme en este mundo científico tan complejo y hermoso a la vez. Porque además de todo el tiempo que has dedicado en formarme, también me has transmitido ilusión, pasión por este trabajo. Contigo no solo he tenido una formación científica brillante sino que además he podido disfrutar a lo largo del proceso. Por supuesto, no todo ha sido disfrute, tú bien lo sabes, pero gracias a ti las fases difíciles han sido más llevaderas y los resultados obtenidos a lo largo de estos años han sido compartidos con entusiasmo y satisfacción. Me has valorado siempre, y has estado ahí tanto para darme apoyo en las complicaciones, como para darme la enhorabuena por los logros. Ahora soy yo quien te debe estas palabras. Esta tesis es tuya, y no me refiero solo al trabajo científico, sino a mis propios logros personales. Espero que tus "*fellows*" venideros sepan apreciar la suerte que es tenerte como directora. Yo siempre te estaré agradecida.

He de dar las gracias también a otra persona que ha dedicado su tiempo en el desarrollo de este trabajo. Laura, mi compañera de poyata por antonomasia a lo largo de esta tesis. Gracias por todo el tiempo que dedicaste en enseñarme desde cero el funcionamiento del laboratorio. Por tu compañía a lo largo de este proceso y porque formas parte de este trabajo y de mi propio aprendizaje.

Quisiera dar las gracias a todo el Departamento de Hepatología donde me he sentido tremendamente acogida a lo largo de estos años.

Al laboratorio 4.03 por recibirme en los inicios de la tesis. A Carlos, Eva y Sara, que me ayudasteis a asentarme al principio de mi llegada. Y a los recién reubicados en el 4.03, Antonio, Ana y Dani, que formáis un grupo excepcional. Gracias por vuestro apoyo, consejo y compañía; especialmente en los cafés y comidas, por la disuasión tan valiosa que hace más llevadero el día a día.

Al laboratorio 4.02, Carmen, Raquel, María Azkona, María Elizalde y la recién llegada María Arechederra. Gracias por vuestra disposición para solucionarme cualquier duda y aportarme consejo y apoyo durante estos años. A Maddalen, con quien he podido compartir mano a mano la aventura de adentrarse en una tesis doctoral. Gracias por todos aquellos momentos en los que me he sentido menos sola al tenerte a mi lado.

A mi laboratorio, 4.01. Uxue, gracias por tu organización. Siempre serás para mí la "*lab manager*" que todo laboratorio necesita. Por ordenar el caos y ser la única persona capaz de lidiar con nuestra querida "máquina del infierno" te mereces estas líneas de agradecimiento.

Iker, doy gracias por tus conocimientos informáticos. Tenerte cerca ha supuesto un alivio frente a cada problema que me ha surgido de esta índole. Pero, sobre todo, por tu amable disposición a ayudarme siempre.

Roberto, gracias. Has sido un apoyo laboral pero también emocional. Por aguantar mis desahogos y darme siempre fuerzas y ánimo para no dejar que perdiera la ilusión. Eres una persona excelente; responsable, trabajador y un gran compañero. Tenemos suerte de poder contar contigo.

Quiero dar las gracias a Gloria, quien se ha comportado como una auténtica amiga desde el principio. Contigo he compartido segundo a segundo los momentos más intensos de esta montaña rusa. Poder tenerte cerca ha sido un regalo. Eres una persona fortísima y trabajadora como la que más. Espero que tengas mucha suerte en tu próxima etapa postdoctoral, porque te lo mereces.

A Leticia que más recientemente se ha embarcado a este viaje que es la tesis doctoral. Has llegado como un aire fresco a este laboratorio. Tu alegría, tu buena disposición y tu compañerismo nos ayuda a todos a ablandar los nervios y paliar nuestra furia. O al menos la mía sí. Gracias por eso. Te deseo lo mejor para tu tesis, estoy segura que harás un gran trabajo.

Gracias también a todas las personas fuera del Departamento que han colaborado de una forma u otra en este proyecto.

A mi familia. A quienes dedico la tesis. Porque nada de lo que aquí he desarrollado habría sido posible sin ellos.

Gracias a mis padres Félix y Lourdes, porque os lo debo todo. Es complicado poner palabras al sentimiento de gratitud que tengo hacia vosotros. Vuestro amor incondicional ha sido el colchón que necesitaba para arriesgar y luchar por lo que quiero. Sin él, no habría sido capaz de convertirme en la persona que soy ahora. Por preocuparos por mi bienestar, incluso cuando ni yo misma lo hago. Porque siempre puedo contar con vosotros y especialmente en etapas complicadas como puede ser una tesis doctoral, dónde demostráis más que nunca vuestro apoyo. Gracias por ayudarme a relativizar las situaciones difíciles. Gracias por transmitirme vuestro sentimiento de orgullo hacia mí, porque ha sido crucial a lo largo de esta tesis, y en mi vida en general, sentirme valerosa y capaz. Gracias por haber luchado tantos años por mi felicidad. Lo habéis logrado. Hoy soy yo quien me siento orgullosa y tremendamente afortunada de teneros como padres.

Papá, Mamá, os quiero.

A mi tato, Sergio. Gracias por soportar el "lastre" que a veces conlleva cargar con una hermana pequeña. Siendo sincera, no se te ha dado nada mal. Eres un pilar fundamental en mi vida. Poder compartir contigo todo lo que nos depara y deparará la vida es un regalo. La "agonías" de tu hermana siempre llamará a tu puerta para pedir ayuda, y contar con que tú siempre estarás ahí para abrirla es un alivio incondicional. Gracias por ser un ejemplo a seguir en mi vida. Por darme templanza ante la adversidad y, por qué no, ser la primera y única persona de la familia capaz de leer y entender esta tesis. Lo que me satisface mucho.

Mi más queridísimo hermano, GRACIAS.

A la que a pesar de no compartir lazos de sangre considero mi hermana, Ane Miren. El vínculo especial que nos une es difícil de explicar. Pero ya sabes lo importante que eres para mí. Gracias por estar ahí, al otro lado del teléfono cada día que lo he necesitado. Tú, que has vivido intensamente cada periodo de mi formación profesional, y has apostado por mí siempre, gracias.

A mis tías, Arancha y Chavela, que desde la distancia siempre me habéis mostrado vuestro apoyo y preocupación. A mis cuñadas, Aida, Mamu y Marta. A vosotras que me habéis conocido de lleno en la inmersión de la tesis, gracias por acogerme entre vuestros brazos y hacerme sentir querida. Por empatizar conmigo y aguantar mis desasosiegos.

También dar las gracias a amigos y amigas que han supuesto un apoyo y una distracción para el día a día. Porque los momentos que he pasado con vosotros a lo largo de estos 3 últimos años los he valorado más que nunca. Especialmente dar las gracias a Garde, que tiene la maravillosa habilidad de sacarme una sonrisa hasta en los días donde me siento más hundida.

Finalmente quiero dar las gracias a Joaquín. Qué decirte que no te haya dicho ya. Eres la persona más consciente de todas de lo que ha supuesto para mí esta tesis doctoral. Nada habría sido igual sin tenerte a mi lado. Como un titiritero que mueve los hilos de una marioneta has sabido en cada momento impulsarme a seguir para adelante. Te has volcado día a día en mi felicidad y no hay manera de agradecer eso. Te has convertido en parte de mí. Y gracias a eso soy una persona mejor e infinitamente más fuerte. Gracias por aparecer en mi vida para quedarte. Te quiero. Esta tesis también está dedicada para ti.

Muchas gracias a todos.

INDEX

ABBREVIATIONS

αSMA	Alpha Smooth Muscle Actin
AdoMet	S-Adenosylmethionine
ADME	Absorption Distribution Metabolism Excretion
AFP	Alpha Fetoprotein
ALB	Albumin
ALDOA	Aldolase A
ALP	Alkaline Phosphatase
ALT	Alanine Aminotransferase
ARID1A	AT-Rich Interaction Domain 1A
ARID2	AT-Rich Interaction Domain 2
AST	Aspartate Aminotransferase
ATP	Adenosine Trisphosphate
BAMBI	BMP-Activin Membrane Bound Inhibitor
BCA	Bicinchoninic Acid
BRD	Bromodomain
BSA	Bovine Serum Albumin
CD31	Cluster of Differentiation 31
CDH1	E-Cadherin
CDKN2A	Cyclin Dependent Kinase Inhibitor 2A
cDNA	Complementary DNA
CEBPα	CCAAT Enhancer Binding Protein Alpha
CI	Combination Index
CLD	Chronic Liver Disease
COLIA1	Type I Collagen Alpha 1 Chain
CTNNB1	Catenin (Cadherin-Associated Protein), Beta 1
CYP7A1	Cholesterol 7 Alpha Hydroxylase 1
DAPI	4’,6-Diamidino-2-Phenylindole
DMEM	Dulbecco’s Modified Eagle’s Medium
DMSO	Dimethyl Sulfoxide
DNA	Deoxyribonucleic Acid
DNMT	DNA Methyltransferase
dNTP	Deoxyribonucleic Triphosphate

DTT	Dithiothreitol
DZNep	Deazaneplanocin A
ECL	Enhanced Chemiluminescence
ECM	Extracellular Matrix
EDTA	Ethylenediaminetetraacetic Acid
EMT	Epithelial-to-Mesenchymal Transition
EpCAM	Epithelial Cell Adhesion Molecule
EPHA2	EPH Receptor A2
ESI	Electrospray Ionization
EZH2	Enhancer of Zeste 2 Polycomb Repressive Complex 2 Subunit
FBP1	Fructose-Bisphosphatase 1
FBS	Fetal Bovine Serum
FDA	Food Drug Administration
FOXA2	Forkhead Box A2
G9a	Histone-Lysine N-Methyltransferase
GEO	Gene Expression Omnibus
GI_{50}	Growth Inhibiting Concentration by 50%
GJC3	Gap Junction Protein Gamma 3
GLP	G9a-Related Protein 1
GLUT1	Glucose Transporter 1
GNAS	Adenylate Cyclase-Stimulating G Alpha Protein
GNMT	Glycine N-Methyltransferase
GPI	Glucose-6-Phosphate Isomerase
GSEA	Gene Set Enrichment Analysis
GO	Gene Ontology
HAT	Histone Acetyltransferase
HBV	Hepatitis B Virus
HCC	Hepatocellular Carcinoma
HCV	Hepatitis C Virus
HDAC	Histone Deacetylase
HEPACAM	Hepatic and Glial Cell Adhesion Molecule
HGH	Hepatocyte Growth Factor
HIF1α	Hypoxia Inducible Factor Alpha

HIF1β	Hypoxia Inducible Factor Beta
HK2	Hexokinase 2
HLA	Human Leukocyte Antigen
HMT	Histone Methyltransferase
HNF4α	Hepatocyte Nuclear Factor 4 Alpha
HP	Heterochromatin Protein
HSC	Hepatic Stellate Cell
ICAM	Intercellular Adhesion Molecule 1
IP	Immunoprecipitation
KC	Kupffer Cells
KLF5	Kruppel-like Factor 5
KRAS	KRAS Proto-Oncogene, GTPase
KR	Keratin
KTM	Lysine Methyltransferase
LB	Lysogeny Broth
LDHA	Lactate Dehydrogenase A
LRAT	Lecithin: Retinol Acyl Transferase
LOX	Lysyl-Oxidase
MAT1A	Methionine Adenosyltransferase Isoform 1
MDR1	Multidrug Resistance 1
MLL2	Myeloid/Lymphoid or Mixed-Lineage Leukemia 2
MRM	Multiple Reaction Monitoring
mRNA	Messenger RNA
MSP	Methylation Specific PCR
MTD	Maximum Tolerated Dose
NASH	Nonalcoholic steatohepatitis
NAV3	Neuron Navigator 3
NFE2L2	Nuclear Factor, Erythroid 2 Like 2
NCAM	Neural Cell Adhesion Molecule
MeCP2	Methyl-CpG-Binding Protein 2
MHC	Major Histocompatibility Complex
MMP	Metalloproteinases
MRM	Multiple Reaction Monitoring
PARP	Poly ADP Ribose Polymerase

PBS	Phosphate-Buffered Saline
PCR	Polymerase Chain Reaction
PCR2	Polycom Repressive Complex 2
PGK1	Phosphoglucokinase 1
PHD	Plant Homeodomain
PHGDH	Phospohoglycerate Dehydrogenase
PI3KCA	Phosphatidylinositol 3-Kinase
PINX1	PIN2/TERF1-Interacting Telomerase Inhibitor 1
PK	Pharmacokinetics
PKM2	Pyruvate Kinase M2
PPARγ	Peroxisome Proliferator-Activated Receptor Gamma
PROM1	Prominin 1
PSAT1	Phosphoserine Aminotransferase 1
PTEN	Phosphatase and Tensin Homolog
PTM	Posttranslational Modifications
qChIP	Quantitative Chromatin Immunoprecipitation
RASSF1A	Ras Association Domain Family Member 1
RMA	Robust Multichip Average
RNA	Ribonucleic Acid
SAR	Structure Activity Relationships
SDS	Sodium Dodecyl Sulfate
SET	Su(var)3-9 Enhancer of Zeste and Trithorax
SETD2	SET Domain Containing 2
SHMT2	Serine Hydroxymethyltransferase 2
SHP	Small Heterodimer Partner
siRNA	Small Interfering -RNA
SKIL	SKI-Like Protooncogene
SSC	Saline Sodium Citrate
TAGLN	Transgelin
TCA	Tricarboxylic Acid
TERT	Telomerase Reverse Transcriptase
TGFβ	Transforming Growth Factor Beta
TGFβR	Transforming Growth Factor Beta Receptor
THY1	Thy-1 Cell Surface Antigen

TIMP1	Tissue Inhibitor of Metalloproteinases 1
TJP3	Thigh Junction Protein 3
TNM	Tumor Node Metastasis
TSG	Tumor Suppressor Gene
UHRF1	Ubiquitin Like with PHD and Ring Finger Domains 1
VDR	Vitamin D Receptor
VEGF	Vascular Endothelial Growth Factor
VHL	Von Hippel-Lindau

Introduction

THE LIVER

The liver is a multifunctional and highly differentiated organ with great regenerative capacity. It performs a wide variety of functions that are essential for the preservation of homeostasis in the organism, playing a central role in metabolism and detoxification. It is responsible for the synthesis, metabolism, storage and redistribution of nutrients, carbohydrates, lipids, vitamins and aminoacids. It also secretes large number of seric proteins and coagulating factors; and eliminates waste products and xenobiotic compounds by metabolic conversion and biliary excretion [1].

The hepatic parenchyma is mainly composed by the epithelial cells called hepatocytes (80%). The other 20% is constituted by different types of cells including cholangiocytes, endothelial cells and resident non-parenchymal cells such as hepatic stellate cells (HSCs), kupffer cells (KCs), macrophages and lymphocytes [1,2]. It has been increasingly recognized that both under normal and pathological conditions, hepatocyte functions are regulated by substances released from these neighboring non-parenchymal cells.

The functional and cellular complexity of the liver remarks its physiological relevance but also its susceptibility to be subjected to systemic insults, metabolic toxics and infectious agents [1]. Its exposure to endogenous and exogenous challenges exerts liver damages that should be quickly and efficaciously repaired to maintain the proper functionality of the organism. Although many different pathogenic agents and processes can affect this organ and liver diseases present high heterogeneity, the progression of chronic liver disease (CLD) goes through a series of common stages that may promote the development of liver cancer.

HEPATOCELLULAR CARCINOMA (HCC)

Liver cancer is a major health problem worldwide. It is the fifth most common cancer and represents the second frequent cause of cancer mortality [3]. Its incidence is increasing, especially in developed countries, with no effective therapies available. Among liver cancers hepatocellular carcinoma (HCC) accounts for 70-85% of malignant primary liver tumors [4,5]. It usually develops on a background of CLD which is the major driver of HCC. CLD is a pathological process of the liver that involves the progressive and sustained destruction and self-regeneration of the liver parenchyma leading to fibrosis and cirrhosis, and in the end stage the development of cancer (Fig. 1). CDL consists of a wide range of liver pathologies which include persistent inflammation, wound-healing response and scars formation that triggers loss of function of the organ and malignant cellular transformation [1,6,7].

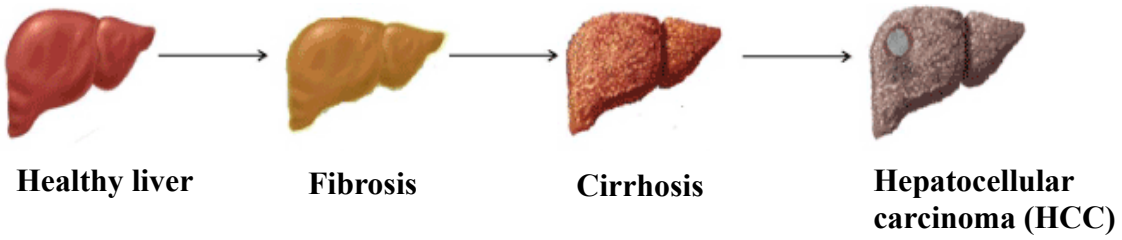

Figure 1. Hepatocarcinogenesis. Representative figure of the consecutive stages of CLD during the process of hepatocarcinogenesis.

There are many different patterns of chronic disease progression and HCC development based on their etiology and influenced by both genetic and environmental factors. Viral infections by hepatitis B virus (HBV) or hepatitis C virus (HCV), certain metabolic liver diseases, heavy alcohol intake, obesity and nonalcoholic steatohepatitis (NASH), or combination of the above are found in almost all HCC cases, contributing to its heterogeneity [4–8]. All these chronic liver injuries are able to establish environmental changes that directly promote HCC onset, maintenance and progression. The unique coexistence of these diseases complicates the prognostic prediction and therapeutic strategies. It is widely accepted that carcinogenesis results from accumulation of genetic alterations in critical genes which regulate cell proliferation, growth, survival, apoptosis, adhesion, and metabolism [9,10]. However, the molecular and cellular heterogeneity of these

tumors, together with the rich tumor microenvironment and stroma, contribute to their therapeutic resistance and their malignant and recurrent development [5,7,11–13].

Current therapeutic approaches include surgical resection, percutaneous radiofrequency ablation, trans-arterial chemoembolization and liver transplantation. Because most patients present multifocal HCC and advanced-stage of liver disease or comorbidities, liver transplantation represents the optimal therapy allowing to remove both tumor and underlying diseases. Consequently, in many countries incidence and mortality rates are equal. Around 70% of HCC patients suffer relapse after resection or ablation, or either are diagnosed in a too late state of the disease with no other therapeutic option than transplantation [4,5]. The unique treatment approved for these patients for almost a decade is the systemic administration of Sorafenib, a multikinase inhibitor that inhibits tumor-cell proliferation and angiogenesis [13,14]. However, the average life expectancy with this therapy is about one year [7–9,13,14]. Recently, two new drugs showed positive results in two phase III studies: the multikinase inhibitors Regorafenib and Lenvatinib, both with similar biological action than Sorafenib [13]. Therefore, novel systemic therapies are clearly needed to improve HCC patient's prognosis. Clinical trials of patients with advanced HCC are being developed testing various targeted therapies such as the promising immunotherapy [15]. However, many phase III clinical trials fail due in part to the high HCC heterogeneity together with an unsatisfactory classification. Classification of HCCs should be based on different genetic and epigenetic alterations and clinical behavior, with the aim to develop tailored treatment strategies. Genomic studies have allowed to categorize HCCs into subsets with distinct molecular and clinical features. For example, the approach performed by Boyault and colleagues in 2007 allowed to obtain a robust classification of HCCs that yielded 6 main subgroups (G1-G6) defined by transcriptome analysis and established a correlation of the groups with significantly associated clinical features [16].

Despite the high variety of molecular alterations causing malignant transformation in hepatocytes, there is a minimum number of alterations leading to the progressive acquisition of the cancer phenotype [17]. During hepatocarcinogenesis, cancer cells acquire several hallmark capabilities which enable them to became tumorigenic and show malignant properties [18] (Fig. 2).

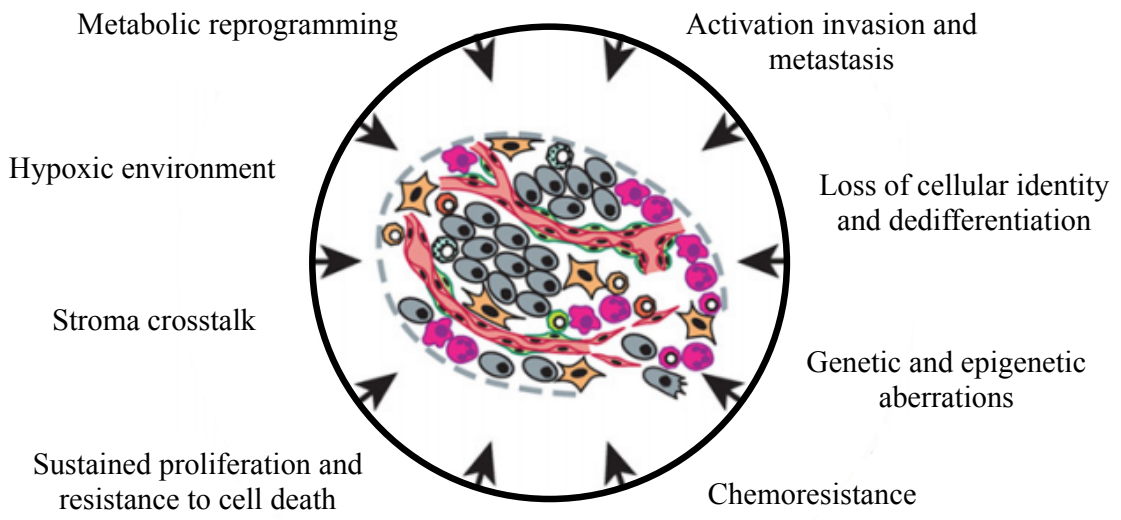

Figure 2. HCC hallmarks. Schematic representation of common features of liver cancer embedded in the tumoral microenvironment. (Adapted from Hanahan & Weinberg, Cell. Rev., 2011)

As was mentioned, HCC is strongly influenced and develops signaling networks with cellular and molecular components of the microenvironment. This crosstalk emphasizes the complexity of the malignant transformation but also correlates with phenotypical features of the liver tumor [7]. However, like most solid tumors, HCC is characterized by common cancer hallmarks such as sustained cell proliferation, evading growth suppressors, resistance to cell death, loss of differentiated phenotype, invasion and metastasis, angiogenesis and deregulated energy metabolism [10,18,19].

Dedifferentiation and metabolic reprogramming of hepatocytes as a hallmark of HCC

Although the most characteristic phenotype is the unrestrained proliferation of cancer cells it has been clarified that tumor proliferation is closely related to tumor cell dedifferentiation in HCC at the early stage [1,18]. As mentioned before, the liver is a highly differentiated organ. To perform its multiple tasks, hepatocytes express a large complement of enabling genes defining their complex phenotype. This phenotype needs to be maintained to guarantee the functionality of the organ [1]. Upon sustained injury, the liver displays a progressive switch from quiescent to active regenerative and proliferative

hepatocytes. This response triggers the loss of hepatocellular differentiation that is characterized by reduction of liver-specific genes expression but also the reactivation of genes expressed in the fetal hepatocytes [1,20]. The loss of hepatocyte identity underlies the liver malfunction in CLD that paves the way for HCC development. Moreover, the presence of stemness features renders the therapies less effective due to chemoresistance, increased survival, resistance to hypoxia, immune-tolerance and active drug-exporting systems among other strategies observed in these cells [21].

The molecular mechanisms driving hepatocellular dedifferentiation during CLD and hepatocarcinogenesis are not completely known, however impaired activity and expression of liver-specific genes has been established [1]. Some studies have assessed a correlation in the gene signature of HCC with that of fetal dedifferentiated hepatocytes [20]. Malignant cancer cells usually have similar properties as embryonic cells showing elevated stemness markers [22], and poorly-differentiated HCC tumors are closely associated with worse patients prognosis [23]. A common transdifferentiation process defined in cancer cells and involving morphological and phenotypical changes is the "epithelial-to-mesenchymal transition" (EMT) [24,25]. This phenotypical reprogramming confers motile abilities to the cancer cells. EMT is integral in development, wound healing and stem cell behavior, but also pathologically contributes to fibrosis and HCC progression. The most common marker of this reprogramming is the down-regulation of the adhesion molecule E-cadherin (CDH1). Consequently, tumor cells lose their contact and are thus enabled to invade out from the primary niche [26]. In HCC, altered expression of *CDH1* is commonly observed and usually correlated with clinical pathological features and cellular dedifferentiation [25].

Metabolic alterations are increasingly thought to participate in cancer biology including HCC. As previously mentioned, liver is a metabolic organ responsible for synthesis, metabolism storage and redistribution of variety of compounds [1]. These functions of the liver are challenged during the dedifferentiation process of cancer cells, resulting in a wide metabolic reprogramming that confers the cancer cells certain advantages for tumor development.

The liver is the main place for the metabolism of S-adenosylmethionine (AdoMet). Expression of enzymes of this metabolic cycle such as glycine N-methyltransferase

(GNMT) are confined mainly to the liver, or even expressed exclusively in this organ, as is the case of methionine adenosyltransferase isoform 1 (MAT1A) [27,28]. Alterations in methionine metabolism are found in patients suffering CLD, especially at the end stages of severe cirrhosis and HCC [28–30]. The importance of this alteration in the metabolism of methionine for the progression of the disease has been sustained in experimental models where AdoMet administration reduces liver damage independently of the etiology of the hepatic disease and improves survival in patients with cirrhosis [31]. Several studies have demonstrated that the main enzymes involved in methionine metabolism are drastically reduced or non-detectable in human cirrhotic liver and HCC [31]. Reduced expression of these enzymes in hepatocytes from damaged liver is an indicative of the progression of the disease and the dedifferentiation process in the cells that induces malignant transformation.

Other relevant metabolic function of the liver is the regulation of bile acid synthesis. Cholesterol 7 Alpha Hydroxylase 1 (CYP7A1) is the enzyme that catalyzes the first reaction of the cholesterol catabolic pathway in the liver, converting cholesterol to bile acids. This reaction is the rate limiting step and the major site of regulation of bile acid synthesis, and also the primary mechanism for the removal of cholesterol from the body. Well differentiated hepatocytes, with normal adult regulation of *CYP7A1* express large amounts of this gene [32], whereas the lack of CYP7A1 has been associated with pathological stages of the liver [33,34].

On the other hand, the liver is responsible for the regulation of glucose homeostasis in the organism, by maintaining the balance between its uptake, storage and synthesis. Abnormal expression of the enzymes responsible for carbohydrate metabolism in hepatocytes is linked to the loss of normal functionality of the liver. Altered carbohydrate metabolism indicators were found in clinical studies demonstrating that patients with Diabetes Mellitus have higher incidence of HCC and also its presence worsens the prognosis of an existing HCC [20,35,36]. Moreover, the extensive screen for enriched and conserved pathways between liver development and liver cancer pointed towards a significant role of carbohydrate metabolism in both conditions [20]. Gluconeogenesis is the metabolic pathway that results in the generation of glucose from certain non-carbohydrate carbon substrates. This pathway is one main mechanisms to maintain homeostatic levels of glucose in the organisms and takes place mainly in the liver. One rate-limiting enzyme

of gluconeogenesis is fructose-bisphosphatase 1 (FBP1), considered a tumor suppressor gene. It was demonstrated that decreased expression of *FBP1* associates with tumor progression in HCC and other cancers [37–39], and its relevance in the pathophysiology of the liver is evidenced due to the important gluconeogenic function of this organ, which is impaired by the malignant transformation of hepatocytes.

In cancer cells the high rate of proliferation increases the biosynthetic demand. Cells must increase the import of nutrients from the environment. A markedly increased consumption of glucose by tumors was first described by the physiologist Otto Warburg [19,40]. Later, it was demonstrated that the influx of glucose into cells is not driven by the immediate bioenergetic need but, on the contrary, it is modulated by extracellular stimuli. Moreover, aberrant activation of oncogenes and loss of tumor suppressors deregulate the glucose metabolic flux in cancer cells from its import to its catabolism. In this sense, cell proliferation not only increases the amount of nutrients but also actively changes the way nutrients are used [19]. Altered energy metabolism is found as a switch from oxidative phosphorylation to glycolysis. This phenomenon known as the *Warburg Effect* has emerged as important hallmark of cancer. Like other solid tumors, metabolic reprogramming from mitochondrial oxidation to aerobic glycolysis is commonly found in human HCC. This effect is characterized by the preferential use of glycolysis as the main program for energy metabolism in tumor cells even in the presence of oxygen [41,42]. Metabolic energy of cells is quantified by adenosine triphosphate (ATP) production, known as the "molecular unit of currency" of intracellular energy transfer. In normal cells, ATP is mainly generated from the tricarboxylic acid (TCA) cycle, followed by oxidative phosphorylation in the mitochondria. This pathway generates 36 molecules of ATP from one molecule of glucose. In contrast, glycolysis only generates 2 molecules of ATP from one molecule of glucose. Thereby, the preferential use of glycolysis in cancer cells is not due to the greater demand of energy. However, glycolysis could generate diverse intermediates for biosynthetic programs that are important for active cell proliferation. It provides a large number of nucleotides, fatty acids, membrane lipids and other intermediates that support the synthesis of macromolecules and are required for rapid tumor growth [19,42]. This reduced dependence of cancer cells on oxidative phosphorylation involves an important reprogramming and compensatory mechanisms that trigger a global remodeling of the metabolism of the cell. On one hand, cancer cells increase glucose intake and catabolism by up-regulating expression of glucose transporters and

glycolytic enzymes, whereas reducing the expression of gluconeogenic enzymes. As metabolic readout of this flux change, increased amounts of lactate are produced.

Glycolysis is classically depicted as a single chain of molecular events that leads to the generation of pyruvate, however, a number of glycolytic intermediates can be diverted into branching pathways, generating diverse biosynthetic precursors. One of these branching pathways is the serine-glycine pathway (Fig. 3). This pathway is the most intensely studied growth-promoting mechanism that shunts metabolites out of the glycolytic pathway by the use of 3-phosphoglycerate as a precursor for the biosynthesis of serine, glycine, and as a means to generate methyl groups donors [19]. Increased serine biosynthesis is one of many metabolic changes that have been reported in cancer cells [43]. Metabolic flux studies reveal that cancer cells may use as much as 50% of glucose-derived carbon in serine biosynthesis and its subsequent catabolism [44]. Thereby, deregulation of the enzymes responsible of the serine-glycine synthesis pathway is found in cancer cells as hallmark of their malignant metabolic reprogramming [43,44].

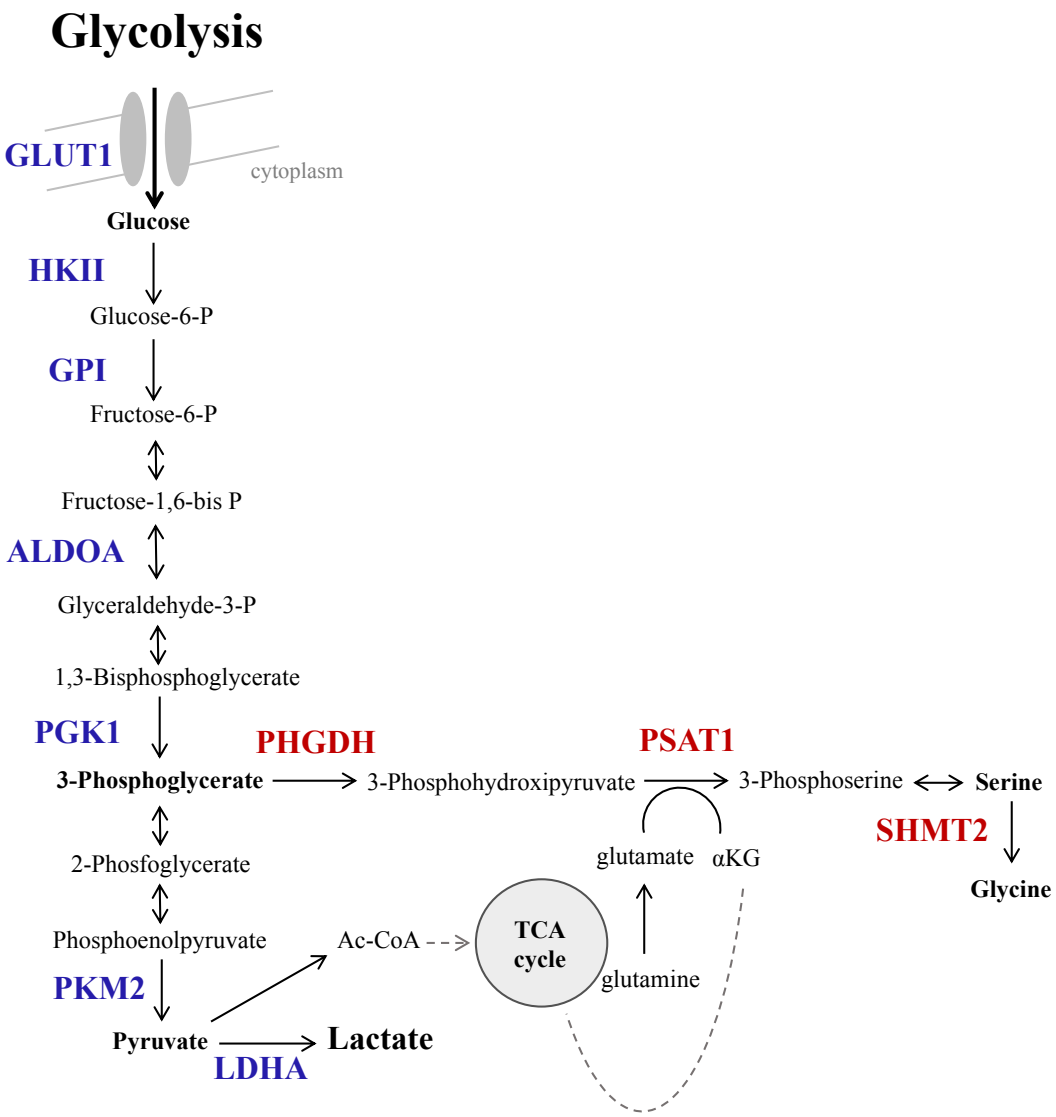

Figure 3. Glycolysis and serine-glycine synthesis pathways. Schematic representation of the glycolysis pathway and its shunt serine-glycine synthesis pathway.

ROLE OF MICROENVIRONMENT IN HCC PATHOGENESIS

HCC development is strictly dependent on environmental cues able to induce and maintain biological changes in tumor cells and in their tissue niche. Taking microenvironment into account will allow the acquisition of better knowledge of the mechanisms involved in hepatocarcinogenesis and the set-up of more effective therapy approaches.

Fibrosis as a tumor promoting background

As was mentioned, HCC development is commonly associated with preexisting CLD and thus it is invariably related to an inflammatory process, high rate of hepatocyte death and regenerative proliferation, and the activation of HSCs into fibril-producing cells. A central event in the beginning of CLD after sustained damage is the hepatocellular death that triggers an inflammatory reaction. This reaction is linked to a potent regenerative response in order to restore the lost hepatic tissue [2]. In this response, there are different cellular and molecular components such as cytokines, growth factors and metabolites playing a complex and controlled interaction. For example, the recruitment of activated inflammatory cells plays an essential role in the stimulation of hepatocytes proliferation. On the other hand, activation of HSCs is essential to produce the extracellular matrix (ECM) necessary to restore the lost liver mass and allow tissue repair [2,45,46]. In the context of acute or self-limited damage, this inflammatory and wound-healing response is transient, and the liver architecture is restored to the normal stage. However, under chronic injury, the response is sustained leading to the accumulation of ECM, a process known as hepatic fibrogenesis. If the situation is prolonged in time, it leads to the progressive substitution of liver parenchyma by scar tissue, resulting in a cirrhotic state where liver function is greatly affected and the chances of developing cancer increase considerably [46–48]. This resulting microenvironment fosters mechanisms in the liver that favor HCC development, growth and migration. The link between fibrosis and cancer is not as simple as a consecutive process, but more like an interactive crosstalk among cellular and molecular processes taking place along the development of CLD. Paracrine crosstalk between tumorigenic and stromal cells leads to rich intracellular networks based on reciprocal signaling. Although most evidences suggest that fibrosis promotes HCC, it

is possible that in some clinical settings fibrosis and HCC might occur due to the same underlying factors rather than one promoting the other. Cells in the microenvironment secret growth factors that support tumor cell growth and angiogenesis, or produce pro-inflammatory cytokines and chemokines, which favor malignant transformation. At the same time, transformed hepatocytes release factors that sustain ECM production by HSCs stimulation, or induces the recruitment of pro-inflammatory cells (Fig. 4).

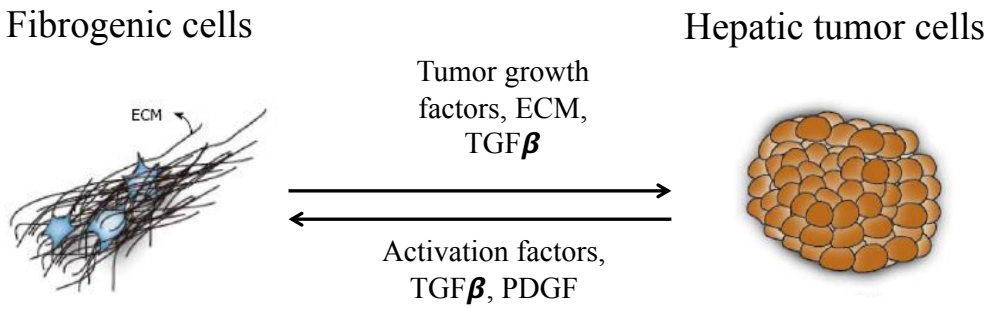

Figure 4. Fibrogenic cells and tumoral cells crosstalk in HCC. Representation of the crosstalk between tumoral and fibrogenic cells that takes place in the liver in the context of HCC.

In fibrotic liver, ECM is in a progressive thickening with ongoing collagen chemical cross-linking. Its composition is also altered. The most important structural components of ECM are: collagens, proteoglycans, laminin, fibronectin and matricellular proteins [48]. Whereas normal liver matrix is mainly composed by type IV collagen, heparan sulfate proteoglycan and laminin, hepatic injury induces the disruption of normal ECM and the replacement of structural components by fibrillar collagens type I and III and fibronectin [49]. The ECM is able to incorporate different molecular components and growth factors that can be bound to the ECM structural scaffold and preserved as latent forms. It has the capacity to modulate cellular activity in hepatocytes and HSCs, prevent apoptosis in damaged liver, avoid growth factor proteolysis and trigger signals of migration, differentiation, angiogenesis and others [49–51]. All these changes alter the matrix microenvironment and create a functional and physical impediment to the normal development of hepatic functions [49]. During this complex crosstalk among all the cellular and molecular components of the liver that takes place along the development of CLD, there are different cell populations contributing to ECM accumulation. However, HSCs activation remains the most dominant pathway leading to hepatic fibrosis perpetuation.

In fact, it has been demonstrated that depletion of HSCs and myofibroblasts in rodent models reduces hepatic injury and fibrosis [52].

HSCs are differentiated mesenchymal cells present in the perisinusoidal space, which embrace endothelial cells and focally provide a double lining for the sinusoid [51]. The most characteristic feature of stellate cells in normal liver is their cytoplasmic storage of vitamin A (retinoid) droplets. Almost all the vitamin A in the liver is stored in stellate cells, and thus the expression of enzymes responsible for retinoid metabolism such as lecithin:retinol acyl transferase (LRAT) are common markers of quiescent HSCs. Other functions of HSCs in normal liver include the control of extracellular matrix turnover, and the regulation of sinusoids contractility [51]. However, hepatocellular damage activates the transformation of quiescent stellate cells into myofibroblast-like cells that play a key role in the development of the inflammatory and fibrogenic response. Thereby, following liver injury HSCs become activated, acquiring a phenotype characterized by the loss of retinoid droplets, increased proliferation and contractile activity and the release of pro-inflammatory, pro-fibrogenic and pro-mitogenic cytokines [46,48,51] (Fig. 5).

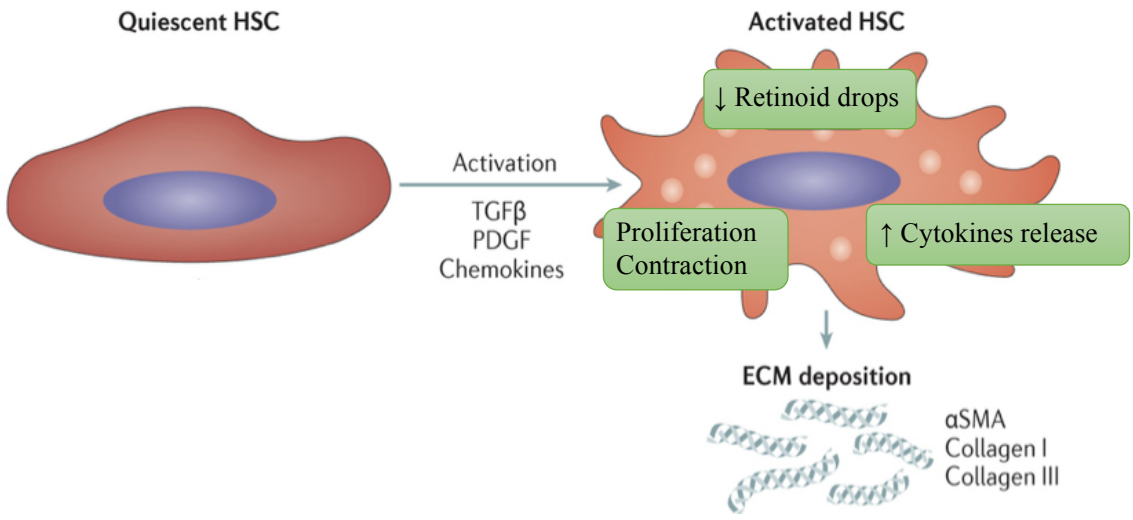

Figure 5. HSCs transdifferentiation process. Representation of the activating process that induce HSCs transdifferentiation. (Adapted from Liu & Brenner, Nat. Rev. Gastro. & Hepatol., 2015)

The transdifferentiation process of HSCs results from either "activating" events as well as loss of repressive signaling [51]. There is a relevant reduction of the expression of genes involved in the maintenance of the quiescent state in HSCs that also participate in functions associated with their normal phenotype. The family of the transcription factors "Peroxisome Proliferator-Activated Receptors" (PPARs) is one example. They are the master regulators of glucose and lipid metabolism in HSC. Among different isoforms, Peroxisome Proliferator-Activated Receptor Gamma (PPARγ) is the most extensively investigated in HSCs and it is considered essential for maintaining the quiescent phenotype. In quiescent cells PPARγ reinforces their adipogenic phenotype, but when activated its expression and activity are downregulated. This downregulation is crucial for enabling transdifferentiation to the myofibroblast phenotype [53,54].

TGFβ signaling as pivotal player in HCC pathogenesis

The pleiotropic transforming growth factor beta (TGFβ) multifunctional cytokine has emerged as a pivotal player in HCC pathogenesis influencing environmental and cell autonomous changes including activation of HSCs [55–57]. TGFβ signaling is involved in all stages of HCC progression, from initial liver injury and inflammation through fibrosis to tumor initiation, development and metastasis. TGFβ is secreted by variety of cell types and presents three isoforms. TGFβ1 is the principal isoform implicated in liver fibrosis [58] and is considered the main factor accelerating the progression of the disease. Once HSCs are stimulated by chronic fibrogenic stimuli, they respond by secreting increased amounts of TGFβ1. This exerts potent fibrogenic effects in both autocrine and paracrine manners, with autocrine being most important [51]. The TGFβ1 signaling pathway involves the binding of the cytokine to serine-threonine kinase type II surface receptor (TGFβRII) that recruits and phosphorylates a type I receptor (TGFβRI). The TGFβRI subsequently phosphorylates downstream effectors, typically SMADs proteins. Phosphorylation leads to activation of SMAD2 and SMAD3, this last one more implicated in fibrosis [59], that are released into the cytoplasm where they form a complex with SMAD4 and translocate into the nucleus. Once in the nucleus, the complex binds to target genes regulating their transcription [58,59]. In addition to the SMAD-dependent pathway, as is represented in Fig. 6, many other pathways are modulated or present a crosstalk with TGFβ signaling.

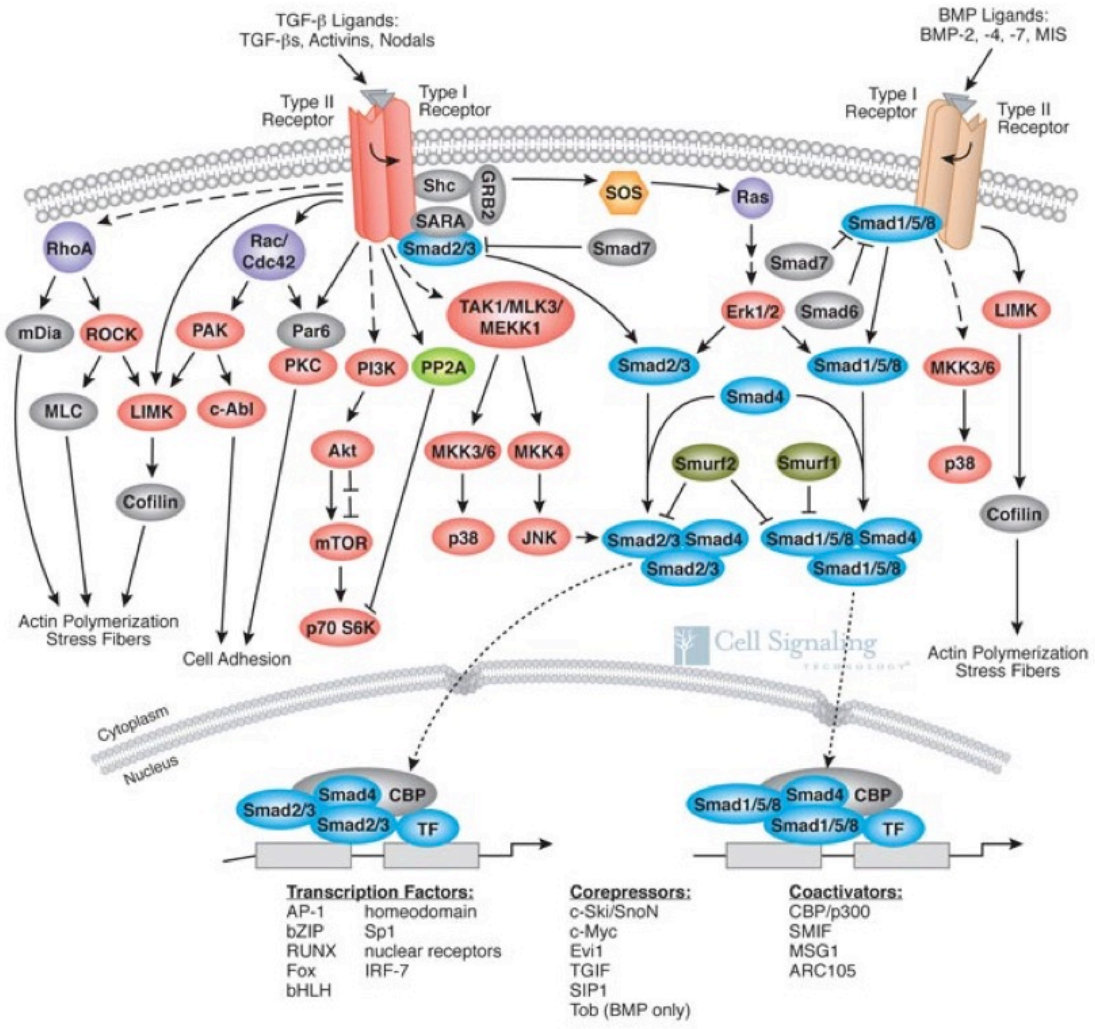

Fig 6. TGFβ signaling pathway. Schematic representation of the TGFβ signaling pathway. (From Cell Signaling Web site; https://media.cellsignal.com/www/pdfs/science/pathways/TGF_beta.pdf)

Type I collagen is the major ECM component of fibrotic tissue produced by HSCs and its production is significantly controlled by TGFβ [58]. In addition to type I collagen gene, there are other target genes such as Alpha Smooth Muscle Actin (*αSMA*) and the *TGFβI* gene itself, that respond to TGFβ. Induction of *αSMA* is the single most reliable marker of stellate cell activation because it is absent from other resident liver cells in either normal or injured liver, with the exception of smooth muscle cells surrounding large vessels [51]. Increased production of these genes is a common hallmark of fibrotic disease and a readout of the TGFβ signaling response. However, TGFβ-mediated activation of HSCs not only induces ECM components but also induces angiogenesis. The increased

expression of angiogenic modulators such as Vascular Endothelial Growth Factor (*VEGF*) also contribute to the pathogenesis of CLD [49].

In addition to HSC, malignant hepatocytes have the ability to produce TGFβ that not only participates in the perpetuation of myofibroblast activation but also works as oncogenic growth factor in HCC. Moreover, when the transformation process of hepatocytes had occurred, TGFβ induces EMT promoting progression and metastasis of primary tumors [60]. Accordingly with its tumor promoting role, TGFβ signaling was found constitutively activated in HCC cell lines [61]. Serum levels of the cytokine were found in advanced-stage HCC patients and correlated with tumor vascularization, metastasis formation, reduced survival and poor prognosis [62].

Hypoxia adaptation as driving force of liver cell transformation

Hypoxia is a common feature of tumor microenvironment of solid tumors. It is an indicative of malignancy and typically arises during CLD not only in tumor regions but also in fibrotic and cirrhotic tissues as there is an increased resistance to blood flow [63]. Many pathogenic mechanisms have been linked with hypoxia such as enhanced tumor-stroma crosstalk, fibrogenesis, malignant transformation, tumor invasiveness and metastasis, and resistance to chemo-, immune- and radio-therapy [64,65].

The events triggered by hypoxia depend to a large extent on the activity of the transcriptional regulator Hypoxia Inducible Factor 1 Alpha (HIF1α) that forms a heterodimer with Hypoxia Inducible Factor 1 Beta (HIF1β). Under normal oxygen levels HIF1α is targeted for ubiquitin-mediated degradation via proline hydroxylation and association with Von Hippel-Lindau (VHL) tumor suppressor complex. But under hypoxia, proline hydroxylases function is impaired and HIF1α is stabilized [64] (Fig. 7). HIF1α/HIF1β heterodimer regulates the transcription of multiple genes relevant to the pathogenesis of HCC. It activates the expression of many genes relevant to the *Warburg Effect* encoding glucose transporters and glycolytic enzymes [64,66]. These enzymes can be expressed as several isoforms, and the ones expressed in hypoxic tumors are different from that on healthy tissues. HIF1α/HIF1β increases the transcription of the particular

isoforms such as glucose transporter 1 (*GLUT1*), hexokinase 2 (*HK2*), aldolase A (*ALDOA*), phospho-glucokinase 1 (*PGK1*) and lactate dehydrogenase A (*LDHA*) [65]. The over-expression of these enzymes after HIF1α stabilization is a key contributor to the *Warburg Effect* and thereby, to the malignant metabolic reprogramming of the cancer cells.

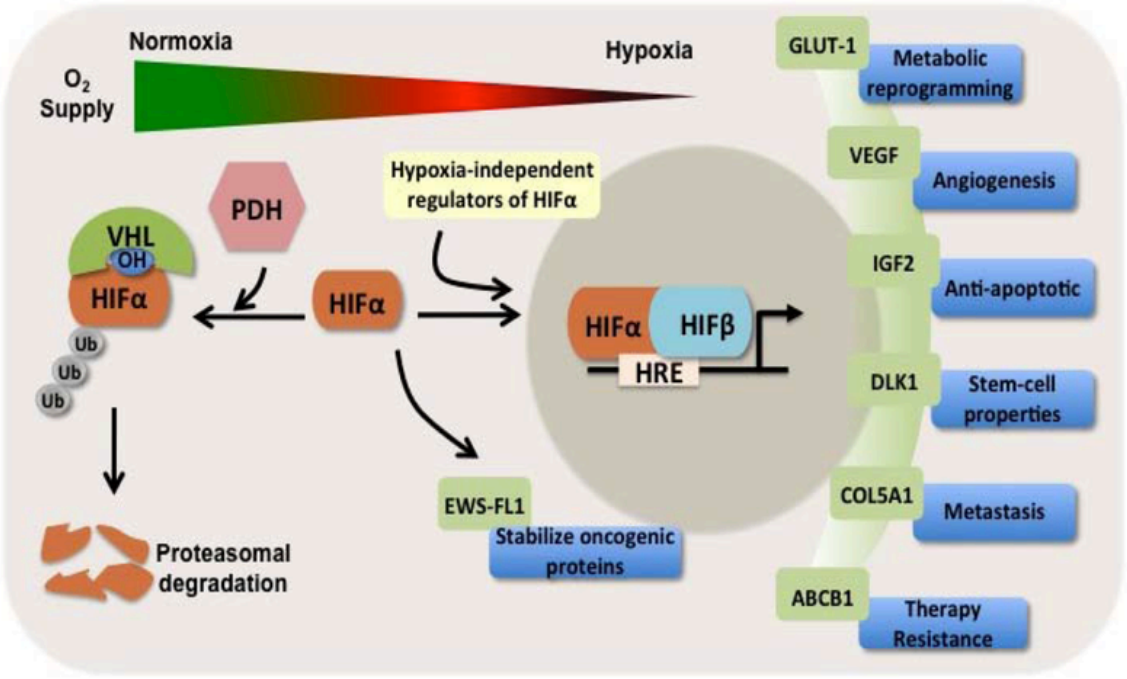

Figure 7. HIF1α stabilization and functions under hypoxia. Representative picture of HIF1α stabilization, heterodimerization and transcriptional regulation of HIF-target genes under hypoxia (Sadri & Zhang, Cancers, 2013).

Angiogenesis is another important feature of cancer highly regulated by the availability of oxygen in the environment. The formation of new blood vessels is a key mechanism in the pathogenesis of CLD irrespective of their underlying etiology. During CLD there is a neovascularization and establishment of an abnormal angio-architecture related to its pathological progression. When tumor mass grows, the tumor cells need to provide enough nutrients and oxygen, at the same time that new vessel formation accelerates proliferation, growth and metastasis of cancer cells [67]. Hypoxic environment is one of the major promoters of angiogenesis, enhancing *VEGF* expression and secretion. It is one of the classical target genes of HIF1 that activates proliferation of endothelial cells and

fibroblasts. Moreover, the hypoxic environment not only stimulates the release of a variety of mediators from cancer cells but also from HSC. Exposure of HSCs to hypoxia increases the synthesis of *VEGF*, *αSMA* and Collagen Type I Alpha 1 Chain (*COLIA1*) indicating that hypoxia also promotes the activation of these cells and therefore may affect the progression of fibrosis [68,69].

EPIGENETICS IN LIVER DISEASE

The term "epigenetic" was initially introduced by Conrad Waddington in 1940, defining it as the branch of biology studying the interactions between genes and their products. In time, the definition has narrowed and it is nowadays used to identify hereditable and long-term changes in gene expression that do not necessarily involve mutations in DNA sequences. Although all the cells within a multicellular organism contain the same genetic material, each tissue and cell type express only specific subsets of genes. How the same genetic information is translated into different cellular identities is a process mainly regulated at the epigenetic level. Epigenetic regulators and transcription factors act to organize the genome into accessible or closed regions, fine-tuning the proper transcriptional program in any given cell type. As such, epigenetic regulation is fundamental to maintain cellular identity and the unique physical characteristics and biological functions of specific tissues and organs.

Epigenetic processes include a wide panel of mechanisms. The most studied ones include DNA methylation events, reversible changes in histones modifications and chromatin remodeling. Importantly, the epigenetic state of a cell is highly malleable, and is the balance between all of them what determinates if particular gene/genes are transcriptionally expressed or silenced [70,71] (Fig. 8). Regulation of genetic expression is an important mechanism for cancer cells to modulate its phenotype during malignant transformation. Alterations in epigenetic information and aberrant expression and activity of epigenetic enzymes are being studied in the process of malignant transformation. Deregulation of gene expression associated with epigenetic events are virtually found in every step of tumor development and progression along with genetic alterations [72,73]. In contrast to genetic mutations, epigenetic alterations arise in a gradual manner leading to the progressive modulation of gene expression. They are believed to appear early in tumor development and may even precede the malignant process. On the other hand, they are induced in response to altered environments. Thereby, epigenetic modifications may also change its pattern once the tumor is established and can be considered in this context as an adaptive processes of cancer cells that participates in signal transduction pathways involved in malignancy [73].

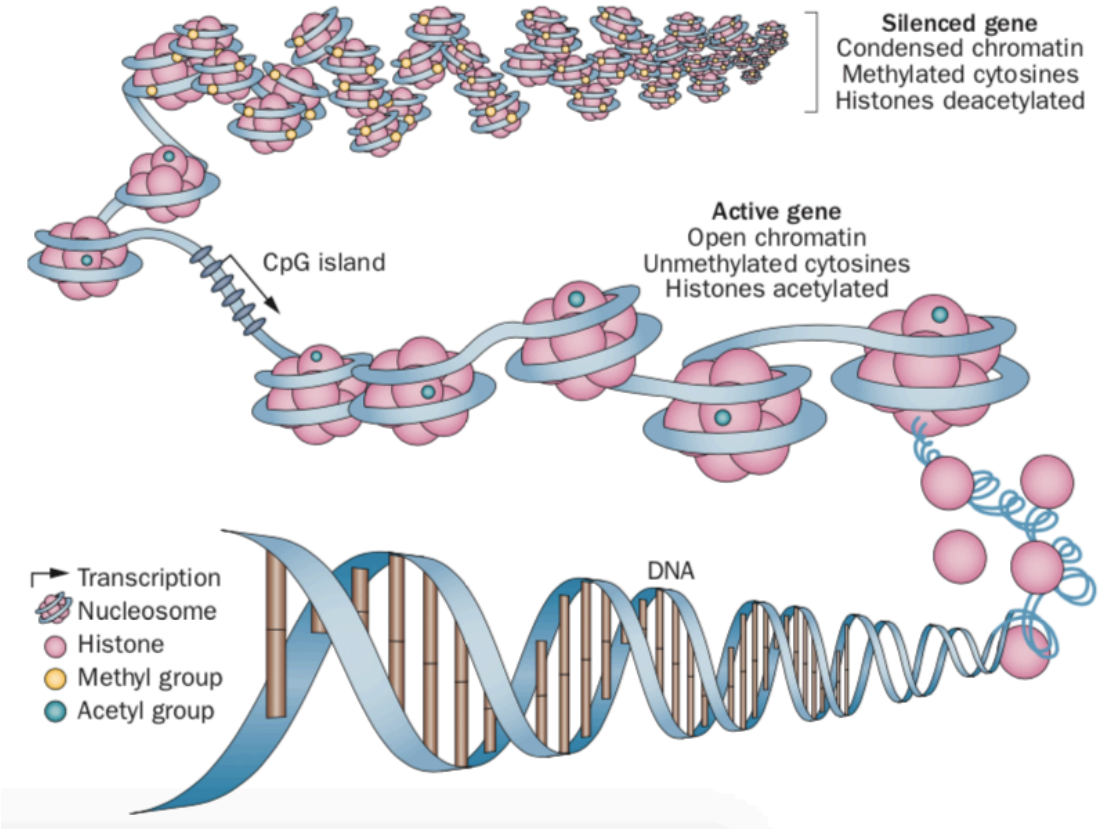

Figure 8. Epigenetic regulation of gene expression. Representative picture of controlled gene expression by combination of DNA methylation status and chromatin configuration in cells (Azad *et al.*, Nat. Rev. Clin. Oncol., 2013).

Traditionally, development of HCC has been viewed as a progressive accumulation of genetic alterations in tumor suppressor genes (TSG) and oncogenes. However, over the past decade, emerging knowledge of the importance of epigenetic regulation in hepatocytes indicates that both genetic and epigenetic aberrations cooperate at all stages of CLD and HCC development [74]. The liver is an organ that must adapt to a constant flux of environmental variations. Thereby, the epigenetic landscape of this organ is acutely sensitive to environmental cues resulting in modifications that impact on its controlled patterns of gene expression [75]. The diverse malignant phenotypes of hepatic cancer associates with several epigenetic alterations in cancer cells, and also with alterations in the regulation of the expression of critical genes along HSC transdifferentiating process [74,75]. Aberrant epigenetic information and its potential application in the diagnosis and treatment of HCC and other cancers are very active fields of investigation. They can be exploited in the clinic as novel tools for early diagnosis, prediction of clinical outcome

and risk assessment, whereas the reversibility of epigenetic modifications make them attractive targets for therapeutic interventions.

HCC and DNA methylation

The first epigenetic abnormality described in HCC, and one of the most common molecular alterations identified in human cancer, is the dysregulation of DNA methylation. DNA methylation occurs in cytosine bases that are located 5' to a guanosine base in a CpG dinucleotide. It is the best understood and most extensively studied epigenetic mechanism. Methylation of CpGs in promoter region is usually linked to inactivation of the expression of the gene, and thus it is commonly considered as repressive mark. However, novel studies are also considering that depending on its location and density along the structure of genes they might be also acting as activating marks [76,77].

Global genomic DNA hypomethylation accompanied by promoter-specific hypermethylation of putative TSGs has been identified in HCC. The global hypomethylation is believed to promote tumor development through activation of cellular proto-oncogenes and induction of chromatin instability [78]. Most of these hypomethylated genes are commonly upregulated in various cancers and predominantly involved in cell proliferation, cell signaling, mobility and invasion [79].

On the other hand, the specific hypermethylation of CpG islands-containing promoters from specific genes is an strategy of cancer cells to silence the expression of large number of cancer-related genes involved in different vital biological processes such as cell-cycle control, apoptosis, cell proliferation, tumor suppression, DNA repair or xenobiotic metabolism [78,80,81]. As examples, two of the most common silenced genes by tumor-related hypermethylation in HCC are the Ras Association Domain Family Member 1 (*RASSF1A*) and the Cyclin Dependent Kinase Inhibitor 2A (*CDKN2A*) [74]. Hypermethylation of the promoter of these genes is considered a biomarker of HCC. On the other hand, there is growing evidence of the importance of coding region hypermethylation in gene inactivation. One example is the association between *MAT1A* coding region hypermethylation and its reduction of expression found in human HCC [82].

The DNA methylation alterations are usually accompanied by aberrant expression of DNA methyltransferases (DNMTs) [83–86]. There are two main categories of DNMTs: those involved in *the novo* DNA methylation (DNMT3A and DNMT3B) and those involved in the maintenance of post-replicative DNA methylation (DNMT1). Progressive overexpression of *DNMT1*, *DNMT3A* and *DNMT3B* has been found from premalignant non-cancerous liver tissues to full-fledged HCC samples, and its contribution to the pathogenesis of liver cancer development along different stages of the disease has been established [74,79,85,87,88]. In fact, the aberrant DNA methylation patterns already mentioned occur not only in HCC, but also in premalignant pathological conditions from the initial acute damage and the onset of fibrosis to the subsequent development of cirrhosis [85,89], suggesting the relevance of this mechanism in pathogenesis and progression of CLD. There is vast potential for alterations in DNA methylation in HCC to be exploited for future drug and biomarker development.

HCC and histone modifications

Within the chromosome, DNA is packaged into chromatin where the DNA coils around an octamer of histones comprising two H2A, two H2B, two H3 and two H4 subunits, forming the repeating unit of chromatin, the nucleosome. Unstructured N-terminal tails of histones protruding out of the nucleosomes are targets of a variety of posttranslational modifications (PTMs), including phosphorylation at serine residues, methylation at arginine or lysine residues and acetylation, ubiquitination, sumoylation and ADP-ribosylation at lysine residues. Altered patterns of histone modifications have been involved in both the silencing and the activating expression of specific genes [78,90]. Histone modifications are high variable and dynamic and conform the so called “histone code”, that can dictate the cellular outcome in many different ways. Its primarily function in transcription is serving as points of recognition for transcriptional regulators and chromatin-associated proteins [78,90]. Acetylation and methylation are the most characterized PTMs so far. Histone acetylation is controlled by two families of enzymes: histone acetyltransferases (HATs), that “write” the acetyl mark, and histone deacetylases (HDACs), that “erase” the acetyl group. On the other hand, histone methylation is catalyzed by histone methyltransferases (HMTs), whereas demethylation comprises histone demethylases (HDMTs) activity. Both epigenetic marks change quickly in

response to cellular environment and stimulus and confers huge power of functional responses [91]. Unlike acetylation, that is considered an activating mark, methylation of histones can be either "activating" or "repressive", depending on the position of the methylated residue and the extent of methylation [70,75].

Histone modifying-mechanisms in HCC are being studied unmasked to get a clearer view of the molecular processes that drive this devastating disease. Global hypo-acetylation and hypermethylation of residues of histone's tails are considered as common epigenetic aberrations found in cancer. It is well documented that HCC is characterized by a prominent dysregulation of several histone-modifying enzymes, and their aberrant expression and activity has been correlated with different clinicopathological features and recurrence of HCC [74]. One example is the Polycomb-group of proteins that are chromatin-modifying complexes mediating heritable gene silencing. Enhancer of Zeste 2 Polycomb Repressive Complex 2 Subunit (EZH2) is a histone lysine methyltransferase that forms part of the Polycomb Repressive Complex 2 (PRC2) and mediates gene silencing by trimethylating lysine 27 of histone 3 (H3K27). Elevated expression of *EZH2* has been reported in many different cancers including HCC [92,93]. Specifically, clinicopathological analysis of paired resected tumor and non-tumor tissues showed that high levels of *EZH2* were strongly associated with aggressive and metastatic features and poor prognosis [92,93]. On the other hand, evaluation of histone methylation status in HCC remains limited to correlative studies with clinicopathological features of HCC. One study demonstrated that high levels of trimethylated histone H3 lysine 4 (H3K4me3) are correlated with reduced overall survival and poor prognosis [94]. Another study showed that high levels of H3K27me3 predicted worse prognosis, and closely correlated with aggressive tumor features, including vascular invasion and poor differentiation [95]. However, there is still a largely unexplored field.

Epigenetics and HSC transdifferentiation

As mentioned above, there is a fundamental role for fibrogenesis and extracellular matrix accumulation in HCC development. Myofibroblasts generated at sites of liver injury are essential cellular elements of wound healing and fibrosis. A paradigm for this process is the transition of quiescent HSCs through transdifferentiation to a profibrogenic

myofibroblastic phenotype. This process requires global epigenetic remodeling to bring about the suppression of adipogenic differentiation factors, *de novo* expression of regulators for the new phenotype and cell cycle entry [96]. Studies of molecular mechanisms that reprogram the HSC transcriptome reveal new regulators of fibrogenesis as well as potential biomarkers and therapeutic targets. Epigenetic events that control HSC activation and function are a highly dynamic process and the phenotype conversion requires changes in expression of hundred different genes [97]. HSCs are highly plastic cells with the ability to respond to cues in their immediate microenvironment, thereby modulation of gene expression is not only important for generation of the activated state, but also for its response to the microenvironment and its persistence in the CLD and cancer development.

As occur in cancer cells, altered expression patterns of epigenetic enzymes have been observed when activation of HSCs. There is an aberrant DNA methylation pattern in myofibroblasts associated with either transcriptional repression or activation [72,75,98]. There is a global DNA hypomethylation that can be found in stably methylated areas of the genome but also in promoter regions of fibrotic genes from the onset of liver fibrosis, whereas there is also a specifically induced repressive hypermethylation of target genes. These events are accompanied by up-regulated levels of DNMTs [75,98] . Up-regulation of various histone-modifications enzymes such as HDACs and HMTs has been also reported [89,99,100]. Histone modification is another active epigenetic alteration during HSC activation. Several findings implicated accumulation of HDACs at matrix metalloproteinases (*MMP*) promoters, specifically HDAC4, as an epigenetic mechanism to repress the expression of these enzymes during HSC activation [101]. Similar regulation was provided via HDAC7, which represses Hepatocyte Growth Factor (*HGF*) and thus increases susceptibility to hepatocellular damage, inflammation, and fibrosis in liver injury [102]. In cultured human skin fibroblasts, HDAC6, HDAC8, but most potently HDAC4 were also identified as crucial epigenetic regulators of TGFβ-induced HSC transdifferentiation, ostensibly by blocking the expression of TGFβ signaling repressor genes [103]. Other study performed by Page and colleagues demonstrated that ethanol exposure promotes rat HSC transdifferentiation by inducing global changes in histone modifying enzymes that upregulate ECM components and collagens [98]. The authors found that ethanol induced the expression of histone 3 lysine 4 (H3K4) methyltransferases, mainly that of *MLL1*. Vitamin D receptor (VDR) ligands also induce

chromatin remodeling as a mechanism to counteract TGFβ-driven HSC activation [104]. TGFβ induces activation by promoting the recruitment of histone-modifying cofactors, p300 and CBP, and by promoting H3 hyperacetylation at a VDR/SMAD co-occupied regulatory region of *COLIA1*. Treatment with VDR ligands antagonized activation by disrupting TGFβ-mediated SMAD/VDR interaction, reducing collagen deposition and fibrotic genes expression [104]. All these studies underscore the critical role of histone modification in HSC transdifferentiation.

One crucial epigenetic mechanism for HSCs activation widely studied by Mann's group is the induction of the expression of the Methyl-CpG-Binding Protein 2 (*MeCP2*), that along with other proteins comprises a nuclear complex able to repress transcription of target genes inducing either DNA methylation or silencing histone marks [54,105,106]. It was demonstrated that this is a mechanism responsible of the epigenetic silencing of *PPARγ* (the master regulator of quiescence in HSC previously mentioned) [54,106]. MeCP2 binds to *PPARγ* promoter where it facilitates methylation of lysine 9 of histone 3 (H3K9), that in turn provides binding sites for Heterochromatin Protein 1 (HP1) that promotes transcriptional silencing. Moreover, MeCP2 moreover stimulates the expression of *EZH2*, which is recruited to the downstream coding region of *PPARγ* where it increases the methylation levels of H3K27 mediating polycomb-regulated transcription silencing [54]. On the other hand, MeCP2 is also able to regulate the induction of expression of positive regulators of profibrogenic genes. It is able to induce the expression of the histone lysine methyltransferase ASH1 that participates in the activation of genes such as *COLIA1*, Tissue Inhibitor Metalloproteinase 1 (*TIMP1*) and *TGFβ1* by catalyzing the methylation of H3K4 [106]. These MeCP2-mediated mechanisms are one example of coordinated activity between DNA methylation and histones modifications, reflecting the relevance of the crosstalk between epigenetic events.

G9a/DNMT1 complex as a promising therapeutic target for HCC

The overall combination of histone marks, as well as their functional relationship with DNA methylation status, together with the presence of other regulatory factors, ultimately determine chromatin conformation and expression level of associated genes. In other

words, numerous associations exist in the recruitment of proteins and enzymatic complexes that can recognize and bind to methylated CpGs or specific histones marks or even both. Thereby all the epigenetic events involve an intimate and complex crosstalk that include DNA methylation regulation, histones modification mechanisms and also the recruitment of transcriptional corepressors/coactivators [73,90].

The mechanisms by which CpG islands remain unmethylated in normal cells and acquire DNA methylation status in cancer cells is likely intimately linked to the underlying histone code. Methylation of H3K9 and DNA methylation are tightly associated in heterochromatin and transcriptionally repressed euchromatic regions [78,90]. Trimethylation of lysine 9 of histone 3 (H3K9me3) in heterochromatin is necessary for maintenance of DNA methylation and is catalyzed by the histone methyltransferase SUV39H1/2. On the other hand, di-methylation of lysine 9 of histone 3 (H3K9me2) and subsequent methylation of DNA plays an equally important role in gene silencing in euchromatin and is catalyzed by the histone methyltransferase G9a and the G9a-related protein (GLP) [78,107,108]. These histone repressive marks are necessary for the maintenance of normal DNA methylation status of genes in differentiated cells and its alteration during carcinogenesis has been demonstrated in various types of tumors [71,109], being promising targets for anti-tumoral approaches.

A model for the coordinated regulation of DNA methylation and H3K9me2 through direct or indirect interactions between G9a and DNMT1 and other proteins such as HP1 and Ubiquitin Like with Plant Homeodomain-PDH- and Ping Finger Domains 1 (UHRF1) has been suggested [78,110,111] (Fig. 9). UHRF1 binds to hemi-methylated DNA and is an essential regulator of DNA methylation during DNA replication, and an adaptor in the crosstalk between DNA and histone methylation. It is overexpressed in many tumors including HCCs and is emerging as an oncogene [78,111]. As an example of the coordinated regulation between DNMTs and G9a, McGarvey and colleagues found that in cancer cells reactivation of TSGs upon treatment with DNMTs inhibitors is achieved by both demethylation of DNA and a decreased H3K9me2 levels, without altering other silencing marks such as H3K9me3 or H3K27me3 [109,112]. Moreover, inhibition of G9a alone is sufficient to induce reactivation of silenced metastasis suppressor genes in cancer cells, but this effect is potentiated by concurrent inhibition of DNMT1 [113]. However, the interactive crosstalk between these enzymes is complex. Dong and colleagues have

demonstrated that G9a-mediated DNA methylation does not require its catalytic activity, suggesting that G9a has additional functions directing DNA methylation such as recruitment of DNMTs or recognition of methyl-lysine residues [108,114].

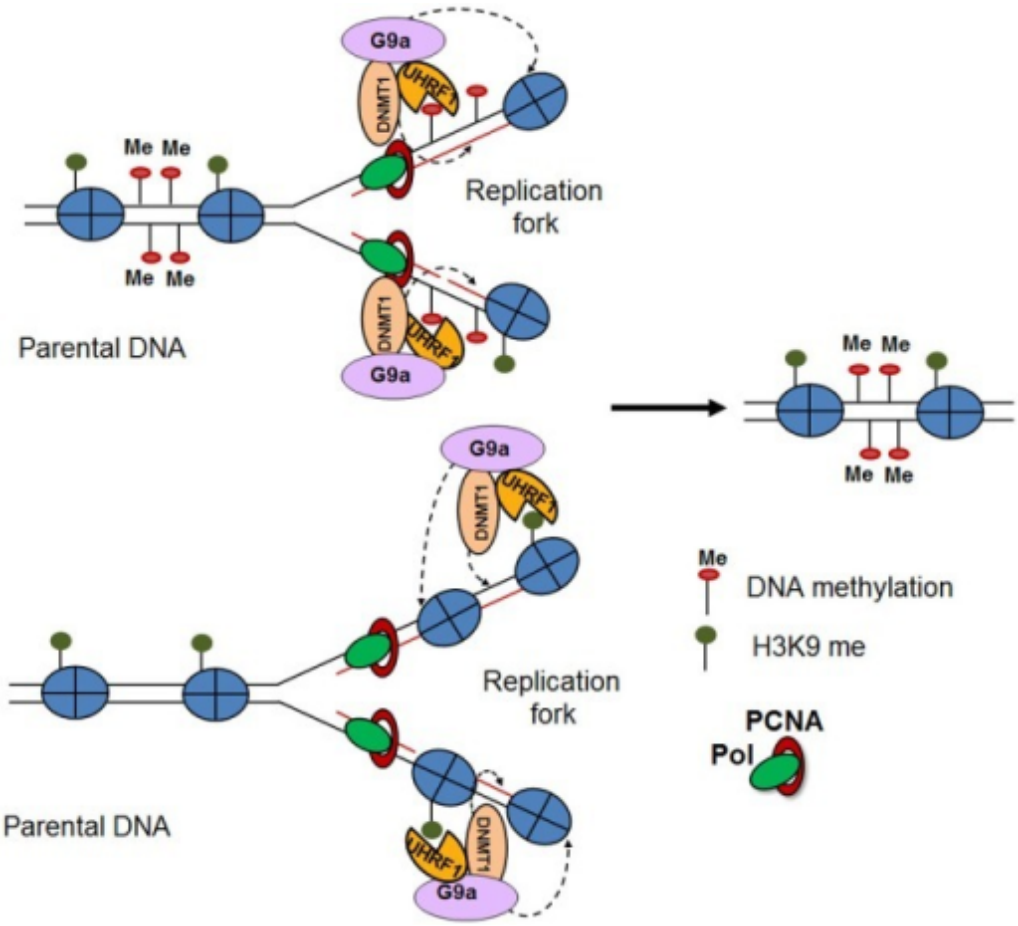

Figure 9. Coordinated regulation of DNA and H3K9 methylation. Representative figure of the functional enzymatic complex formed by G9a, DNMT1 and UHRF1 at replication fork in the chromatin (Cheedipudi *et al.*, Front. Genet., 2014).

G9a was first identified as a gene located in the Major Histocompatibility Complex (*MHC*) locus in mice and Human Leukocyte Antigen (*HLA*) locus in humans. It is made up of 28 exons that code for a 1263 amino acid protein. A splice form lacking exon 10 that codes 34 amino acids has also been identified, although its functional significance is still unknown. G9a forms a heterodimer with GLP *in vivo* and is critically required for the H3K9me2 methylation activity. However, mutational studies of active sites demonstrated that the methyltransferase activity of G9a plays a larger role in H3K9me2

methylation *in vivo* [115]. The Su(var)3-9, Enhancer-of-Zeste and Trithorax (SET) domain of G9a is able to mono- and dimethylate H3K9 but is less efficient in mediating trimethylation. Additionally, several studies have shown that G9a is also able to methylate a wide range of non-histone targets, including the tumor suppressor p53 and G9a itself [116,117]. Although the precise role of posttranslational methylation on protein function remains unclear, methylation of non-histone proteins may affect protein stability, protein-protein interactions, subcellular localization, or function. Apart from its ability to methylate substrates, G9a has also been shown to have methyltransferase-independent activities through the N-terminal domain of the G9a protein. A work from the Stallcup's group showed that G9a was a strong coactivator of nuclear hormone receptor activity by associating with transcriptional coactivators including p300 [118]. Thus, in addition to repressive functions, G9a can positively influence gene expression at selected genetic loci.

Previously, G9a has been identified to serve critical roles in various biological processes such as lymphocyte development, stem cell differentiation and tumor cell growth. The expression level of *G9a* is increased in numerous types of cancer compared with their corresponding normal tissues. The elevated expression of *G9a* in HCC was recently reported, suggesting this enzyme as a novel epigenetic target for the treatment of liver tumors [119–121]. *G9a* overexpression was correlated with increased H3K9 and DNA methylation, leading to the inhibition of important TSGs, and was associated with poor patients' prognosis [122]. Bai and colleagues recently reported that *G9a* overexpression serves as a predictor of unfavorable survival rates after liver resection in patients with HCC [120]. Although this finding indicates a relevance of G9a in HCC, its role in this disease remains to be elucidated.

The growing knowledge on the involvement of G9a in the promotion of tumorigenesis in other cancers serves as starting point to study its potential role in the liver. On one hand, G9a participates in the expression of genes associated with cellular migration and motility and, in consequence with metastatic features of cancer cells [123,124]. This role of G9a has been found in various cancers including breast, lung, endometrial and ovarian cancers [122]. Its involvement in the EMT processes has been also established. It is clear that an appropriate G9a activity is required to maintain the normal phenotype in a cell. However, it is not known how G9a is increased in tumorigenesis, and its specific functions along

the malignant transformation. Hypoxia has been reported to upregulate G9a protein levels without affecting its mRNA, resulting in a global increase of H3K9 methylation [125,126]. Its function in this context is still unclear but G9a is thought to be a modulator of hypoxia-mediated gene expression control, by either direct or indirect mechanisms. Hypoxia is considered to be an important factor in the development of aggressive phenotypes in cancer. Thereby the role of G9a in this context may be relevant to elucidate potential targets for cancer treatment. Furthermore, G9a has been very recently identified as a key enzyme in the maintenance of the serine-glycine biosynthetic pathway, an integral part of cancer metabolism [127]. Altogether these findings suggest that G9a is involved in general mechanisms of cancer development and thus its pharmacological inhibition represents a novel approach for treatment of various cancers.

Epigenetic therapeutical approaches in HCC

Many epigenetic drugs are currently being tested in clinical trials, while several of them are already used in the clinic. Treatments with DNMTs inhibitors such as 5-azacytidine and decitabine efficiently reactivate the expression of aberrantly silenced genes in variety of cancer cells, including HCC, and suppress tumor growth [90]. They have been approved by the Food and Drug Administration (FDA) for hematological diseases and are being tested in clinical trials for solid tumors [90]. Histone modifiers inhibitors have been also developed. HDAC inhibitors such as SAHA and Trichostatin A cause the induction of differentiation, growth arrest and/or apoptosis in various transformed cells, and have been tested in clinical trials demonstrating encouraging results [90,128]. Lysine methyl transferases (KTMs) inhibitors are also in early stages of clinical trials, and the relevance of these enzymes in cancer phenotype suggests great promise for this kind of inhibitors. However, current commercialized epigenetic drugs, such as the HDAC inhibitors (SAHA and Trichostatin A) and the EZH2 inhibitor 3-Deazaneplanocin A (DZNep), did not improve the response of HCC cells to Sorafenib [128]. Different epigenetic agents have been used in combination demonstrating impressive preclinical results. Evidence of a self-reinforcing interaction between DNA methylation and histone modifications in the control of gene expression has paved the way for these combinatorial epigenetic therapies. These combinations allow the use of reduced doses of the drugs while obtaining higher efficacies [90,129].

Nevertheless, there are some important aspects to keep in mind when considering an epigenetic drug for systemic treatments. The most relevant problems found in clinical trials using epigenetic inhibitors are their relatively low efficacy in solid tumors, high cytotoxicity, lack of specificity and poor tolerability in patients [90,129]. The effects of epigenetic drugs have to be considered in the cellular context. They might have different effects depending on the cells type, the molecular signature of cancer cells, the tumor microenvironment and also on the stage of the disease. The intrinsic molecular heterogeneity and the subsequent development of treatment resistance may limit the efficacy of epigenetic drugs against solid tumors. However, epigenetic therapies have the positive feature of being able to modulate the tumor microenvironment. Thus, studies of the epigenetic changes in both the tumor cells and the different cells of the tumor niche in HCC can open the window for innovative targeted epigenetic therapies.

Development of small molecule dual inhibitors of G9a and DNMT1

Based on the potential biological relevance of the epigenetic complex formed by G9a and DNMT1 in the context of tumorigenesis, new series of proprietary G9a and DNMT1 inhibitors (EPOPatent application #14-382230.2-1462) were developed in our Institute (Molecular Therapeutics Program, CIMA, Pamplona). Knowledge- and structure-based approaches guided to design and identify first-in-class dual inhibitors of epigenetic targets G9a and DNMT1 [130–132]. Based on reported structure-activity relationships (SAR) data from G9a substrate competitive inhibition [133–135] together with the available structural information, X-ray co-crystal structure for G9a-UNC0638 complex (PDB 3RJW) [136] and DNMT1-hemimethylated CpG complex (PDB 4DA4) [137] compounds were designed and synthesized to interact with the epigenetic enzymes [130,131]. The design was directed to look for ligand- receptor interaction at substrate binding sites in such way that the mechanism of action would be based on competition with the binding of the enzymes with the substrates, namely lysine 9 in histone 3 (K9H3) and CpGs in DNA (Fig. 10C). Consequently, a novel chemical series bearing key chemical functionalities that cover critical pharmacophoric features were designed [130,132].

Detailed exploration of these novel chemical series, including more than 100 compounds, showed their dual activity against G9a and DNMT1 (Fig. 10A). All this information has

been recently published [132]. More promising compounds resulting from these series were tested in different human HCC cells showing wide differences in the drug inhibiting cell growth by 50% (GI_{50}) values (Fig. 10B). However, various molecules demonstrated promising GI_{50} values in the nanomolar range. After the initial efficacy screenings, only a few compounds reached the toxicity and ADME (Absorption, Distribution, Metabolism and Excretion) studies phase. These studies pointed out to CM-272 as a lead pharmacological tool compound (detailed in San José-Eneriz *et al* [132]). The selected compound presented dual activity potent enough against both targets *in vitro*; 8 and 382 nM IC_{50} values for G9a and DNMT1 respectively. Of note, CM-272 also inhibited DNMT3A (85 nM IC_{50}), DNMT3B (1200 nM IC_{50}) and GLP (2 nM IC_{50}). However, it did not present relevant inhibitory effects against a panel of 36 proteins implicated in the regulation of epigenetic mechanisms (Table 1). These analyses demonstrated a high selectivity of CM-272 against its specific targets.

In order to evaluate CM-272 properties *in vivo*, San José-Eneriz and colleagues developed CM-272 pharmacokinetic (PK) studies. It was observed that intravenous administration of CM-272 at 2.5 mg/Kg reached a sustained plasmatic concentration, below the toxic level defined in THLE-2 cell line (1.78 μM GI_{50}). Moreover, the potential toxicity of CM-272 in mice was evaluated. No weight loss, other physical indicators of sickness, or major changes in hematological parameters were found. Materials and methods developed for these experimental procedures are detailed in San José-Eneriz *et al* [132]. Overall, these results demonstrated that CM-272 might be a safe molecule for administration in mice. Furthermore, San José-Eneriz and colleagues demonstrated that CM-272 presents a potent *in vivo* activity against hematological malignances and claimed that CM-272 represent a novel approach for targeting cancer safely and efficiently, paving the way for treating a broad series of human tumors with poor prognosis including HCC.

A

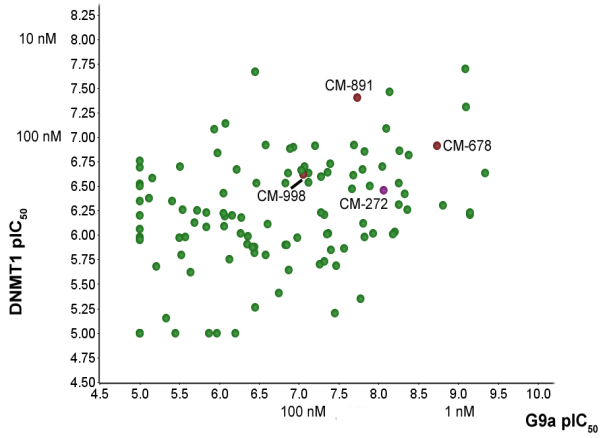

B

Dual DNMT1 and G9a inhibitors

Compound	HepG2 (GI_{50})	Hep3B (GI_{50})	PLC (GI_{50})
272	302.5	450.4	437.3
579	540.2	948	874.3
631	2697	2469	3163
660	2177	N/A	2104
678	423	305	255
679	2253	1701	991
697	761.5	497.8	744.9
891	75.8	319.0	110
905	2242	2217	2140
906	2056	2244	2234
952	2090	1154	1470
953	N/A	N/A	N/A
958	N/A	N/A	N/A
962	655.9	614.2	837.1
974	N/A	1080	N/A
975	623.5	497.7	675.1
981	587.0	505.1	584.9
986	161.9	356.5	160.3
987	9400	2200	972.1
997	N/A	N/A	N/A
998	257.9	155.3	852.5
999	N/A	N/A	N/A
1002	488.5	597.7	321.8

C

DNMT1 binding CM-272

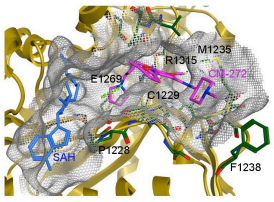

G9a binding CM-272

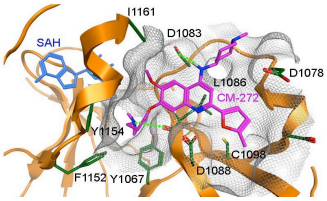

Figure 10. Development of small molecule dual inhibitors of G9a and DNMT1. A) pIC_{50} values against G9a and DNMT1 of a wide panel of small molecule dual inhibitors. **B)** GI_{50} values of several dual inhibitors of G9a and DNMT1 tested in HepG2, Hep3B and PLC/PRF5 cells. **C)** CM-272 chemical structure and representative picture of its binding sites to G9a and DNMT1. (San José-Eneriz *et al.*, Nat. Comm., 2017)

Table 1. Percentage of inhibition of CM-272 at 10 μM against a panel of 36 epigenetic targets.

Target	% of inhibition by CM-272	Family
EZH1	6	HMT
EZH2	1	HMT
MLL-WARD	4	HMT
PRMT1	73	HMT
PRMT3	7	HMT
PRMT4	5	HMT
PRMT5	6	HMT
PRMT6	82	HMT
PRMT8	11	HMT
SET7-9	3	HMT
SETD2	8	HMT
SUV39H1	1	HMT
SUV39H2	4	BRD
ATAD2A	0	BRD
ATAD2B	0	BRD
BAZ2B	0	BRD
BRD1	0	BRD
BRD2(BD1+BD2)	0	BRD
BRD4(BD1+BD2)	56	BRD
BRDT(BD1)	8	BRD
CREBBP	5	BRD
TAF1	0	BRD
TRIM24	0	BRD
JMJD1A	8	HDMT
JMJD2A	1	HDMT
JMJD2B	2	HDMT
JMJD2C	12	HDMT
JMJD2D	5	HDMT
JMJD2E	1	HDMT
JMJD3	9	HDMT
Jarid1A	2	HDMT
Jarid1B	5	HDMT
Jarid1C	1	HDMT
LSD1	0	HDMT
HDAC1	0	HDAC
HDAC6	0	HDAC

HMT: Histone Methyltransferase; BRD: Bromodomains; HDMT: Histone Demethylase; HDAC: Histone Deacetylase. (adapted from San José-Eneriz *et al*., Nat. Comm., 2017)

Hypothesis and Objectives

Liver cancer is a deadly disease that usually develops on a background of chronic inflammation in which the interaction of transformed cells with a fibrous stroma is a strong determinant in cancer progression. HCC is highly resistant to conventional chemotherapeutics, and molecules targeting growth factor signaling pathways have shown suboptimal clinical efficacies. Therefore, it is necessary to characterize new targets and develop novel therapeutic strategies for HCC. The stromal compartment actively contributes to tumorigenesis, while the tumor itself influences the stroma to create a favorable background for its own growth. In order to achieve an adequate therapeutic response, it may be necessary to hit not only the tumoral cell, but also its microenvironment. From recent literature it appears that dysregulation of epigenetic mechanisms, such as DNA and histone methylation, might be playing a crucial role in hepatocarcinogenesis. The deposition of methyl marks of histones and DNA are very dynamic enzymatic processes amenable to pharmacological intervention and, thus, constitute attractive therapeutic targets. Although these epigenetic events are carried out by different enzymes they engage in a close biological crosstalk, cooperatively modulating gene expression through a system which could be defined as a "double lock". One example of this coordinated activity is the epigenetic complex previously described that includes the DNA methyltrasferase 1, the histone methyltransferase G9a and the molecular adaptor UHRF1.

Our hypothesis is that the epigenetic complex formed by G9a, DNMT1 and UHRF1 is playing a relevant role in hepatocarcinogenesis and CLD progression, and thus directly targeting the epigenetic activity of these enzymes would be a novel and effective therapeutical approach to quell this disease.

Our proposal has two general objectives:

1. Analyze the expression and pathological significance of *DNMT1*, *G9a* and *UHRF1* in HCC patients, study their coordinated activity and evaluate their biological functions in hepatocarcinogenesis.

2. Study the possible beneficial effects of simultaneously inhibition of DNMTs and G9a against HCC and evaluate the effectivity of the novel and proprietary small molecule dual inhibitor (CM-272) as potential therapeutical approach for HCC.

Materials and Methods

Human liver samples

1. For bioinformatic studies

Bioinformatic studies were performed with data bases from sequenced human samples kindly ceded by Prof. Jessica Zucman-Rossi, University Paris Descartes-HEGP, France. A cohort of 268 liver tumor samples (T), 154 peritumoral liver samples (NT) and 5 samples of normal liver tissues were collected from patients surgically treated in Bordeaux and Créteil hospitals in France. The study was approved by institutional review board committees (CCPRB Paris Saint-Louis, 1997, 2004, and 2010, #01-037; Bordeaux #2010-A00498-31). Written informed consent was obtained in accordance with French legislation. These patients and samples have been described previously [138,139] and are summarized in Table 2.

Table 2. Clinical, histological and molecular data of HCC patients.

HCC (n=268)			
Variable		**n. of cases**	**%**
Gender (n=268)	F	47	17.54%
	M	221	82.46%
Age (n=268)	median (min-max)	65 (18-90)	
Etiology (n=268)	AL	65	24.25%
	AL HBV	7	2.61%
	AL HBV HCV	2	0.75%
	AL HBV METAB	1	0.37%
	AL HCV	17	6.34%
	AL HM	4	1.49%
	AL METAB	19	7.09%
	HBV	40	14.93%
	HBV HCV	5	1.87%
	HCV	32	11.94%
	HCV METAB	2	0.75%
	HM	17	6.34%
	HM METAB	2	0.75%
	METAB	20	7.46%
	OTHER	1	0.37%

Table 2. Clinical, histological and molecular data of HCC patients. (*Continuation*)

	W/O Etiology	34	12.69%
Edmonson grade (n=265)	I	8	3.02%
	II	114	43.02%
	III	117	44.15%
	IV	26	9.81%
Macroscopic vascular invasion (n=267)	no	229	85.7%
	yes	38	14.2%
TNM (n=235)	T1	82	36.1%
	T2	98	41.7%
	T3	55	23.4%
AFP recod (n=252)	<=20	139	55.1%
	>20	113	44.8%
G1G6 (n=268)	G1	16	5.97%
	G2	23	8.58%
	G3	47	17.54%
	G4	87	32.46%
	G5	56	20.90%
	G6	39	14.55%
Differentiation WHO (n=267)	Good	69	25.84%
	Medium	156	58.43%
	Weak	42	15.73%
5 gene score (n=257)	P1	142	55.25%
	P2	115	44.75%
TERT (n=252)	M	160	63.49%
	NM	92	36.51%
CTNNB1 (n=258)	M	106	41.09%
	NM	152	58.91%

2. For western blot and DNA methylation studies

Healthy liver tissues from patients were obtained and ceded by Dr. Bioulac-Sage and Dr. Balabaud from the French National Cancer Biobank at the Hospital de Bordeaux (France). Samples were collected under informed consent by the patient, and anonymized for their use, from patients with digestive tumors or submitted to percutaneous biopsies of healthy or with minimal changes. All the samples were frozen immediately after

obtaining them in liquid nitrogen for further processing. We have used them for protein and DNA extraction and were included in western blots and DNA methylation studies as healthy controls.

Cell lines and human hepatic stellate cells (hHSCs) culture

The origin and culture of the 32 HCC cell lines used in this study has been previously described in Rebouissou and colleagues [140]. The panel of 32 cell lines is summarized in Table 3. All the cells were adapted and grown in Dulbecco's modified Eagle's medium (DMEM) except JHH5 and JHH6 that were grown in William's E medium. Culture media were supplemented with 10% Fetal Bovine Serum (FBS) and 100 U/mL penicillin/streptomycin.

Table 3. Human liver cancer cell lines.

Cell line ID	Tumor type	Supplier
Hep3B	Hepatocellular carcinoma	American Type Culture Collection
Huh7	Hepatocellular carcinoma	American Type Culture Collection
HLE	Hepatocellular carcinoma	Health Science Research Resources Bank
HLF	Hepatocellular carcinoma	Health Science Research Resources Bank
SNU182	Hepatocellular carcinoma	American Type Culture Collection
SNU387	Hepatocellular carcinoma	American Type Culture Collection
SNU398	Hepatocellular carcinoma	American Type Culture Collection
SNU423	Hepatocellular carcinoma	American Type Culture Collection
SNU449	Hepatocellular carcinoma	American Type Culture Collection
SNU475	Hepatocellular carcinoma	American Type Culture Collection
PLC/PRF/5	Hepatocellular carcinoma	American Type Culture Collection
Mahlavu	Hepatocellular carcinoma	American Type Culture Collection
Li7	Hepatocellular carcinoma	RIKEN BioResource Center
Huh1	Hepatocellular carcinoma	Japanese Collection of Research Bioresources Cell Bank
JHH1	Hepatocellular carcinoma	Japanese Collection of Research Bioresources Cell Bank

(Rebouissou *et al.*, Clin. Cancer. Res., 2017)

Table 3. Human liver cancer cell lines. (*Continuation*)

JHH2	Hepatocellular carcinoma	Japanese Collection of Research Bioresources Cell Bank
JHH4	Hepatocellular carcinoma	Japanese Collection of Research Bioresources Cell Bank
JHH5	Hepatocellular carcinoma	Japanese Collection of Research Bioresources Cell Bank
JHH6	Hepatocellular carcinoma	Japanese Collection of Research Bioresources Cell Bank
JHH7	Hepatocellular carcinoma	Japanese Collection of Research Bioresources Cell Bank
SNU354	Hepatocellular carcinoma	Korean Cell Lines Bank
SNU368	Hepatocellular carcinoma	Korean Cell Lines Bank
SNU739	Hepatocellular carcinoma	Korean Cell Lines Bank
SNU761	Hepatocellular carcinoma	Korean Cell Lines Bank
SNU878	Hepatocellular carcinoma	Korean Cell Lines Bank
SNU886	Hepatocellular carcinoma	Korean Cell Lines Bank
MHCC97H	Hepatocellular carcinoma	Woodland Pharmaceuticals
BEL7402	Hepatocellular carcinoma	Woodland Pharmaceuticals
B1	Hepatocellular carcinoma	A gift from Bettina Grasl-Kraupp (Austria)
HCC-1.2	Hepatocellular carcinoma	A gift from Bettina Grasl-Kraupp (Austria)
HepG2	Hepatoblastoma	American Type Culture Collection (ATCC)
Huh6	Hepatoblastoma	RIKEN BioResource Center

(Rebouissou *et al.*, Clin. Cancer. Res., 2017)

The human HSC cell line LX2 (Millipore-Merck, Darmstadt, Germany), was cultured in DMEM supplemented with 2% FBS and 100 U/mL penicillin/streptomycin. Primary hHSCs were obtained and ceded by Dr. Krista Rombouts from UCL Institute for Liver & Digestive Health, United Kingdom. They were isolated from resected liver wedges obtained from patients undergoing surgery at the Royal Free Hospital (London, United Kingdom) after giving informed consent (#EC01.14-RF). Isolation and purity of hHSCs were as published [141]. The obtained hHSCs were cultured in Iscove's Modified DMEM (IMDM), supplemented with 20% performance FBS, 2 mM Glutamine, 1X nonessential amino acids, 1.0 mM sodium pyruvate, 1X antibiotic-antimycotic (all from Life

Technologies, Paisley, UK). Experiments were performed on hHSCs from at least three independent cell preparations, used between passages 3-8.

All cells were maintained at 37ºC in a humified incubator (95% wet) in 21% O_2 and 5% CO_2. For hypoxic culture conditions cells were incubated under 1% O_2, 5% CO_2 and 94% N2 atmosphere in the H35 Hypoxystation incubator (Don Whitley Scientific Ltd., Shipley, United Kingdom).

Analysis of gene expression

1. **Human tissue**

Human tissue RNA was extracted as described [138]. Quantitative Real-Time PCR (qRT-PCR) was performed using Fluidigm 96.96 Dynamic Arrays and specific TaqMan pre-designed assays for *G9A* (Hs00198710_m1), *DNMT1* (Hs02558036_s1), *UHRF1* (Hs00273589_m1), *FBP1* (Hs00166829_m1) and *ABCB1* (Hs00184491_m1). Gene expression was normalized with the RNA ribosomal *18S* (Hs03928990_g1), and the level of expression of T and NT samples was compared with the mean level of gene expression in normal liver tissues, being expressed as an n-fold ratio. The relative amount of RNA was calculated with the -ΔΔCT method:

$$2^{\Delta CT}=2^{(\text{CT reference gene- CT measured gene})}$$

2. **Cultured Cells**

Total RNA from cells was isolated and DNase treated by LEV Simply RNA Cells and Tissue kit using Maxwell^{R} 16 machine (Promega, Madison, WI), following manufacturer's instructions. Concentration and amount of RNA was evaluated through absorbance lecture at 260 and 280 nm in NanoDrop ND-1000 spectrophotometer (Thermo Scientific). For retro-transcription PCR samples were exposed for 1 min at 90ºC for denaturalization followed by 1 h at 37ºC using a mix containing: 50 mM Tris-HCl pH 8.3, 75 mM KCl and 3 mM $MgCl_2$, 10 ng/μL of random primers, 0.5 mM of each

deoxyribonucleic triphosphate (dNTP), 5 mM of dithiothreitol (DTT), 1.2 U/μL RNase inhibitors (RNase out) and 6 U/μL of M-MLV inverse transcriptase enzyme. All reagents from Invitrogen, less dNTPs from Roche Diagnostics (Mannheim, Germany). Resulting complementary DNA (cDNA) was used to measure differences among genic expression levels. Reactions were performed by quantitative real-time PCR (qRT-PCR) in CFX-96 Real-Time System thermocycler using iQ SYBR Green Supermix reagent (BioRad) following manufacturer's instructions. Sequences of primers used can be found in Table 4, and reaction conditions were the following:

Initial denaturalization		95ºC, 3 min
X45	Denaturalization	95ºC, 30 sec
	Hybridizing	60ºC, 15 sec
	Extension	72ºC, 25 sec
Lecture		80ºC, 10 sec

Relative quantification of mRNA was calculated with the -ΔΔCT method using the reference gene of constitutive expression *H3F3A*.

Table 4. qRT-PCR primer sequences.

Gene	Sequence	
aSMA	Fw	5′-CCAGGGCTGTTTTCCCATCC-3′
	Rev	5′-GTCATTTTCTCCCGGTTGGCC-3′
ALDOA	Fw	5′-AGTCCATTGGCACCGAGAAC-3′
	Rev	5′-AACATTGGCATTTTCCATGA-3′
BAMBI	Fw	5′-CTCCAGCTACATCTTCATCTGG-3′
	Rev	5′-CTGCTACCATCATGCTGATACC-3′
CDH1	Fw	5′-CTGGTTCAGATCAAATCCAAC-3′
	Rev	5′-GAGGTTCCTGGAAGAGC-3′
COLIA1	Fw	5′-GGCTCCTGCTCCTCTTAGCGG-3′
	Rev	5′-CGGGACAGCACTCGCCCTCGG-3′
CYP7A1	Fw	5′-TTGCTACTTCTGCGAAGGCA-3′
	Rev	5′-TCCGTGAGGGAATTCAAGGC-3′
DNMT1	Fw	5′-GAGGCCCGAAGAAAAAGAAC-3′
	Rev	5′-TGAAGCAGGTCAGTTTGTGC-3′

Table 4. qRT-PCR primer sequences. (*Continuation*)

EPHA2	Fw	5′-GCTTCTACCTGGCCTTCCA-3′
	Rev	5′-GGCTCTCAGATGCCTCAAAC-3′
FBP1	Fw	5′-ACATCGATTGCCTTGTGTCC-3′
	Rev	5′-CATGAAGCAGTTGACCCCAC-3′
G9a	Fw	5′-GCAGCACTGCACGTGTGTGGA-3′
	Rev	5′-ACATCAGCCTCAGCATCAGA-3′
GJC3	Fw	5′-CTTCCAGGTCATCTTGGTGG-3′
	Rev	5′-AACCGCTGACTCCAAACATG-3′
GLUT1	Fw	5′-CCTTTGAGATGCTGATCCTG-3′
	Rev	5′-TCTTGGCCCGGTTCTCCTCG-3′
GNMT	Fw	5′-AAGAGGGCTTCAGTGTGACG-3′
	Rev	5′-AGGCTTGAAGTCGCCCAGGA-3′
H3F3A	Fw	5′-AAAGCCGCTCGCAAGAGTGCG-3′
	Rev	5′-ACTTGCCTCCTGCAAAGCAC-3′
HEPACAM	Fw	5′-GACAAGCCAGTGACCGTGG-3′
	Rev	5′-CTCCAGCACAGTGGTTGAAG-3′
HK2	Fw	5′-TTGACCAGTATCTCTACCACATGCG-3′
	Rev	5′-CAATGTGGTCAAACAGCTGGG-3′
KLF5	Fw	5′-AGCTCAGAGCCTGGAAGTC-3′
	Rev	5′-CCTCAGGTGAGCTTTTAAATGAGA-3′
LDHA	Fw	5′-GTTGGTGCTGTTGGCATGGC-3′
	Rev	5′-GTGATAATGACCAGCTTGGAG-3′
LOX	Fw	5′-CCCCAAAGAGTGAAAAACCA-3′
	Rev	5′-CCAGGACTCAATCCCTGTGT-3′
LRAT	Fw	5′-CAGAAGGTGGTCTCCAACAA-3′
	Rev	5′-CCAAGACTGCTGAAGCAAGA-3′
MAT1A	Fw	5′-TCTTCATGTTCACATCGGAG-3′
	Rev	5′-TGCACTCCTCTGTCTCGTCG-3′
PGK1	Fw	5′-GTTCCTATGAAGAACAACCAG-3′
	Rev	5′-CATCTTTTCCCTTCCCTTCTTCC-3′
PINX1	Fw	5′-GAGAAGATGGGGTGGTCTAAAG-3′
	Rev	5′-CGGTTTTTGGAGATTTTGGA-3′
PKM2	Fw	5′-AGAAACAGCCAAAGGGGACT-3′
	Rev	5′-CTGCCAGACTTGGTGAGGACG-3′
PPARγ	Fw	5′-GCTGTTATGGGTGAAACTCTG-3′
	Rev	5′-GAATAATAAGGTGGAGATGCAGG-3′
RASSF1A	Fw	5′-AAGTTCACCTGCCACTACCG-3′
	Rev	5′-CTGGAGGGCACAGAGACAG-3′

Table 4. qRT-PCR primer sequences. (*Continuation*)

SKIL	Fw	5′-GGAGAAAAGAGACTCTGTTTGCC-3′
	Rev	5′-CCACTTCAAAGGCACTGCC-3′
TAGLN	Fw	5′-GACCAAGAATGATGGGCACTA-3′
	Rev	5′-ATGACATGCTTTCCCTCCTG-3′
TGFβ1	Fw	5′-TGGTGGAAACCCACAACGAA-3′
	Rev	5′-GGCCATGAGAAGCAGGAAAG-3′
TJP3	Fw	5′-GTGGGCAGTTCCTGGTGAAC-3′
	Rev	5′-CCACGATCCTCCATGCTCTG-3′
UHRF1	Fw	5′-CAAGAAGAAGGCGAAGATGG-3′
	Rev	5′-AAAAATTCCCATGGTCCACA-3′
VEGF	Fw	5′-CTGCTGTCTTGGGTGCATTGG-3′
	Rev	5′-CACCGCCTCGGCTTGTCACA-3′

Western blot

Cells and tissues were lysed in RIPA buffer (150 mM NaCl, 50 mM Tris pH 7.5, 01% Sodium Dodecyl Sulfate (SDS), 1% Triton X-100, 0.5% sodium deoxycolate) containing phosphatases inhibitors (1 mM sodium orthovanadate, 10 mM sodium fluoride and 100 mM β-glycerophosphate from Sigma) and proteases inhibitor cocktail (1X Complete from Roche). Lysate samples were sonicated in ice and centrifuged at 13000 rpm during 45 min at 4ºC. Supernatants were collected and protein quantification was performed by Bicinchoninic Acid (BCA) assay (Pierce Technologies, Rockford, IL) according to manufacturer's specifications and using standard curve of Bovine Serum Albumin (BSA). Protein lysates were prepared to electrophoresis by mixing 5-30 μg of protein with 1X loading buffer (50 mM Tris pH 6.8, 100 mM β-mercaptoethanol, 2% SDS, 10% glycerol, 0.01% bromophenol blue) and incubating 5 min at 95ºC for denaturalization.

Electrophoresis was performed using polyacrylamide gels (stacking of 6% and resolving of 8-15% of acrylamide depending on the protein weigh of study) under denaturalizing conditions (SDS-PAGE) and running buffer (25 mM Tris, 192 mM glycine, 0.1% SDS) from Sigma (10X stock). Electrophoresis was carried out at constant voltage (120 V). Resolved proteins were then transferred to nitrocellulose membrane of 0.2 or 0.45 μm

(Hybond-C Extra from Amersham Biosciences, Buckinghamshire, United Kingdom) under transference buffer (25 mM Tris, 192 mM glycine and 20% methanol) at 120 V during 45 min-1 h at 4ºC. After transference, Ponceau S solution (Sigma) staining was performed to demonstrate equal loading of proteins. Then, membrane was washed in tap water and blocked by 5% of skimmed milk or 5% BSA on T-TBS (25 mM Tris pH 7.5, 200 mM NaCl (TBS), 0.1% Tween) during 1 h at room temperature, and incubated overnight at 4ºC with corresponding primary antibody (at manufacture instruction's concentrations). Antibodies used are listed in Table 5.

Table 5. Antibodies.

Antibodies	**Reference & Supplier**
Primary antibodies	
anti-5meC	BI-MECY-1000, Eurogentec, Liege, Belgium
anti-alpha-Smooth Muscle Actin	A2547, Sigma Aldrich, St. Louis, MO
anti-alpha-Tubulin	2144S, Cell Signalling Technology, Leiden, The Netherlands
anti-CD31	77699S, Cell Signalling
anti-DNMT1	5032S, Cell Signalling Technology, Leiden, The Netherlands
anti-FBP1	HPA005857, Sigma Aldrich, St. Louis, MO
anti-G9a	3306S, Cell Signalling Technology, Leiden, The Netherlands
anti-GNMT	provided by Dr M. Martinez-Chantar, CIC-BioGune, Bilbao, Spain
anti-H3K4me3	ab8580, Abcam, Cambridge, UK
anti-H3K9me2	ab1220, Abcam, Cambridge, UK
anti-H3K27me3	ab6002, Abcam, Cambridge, UK
anti-HIF1-alpha	NB100-105, Novus Biologicals, Littleton, USA
anti-HK2	sc28889, Santa Cruz Biotechnology, Santa Cruz, CA
anti-normal rabbit IgG	2729S, Cell Signalling Technology, Leiden, The Netherlands
anti-phospho-SMAD3 (Ser423/425)	9520S, Cell Signalling Technology, Leiden, The Netherlands
anti-total H3	07-690, Millipore-Merck, Darmstadt, Germany
anti- total SMAD3	9513S, Cell Signalling Technology, Leiden, The Netherlands
anti-UHRF1	ab57083, Abcam, Cambridge, UK
Secondary antibodies	
anti-rabbit IgG HRP-linked antibody	7074S, Cell Signalling Technology, Leiden, The Netherlands
Goat anti-mouse IgG:HRPO	M15345, Transduction Laboratories, USA

After incubation, membranes were washed three times with T-TBS during 5 min at room temperature and incubated with the corresponding secondary antibody (1:5000 dilution) in T-TBS for 1 h at room temperature. Finally, two washes with T-TBS followed by two washes with TBS of 5 min each were performed at room temperature. Western Lightning-Enhanced Chemiluminescence (ECL) from Perkin Elmer Inc. (Waltham, MA, EEUU) was used for chemiluminescence illuminating of membranes following manufacturer's instructions and using Amersham Hyperfilm ECL films (Amersham Biosciences).

Small interfering RNAs (siRNAs)

Human *G9a* and *DNMT1*-specific siRNAs and control siRNA (siCtrl) used in this project were from Santa Cruz Biotechnology (Santa Cruz, CA). For experiments, 150000-200000 cells where seeded in each well of 6 multi-well plates with complete DMEM medium. After overnight incubation, cells were washed with phosphate-buffered saline (PBS) and transfections were performed with 75 nM of each siRNA using 3 μL/well of Lipofectamine RNAiMAX (Invitrogen, Grand Island, NY) transfection reagent in Opti-MEM Reduced Serum Medium from Gibco (Thermo Fisher Scientific) without antibiotics. In those cases where combined siRNAs transfections were performed, each specific siRNA was used at 32.5 nM. After 4-6 h of transfection, medium was refresh with complete DMEM medium. Cells were harvested 48 or 72 h after transfection. Silencing was confirmed by qPCR and western blot.

Plasmid transfections

Expression vectors were produced by transforming competent *E.coli* bacteria grown in lysogeny broth (LB) (Sigma) under sterile conditions at 37ºC in agitation overnight. Plasmids were purified by Endofree Plasmid Maxi Kit from Quiagen (Hilden, Germany) following manufacturer's instructions. Concentration was measured in NanoDrop ND-1000 Spectrophotometer de Thermo Fisher Scientific (Wilmington, DE, EEUU). For overexpression experiments 150000-200000 cells where seeded in each well of 6 multi-well plates with complete medium. After overnight incubation, cells were washed with PBS and transfections were performed with 1.8 μg of pEGFP-G9a (Cat. Nos 33025,

Addgene, Cambridge, MA) or empty vector, pEGFP-Ctrl (Cat. Nos 86775, Addgene, Cambridge, MA), using 3 μl/well of Lipofectamine 2000 (Invitrogen, Carlsbad, CA) transfection reagent in Opti-MEM Reduced Serum Medium from Gibco (Thermo Fisher Scientific) without antibiotics. In each set of experiments, equal amounts of plasmid were used by adding the empty vector pEGFR-Ctrl. After 6 h of transfection, medium was refresh with complete DMEM medium. Cells were harvested 48 h after transfection. Gene expression was confirmed by western blot.

In vitro treatments

Cells were treated with CM-272 diluted in dimethyl sulfoxide (DMSO) (Sigma). The concentration of CM-272 used is indicated in each experiment. In all cases, control cells were treated by vehicle (DMSO) at the highest concentration used in each experiment. For recombinant human-TGFβ1 (240-B-002, R&D Systems) treatments in hHSC incubation in serum free medium for 24 h before each experimental treatment was performed to avoid interference with growth factors and amino acids enriched in FBS. On the other hand, treatments of LX2 cells were performed in presence of 2% FBS supplemented medium. Concentration of recombinant human-TGFβ1 was stipulated at 5 ng/mL. TGFβ1 vehicle (4 mM HCl, 1 mg/mL BSA) was added to control cells. Duration of treatments are indicated in each experiment.

Cell proliferation assay

Cell proliferation assays were performed in different experiments over cells transfected with siRNA (siG9a and siDNMT1) or pEGFP-G9a plasmid transfections and cells treated with CM-272, Decitabine (5-aza-2'-deoxycytidine) (Sigma, St. Louis, MO) or BIX-01294 (Sigma, St. Louis, MO). Cells were seeded at a density of 2000–3000 cells/well (depending on cell line) in 96-well plates (triplicates). After overnight incubation, cells were transfected or treated for 48-72 h with corresponding controls (siCtrl, pEGFP-Ctrl or 0.1% DMSO vehicle) in complete medium (100 μL/well). Experiments were repeated three times for each assay and cell line and treatment conditions were performed by

triplicates. In all cases, only 60 inner wells were used to avoid any border effects. Cell viability was measured using the Cell Titer 96 Aqueous One Solution Cell Proliferation Assay (Promega, Madison, WI, USA) adding 30 μL/well of reagent over 100 μL/well of medium. Then, plates were incubated during 3 h at 37ºC protected from light and absorbance was measured at 490 nM in 96-well plate reader spectrophotometer. This is a colorimetric method for determining the number of viable cells in proliferation. The background absorbance was obtained from wells containing only cell culture medium and solution reagent. First, the average of the absorbance from the control wells was subtracted from all other absorbance values. Data were then calculated as the percentage of total absorbance of treated cells/absorbance of non-treated cells. For CM-272 treatments assays, the GI_{50} value, relative to the untreated control, was calculated using non-linear regression plots with GraphPad-Prism-v5 software.

Combination assay

For the calculation of combination index (CI) values, growth inhibition was determined at different concentrations of the G9a inhibitor (BIX-01294) (Sigma, St. Louis, MO, USA) (1.25, 2.5, 5 and 10 μM) in combination with different concentrations of the DNMTs inhibitor Decitabine (5-aza-2'-deoxycytidine) (Sigma, St. Louis, MO, USA) (2.5, 5, 10 and 20 μM). Briefly, 2000 cells were cultured in a 96-well plate in triplicates. After overnight incubation, the different concentrations of compounds were added in a final volume of 100 μL/well. After 48 h of treatments, viability was measured using the Cell Titer 96 Aqueous One Solution Cell Proliferation Assay (as described in previous section). Resulting data were analyzed according to the method described by Chou [142], using the Calcusyn software (Biosoft, Cambridge, UK). The CI determined whether the effects of drug combinations were additive (CI=1) or synergistic (CI<1).

Evaluation of CM-272 as MDR1 substrate

To evaluate the Multidrug Resistance 1 (MDR1) transporter mediated cellular efflux of CM-272 studies were performed by WuXi AppTec company (http://www.wuxi.com/). Briefly, test and reference compounds were diluted with transport buffer (HBSS with 10

mM Hepes, with and without Elacridar, GF-120918, pH 7.4) from stock solutions to a concentration of 2 μM (10 μM for digoxin) (DMSO<1%) and applied to the apical or basolateral side of the cell monolayer. Wild type MDCK II cells, and MDCK II cells overexpressing MDR1 (MDR1-MDCK II) obtained from Dr. Piet Borst (Netherlands Cancer Institute, Amsterdam, The Netherlands) were used. Permeation of the compounds from A to B direction or B to A direction was determined in duplicate with/without MDR1 inhibitor (Elacridar, 10 μM) over 150 min incubation at 37ºC and 5% CO_2 with relative humidity of 95%. Test and reference compounds were quantified by LC-MS/MS analysis (Waters Aquity UPLC, API4000) based on the peak area ratio of analyte/internal standard (Tolbutamidine). Results were interpreted according to the FDA guideline 2012 (Guidance for Industry Drug Interaction Studies-Study Design, Data Analysis, Implications for Dosing, and Labeling Recommendations; https://www.fda.gov/downloads/drugs/guidances/ucm292362.pdf). Lucifer yellow rejection assay were applied to determine the cell monolayer integrity.

Colony formation assay

Colony formation assays were performed with HepG2 and PLC/PRF5 cells. 5000 cells were seeded in complete medium in six-well plates and treatments were added next day. Media was changed every two days and cultures maintained until differences between treatment conditions were noticeable (2-3 weeks). Plates were washed with PBS, fixed with 4% formaldehyde (Sigma-Aldrich, Saint Louis, MO, USA) in PBS for 10 min and stained with crystal violet. Representative pictures were taken. At least two biological replicates with three technical replicates each were performed.

ELISA Apoptosis

Apoptosis assay was performed by Cell Death Detection ELISA^{PLUS} tool (11-920-685-001, Roche) following manufacturer's instructions.

Cell cycle

For cell cycle analysis, 200000 cells/well were cultured in 6-well plates. After overnight incubation treatments by CM-272 were performed at 400 nM or 800 nM for 48 h. After treatments, cells were harvested and aliquoted in 1 million cells/tube, washed twice with 2.5 M ethylenediaminetetraacetic acid (EDTA)-PBS and resuspended in 200 µL of 2.5 M EDTA-PBS. Subsequently, cells were fixed by adding 1.8 mL of 70% ethanol drop by drop while vortex. Fixed cells were stored at 4ºC overnight. Prior to cell cycle assay, fixed cells were centrifuged (1200 rpm/ 5 min) and washed twice in 2.5 M EDTA-PBS. Pellet was resuspended in 250 µL of 2.5 M EDTA-PBS and 5 µL of Rnase A (Ribonuclease A Type III-A from bovine pancreas, Sigma) at 10 mg/mL was added. After 1 h of incubation at 37 ºC, 10 µL of propidium iodide at 1 mg/mL (Sigma) was added and incubated 10 min in dark. A final wash with 2.5 M EDTA-PBS was performed to eliminate excess of propidium iodide. Resuspended stained cells were analyzed using a BD FACSCalibur flow cytometer (Becton Dickinson, San Jose, CA, USA).

Measurement of glucose uptake and lactate production in cultured cells

HCC cells were seeded and treated the day after (by corresponding treatments) during 48 h. Prior to assay, cells were incubated for 90 min in regular media without glucose. The medium was then replaced with media containing 1 µCi/mL [14C]-2-deoxyglucose (Perkin Elmer, Waltham, MA, USA). After 15 min, cells were quenched and washed in ice-cold PBS and lysed in 1 M NaOH and Triton-X100. 80% of each lysate was subjected to liquid scintillation counting using a Beckman Coulter (Brea, CA, USA) LS6500 scintillation counter. Protein content in the remaining lysate was quantified with the dye-binding assay of Bradford (Bio-Rad, Hercules, CA, USA) following manufacturer's instructions. Uptake was normalized for protein content.

Lactate production was measured on cell's conditioned media with the Lactate Colorimetric Assay Kit from Biovision (Milpitas, CA, USA) according to manufacturer's instructions. The resulting lactate quantification was normalized for protein content.

Microarray hybridization and gene expression analysis

RNA was extracted using the automated Maxwell system from Promega (Madison, WI, USA). Before cDNA synthesis, RNA integrity from each sample was confirmed on Agilent RNA Nano LabChips (Agilent Technologies, Santa Clara, CA, USA). The sense cDNA was prepared from 200 ng of total RNA and then fragmented and biotinylated using Affymetrix GeneChip® WT PLUS Reagent Kit. Labeled sense cDNA was hybridized to the Affymetrix Human Gene 2.0 ST microarray according to the manufacturer protocols and using GeneChip® Hybridization, Wash and Stain Kit. Genechips were scanned with the Affymetrix GeneChip® Scanner 3000. Both background correction and normalization were done using RMA (Robust Multichip Average) algorithm [143]. After quality assessment, a filtering process was performed to eliminate low expression probe sets. Applying the criterion of an expression value greater than 16 in 2 samples for each experimental condition (control and CM-272 treatment), 26432 probe sets for experiments performed in HepG2 cells and 29762 probe sets for those performed in LX2 cells were selected for statistical analysis. R and Bioconductor [144] were used for preprocessing and statistical analysis. LIMMA (Linear Models for Microarray Data) was used to find out the probe sets that showed significant differential expression between experimental conditions [145]. Genes were selected as significant using a criterion of P-value<0.01, |logFC|>0.56.

Functional enrichment analysis of Gene Ontology (GO) categories (*Gene Ontology Consortium 2013 Nucleic Acids Research*) was carried out using standard hypergeometric test and the gene list ranked by logFC was also analyzed with Gene Set Enrichment Analysis (GSEA) (*Subramanian 2005 Proceedings of the National Academy of Sciences*). Microarray data can be downloaded from Gene Expression Omnibus (GEO) public functional genomics data repository under the accession number GSE110418.

Histones extraction

Histones were isolated as previously described [146]. Briefly, cells were lysed in a buffer containing 10 mM Tris-HCl pH 7.4, 10 mM NaCl and 3 mM $MgCl_2$. After centrifugation at 2500 rpm for 10 min at 4°C supernatants were removed and pellets were lysed in the

previous buffer but containing 0.5% NP40 on ice for 10 min with gentle stirring. Nuclei were pelleted by centrifugation at 2500 rpm for 10 min at 4°C and resuspended in 5 mM $MgCl_2$ and 0.8 M HCl. Nuclei were incubated in this buffer during 30 min at 4ºC to extract the histones. Samples were then centrifuged at 14000 rpm for 10 min at 4°C to pellet debris and supernatants were transfered to a clean tube where Trichloroacetic Acid (TCA) 50% was added to precipitate the histones. After washing the pellets with acetone they were air-dried and resuspended in 100 mM Tris-HCl pH 7.5, 1 mM EDTA and 1% SDS. The histone concentration in the extract was measured using the BCA assay (Pierce Technologies, Rockford, IL, USA) according to manufacturer's specifications. Histone samples were then analyzed by western blot.

Quantitative chromatin immunoprecipitation (qChIP)

For ChIP analysis, 8 millions of HepG2 and 5 millions of LX2 cells were seeded and treated with CM-272 (400 nM and 200 nM respectively) or vehicle for 48 h. For crosslinking of DNA and proteins cells were trypsinized, counted and aliquoted in 10 million cells/falcon. After centrifugation (1800 rpm/ 5 min/ 4ºC), cellular pellets were resuspended in 10 mL of ice-cold PBS and treated with 1% formaldehyde for 15 min rolling at room temperature before quenching with 0.125 M glycine (5 min rolling at room temperature). Fixed cells were centrifuged, washed twice (5 min rolling at room temperature each) and harvested in 10 mL of ice-cold PBS with proteases inhibitors. Samples were then incubated with lysis buffer (10 mM EDTA, 50 mM Tris-HCl pH 8.1, 1 % SDS and proteases inhibitor mixture) and sonicated on ice to yield 200-800 bp DNA fragments (35 cycles of 30 sec pulse + 30 sec rest for HepG2 and 45 cycles for LX2). After centrifugation at 14000 rpm for 10 min at 4ºC, supernatant was collected and frozen at -80°C to obtain the chromatin. Prior to continue with ChIP analysis, purified DNA (Macherey-Nagal, Thermo Fisher Scientific, Waltham, MA, USA) of 100 µL aliquoted from sonicated chromatin products were electrophoresed and visualized in GelRed Nucleic Acid (41003, Biotium, Fremont, CA, USA)-stained 2% agarose gels under UV light). DNA concentration of chromatin was measured using NanoDrop ND-1000 spectrophotometer (Thermo Fisher Scientific, Waltham, MA, USA). 50 µg of DNA were used per immunoprecipitation (IP). Chromatin was diluted 1/4 in IP dilution buffer (0.01 % SDS, 1.1 % Triton-X100, 1.2 mM EDTA, 16.7 mM Tris-HCl pH 8.1, 167 mM NaCl)

and pre-cleared with protein A-agarose/salmon sperm DNA (Upstate Biotechnology, Merck, Darmstadt, Germany), centrifuging at 3000 rpm for 1 min and collecting supernatant. Samples were incubated overnight at 4°C with 5 µg of anti-H3K9me2 or 5 µg non-specific IgGs antibodies (listed in Table 5). Immuno-complexes were precipitated by incubation for 1 h with protein A-agarose/salmon sperm DNA at 4ºC and centrifuging at 3000 rpm for 1 min. Bound DNA-protein complexes were eluted and cross-links were reversed after a series of washes. Purified DNA by phenol/chloroform extraction was resuspended in DNase free water for qPCR (performed as described in previous section). The specific primers used were described previously by Mitro *et al*. for *CYP7A1* [147], by Huidobro *et al.* for *GNMT* [148] by Dong *et al.* for *FBP1* [149] and by Jiang *et al.* for *PPARγ* [150] and their sequences are listed in Table 6. Independent ChIP assays were performed at least two times in duplicates. The proportion of H3K9me2 of each gene was quantified calculating:

$$\% \text{ H3K9me2} = (2(-\Delta\Delta Ct) \text{ CM-272 sample}/2(-\Delta\Delta Ct) \text{ Control}) * 100$$

Table 6. qChIP primer sequences.

Gene	Sequence	
CYP7A1	Fw	5´-CATAATTCAGTCACCTCCTACCAGG-3´
	Rev	5´-AGGCATGGTAGTGTGACATGGTT-3´
FBP1	Fw	5´-GACAGAAGGGCCAGGTGA-3´
	Rev	5´-GCCAGAGAGAAAGCTATGACTG-3´
GNMT	Fw	5´-AAGGACCTAGCCCAGGATTG-3´
	Rev	5´-CCGCATTAAAGCATAAGCA-3´
PPARγ	Fw	5´-GGACGCACGGAGCACTTCCG-3´
	Rev	5´-TGTCCTTCCTCCACAGCCCCT-3´

DNA methylation studies

After the corresponding treatments of cells, total DNA was extracted from cells (or control liver tissues) by LEV Blood DNA kit using Maxwell^{R} 16 machine (Promega, Madison, WI, USA) following manufacturer's instructions. DNA purity and

concentration were measured using a NanoDrop ND-1000 spectrophotometer (Thermo Fisher Scientific, Waltham, MA, USA).

1. Global DNA methylation analysis: Slot blot assay

Aliquots of 500 ng of genomic DNA were loaded onto a nitrocellulose membrane (Amersham Hybond N+, RPN203B, GE Healthcare, Little Chalfont, UK), pre-wetted in 6X Saline-Sodium Citrate (SSC) (20X stock solution consists of 3 M NaCl and 300 nM $Na_3C_6H_5O_7$, adjusted to pH 7.0) for 10 min, using the Bio-Dot microfiltration apparatus (170-6545, BioRad, Hercules, CA, USA). Then the membrane was incubated with 2X SSC for 5 min and was cross-linked for 2 h at 80 ºC. The membrane, after being blocked with Tropix I- block blocking reagent (AI300, Tropix-Thermo Fisher Scientific) in PBS with 0.1 % of Tween-20 and 0.02 NaN_3, was incubated overnight at 4ºC with an antibody against 5-methylcytosine (see Table 5). After incubation, membranes were treated as western blot: washed three times by T-TBS during 5 min at room temperature and incubated with the corresponding secondary antibody (1:5000 dilution) in T-TBS for 1 h at room temperature. Finally, two washes of T-TBS followed by two washes of TBS of 5 min each were performed at room temperature. Western Lightning-ECL from Perkin Elmer Inc. (Waltham, MA, USA) was used for chemiluminescence illuminating of membranes following manufacturer's instructions and using Amersham Hyperfilm ECL films (Amersham Biosciences). Equal DNA loading in membranes was assessed by methylene-blue staining (Sigma).

2. Specific DNA methylation analysis: methylation-specific PCR (MSP) and pyrosequencing

DNA methylation status of the genes promoters was analyzed by MSP and pyrosequencing techniques. HepG2, PLC/PRF5 and LX2 cells were treated with vehicle (DMSO), decitabine (5 μM) or CM-272 (50-200 nM) for 3-5 days, with daily medium change. At the end of treatments cells were washed twice with PBS and genomic DNA was extracted using a DNA kit (Maxwell 16 LEV Blood DNA Kit, Promega, Madison, WI, USA) following the manufacturer's instructions. DNA purity and concentration were

measured using a NanoDrop spectrophotometer (Thermo Fisher Scientific). 1 µg of genomic DNA was treated and modified using the CpGenome DNA modification Kit (S7820, Chemicon International, Fisher Scientific) following the manufacturer's instructions. Bisulfite-modified DNA was stored at -20ºC until used for MSP and pyrosequencing analysis. Bisulfite-modified DNA from human liver tissues was used as control of unmethylated sample in both techniques.

MSP was performed using a set of primers for *FBP1*, *RASSF1A* and *PPARγ* either designed by MethPrimer software (The Li Lab, www.urogene.org) or subtracted from literature (specific sequences listed in Table 7). MSP reactions were performed in pairs: one for specific methylated PCR and the other for specific unmethylated PCR at the same time using corresponding primers for each gene. MSP reactions were performed using Phusion U Hot Start DNA Polymerase kit (F-555S, Thermo Fisher Scientific) under these conditions:

Pre-hit		95ºC, 10 min
Initial denaturalization		98ºC, 30 sec
X35	Denaturalization	98ºC, 10 sec
	*Hybridizing	XºC, 20 sec
	**Extension	72ºC, X sec
Final extension		22ºC, 10 min

**FBP1* (56ºC), *RASSF1A* (58ºC), *PPARγ* (60ºC)

** *FBP1* (20 sec), *RASSF1A* (15 sec), *PPARγ* (20 sec)

PCR products were electrophoresed and visualized in GelRed Nucleic Acid (41003, Biotium, Fremont, CA, USA)-stained 2% agarose gels under UV light.

For pyrosequencing, "hot start" PCR (PyroMark PCR Kit, 978703, Qiagen, Hilden, Germany) was performed using 2 µl of bisulfite-modified DNA, 12.5 µl of 2X Buffer, 1 µl of 10 µM of each specific primer for *FBP1* promoter region (specific sequences listed in Table 7 and were design by MethPrimer software, The Li Lab, www.urogene.org) in a final volume of 25 µl; following the reaction:

Initial denaturalization		95ºC, 15 min
X45	Denaturalization	94ºC, 1 min
	Hybridizing	55ºC, 1 min
	Extension	72ºC, 1 min
Final extension		72ºC, 10 min

Prior to pyrosequencing assay, 2 μL of the PCR products were electrophoresed and visualized in GelRed Nucleic Acid (41003, Biotium, Fremont, CA, USA)-stained 2% agarose gels under UV light, to confirm the purity of the product. The rest of biotinylated PCR products were immobilized to streptaviding Sepharose High Performance beads (GE Healthcare, Little Chalfont, UK) and processed to yield high quality ssDNA using the PyroMark Vacuum Prep Workstation (Biotage, Uppsala, Sweden), according to the manufacturer's instructions. The specific sequence of the pyrosequencing primer used is listed in Table 7 and was design by MethPrimer software (The Li Lab, www.urogene.org). The pyrosequencing reaction was performed using the PyromarkTM ID (Biotage) and sequence analysis was obtained using the PyroQ-CpG analysis software (Biotage).

Table 7. MSP and Pyrosequencing primer sequences.

Gene	Sequence	
MSP		
M_FBP1	Fw	5′-GTTAGTTTTTTCGTTAGGTTTCGC-3′
	Rev	5-AATCAAAATATTAACGTCCGTATCG-3′
U_ FBP1	Fw	5′-TTAGTTTTTTTGTTAGGTTTTGTGG-3′
	Rev	5′-TCAAAATATTAACATCCATATCAAA-3′
M_PPARɣ	Fw	5′-GAGATTAGCGGTTTTTTGAAC-3′
	Rev	5-TAAATAAAAACGAAATAAAAACGTA-3′
U_PPARɣ	Fw	5′-TTTAGGAGATTAGTGGTTTTTTGAAT-3′
	Rev	5′-ACAACATAAATAAAAACAAAATAAAAACAT-3′
M_RASSF1A	Fw	5′-GTGTTAACGCGTTGCGTATC-3′
	Rev	5-AACCCCGCGAACTAAAAACGA-3′
U_RASSF1A	Fw	5′-TTTGGTTGGAGTGTGTTAATGTG-3′
	Rev	5′- CAAACCCCACAAACTAAAAACAA-3′

Table 7. MSP and Pyrosequencing primer sequences. (*Continuation*)

Pyrosequencing		
PYRO-PCR_FBP1	Fw	5´-GATTTTGTTTGAAGATTTAAGTAGG-3´
	Rev	5- biotin- ACAAAAAAAAACAATAAACACTAAC-3´
PYRO-SEQ_FBP1	Fw	5´-GTTTGGTTTGGTTTAGTTGTATTA-3´

Mouse models, ethical statement

All animal used received humane care according to the criteria outlined in the "Guide of the Care and Use of Laboratory Animals" prepared by the National Academy of Sciences and published by the National Institutes of Health (NIH publication 86-23 revised 1985). Protocols were also approved and performed according to the guidelines of the Animal Care Committee of the University of Navarra (#R-CP001-15GN).

1. **Subcutaneous tumor xenograft mouse models**

The subcutaneous tumor model was established injecting 10 million PLC/PRF5 or HepG2 cells, or 5 million PLC/PRF5 cells plus 5 million LX2 cells, on the right flank region of male athymic nude mice (6-8 weeks) (Envigo, Valencia, Spain). When tumors reached ~100 mm^3 (3-15 days from implanting cells), mice were randomized into control (n=5) and treatment (n=5) groups. Mice received 5 mg/kg (i.p.) of CM-272 or same volume of vehicle (PBS). Total of 13 doses were administered (6 consecutive days of injection followed by 1 resting day). This dose was selected based on previous toxicity and pharmacological studies [132]. Tumor growth were measured every 3-4 days. At the end of the treatment tumors were harvested, weighed and fixed with 4% formalin for histological analyses or snap-frozen and stored at -80ºC. Blood was harvested for serum determinations.

2. Orthotopic tumor xenograft mouse model

Subcutaneous xenograft tumors were generated with PLC/PRF5 cells in nude mice as described in the previous section. When tumors reached approximately 1 cm of diameter, animals were sacrificed and tumor tissue was sliced into equal fragments of ~1 mm^3. These fragments were implanted orthotopically by laparotomy in the left lobe of the liver of a second group of nude mice. Tumor engraftment was monitored by ultrasound scan using Vevo 770 High-Resolution Imaging System (Visualsonics, Toronto, Canada) enabling *in vivo* visualization, assessment, and measurement of tumors. When lesions reached ~2 mm^3 mice were randomized into control and treatment groups (n= 5 per group). Mice received 5 mg/kg (i.p.) of CM-272 or same volume of vehicle (PBS). Total of 13 doses were administrated (6 consecutive days of injection followed by 1 resting day). Tumor growth were measured every week. At the end of treatment tumors were harvested, weighed and fixed with 4% formalin for histological analyses or snap-frozen and stored at -80ºC. Blood was harvested for serum determinations.

Serum biochemistry determinations

For serum determinations, blood obtained from mice was preserved at 4ºC overnight to allow the complete formation of the blood clot. Supernatants were then centrifuged at 2500 rpm during 10 min at 4ºC to obtain serum from upper phase and stores at -20ºC until analysis. Serum levels of alanine aminotransferase (ALT), aspartate aminotransferase (AST), alkaline phosphatase (ALP), cholesterol, urea, albumin, bilirubin and creatinine were measured using a C311 Cobas Analyzer (Roche Diagnostics) following manufacturer's instructions.

CM-272 determination in mice serum, liver and tumor tissue samples

CM-272 was measured in serum, liver and tumor tissues using a Xevo-TQ MS triple quadrupole mass spectrometer with an electrospray ionization (ESI) source and Acquity UPLC (Waters, Manchester, UK) as previously described [132].

Chromatographic separation was performed by gradient elution at 0.6 mL/min using an Acquity UPLC BEH C18 column (50 x 2.1 mm, 1.7 μm particle size; Waters). The mobile phase consisted of A: water with 0.1% formic acid, B: methanol with 0.1% (CM-272) formic acid. The auto- sampler temperature was set at 7ºC and column temperature at 50ºC. For detection and quantification, the electrospray ionization operated in the positive mode, and the collision gas used was ultra-pure argon at a flow rate of 0.15 mL min^{-1}. The compound was detected using multiple reaction monitoring (MRM). Quantification was achieved by external calibration using matrix-matched standards. Concentrations were calculated using a weighted least-squares linear regression (W= 1/x). Calibration standards were prepared by adding the appropriate volume of diluted solutions of the compound (made in a mixture of methanol and water, 50:50, v:v) to aliquots of 25 μL of blank plasma. 2% formic acid in acetonitrile was added to precipitate the proteins. The mixture was then agitated for 5 min and centrifuged at 13200 rpm for 10 min at 4ºC. A 5 μL aliquot of the resulting supernatant was injected onto the LC-MS/MS system for analysis. Frozen plasma samples were thawed at room temperature, vortexed thoroughly and subjected to the above described extraction procedure.

Immunofluorescence

Immunofluorescent staining of 3 μM thick formalin-fixed paraffin embedded tissues was performed following standard protocols. The paraffin was removed and the tissues rehydrated using a slide wash/incubation sequence with Histoclear II (Nottingham, UK), ethanol 10%, 90%, 70% and ddH_20. Antigen retrieval was performed with citrate buffer (pH 6.0) (Dako, Glostrup, Denmark) and sections were blocked in 1% BSA in PBS and incubated with primary antibodies diluted in blocking solution for 1 h at room temperature. After washing, sections were incubated with secondary antibodies diluted in 1% BSA in PBS for another 1 h at room temperature and then washed and counterstained with 4',6-diamidino-2-phenylindole (DAPI). The primary antibody for cluster of differentiation 31 (CD31) detection was diluted 1:100 (77699S, Cell Signalling) and the secondary antibody, Alexa Fluor conjugate (594, A21207 Invitrogen- Life technologies), was diluted 1:400. Images were obtained using an Axoimagen M1 microscope (Zeiss, Oberkochen, Germany). Controls were performed using only secondary antibody. Images

from multiple fields (at least 5) and tissue samples from each mouse xenograft were taken, processed and signal was quantitated with a Zen 2.1 Zeiss Image Analysis System.

Statistical analysis

Human samples data visualization and statistical analyses were performed using R software version 3.3.2 (R Foundation for Statistical Computing, Vienna, Austria. https://www.R-project.org) and Bioconductor packages. Comparison of the different gene expression levels between groups were evaluated using Mann-Whitney U test or Kruskal-Wallis Test. Spearman correlation analysis was used to test the association between continuous variables. Univariate survival analysis was performed using Kaplan-Meier curve with log-rank test. The median *G9A*, *DNMT1* and *UHRF1* expression levels on the total number of analyzed samples was used to determine the low- and high-expression groups. For the rest of the data of this work, the statistical analysis was performed using GraphPad Prism-v5 program. For comparison between two groups, parametric Student t-test was used. All reported P-values were two-tailed and differences were considered significant when $P<0.05$. (*<0.05; **<0.01; ***<0.001)

Results

1. Overexpression of G9a, DNMT1 and UHRF1 in HCC

So far, up-regulated levels of *G9a*, *DNMT1* and *UHRF1* have been independently described in various cancers and pathological processes including liver cancer [85,121,151]. Our first objective was determine the possible biological relevance of G9a-DNMT1-UHRF1 complex in HCC. Thus, we first studied the expression of *G9a*, *DNMT1* and *UHRF1* in HCC, and evaluated whether there was a correlation between the expression of these genes. Additionally, we assessed if their expression levels could be associated with different molecular signatures and clinicopathological features of liver cancer.

1.1. Expression in human HCC samples

We evaluated the expression of these genes in a cohort of 268 HCC patients. Detailed information of these samples is summarized in Materials & Methods Table 2. In these samples, we examined the expression of *G9a*, *DNMT1* and *UHRF1* in normal liver tissues (n=5), peritumor non-transformed liver tissues (NT, n=154) and tumor liver tissues (T, n=268) (Fig. 11). Consistently, we observed that the expression of these enzymes was significantly elevated in HCC tissues compared to normal and peritumoral tissues.

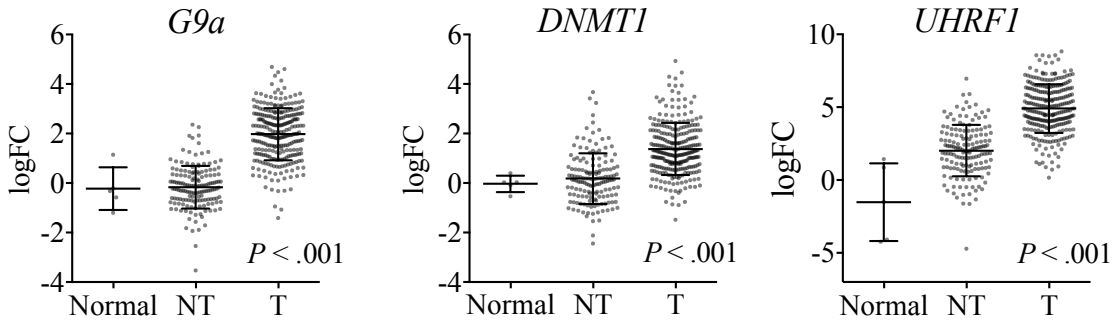

Figure 11. *G9a*, *DNMT1* and *UHRF1* overexpression in human HCC. *G9a*, *DNMT1* and *UHRF1* mRNA levels in normal, NT and T human liver tissues (NT: peritumoral liver tissue; T: tumoral liver tissue). *18S* was used as reference gene of constitutive expression.

We next performed Spearman correlation analyses to test the association between the expression of *G9a*, *DNMT1* and *UHRF1* in these samples (Fig. 12). Interestingly, we observed a significant positive correlation between the expression of all these enzymes; *DNMT1* and *G9a*, *UHRF1* and *G9a*, as well as *DNMT1* and *UHRF1*.

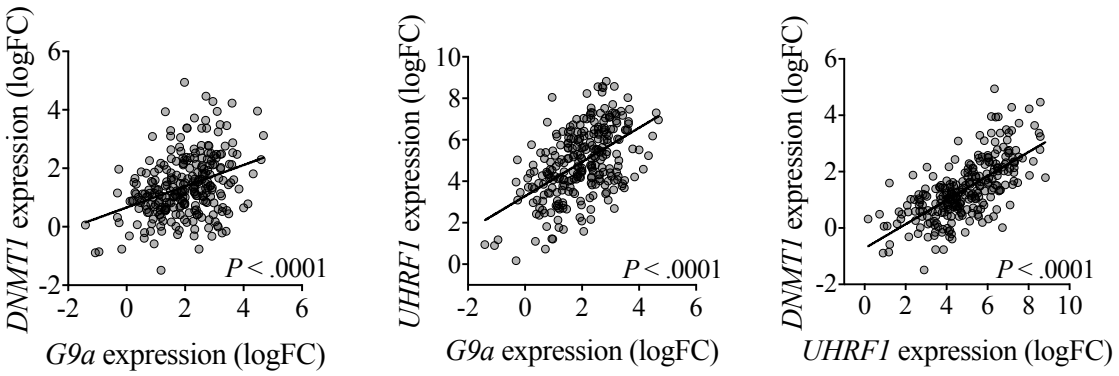

Figure 12. *G9a*, *DNMT1* and *UHRF1* expression correlation in human HCC. Spearman correlation analysis of *G9a*, *DNMT1* and *UHRF1* mRNA levels in tumoral liver tissue samples. *18S* was used as reference gene of constitutive expression.

1.2. Correlation of *G9a*, *DNMT1* and *UHRF1* overexpression with molecular signatures in human HCC samples

The HCC patients cohort analyzed has been perfectly characterized at the clinical, genetic and transcriptomic level [138,139]. We decided to study the possible correlation between the expression of *G9a*, *DNMT1* and *UHRF1* with previously established molecular and clinicopathological parameters that can classify these tumors in cohorts of varying disease severity. Clinical, histological and molecular characteristics were contrasted, including gender, age, geographical origin, etiology (hepatitis B virus, hepatitis C virus, alcohol abuse, hemochromatosis), histological grade of tumor differentiation assigned according to the Edmondson and Steiner grading system, tumor size, α-fetoprotein (AFP) levels, macroscopic and/or microscopic vascular invasion, satellite tumors, BCLCB classification or mutational status in numerous genes such as *TP53*, *CTNNB1*, *AXIN1*, *PIK3CA*, *NFE2L2*, *GNAS*, *PTEN*, *MLL2*, *ARID2*, *SETD2*, *ARID1α*, *KRAS* or *TERT*, and others. Among a big number of classifications we found that *G9a*, *DNMT1* and *UHRF1*

expression was significantly higher in HCC tissues from patients classified as poor prognostic group (P2) (Fig. 13A) by the molecular signature of Nault J-C and colleagues [152]. This classification describes a molecular signature based on the expression of 5 genes that accurately identified patients with aggressive tumors and a poor prognosis. We also found that the expression of the three enzymes was higher in those samples classified within groups G1-G3 compared to G4-G6 (Fig. 13A), based on Boyault and colleagues categorization [16] that classified HCCs in six subgroups (G1 to G6) with worse survival for patients within subgroups G1-G3. *G9a*, *DNMT1* and *UHRF1* expression was also higher in HCC tissues displaying macroscopic vascular invasion, and patients with more advanced Edmondson grades and "tumor, node, metastasis" (TNM) stages (Fig. 13A), which are all clinically relevant features of worse phenotypes. Finally, patients with higher *G9a* and *DNMT1* mRNA levels showed significant worse survival, and a similar trend was observed for *UHRF1* although it did not reach statistical significance (Fig. 13B). These results reinforced the hypothesis that this enzymatic complex could be playing a relevant role in the pathogenesis of liver cancer, and demonstrated that overexpression of *G9a*, *DNMT1* and *UHRF1* is correlated with worse phenotype and prognosis in human HCC.

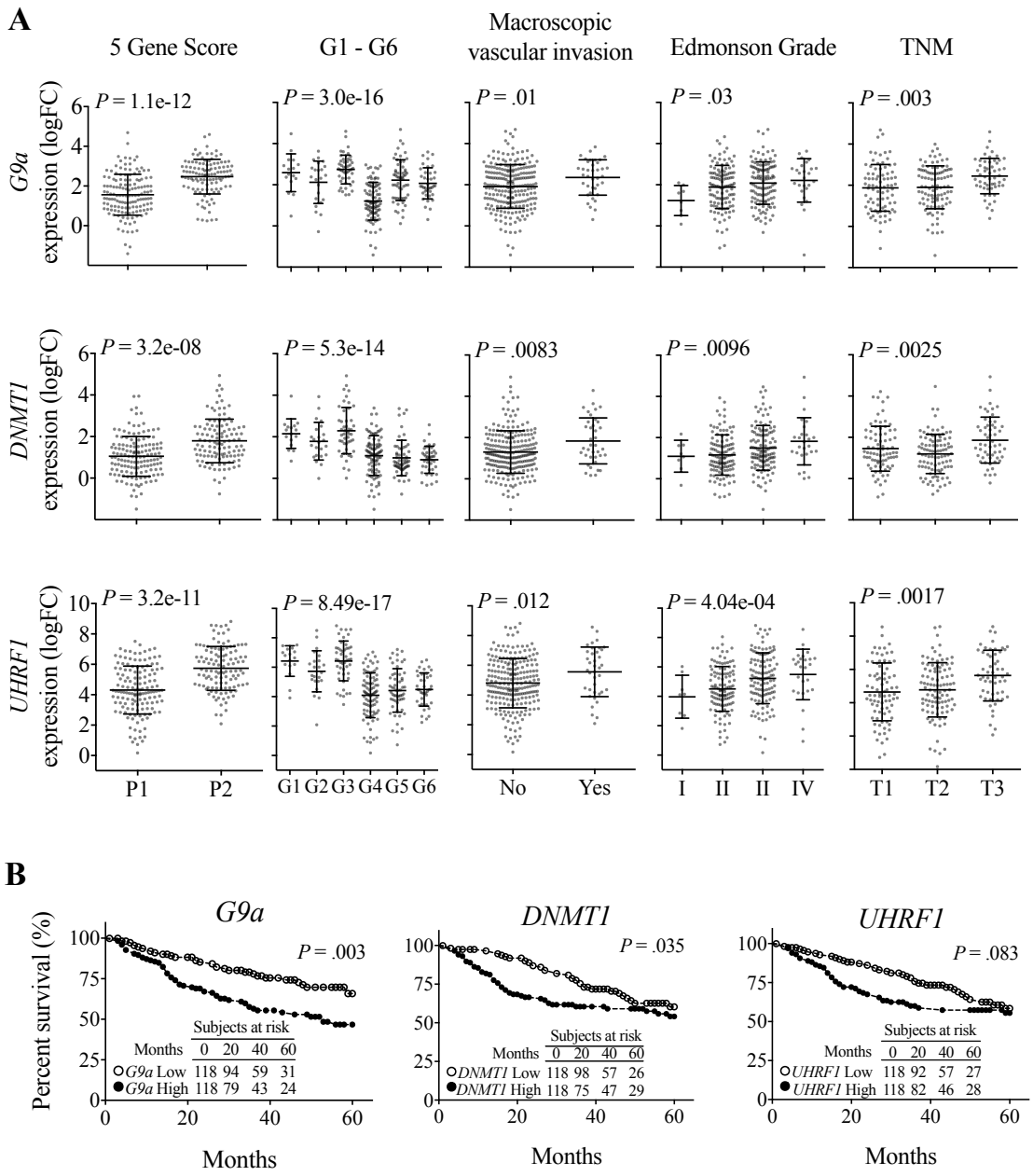

Figure 13. *G9a*, *DNMT1* and *UHRF1* expression correlation with worse phenotypes and prognosis in human HCC. A) *G9a*, *DNMT1* and *UHRF1* gene expression in tumoral liver tissues from patients classified according to the 5-gene score, the G1 to G6 transcriptomic groups, the presence of macroscopic vascular invasion, the Edmonson Grade and the "tumor, node, metastasis" (TNM) score. **B)** Post-operative survival of HCC patients according to *G9a*, *DNMT1* and *UHRF1* expression levels. *18S* was used as reference gene of constitutive expression.

1.3. G9a, DNMT1 and UHRF1 levels in HCC cell lines vs. normal liver

Next, we examined *G9a*, *DNMT1* and *UHRF1* expression levels in a wide panel of human HCC cell lines (described in Materials and Methods Table 3). We found significantly higher expression levels in these cell lines compared to normal and peritumoral liver tissues (Fig. 14A). Protein levels of these genes were consistently higher in four representative HCC cell lines compared to primary human hepatocytes (Fig. 14B).

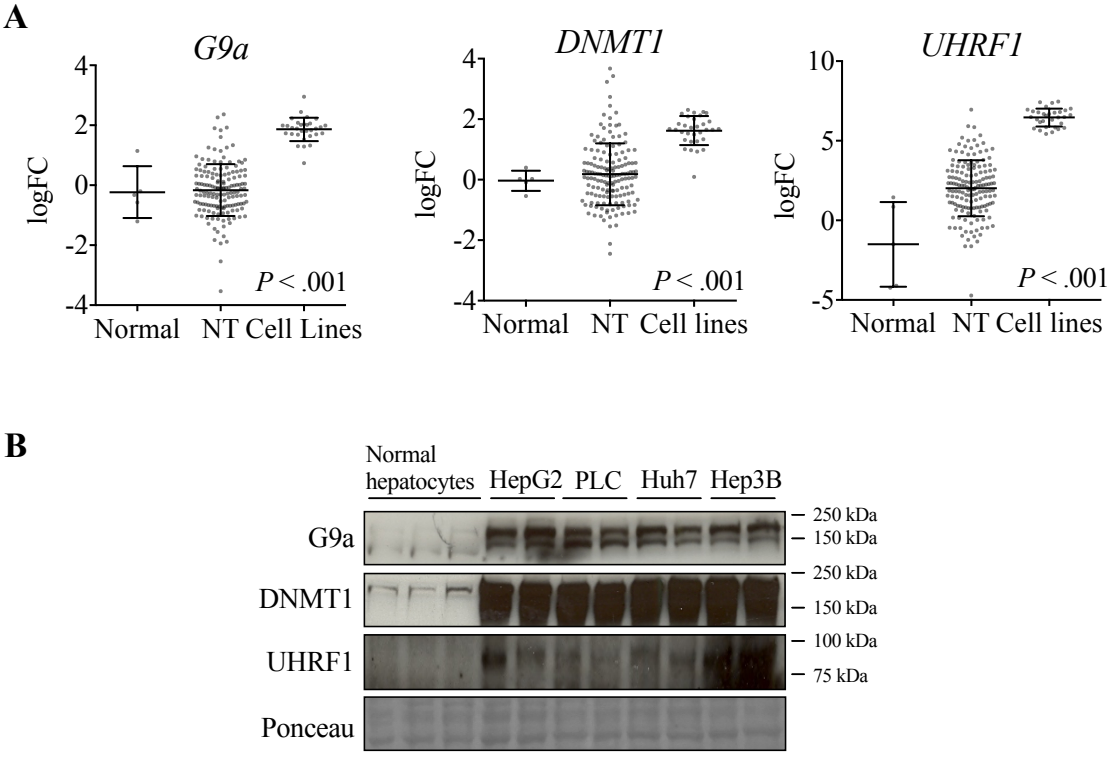

Figure 14. Increased levels of G9a, DNMT1 and UHRF1 in human HCC cell lines. A) *G9a*, *DNMT1* and *UHRF1* mRNA levels in normal, NT and human HCC cell lines (NT: peritumoral liver tissue). *18S* was used as reference gene of constitutive expression. **B)** Western blot of G9a, DNMT1 and UHRF1 in primary human hepatocytes and the four human HCC cell lines HepG2, PLC/PRF5, Huh7 and Hep3B. Ponceau staining is shown to demonstrate equal loading of proteins.

Interestingly, and according to the studies performed in patients' samples, we also found a significant positive correlation between *DNMT1* and *G9a* mRNA levels and between *UHRF1* and *DNMT1* mRNA levels, while between *UHRF1* and *G9a* the correlation showed a positive trend (Fig. 15), when we performed Spearman correlation analysis.

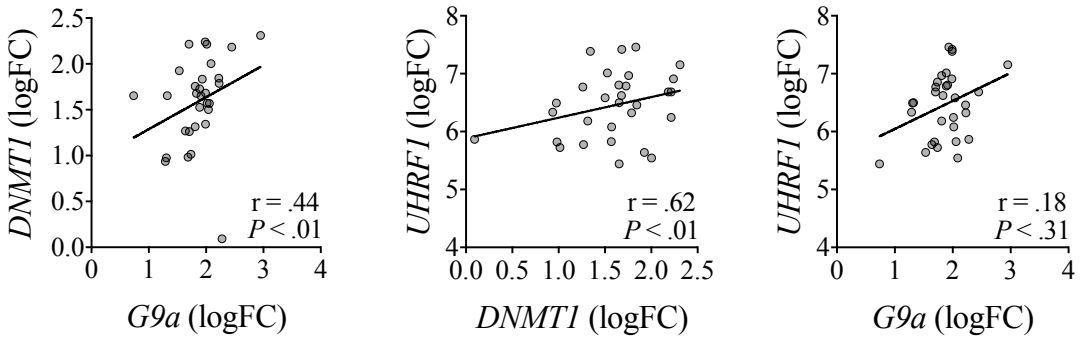

Figure 15. *G9a*, *DNMT1* and *UHRF1* expression correlation in human HCC cell lines. Spearman correlation analysis of *G9a*, *DNMT1* and *UHRF1* mRNA levels in human HCC cell lines. *18S* was used as reference gene of constitutive expression.

2. Dual targeting of G9a and DNMT1 in HCC cells *in vitro*

We demonstrated that overexpression of *G9a* and *DNMT1* in HCC showed a positive correlation and both were associated with worse phenotypes and prognosis in HCC patients. Moreover, we observed that the key molecular adaptor of the G9a-DNMT1 complex, UHRF1, is also overexpressed in HCC and correlates with the same HCC phenotypes. This suggested that the role of G9a and DNMT1 in HCC might be closely linked to their activity displayed as an enzymatic complex. Thereby, we decided to evaluate the possible enhancing effects by simultaneous inhibition of G9a and DNMT1 in HCC cells.

2.1. Combined inhibition of G9a and DNMT1 either by specific siRNAs or chemical inhibitors.

To evaluate the effects of the dual targeting of G9a and DNMT1 in HCC cells we performed transfections with siRNAs specific for *G9a* and/or *DNMT1* in HepG2 and PLC/PRF5 cells. With this molecular tool, we have tested cell viability after 72 h of transfection to evaluate how the simultaneous inhibition of G9a and DNMT1 could affect HCC cell growth. The transfection with siG9a or siDNMT1 significantly reduced HepG2 and PLC/PRF5 cells survival and the simultaneous molecular inhibition with both specific siRNAs led to a significant additive effect (Fig. 16).

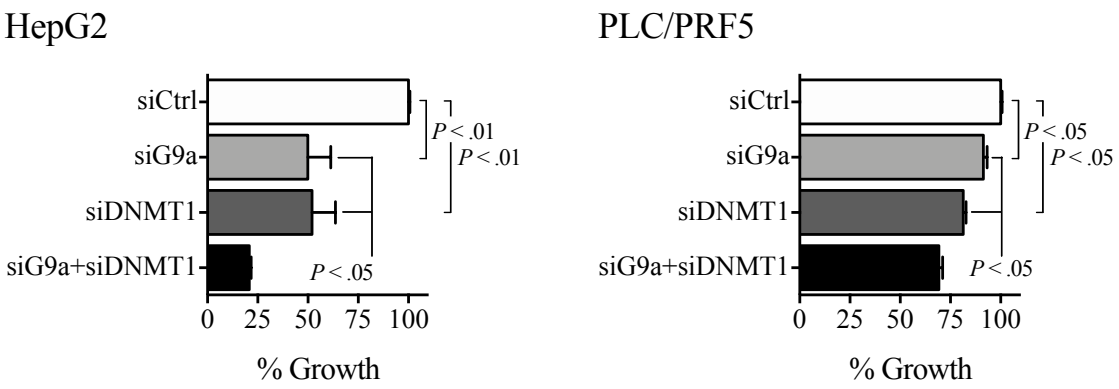

Figure 16. Additive effect of simultaneous silencing *G9a* and *DNMT1* in human HCC cell lines. Effects on cells viability after *G9a* and *DNMT1* expression knockdown upon 72 h of specific siRNA transfections in HepG2 (left) and PLC/PRF5 (right) cells. (siCtrl: control siRNA; siG9a: *G9a* specific siRNA; siDNMT1: *DNMT1* specific siRNA).

Validation of the knockdown efficiency was obtained by measuring their respective mRNA and protein expression levels (Fig. 17). After 72 h of transfection we observed a reduction in mRNA expression levels of around 75% (Fig. 17A) and almost undetectable protein levels of the enzymes (Fig. 17B) either with siG9a, siDNMT1 and combination of siRNAs in the two HCC cell lines.

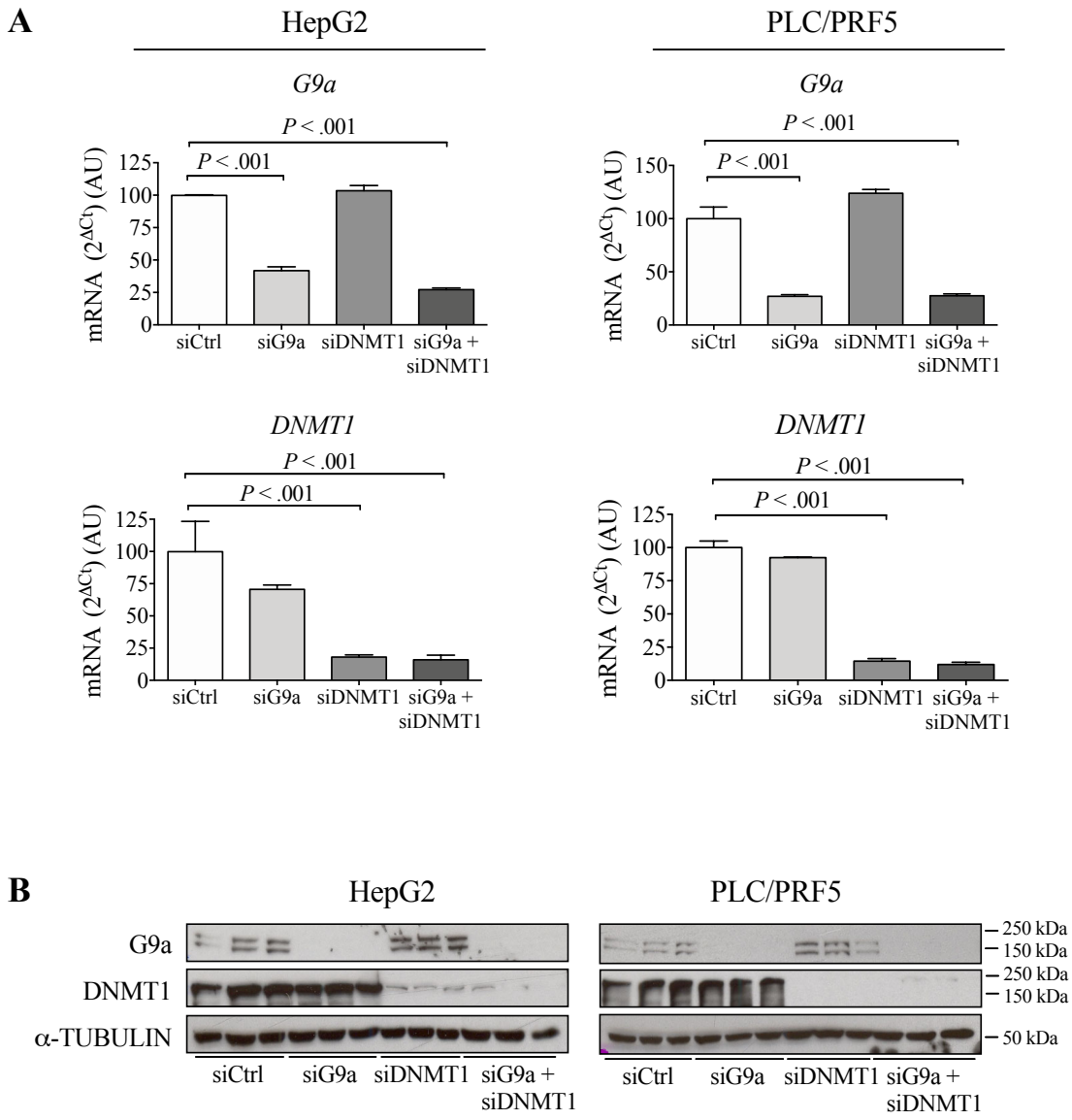

Figure 17. Validation of *G9a* and *DNMT1* expression knockdown upon specific siRNA transfections in HCC cells. A) mRNA expression levels of *G9a* and *DNMT1* after 72 h of indicated siRNA transfections in HepG2 (left) and PLC/PRF5 (right) cells. *H3F3A* was used as reference gene of constitutive expression. **B)** Western blot of G9a and DNMT1 after 72 h of indicated siRNA transfections in HepG2 (left) and PLC/PRF5 (right) cells. α-TUBULIN western blots are loading controls. (siCtrl: control siRNA; siG9a: *G9a* specific siRNA; siDNMT1: *DNMT1* specific siRNA).

After these results, we decided to corroborate the advantageous effect of dual targeting G9a and DNMT1 by chemical inhibition using their respectively commercially available compounds. We treated HepG2 and PLC/PRF5 cells combining the G9a inhibitor BIX01294, and the DNMTs inhibitor Decitabine at different concentrations. Both drugs were administered at a concentration range from 2 GI_{50}, to 1/4 GI_{50} (previously calculated for each cell line and indicated in Figure 18) and cell viability was measured after 48 h of treatment. The combination of these drugs showed a synergistic inhibition of both HCC cell growth at all concentrations tested by using Calcusyn software (Fig. 18). This effect was stronger in HepG2 cells, reaching strong synergisms (CI <0.3) at two points of combinatory treatments. These results corroborated our hypothesis that dual targeting of G9a and DNMTs potentiates the anti-tumoral properties of inhibiting these epigenetic enzymes independently and could therefore represent a novel approach to liver cancer therapeutics.

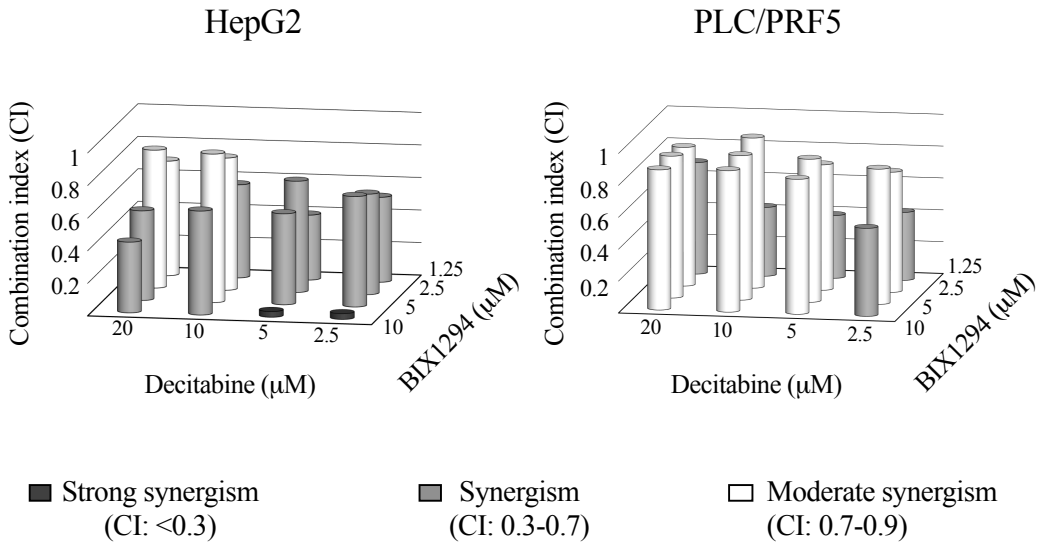

Figure 18. Synergistic effects of simultaneous targeting of G9a and DNMT1 in human HCC cell lines. Combination study of the growth inhibitory effects of G9a (BIX01294) and DNMT1 (Decitabine) inhibitors after 48 h of treatment in HepG2 (left) and PLC/PRF5 (right) cells. Cells were treated combining the doses of 1/4 GI_{50}, 1/2 GI_{50}, GI_{50} and 2GI_{50} of BIX01294 (1.25, 2.5, 5 and 10 μM) and Decitabine (2.5, 5, 10 and 20 μM).

2.2. Testing the activity of the small molecule dual inhibitor of G9a and DNMT1 CM-272 in HCC cell lines

As it was previously described, novel and proprietary small molecule dual inhibitors of G9a and DNMT1 have been developed in our Institution. These compounds present a novel mechanism of action based on substrate competition., anthe lead compound, CM-272, already demonstrated its anti-tumoral effectivity against hematological malignances *in vivo* presenting good pharmacokinetic, high specificity and lack off side effects [132]. In order to explore the biological relevance of dual inhibiting G9a and DNMT1 for HCC development using this compound we first evaluated the anti-proliferative effects of CM-272 in the panel of 32 HCC cell lines (Fig. 19). CM-272 showed GI_{50} in the nM range for most HCC cell lines, which is an acceptable therapeutic window, as toxicity of CM-272 on non-tumoral hepatic cell line THLE-2 was GI_{50} of 1.78 μM (data from San José-Eneriz *et al*. [132]).

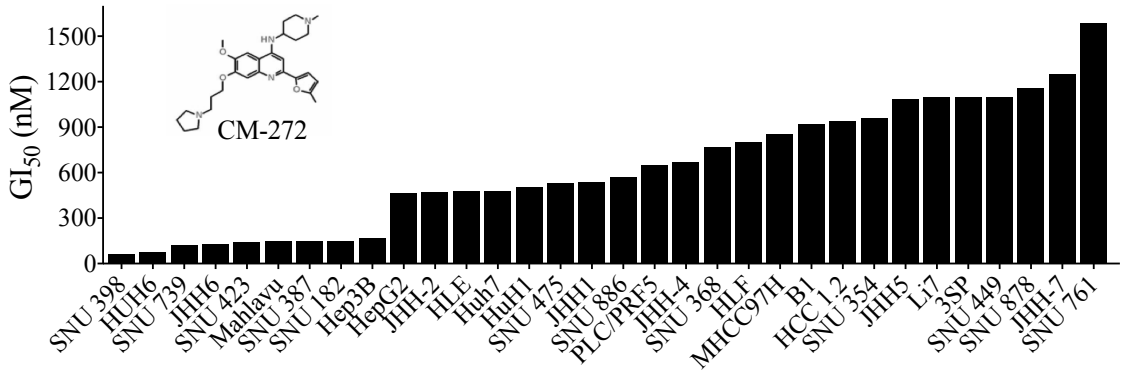

Figure 19. HCC cells are sensitive to CM-272 treatment. Representation of the GI_{50} values of CM-272 in 32 human HCC cell lines after 48 h of treatment.

Although good sensitivity of the different HCC cell lines to CM-272 was demonstrated, we found considerable differences among the cell lines GI_{50} values. This can be a very important issue from a translational perspective, and thus we tried to find an explanation for this variability. We first hypothesized that these differences could be due to different expression levels of the enzymatic complex formed by *G9a*, *DNMT1* and *UHRF1*. We studied the possible correlation between the CM-272 GI_{50} values of HCC cells and their

enzymes expression levels (Fig. 20). This assay showed a negative correlation trend in all cases but did not reach statistical significance.

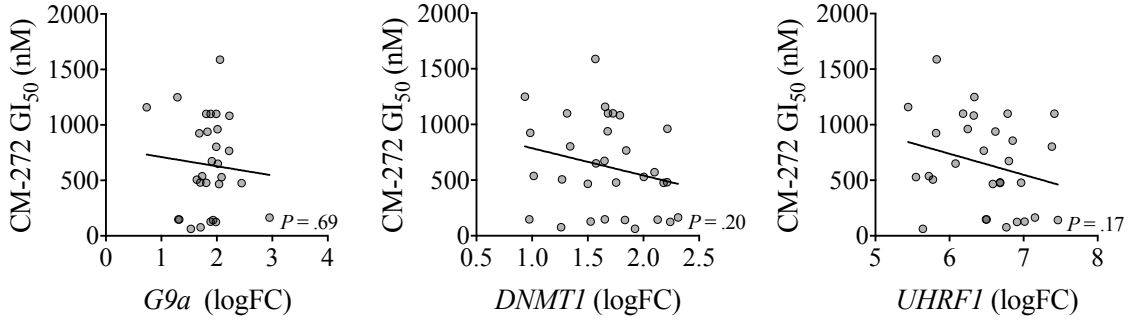

Figure 20. Correlation between GI_{50} values of CM-272 in HCC cells and *G9a*, *DNMT1* and *UHRF1* expression levels. Spearman correlation analysis of the GI_{50} values of CM-272 in 32 human HCC cell lines vs. their *G9a*, *DNMT1* and *UHRF1* expression levels. *18S* was used as reference gene of constitutive expression.

We decided to explore other possible correlations and we analyzed an extensive panel of genes related with different phenotypic characteristics of these HCC cells such as indicators of differentiation status (*ALB*, *HNF4α*, *CEBPα*), established markers of progenitor cells (*AFP*, *KRT7*, *KRT19*, *EpCAM*, *NCAM*, *PROM1*, *THY1*, *FOXA2*), vascular markers and proteins involved in migration and metastasis (*CD34*, *CD44*, *NAV3*, *CDH1*, *ICAM*). In all cases we were not able to find significant association, except a positive correlation between *ICAM* and *HNF4α* with the GI_{50} values.

We then studied if the sensitivity of HCC cells to CM-272 could be attributed to the expression of the drug efflux pump MDR1, coded by the *ABCB1* gene. This transporter is able to pump many foreign substances out of the cells, conferring a chemoresistance mechanisms in cancer cells. We determined the expression of *ABCB1* in our collection of HCC cell lines and evaluated whether there was a correlation with the CM-272 GI_{50} values. Interestingly, a highly significant positive correlation was found between the two parameters (Fig. 21), suggesting that CM-272 might be a potential substrate of this transporter. To validate this hypothesis, functional experiments aimed at directly evaluating the role of MDR1 in CM-272 cellular efflux were performed by WuXi AppTec company (Hong Kong). The experiment was based on the measurement of the efflux ratio

(permeability value in the B-A direction divided by the permeability value in the A-B direction) of CM-272 in the control cell line MDCK (MDCK-II) and the same cell line overexpressing MDR1 (MDR1-MDCK-II). For the experiment, Elacridar, an inhibitor of the MDR1, and Digoxin, a known substrate of MDR1, were used. As shown in Fig. 21, we could demonstrate that CM-272 was indeed a substrate of this drug transporter. Its net efflux ratio was similar than Digoxin and inhibited upon Elacridar administration in MDR1-MDCK-II cells.

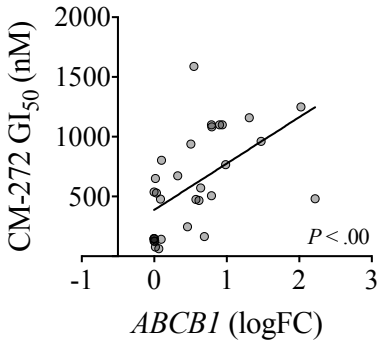

Compound ID	+/- Elacridar	Cell Line	Mean Papp (10^{-6}cm/s) A to B	Efflux Ratio	Net Efflux Ratio
Digoxin	-	MDCK II	0.79	8.84	6.73
	-	MDR1-MDCK II	0.19	59.46	
	+	MDCK II	1.97	1.73	1.35
	+	MDR1-MDCK II	1.37	2.34	
CM-272	-	MDCK II	0.40	4.02	5.35
	-	MDR1-MDCK II	0.18	21.50	
	+	MDCK II	0.37	2.16	1.36
	+	MDR1-MDCK II	0.20	2.94	

Figure 21. HCC cells sensitivity to CM-272 treatment correlates with *ABCB1* expression as CM-272 is a MDR1 substrate. Left panel; spearman correlation analysis of GI_{50} values of CM-272 in 32 human HCC cell lines vs. their *ABCB1* expression levels. *18S* was used as reference gene of constitutive expression. Right panel; evaluation of CM-272 as MDR1 substrate. Efflux ratio measurements of CM-272 performed in MDCK cells expressing MDR1 (MDR1-MDCK II) or control MDCK cells (MDCK II). Elacridar was used as inhibitor of the MDR1 and Digoxin was used as control substrate of MDR1.

We wanted to study the activity and specificity of CM-272 in HCC cells. To this aim we purified total histones and DNA from HepG2 and PLC/PRF5 cells after 48 h of treatment with CM-272 at GI_{50}. Inhibition of G9a and DNMTs was demonstrated by a decrease in total levels of H3K9me2 and DNA methylation (5-methylated-cytosine, 5meC) respectively (Fig. 22A). Specificity of CM-272 was evaluated by measuring other methylation histone marks (H3K4me3 and H3K27me3), that were not apparently reduced by CM-272 treatment in HepG2 (Fig. 22B).

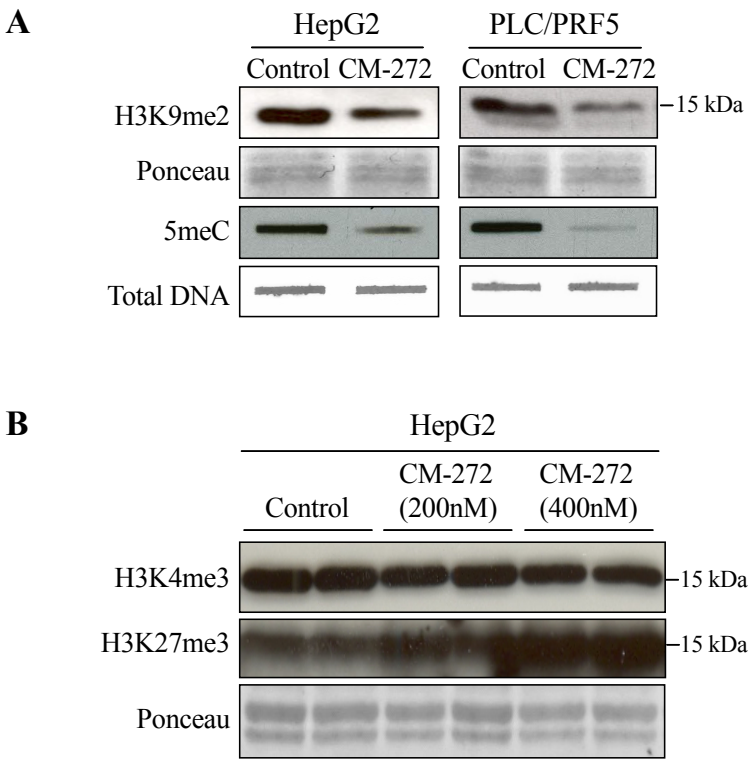

Figure 22. CM-272 treatment reduces H3K9me2 and 5meC levels without reducing other methylation-dependent epigenetic marks in human HCC cells *in vitro*. A) H3K9me2 (western blot) and 5meC (slot blot) levels in HepG2 (left) and PLC/PRF5 (right) cells treated for 48 h with CM-272 at its GI_{50} (400 nM). **B)** Western blot of H3K4me3 and H3K27me3 in HepG2 cells treated for 48 h with CM-272 at 1/2 of its GI_{50} (200 nM) and its GI_{50} (400 nM). Ponceau staining of histones and methylene blue staining of DNA are loading controls.

We next decided to study the protein and expression levels of the epigenetic complex after CM-272 treatment in our cells. Interestingly, a decrease in the protein levels of G9a, DNMT1 and UHRF1 in HepG2 and PLC/PRF5 cells was observed upon CM-272 treatment (Fig. 23A). We then analyzed the mRNA expression levels of these enzymes after CM-272 treatment (Fig. 23B), and we found that while mRNA levels of *G9a* and *DNMT1* were not significantly affected by the drug, those of *UHRF1* were significantly reduced in HepG2 cells. These new findings provided further insights into the mechanisms of action of CM-272 and are consistent with previous reports that have demonstrated that the inhibition of epigenetic enzymes activity can induce their destabilization and consequently degradation [113,153].

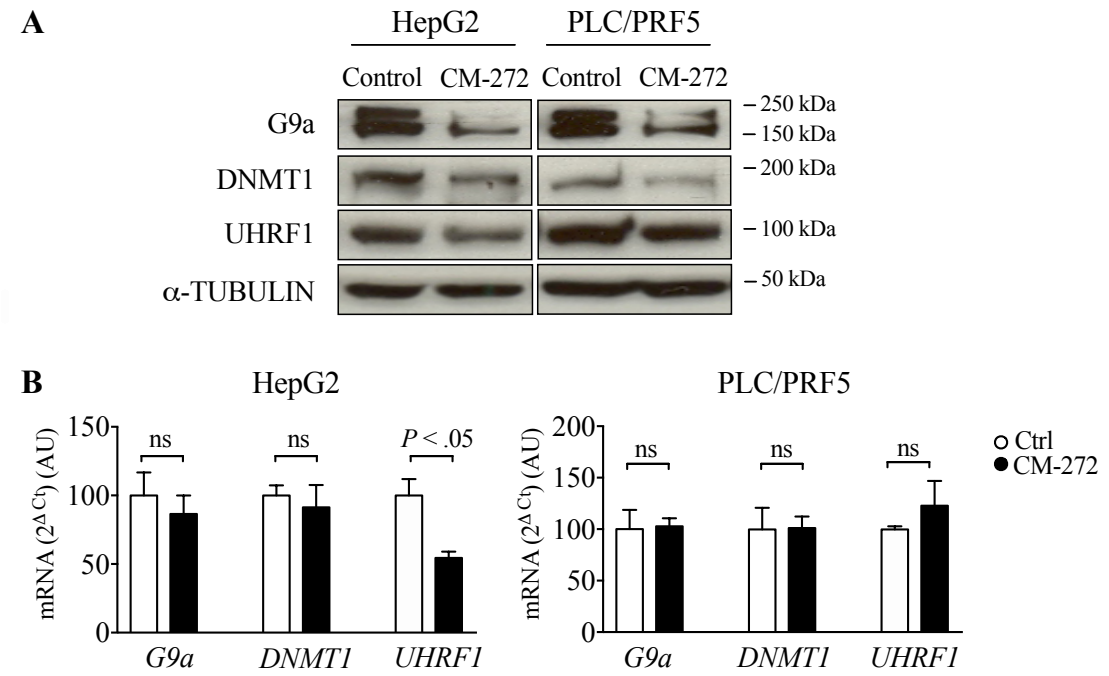

Figure 23. G9a, DNMT1 and UHRF1 levels upon CM-272 in human HCC cells. A) Western blot of G9a, DNMT1 and UHRF1 in HepG2 (left) and PLC/PRF5 (right) cells upon 48 h of CM-272 treatment at its GI_{50} (400 nM). α-TUBULIN western blot is loading control. **B)** *G9a*, *DNMT1* and *UHRF1* mRNA levels in HepG2 (left) and PLC/PRF5 (right) cells upon 48 h of CM-272 treatment at its GI_{50} (400 nM). *H3F3A* was used as reference gene of constitutive expression.

Once we demonstrated the activity and specificity of CM-272 in our cell lines, we tested if CM-272 presented anti-tumoral properties *in vitro*. We performed a colony formation assay on HepG2 and PLC/PLF5 cells, and we could observe a markedly impairment of their clonogenic capacity mediated by CM-272 (Fig. 24).

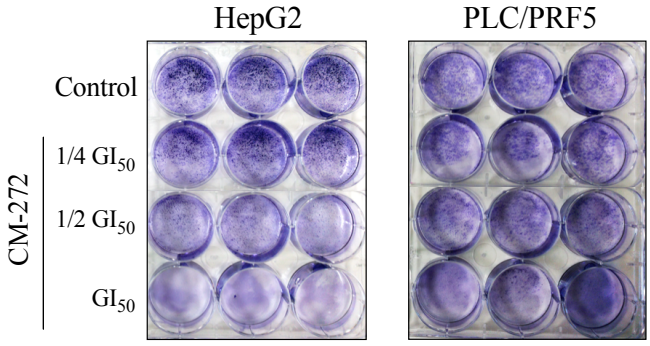

Figure 24. Clonogenic assay in HCC cells treated with CM-272. Representative pictures of the colony formation assay in HepG3 (left) and PLC/PRF5 (right) cells. Treatment was performed at 1/4 GI_{50} (100 nM), 1/2 GI_{50} (200 nM) and GI_{50} (400 nM) concentration for each cell line during 2-3 weeks.

We also evaluated if CM-272 induces either apoptosis and autophagy in HCC cells. Apoptosis was measured by western blot of cleaved Poly (ADP-ribose) polymerase (PARP) (Fig. 25A) and validated by ELISA apoptosis assay (Fig. 25B). We did not observe any trace of apoptosis induction mediated by CM-272 neither in HepG2 nor PLC/PRF5 cells treated at their respective GI_{50} values.

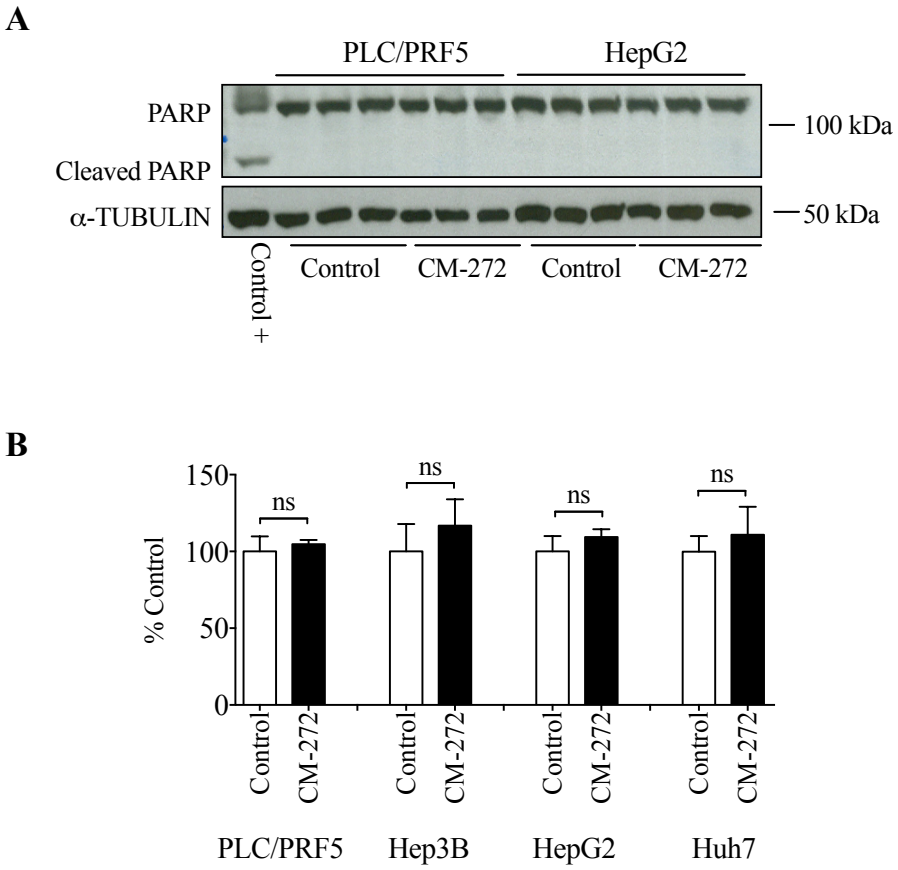

Figure 25. Apoptosis assay in HCC cell lines upon CM-272 treatment. A) Western blot of cleaved PARP in HepG2 and PLC/PRF5 cells after 24 h of treatment with CM-272 at its GI_{50} (400 nM), including a positive control for cleaved PARP. α-TUBULIN western blot is loading control. **B)** ELISA apoptosis assay of HepG2 and PLC/PRF5 cells together with other two HCC cell lines (Hep3B and Huh7) treated at 24 h with CM-272 at its GI_{50} (400 nM except Hep3B at 300 nM).

On the other hand, we assessed autophagy by measuring protein levels of LC3-I and LC3-II using Sorafenib treatment as a positive control in PLC/PRF5, Hep3B and HepG2 cells (Fig. 26). Contrary to the intense autophagy induced by Sorafenib, CM-272 did not show an increase in LC3-I and LC3-II levels.

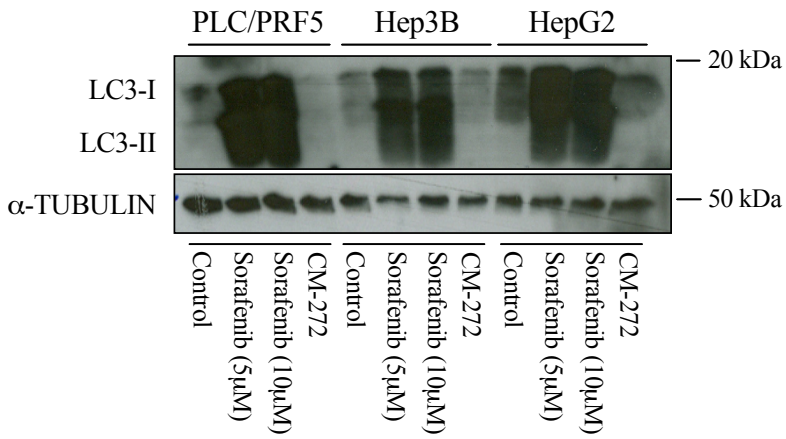

Figure 26. CM-272 does not induce autophagia in human HCC cell lines. Western blot of LC3-I and LC3-II in PLC/PRF5, Hep3B and HepG2 cells after 24 h of treatment with vehicle, Sorafenib (5, 10 μM) or CM-272 at its GI_{50} (all 400 nM except Hep3B at 300 nM). α-TUBULIN western blots is loading control.

As we did not observe increased apoptosis or autophagy mediated by CM-272 we decided to evaluate its potential effects in cell cycle progression (Fig. 27). Surprisingly, we did not find significant effects on cell cycle when HepG2 cells were treated at GI_{50}, but we found an effect of cell cycle arrest when treatment was performed at $2GI_{50}$. The S-phase almost disappeared in these treated cells increasing the percentage of cells arrested in G1 phase. Thus, CM-272 treatment was able to induce cell cycle arrest but this effect was only achieved at higher doses than the GI_{50} concentration.

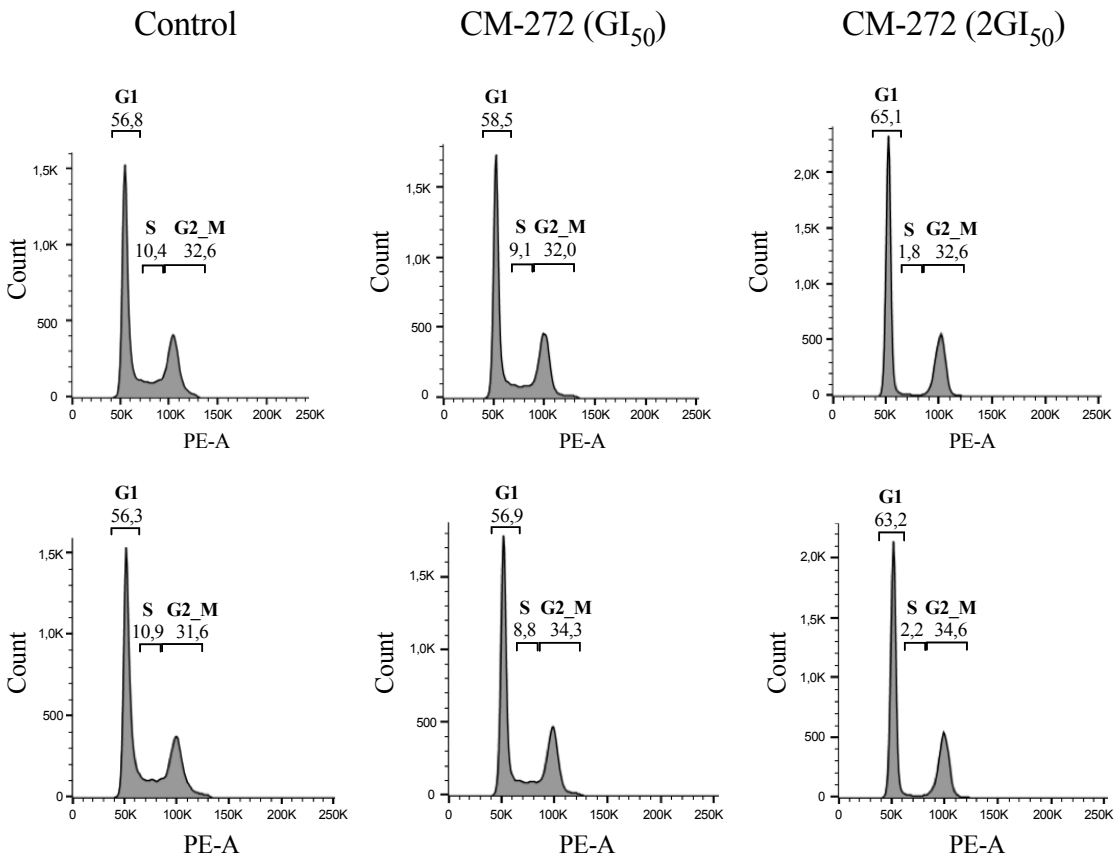

Figure 27. Cell cycle assay of HepG2 cells upon CM-272 treatment. Representative figures of HepG2 cell cycle including the three main cell cycle phases (G1, S and G2_M) after 48 h of treatment of CM-272 at its GI_{50} (400 nM) and $2GI_{50}$ (800 nM).

3. Mechanisms of CM-272 anti-tumoral activity in human HCC cells

We observed that CM-272 presents anti-tumoral properties against human HCC cells *in vitro* reducing its growth and clonogenic capacities, however we did not find evidences that these anti-tumoral properties were mediated by induction of apoptosis or autophagy in HCC cells. Moreover, no strong effect on cell cycle arrest was observed by CM-272. Thereby, to gain insight into the mechanisms of the anti-tumoral effect of CM-272 we performed a microarray analysis of gene expression in HepG2 cells treated at GI_{50} during 48 h. We detected 388 upregulated and 509 downregulated genes compared to controls ($P<0.01$). A representative volcano-plot of the differentially expressed genes can be found in Fig. 28A. To classify these differences in biological categories, GO functional classification of the significantly differentially expressed genes ($P<0.01$) was performed (Fig. 28B). In this study, we identified general categories related to relevant aspects for cancer including regulation of cell growth and proliferation ("growth factor activity" and "cell proliferation"), and interaction with the cellular microenvironment ("response to extracellular stimulus", "regulation of signaling", "blood vessel formation", "regulation of cell communication", "wound healing", "regulation of response to stimulus" and "extracellular space"). This analysis only indicated altered pathways by CM-272 treatment but did not distinguish between those that were activated or inhibited by the treatment. Thereby, microarray gene expression data scrutiny using GSEA was performed to elucidate positive and negative enrichments mediated by CM-272 in numerous pre-established biological pathways. The results revealed very interesting categories summarized in Table 8. Positive enrichments were found in those gene-sets related to anti-tumoral properties such as adhesion and thigh junctions or specific metabolic functions. On the other hand, gene-sets related to common hallmarks of cancer such as cell proliferation, growth factor signaling, metastasis, dedifferentiation, hypoxic response, and interaction with the microenvironment presented negative enrichment in CM-272 treated cells (Table 8). Among these negative enriched gene-sets we found characteristic signatures of more aggressive HCC subclasses, such as the S2 subclass from Hoshida and colleagues [154], and the previously mentioned G1-G3 subgroups identified by Boyault and colleagues [16] (Fig. 28C). These findings reinforce the involvement and correlation of the epigenetic complex G9a-DNMT1 with the malignancy of HCC, as we previously observed that expression levels of the complex in the cohort of

patients were significantly higher in these G1-G3 subgroups. On the other hand, one of the gene-sets with strong positive enrichment encompassed the genes defining the human liver-specific transcriptome, abundant in metabolic genes [155] (Fig. 28C).

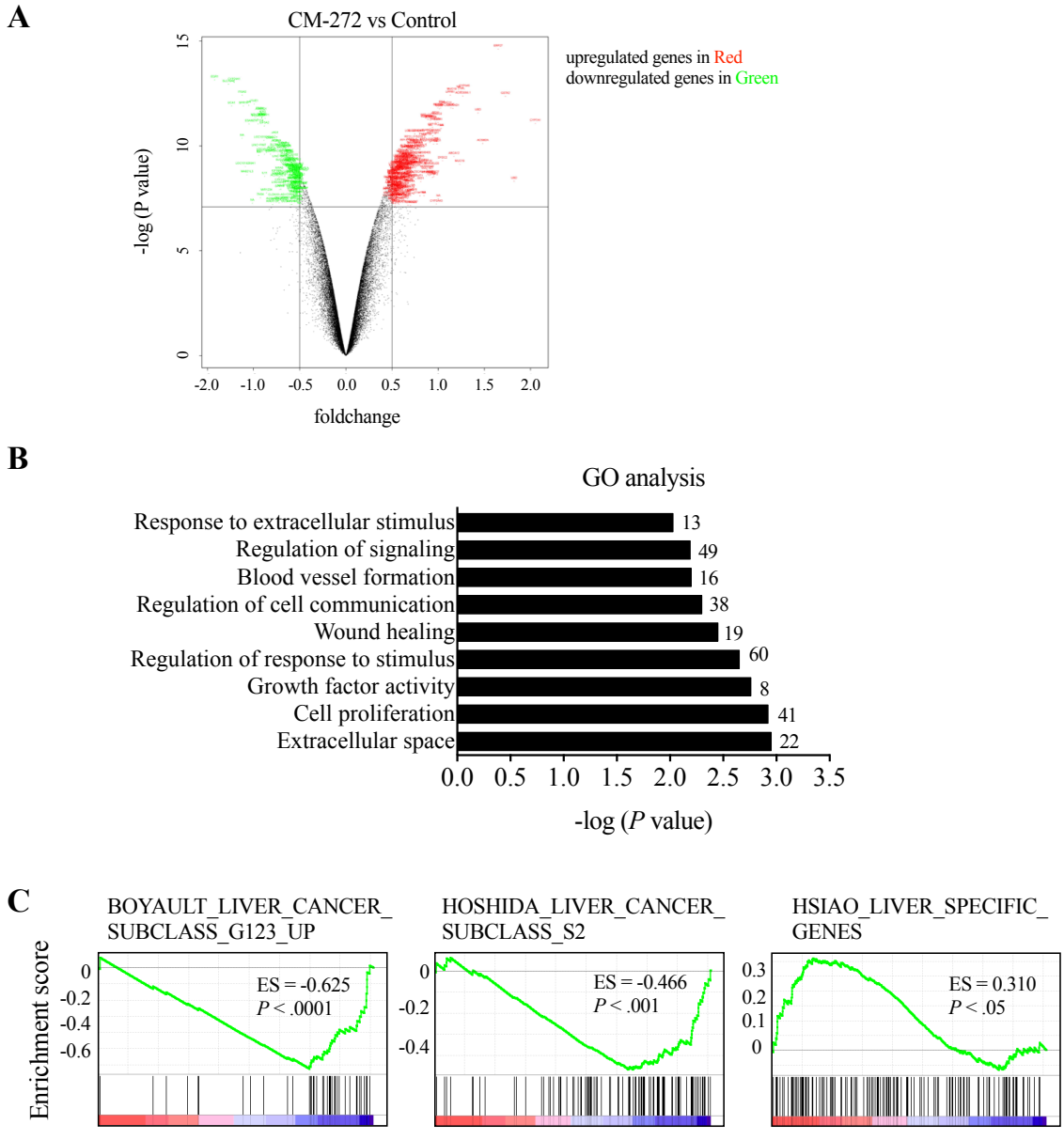

Figure 28. Microarray analysis of gene expression in HepG2 cells treated with CM-272. A) Volcano-plot representation showing the differentially expressed genes after 48 h of CM-272 at GI_{50} (400 nM) in HepG2. **B)** Representative graph of most relevant GO categories of genes undergoing changes in mRNA expression upon CM-272 treatment. **C)** Representative gene-set enrichment plots: negative enriched gene-set plots (subclass G1-G3 defined in Boyault *et al.* dataset and subclass G1-G3 defined in Hoshida *et al.* dataset) and positive enriched gene-set plot (liver-specific genes defined in Hsiao *et al.* dataset) upon CM-272 treatment.

Table 8. GSEA of target gene-sets regulated by CM-272 in HepG2 cells.

Enrichment in phenotype: na_POS		
Liver healthy & Liver cáncer		
GSEA	**Systematic name**	**NOM p-val**
HSIAO_LIVER_SPECIFIC_GENES	M13283	0.020
OHGUCHI_LIVER_HNF4A_TARGETS_UP	M2193	0.024
SERVITJA_LIVER_HNF1A_TARGETS_DN	M2398	0.012
CHIANG_LIVER_CANCER_SUBCLASS_UNANNOTATED_UP	M19610	0.034
CHIANG_LIVER_CANCER_SUBCLASS_INTERFERON_DN	M14353	0.017
LEE_LIVER_CANCER	M3879	0.063
LEE_LIVER_CANCER_DENA_UP	M16524	0.05
CHIANG_LIVER_CANCER_SUBCLASS_INTERFERON_UP	M16141	0.061
CHIANG_LIVER_CANCER_SUBCLASS_CTNNB1_DN	M8689	0.053
ACEVEDO_LIVER_TUMOR_VS_NORMAL_ADJACENT_TISSUE_DN	M13014	0.002
YAMASHITA_LIVER_CANCER_STEM_CELL_DN	M9206	0.016
Down regulation of cancer marks		
GSEA	**Systematic name**	**NOM p-val**
ZUCCHI_METASTASIS_DN	M16826	0.009
JAEGER_METASTASIS_DN	M10702	0.004
BOQUEST_STEM_CELL_DN	M1578	0.0
JECHLINGER_EPITHELIAL_TO_MESENCHYMAL_TRANSITION_DN	M1417	0.0
AMIT_DELAYED_EARLY_GENES	M10550	0.006
ENGELMANN_CANCER_PROGENITORS_DN	M9246	0.002
AZARE_NEOPLASTIC_TRANSFORMATION_BY_STAT3_DN	M2311	0.020
SARRIO_EPITHELIAL_MESENCHYMAL_TRANSITION_DN	M11513	0.0
GRAHAM_NORMAL_QUIESCENT_VS_NORMAL_DIVIDING_UP	M4406	0.008
RAFFEL_VEGFA_TARGETS_DN	M2358	0.025
LOPEZ_MESOTELIOMA_SURVIVAL_TIME_DN	M5899	0.014
MCBRYAN_PUBERTAL_TGFB1_TARGETS_DN	M1125	0.028
LABBE_TARGETS_OF_TGFB1_AND_WNT3A_DN	M1843	0.008
Adhesion & Thigh junctions		
GSEA	**Systematic name**	**NOM p-val**
ONDER_CDH1_TARGETS_3_DN	M11790	0.010
ONDER_CDH1_TARGETS_2_DN	M4306	0.0
KEGG_CELL_ADHESION_MOLECULES_CAMS	M16476	0.023

Table 8. GSEA of target gene-sets regulated by CM-272 in HepG2 cells. (*Continuation*)

Metabolism		
	Systematic name	**NOM p-val**
REACTOME_GLUCONEOGENESIS	M13748	0.83
KEGG_FOLATE_BIOSYNTHESIS	M2220	0.783
KEGG_GLYCINE_SERINE_AND_THREONINE_METABOLISM	M766	0.211
Enrichment in phenotype: na_NEG		
Cell Cycle and Proliferation		
GSEA	**Systematic name**	**NOM p-val**
CHIANG_LIVER_CANCER_SUBCLASS_PROLIFERATION_UP	M3268	0.0
BENPORATH_PROLIFERATION	M2114	0.0
REACTOME_CELL_CYCLE_CHECKPOINTS	M16647	0.0
REACTOME_DNA_REPLICATION	M1017	0.0
KEGG_CELL_CYCLE	M7963	0.001
LEE_LIVER_CANCER_SURVIVAL_DN	M7987	0.0
SCIAN_CELL_CYCLE_TARGETS_OF_TP53_AND_TP73_DN	M9402	0.011
GRAHAM_NORMAL_QUIESCENT_VS_NORMAL_DIVIDING_DN	M5198	0.00
ZHANG_PROLIFERATING_VS_QUIESCENT	M16992	0.057
FIRESTEIN_PROLIFERATION	M5354	0.022
REACTOME_CELL_CYCLE_MITOTIC	M5336	0.0
EGUCHI_CELL_CYCLE_RB1_TARGETS	M4455	0.001
TGFβ signaling		
GSEA	**Systematic name**	**NOM p-val**
REACTOME_DOWNREGULATION_OF_SMAD2_3_SMAD4_TRANSCRIPTIONAL_ACTIVITY	M669	0.0
REACTOME_TGF_BETA_RECEPTOR_SIGNALING_ACTIVATES_SMADS	M646	0.001
REACTOME_DOWNREGULATION_OF_TGF_BETA_RECEPTOR_SIGNALING	M628	0.001
REACTOME_SIGNALING_BY_TGF_BETA_RECEPTOR_COMPLEX	M1041	0.0
SARRIO_EPITHELIAL_MESENCHYMAL_TRANSITION_UP	M4288	0.0
KARAKAS_TGFB1_SIGNALING	M17300	0.007
KOINUMA_TARGETS_OF_SMAD2_OR_SMAD3	M2356	0.0
REACTOME_TRANSCRIPTIONAL_ACTIVITY_OF_SMAD2_SMAD3_SMAD4_HETEROTRIMER	M665	0.005
PID_SMAD2_3PATHWAY	M228	0.016
BIOCARTA_TGFB_PATHWAY	M18933	0.029
CHANG_CORE_SERUM_RESPONSE_DN	M5793	0.007
PID_TGFBR_PATHWAY	M286	0.029
KARLSSON_TGFB1_TARGETS_DN	M2081	0.007

Table 8. GSEA of target gene-sets regulated by CM-272 in HepG2 cells. (*Continuation*)

Metastasis & EMT & Cell adhesion		
GSEA	**Systematic name**	**NOM p-val**
ROESSLER_LIVER_CANCER_METASTASIS_DN	M2545	0.011
GOTZMANN_EPITHELIAL_TO_MESENCHYMAL_TRANSITION_DN	M1376	0.0
SUNG_METASTASIS_STROMA_UP	M9483	0.006
CHANDRAN_METASTASIS_UP	M16036	0.0
TOMLINS_METASTASIS_DN	M7090	0.048
ZUCCHI_METASTASIS_UP	M14951	0.05
PID_ECADHERIN_NASCENT_AJ_PATHWAY	M156	0.01
Differentiation & Cancer signature		
GSEA	**Systematic name**	**NOM p-val**
RICKMAN_TUMOR_DIFFERENTIATED_WELL_VS_MODERATELY_UP	M7141	0.012
RICKMAN_TUMOR_DIFFERENTIATED_MODERATELY_VS_POORLY_UP	M15672	0.038
LIU_COMMON_CANCER_GENES	M18694	0.002
Liver cancer subclass		
GSEA	**Systematic name**	**NOM p-val**
BOYAULT_LIVER_CANCER_SUBCLASS_G123_UP	M13831	0.0
BOYAULT_LIVER_CANCER_SUBCLASS_G3_UP	M18436	0.0
CHIANG_LIVER_CANCER_SUBCLASS_UNANNOTATED_DN	M10986	0.0
IIZUKA_LIVER_CANCER_PROGRESSION_G1_G2_DN	M16374	0.0
HOSHIDA_LIVER_CANCER_SUBCLASS_S2	M7995	0.001
YAMASHITA_LIVER_CANCER_WITH_EPCAM_UP	M16542	0.0
WANG_RECURRENT_LIVER_CANCER_UP	M10922	0.001
CAIRO_HEPATOBLASTOMA_CLASSES_UP	M4772	0.0
PATIL_LIVER_CANCER	M1195	0.0
ACEVEDO_LIVER_CANCER_UP	M15709	0.0
KUROKAWA_LIVER_CANCER_CHEMOTHERAPY_DN	M11545	0.001
CAIRO_HEPATOBLASTOMA_UP	M14601	0.0
BOYAULT_LIVER_CANCER_SUBCLASS_G1_UP	M14146	0.005
MIDORIKAWA_AMPLIFIED_IN_LIVER_CANCER	M1065	0.027
SMITH_LIVER_CANCER	M18761	0.031
ACEVEDO_LIVER_TUMOR_VS_NORMAL_ADJACENT_TISSUE_UP	M4950	0.0
Hypoxia		
GSEA	**Systematic name**	**NOM p-val**
MANALO_HYPOXIA_DN	M18562	0.0
JIANG_HYPOXIA_CANCER	M7547	0.025

Table 8. GSEA of target gene-sets regulated by CM-272 in HepG2 cells. (*Continuation*)

KRIEG_HYPOXIA_NOT_VIA_KDM3A	M2469	0.0
JIANG_HYPOXIA_VIA_VHL	M2522	0.039
JIANG_HYPOXIA_NORMAL	M3996	0.0
GROSS_HYPOXIA_VIA_ELK3_UP	M1303	0.017
BIOCARTA_HIF_PATHWAY	M13324	0.013
KRIEG_HYPOXIA_NOT_VIA_KDM3A	M2469	0.0
JIANG_HYPOXIA_VIA_VHL	M2522	0.039
JIANG_VHL_TARGETS	M18850	0.002
GROSS_HYPOXIA_VIA_ELK3_UP	M1303	0.017
MIKHAYLOVA_OXIDATIVE_STRESS_RESPONSE_VIA_VHL_UP	M2263	0.141
Angiogenesis		
GSEA	**Systematic name**	**NOM p-val**
HU_ANGIOGENESIS_DN	M18833	0.015
PID_VEGFR1_2_PATHWAY	M237	0.030
WESTON_VEGFA_TARGETS_6HR	M1521	0.074
Metabolism		
GSEA	**Systematic name**	**NOM p-val**
KEGG_PYRUVATE_METABOLISM	M7934	0.003
CHEN_LIVER_METABOLISM_QTL_CIS	M1947	0.030
PENG_GLUCOSE_DEPRIVATION_DN	M7970	0.028
REACTOME_REGULATION_OF_PYRUVATE_DEHYDROGENASE_PDH_COMPLEX	M716	0.213
REACTOME_SIGNALING_BY_INSULIN_RECEPTOR	M1021	0.043
Growth factor signaling & Microenvironment		
GSEA	**Systematic name**	**NOM p-val**
NAKAMURA_CANCER_MICROENVIRONMENT_DN ST_INTEGRIN_SIGNALING_PATHWAY	M2427	0.002
PID_ERBB1_INTERNALIZATION_PATHWAY	M214	0.0
PID_IL2_PI3K_PATHWAY	M143	0.004
PID_IL1_PATHWAY	M110	0.0
STEIN_ESRRA_TARGETS_RESPONSIVE_TO_ESTROGEN_DN	M19002	0.007
REACTOME_SIGNALING_BY_EGFR_IN_CANCER	M563	0.016
REACTOME_SIGNALING_BY_PDGF	M2049	0.040
REACTOME_PLATELET_ADHESION_TO_EXPOSED_COLLAGEN	M9450	0.031
Histone/DNA remodeling		
GSEA	**Systematic name**	**NOM p-val**
KAMMINGA_EZH2_TARGETS	M1486	0.0

Table 8. GSEA of target gene-sets regulated by CM-272 in HepG2 cells. (*Continuation*)

NUYTTEN_EZH2_TARGETS_DN	M17122	0.0
NUYTTEN_NIPP1_TARGETS_DN	M18090	0.0
MISSIAGLIA_REGULATED_BY_METHYLATION_DN	M6866	0.0
ZHONG_RESPONSE_TO_AZACITIDINE_AND_TSA_DN	M3988	0.001
LIANG_SILENCED_BY_METHYLATION_DN	M6302	0.007
MARIADASON_REGULATED_BY_HISTONE_ACETYLATION_DN	M1552	0.032
NUYTTEN_EZH2_TARGETS_UP	M4196	0.0

All the findings from the microarray gene expression led us to think that enhanced G9a-DNMT1 complex activity in HCC could contribute to the growth of tumor cells and to their interaction with extracellular milieu, but also evidenced their strong negative impact on the expression of metabolic genes characteristic of the differentiated hepatocyte.

We observed some potential functions were G9a and DNMT1 could be involved as their molecular inhibition by CM-272 altered these biological pathways. Many of these functions have been already described in other type of tumors. However, we also observed novel biological pathways where the enzymatic complex might be playing a relevant role in the context of HCC development that also could be extrapolated to other pathologies.

We validated a wide panel of differentially expressed genes by qPCR in three independent experiments. A selection of relevant genes down-regulated by CM-272 in HepG2 cells is represented in Fig. 29A including the genes: Kruppel Like Factor 5 (*KLF5*), EPH receptor A2 (*EPHA2*), PIN2/TERF1-interacting telomerase inhibitor 1 (*PINX1*) and transforming growth factor beta-1 (*TGFβ1*). The negative effect on the expression of these genes mediated by CM-272 was also validated by siRNA specific for G9a (Fig. 29B). These genes represent malignant markers of cancer cells commonly overexpressed in many different cancers including HCC [57,156–158]. The capability of CM-272 to revert their aberrant over-expression demonstrated an anti-tumoral mechanism of this molecule.

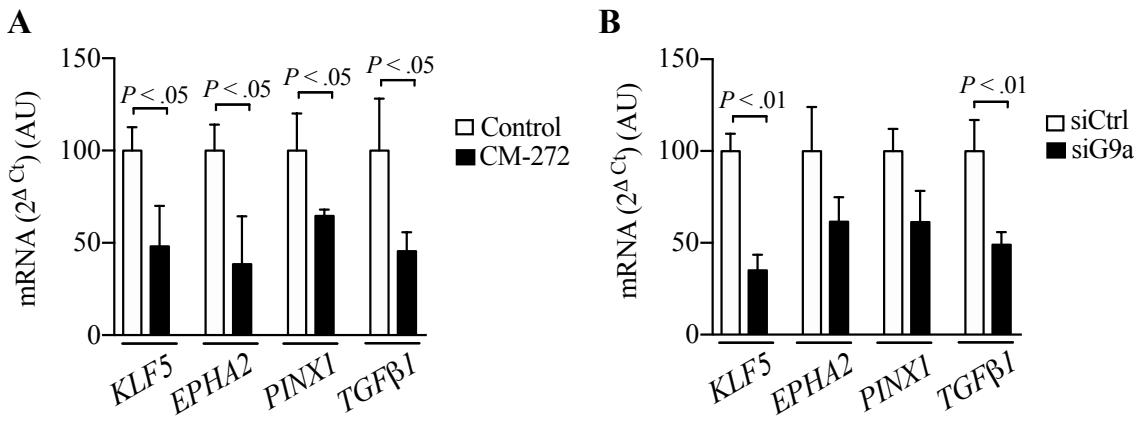

Figure 29. Down-regulation of malignant markers of cancer cells by CM-272 treatment and specific siRNA for *G9a* in HepG2 cells. qRT-PCR of *KLF5, EPHA2, PINX1* and *TGFβ1* in HepG2 cells after **A)** 48 h of CM-272 treatment at its GI_{50} (400 nM) or **B)** 48 h of either siCtrl or siG9a transfection (siCtrl: control siRNA; siG9a: *G9a* specific siRNA). *H3F3A* was used as reference gene of constitutive expression.

On the other hand, the effects observed in the microarray analysis on genes associated with adhesion and thigh junctions, and consequently with non-metastatic phenotypes [24,159] were corroborated by Gap Junction Protein Gamma 3 (*GJC3*), Hepatic And Glial Cell Adhesion Molecule (*HEPACAM*) and Tight Junction Protein 3 (*TJP3*) mRNA up-regulation mediated by CM-272 (Fig. 30A) and also validated by siG9a in HepG2 cells (Fig. 30B).

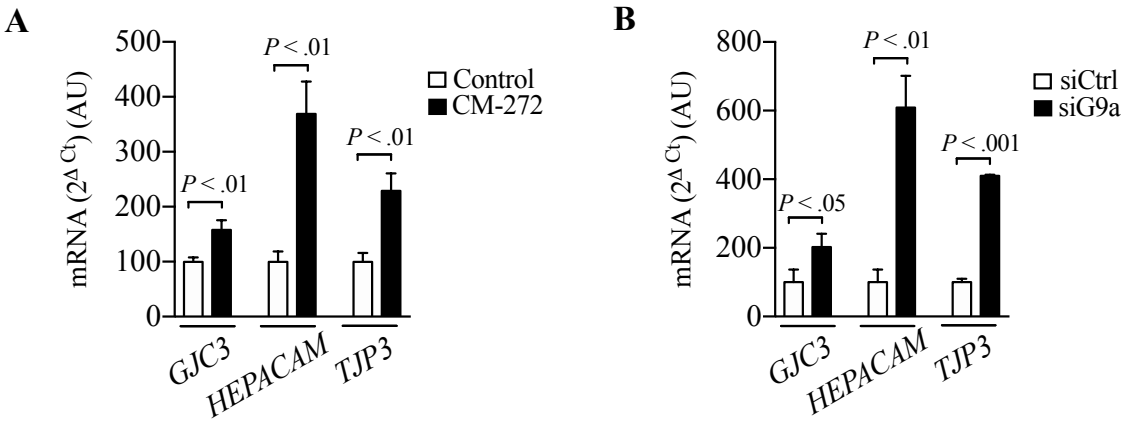

Figure 30. Up-regulation of genes associated to adhesion and thigh junctions by CM-272 treatment and specific siRNA for *G9a* in HepG2 cells. qRT-PCR of *GJC3*, *HEPACAM* and *TJP3* in HepG2 cells after **A)** 48 h of CM-272 treatment at its GI_{50} (400 nM) or **B)** 48 h of either siCtrl or siG9a transfection (siCtrl: control siRNA; siG9a: *G9a* specific siRNA). *H3F3A* was used as reference gene of constitutive expression.

From these results we concluded that anti-tumoral mechanisms of dual targeting of G9a and DNMT1 with our molecule could be assessed either by inhibiting or inducing the expression of pro-tumorigenic or anti-tumorigenic genes, respectively. More interesting for us, and in addition to general anti-tumoral mechanisms of CM-272, we observed relevant mechanisms of our molecule specifically in the context of liver disease and HCC. We found that treatment of HepG2 cells with CM-272 resulted in the mRNA up-regulation of liver-specific genes (Fig. 31A) and their protein levels (Fig. 31B) whose expression is lost during HCC development and are critical markers of the disease. These are, the epithelial marker CDH1 whose relevance in HCC is well documented [160] and the enzymes CYP7A1, FBP1, GNMT, MAT1A, all involved in key liver metabolic functions [28,161]. The positive effect on the expression of these genes mediated by CM-272 was validated by siRNA specific for *G9a* (Fig. 31C).

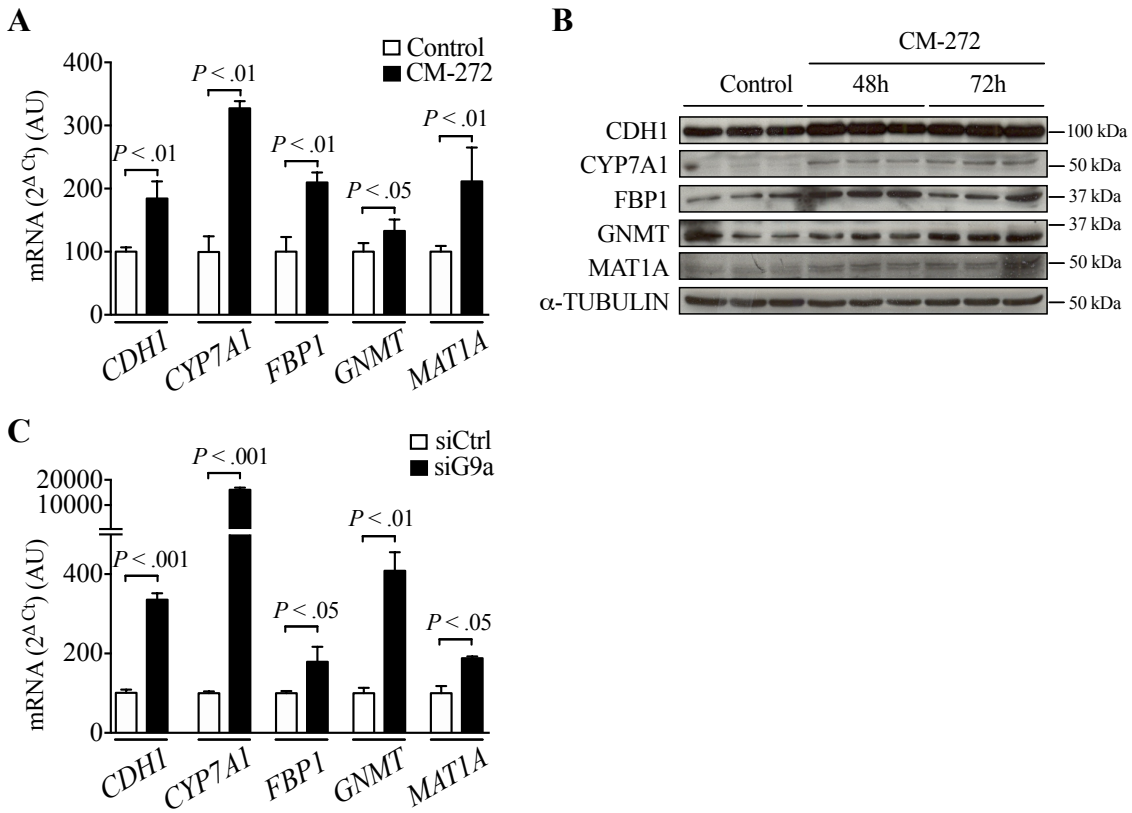

Figure 31. CM-272 strongly influences HCC cells gene expression promoting a quiescent and differentiated phenotype. mRNA expression **A)** and protein levels **B)** of CDH1, CYP7A1, FBP1, GNMT and MAT1A are increased upon 48 h of CM-272 treatment at GI_{50} (400 nM) in HepG2 cells. α-TUBULIN western blot is loading control. **C)** The effect on mRNA expression is validated by siRNA specific for *G9a*. Cells were transfected with siRNAs (siCtrl: control siRNA; siG9a: *G9a* specific siRNA) during 72 h. *H3F3A* was used as reference gene of constitutive expression.

In order to demonstrate that these expression changes mediated by CM-272 are, at least in part, a consequence of its G9a inhibitory activity we performed ChIP using a specific antibody against H3K9me2. Resulting qChIP analyses showed a decrease in the levels of this epigenetic mark in *CYP7A1*, *FBP1* and *GNMT* gene promoters upon CM-272 treatment in HepG2 cells (Fig. 32).

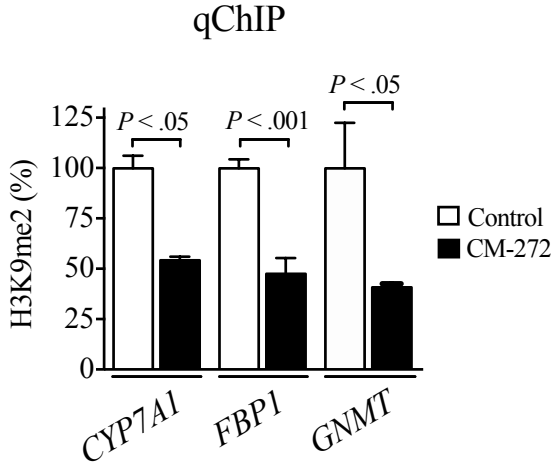

Figure 32. CM-272 treatment reduces H3K9me2 levels at the promoter regions of *CYP7A1*, *FBP1* and *GNMT* in HepG2 cells. qChIP analysis reveals a fall of the epigenetic mark H3K9me2 in *CYP7A1*, *FBP1* and *GNMT* gene promoters in HepG2 cells after 48 h of treatment with CM-272 at its GI_{50} (400 nM).

As was explained in the introduction, promoter hypermethylation and the consequent mRNA downregulation of tumor suppressor genes is a common hallmark of cancer including HCC and it is the most studied epigenetic event in hepatocarcinogenesis. Due to the potent inhibitory effect of CM-272 over DNMTs, we expected that this compound would be able to up-regulate the expression of genes that are aberrantly silenced by hypermethylation. To test this, we performed an experiment of HepG2 and PLC/PRF5 cells after CM-272 treatment during several days at indicated doses. Simultaneously, Decitabine was used as a control of demethylating agent. In this experiment, we first studied the mRNA levels of *RASSF1A*, as it is one of the most frequently hypermethylated genes in HCC. We observed that both CM-272 and Decitabine treatments were able to induce the expression of this gene in HCC cells, being CM-272 even more efficient (Fig. 33A). After this observation, isolated DNA from cells was subjected to bisulfite conversion and MSP was performed over specific promoter region previously described in *RASSF1A* [162]. Both products obtained in the MSP assay (the unmethylated-specific

PCR and the methylated-specific PCR) from each sample were loaded on a gel to test for the presence or absence of specific bands and their intensity.

DNA methylation levels of *RASSF1A* upon CM-272 treatment were found decreased in both HepG2 and PLCR/PRF5 cells (Fig. 33B). In HepG2 cells the hypermethylation of this region was not total as we detected a specific band from the unmethylated-PCR product in control cells. However, there was an increase in the intensity of this band upon CM-272 treatment and also after Decitabine treatment. In the case of PLC/PRF5 cells, the result was more evident, as there was no specific band in the unmethylated-PCR product in control cells while an intense band appeared upon CM-272 or Decitabine treatment.

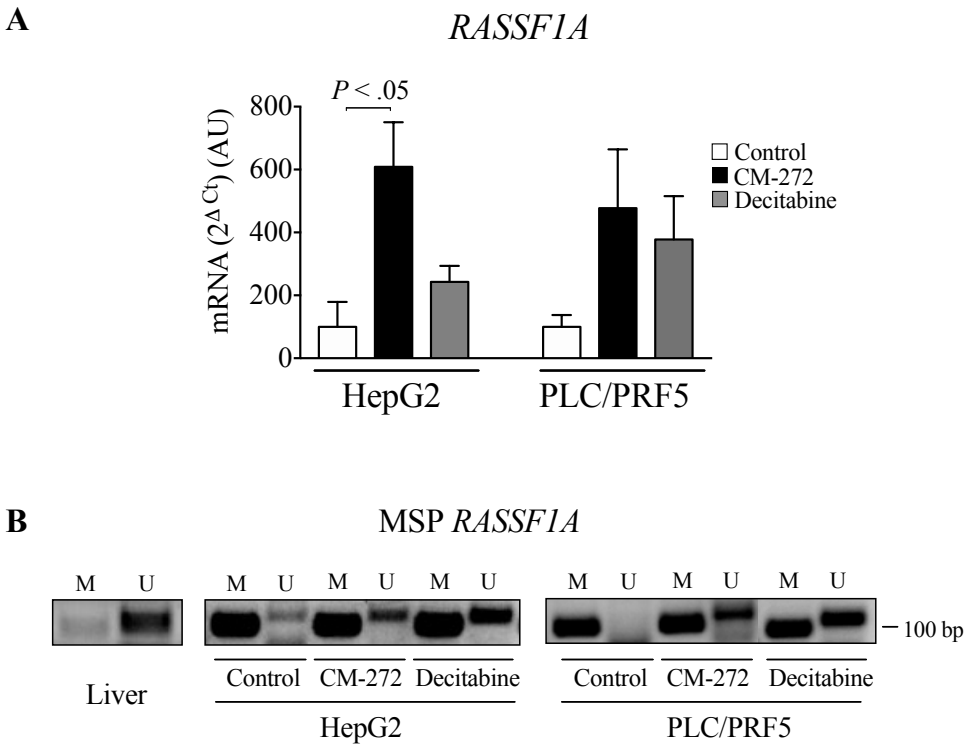

Figure 33. *RASSF1A* mRNA induction and promoter demethylation upon CM-272 treatment in HCC cells. A) mRNA expression levels of *RASSF1A* in HepG2 and PLC/PRF5 cells after CM-272 treatment (1/2 GI_{50}: 200 nM; 4 days and 3 days respectively). *H3F3A* was used as reference gene of constitutive expression. **B)** MSP of *RASSF1A* promoter region in HepG2 (left) and PLC/PRF5 (right) cells after CM-272 treatment (1/2 GI_{50}: 200 nM; 4 days and 3 days respectively). Human liver tissue MSP product is loaded has a control of demethylated specific PCR band. Decitabine treatment (5 μM) is used as a control of demethylation activity.

Once we studied the effects of CM-272 on *RASSF1A* gene methylation and expression, we focused our studies on *FBP1* regulation. It was recently reported that *FBP1* expression in HCC is lost by promoter hypermethylation [37]. Due to the fact that *FBP1* expression is transcriptionally regulated by G9a (Fig. 32), we decided to study the DNA methylation levels in the same promoter region where we observed CM-272-mediated H3K9me2 downregulation, to evaluate if this gene could be simultaneously co-regulated by G9a and DNA methylation events. We designed MSP primers that cover a CpG -enriched region in the *FBP1* promoter (ANNEX 1). When we performed the MSP analysis after CM-272 treatment in HepG2 cells, we observed DNA demethylation of *FBP1* (Fig. 34A). No specific band was observed in the unmethylated-PCR product in control cells while a specific band appeared upon CM-272 or Decitabine treatment. To corroborate this result, we performed a pyrosequencing analysis that demonstrated a consistent fall in DNA methylation levels at this region (Fig. 34B). All cytosines within CG dinucleotides were demethylated in treated cells compared to control cells.

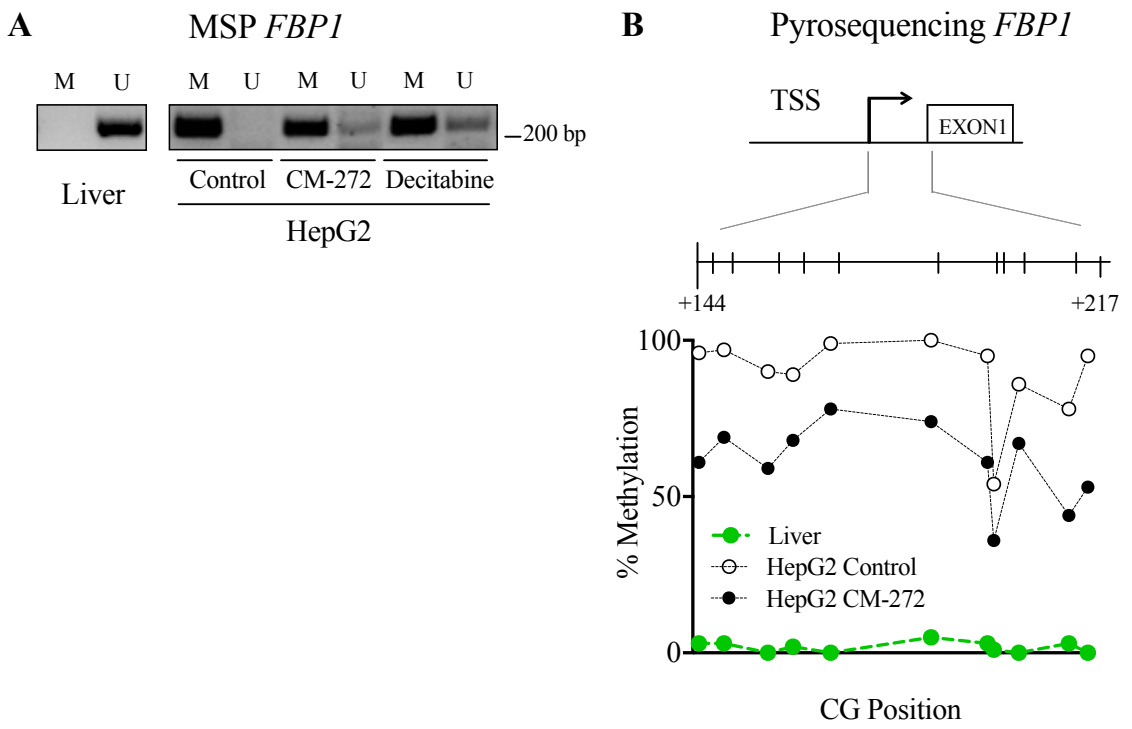

Figure 34. Demethylation effect on DNA promoter region of *FBP1* upon CM-272 treatment in human HCC cells. A) MSP of *FBP1* promoter region in HepG2 cells after 4 days of CM-272 treatment at 1/2 GI_{50} (200 nM). Human liver tissue MSP product is loaded as a control of demethylated specific PCR band. Decitabine treatment (5μM) is used as a control of demethylation activity. **B)** Pyrosequencing analysis of *FBP1* promoter DNA methylation status in HepG2 after treatment by CM-272 (1/2 GI_{50}: 200 nM; 4 days). Human liver tissue pyrosequencing was performed as a control of demethylated *FBP1* promoter.

These results demonstrated an important epigenetic regulation of *FBP1* in HCC cells modulated by CM-272 treatment, and suggested that *FBP1* expression might be co-regulated by our epigenetic complex of interest. The relevance of these results also lies in the fact that FBP1 is one key gene for the development of CLD and HCC. *FBP1* encodes a rate limiting enzyme in gluconeogenesis and is emerging as a TSG in HCC. Due to its biological relevance in the progression of the disease we decided to extrapolate our studies to our cohort of patients. We first corroborated its downregulation in tumor samples compared to normal tissues (Fig. 35A). After that, we directly analyzed the correlation between *FBP1* expression and the molecular and clinical characteristics of tumor aggressiveness (5 gene score, G1-G6 classification, macroscopic vascular invasion, Edmonson grade and TNM score) that we previously found to be correlated with the expression of *G9a*, *DNMT1* and *UHRF1* (Fig. 12A). Very interestingly, we observed an inverse association with those subclasses and clinical features that positively correlated with *G9a*, *DNMT1* and *UHRF1* expression (Fig. 35B). In other words, *FBP1* expression was found significantly lower in HCC samples classified as poor prognostic group (P2), in those within groups G1-G3, and in patients with more advanced Edmonson grades and TNM stages. *FBP1* expression trended to be also lower in tissues from patients displaying macrovascular invasion although it did not reach statistical significance.

In view of all this, we also studied the correlation between *FBP1* expression and the expression of our epigenetic enzymes of interest. Interestingly, we found a statistically significant negative correlation between *FBP1* and *G9a* or *UHRF1* mRNA levels in our set of HCC samples, and a similar trend with *DNMT1* mRNA levels (Fig. 35C). These results pointed out to a strong association between *FBP1* expression and the epigenetic complex G9a-DNMT1-UHRF1, with a translational link with clinical features of HCC. It also highlights the possible therapeutic benefits of the simultaneous inhibition of G9a and DNA methylation in the context of HCC.

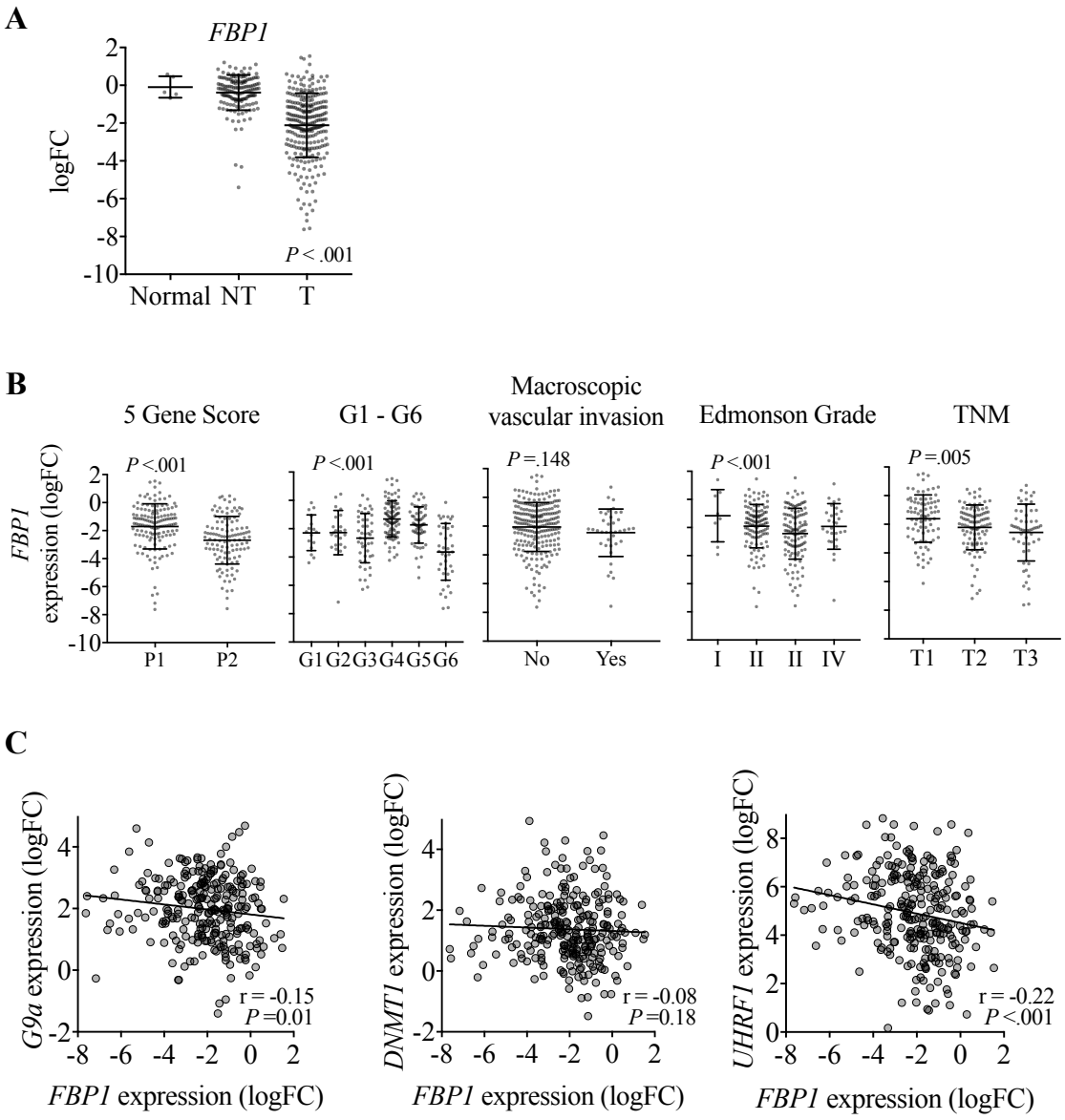

Figure 35. *FBP1* downregulation in HCC patients is inversely associated with worse HCC phenotypes and negatively correlated with *G9a*, *DNMT1* and *UHRF1* expression. A) *FBP1* mRNA levels in normal, NT and T human liver tissues. **B)** *FBP1* gene expression in tumoral liver tissues from patients classified according to the 5-gene score, the G1 to G6 transcriptomic groups, the presence of macroscopic vascular invasion, the Edmonson Grade and the TNM score. **C)** Spearman correlation analysis of *FBP1* expression with that of *G9a*, *DNMT1* and *UHRF1* in tumoral liver tissue samples. *18S* was used as reference gene of constitutive expression.

It is known that reduced *FBP1* expression stimulates tumor progression by enhancing glucose metabolism to lactate. As a readout of the restoration of *FBP1* levels in HepG2 cells by CM-272 treatment, we decided to measure glucose consumption (Fig. 36A) and

lactate production (Fig. 36B). The results demonstrated a CM-272-mediated impairment of glucose uptake and lactate secretion of the cells.

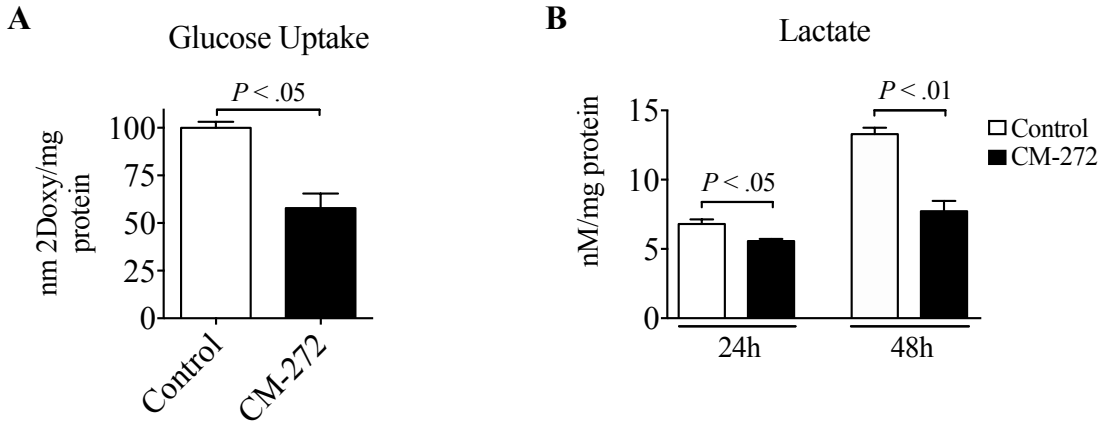

Figure 36. CM-272 impairs the glycolytic pathway in human HCC cells. A) Glucose (2-deoxyglucose) uptake in control and CM-272 treated HepG2 cells (48 h). **B)** Lactate production in control and CM-272 treated HepG2 cells (24 and 48 h). Both experiments were treated at GI_{50} (400 nM) of CM-272 and data were normalized with total protein levels. Experiments were performed twice in triplicates.

4. CM-272 inhibits the growth and metabolic adaptation of HCC cells to hypoxia.

In view of the relevance of hypoxia in the context of hepatocarcinogenesis, we decided to perform several experiments in this context. It was recently found that G9a protein levels are increased in several tumor cells when exposed to hypoxic conditions, and that this increase corresponded to an elevation of the global levels of H3K9me2 [163]. We evaluated the protein levels of G9a in various human HCC cell lines subjected them to a hypoxic environment (1% O_2), and in all cases we observed an increase in the G9a protein levels (Fig. 37).

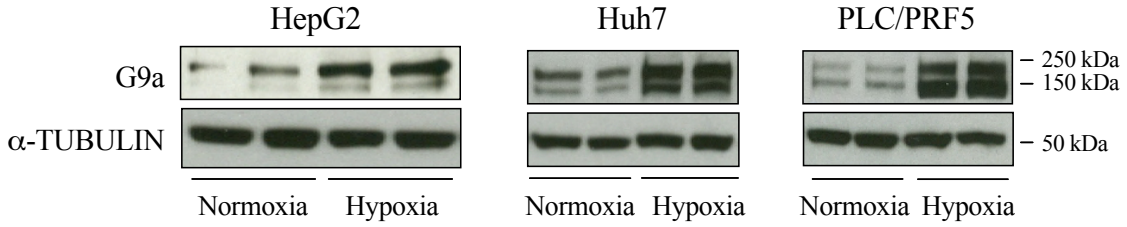

Figure 37. G9a protein levels are stabilized in human HCC cells under hypoxic environment. Western blot of G9a in HepG2, Huh7 and PLC/PRF5 cells under 24 h of hypoxic environment (1% O_2). α-TUBULIN western blots are loading controls.

Testing the anti-tumoral properties of CM-272 under this environmental condition, we found that the hypoxia-stimulated growth of HepG2 and PLC/PRF5 HCC cells was markedly reduced upon treatment (Fig. 38A). This effect was reproduced in HepG2 cells after *G9a* expression knockdown (Fig. 38B). At this point, and as a complementary approach, we examined the effects of transient overexpress *G9a* overexpression in HepG2 cells. Conversely, *G9a* overexpression enhanced hypoxia-stimulated proliferation of HepG2 cells (Fig. 38C).

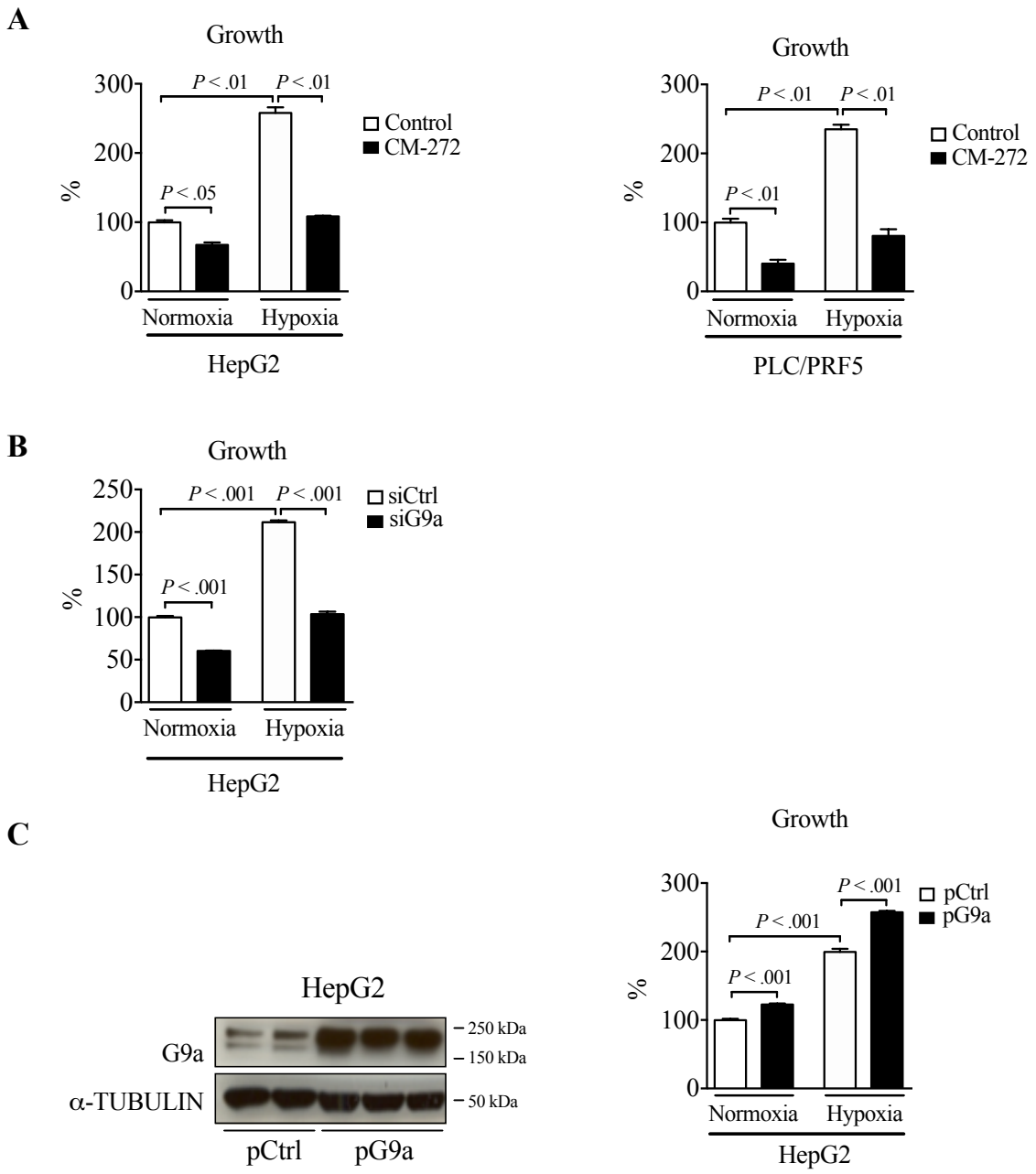

Figure 38. CM-272 or siG9a-mediated growth inhibition and pG9a-mediated growth increase of hypoxia-stimulated HCC cells. A) Effect of CM-272 (GI_{50}: 400 nM) on hypoxia-induced HepG2 and PLCR/PRF5 cells growth. Cells were pre-treated with CM-272 for 24 h and then kept in normoxic or hypoxic conditions (1% O_2) for another 24 h. **B)** Effect of silencing *G9a* on hypoxia-induced HepG2 cells growth. **C)** Left panel: validation of *G9a* overexpression in HepG2 cells by western blot of G9a. α-TUBULIN western blot is a loading control. Right panel: effect of overexpressing *G9a* on hypoxia-induced HepG2 cells growth. Cells were transfected with siRNAs (siCtrl: control siRNA; siG9a: *G9a* specific siRNA) or plasmids (pCtrls: empty pEGFP; pG9a: *G9a* expression plasmid pEGFP) 24 h prior to being kept in normoxic or hypoxic conditions (1% O_2) for another 24 h.

One of the most relevant pathways exacerbated by the pro-tumorigenic hypoxic environment in HCC is glycolysis. Dysregulated metabolic pathways under hypoxia play a relevant role in the pathogenesis of HCC. Thereby, we decided to evaluate the effects of CM-272 on the expression of key glycolytic enzymes triggered by hypoxia and upregulated in HCC: *GLUT1, HK2*, glucose-6-phosphate isomerase (*GPI*), *ALDOA*, *PGK1*, pyruvate kinase-M2 (*PKM2*) and *LDHA*. The overexpression of all these genes was markedly reduced upon CM-272 treatment under hypoxia (Fig. 39A) and consistently lactate production was inhibited in HepG2 cells (Fig. 39B). The effect of CM-272 on the mRNA expression levels of these glycolytic enzymes was reproduced upon *G9a* expression knockdown (Fig. 39C). Interestingly, *G9a* overexpression enhanced this hypoxia-stimulated mRNA expression in the same cell line (Fig. 39D).

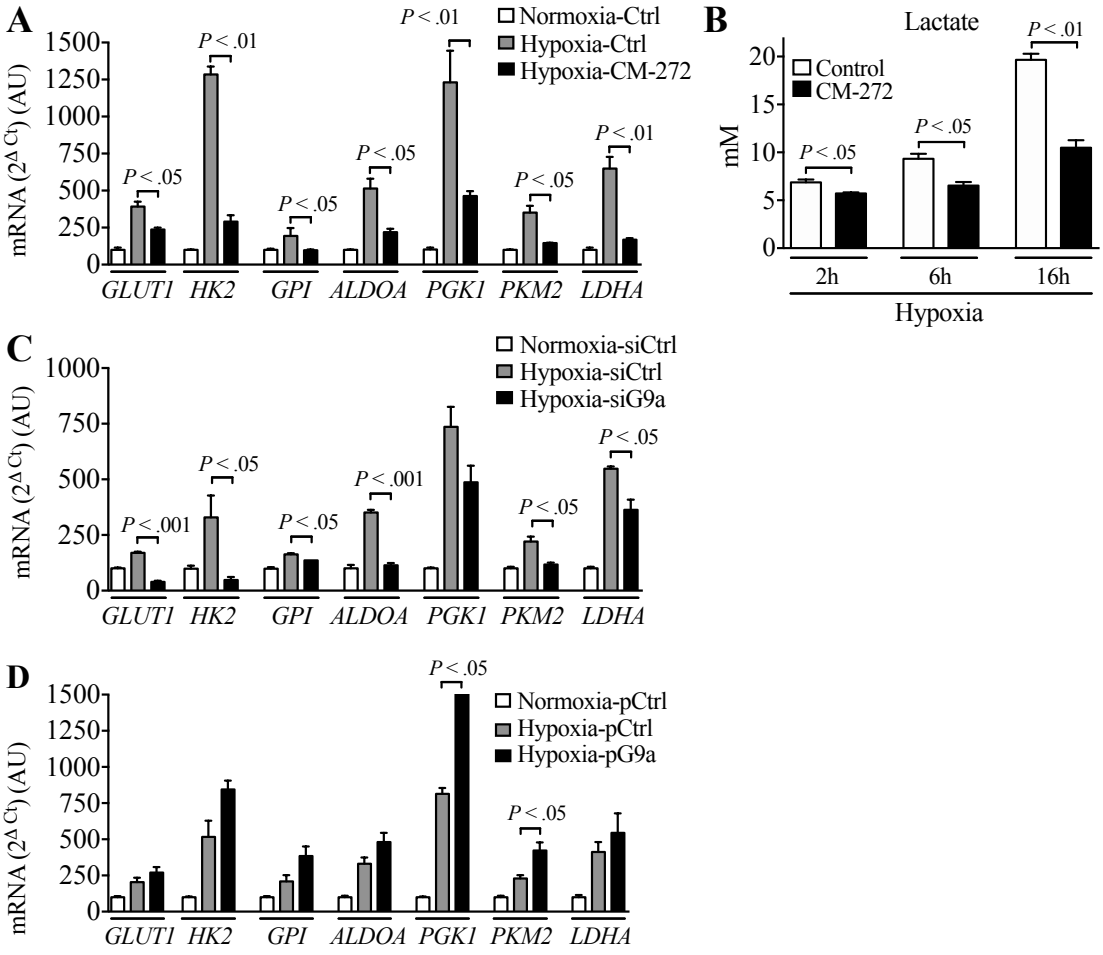

Figure 39. G9a inhibition impairs the hypoxia-stimulated overexpression of glycolytic enzymes in HCC cells whereas G9a overexpression enhances this hypoxia-mediated expression regulation. A) Effect of CM-272 (GI_{50}: 400 nM) on hypoxia-induced glycolytic genes mRNA expression in HepG2 cells. Cells were pre-treated with CM-272 for 24 h and then kept in normoxic or hypoxic conditions (1% O_2) for

another 24h. **B)** Effect of CM-272 (GI_{50}: 400 nM) on lactate production in HepG2 cells under hypoxia (1% O_2) during indicated times. Effect of transiently silencing **C)** or overexpression **D)** of *G9a* on hypoxia-induced glycolytic genes in HepG2 cells. Cells were transfected with siRNAs (siCtrl: control siRNA; siG9a: *G9a* specific siRNA) or plasmids (pCtrls: empty pEGFP; pG9a: *G9a* expression plasmid pEGFP) 24 h prior to being kept in normoxic or hypoxic conditions (1% O_2) for another 24 h. *H3F3A* was used as reference gene of constitutive expression.

Being the serine-glycine synthesis pathway a glycolysis-diverting pathway, and because G9a is implicated in its regulation, we analyzed the expression of the most relevant enzymes involved in this pathway: phosphoglycerate dehydrogenase (*PHGDH*), phosphoserine aminotransferase 1 (*PSAT1*) and serine hydroxymethyltransferase 2 (*SHMT2*) in HepG2 cells under normoxia and hypoxia upon CM-272 treatment. We observed that CM-272 treatment is able to reduce the expression of these enzymes, demonstrating an impairing of their up-regulation when subjected to hypoxia and being able to reduce theirexpression also under normal oxygen levels (Fig. 40A). Opposite results were found when *G9a* was transiently overexpressed under hypoxia (Fig. 40B). Based on these results we could confirm the relevant role of G9a in the hypoxic-adaptive metabolic regulation of HCC cells, and the fact that this adaptation can be blocked by CM-272 treatment.

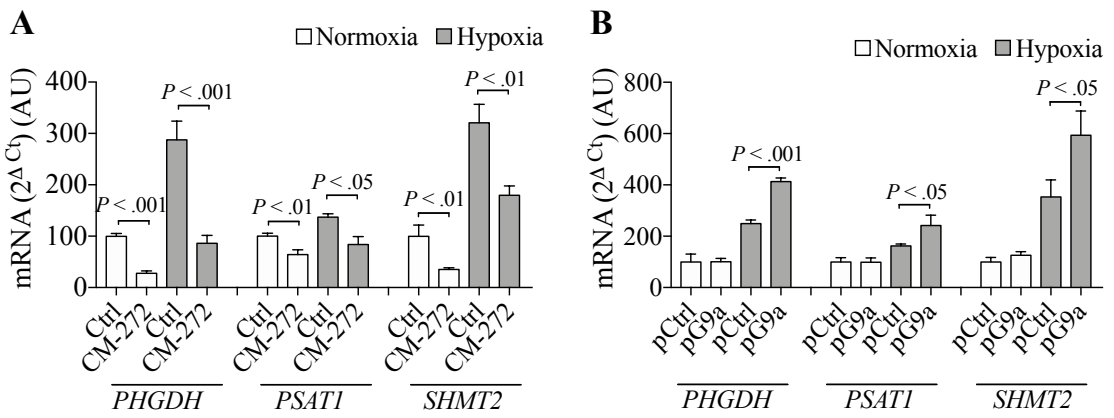

Figure 40. CM-272 impairs the overexpression of serine-synthesis pathway enzymes in HCC cells (either in normoxia or hypoxia), whereas G9a overexpression enhances this hypoxia-mediated expression regulation. A) Effect of CM-272 (GI_{50}: 400 nM) or **B)** *G9a* overexpression on mRNA expression of serine-synthesis pathway enzymes genes in HepG2 cells. Cells were pre-treated with CM-272 or transfected with plasmids (pCtrls: empty pEGFP; pG9a: *G9a* expression plasmid pEGFP) for 24 h prior to being kept in normoxic or hypoxic conditions (1% O_2) for another 24 h. *H3F3A* was used as reference gene of constitutive expression.

Hypoxia also fosters HCC development through the stimulation of angiogenesis and liver fibrosis. We evaluated the effects of CM-272 on the expression of the pro-angiogenic and pro-fibrogenic factors *VEGF* and *TGFβ1*. We found that CM-272 treatment significantly inhibited hypoxia-triggered *VEGF* and *TGFβ1* expression (Fig. 41). And once again, the effect of CM-272 on the mRNA expression of these genes was reproduced by silencing *G9a*, while *G9a* overexpression exerted the opposite effect (Fig. 41).

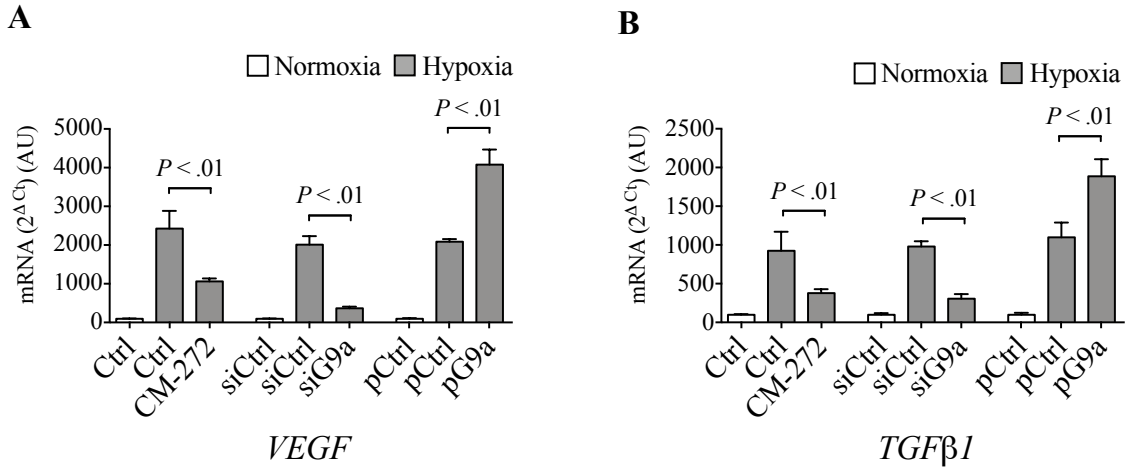

Figure 41. G9a inhibition impairs pro-angiogenic and pro-fibrogenic signals in HCC cells. CM-272 and silencing *G9a* block the increased expression of pro-angiogenic and pro-fibrogenic genes under hypoxia in HepG2 cells, whereas *G9a* overexpression reinforce their up-regulation. Cells were pre-treated with CM-272 (GI_{50}: 400 nM) or transfected with siRNAs (siCtrl: control siRNA; siG9a: *G9a* specific siRNA) or plasmids (pCtrls: empty pEGFP; pG9a: *G9a* expression plasmid pEGFP) for 24 h prior to being kept in normoxic or hypoxic conditions (1% O_2) for another 24 h.

All these results showed a relevant pro-tumorigenic role for G9a in the context of hypoxia adaptation of HCC cells, and that this response is impaired by CM-272 treatment. G9a inhibition by CM-272 was able to reduce the enhanced glycolysic and serine-glycine synthetic pathways triggered by low oxygen tension in HCC cell lines. It also reduced pro-angiogenic and pro-fibrogenic signals relevant for HCC development and the tumor microenvironment. Little is known about the mechanisms underlying G9a activity in hypoxia adaptive responses. As we observed that G9a inhibition altered the expression of genes involved in different but related pathways, we proposed that G9a might interfere with the master regulator of gene expression HIF1α. As preliminary data on this hypothesis we observed that CM-272 treatment was able to impair the stabilization of

HIF1α under hypoxia in HepG2 cells (Fig. 42). Further studies are necessary to understand these mechanism. However, they allowed us to better understand that HepG2 cells treated with CM-272 displayed impaired adaptive responses when subjected to a hypoxic environment.

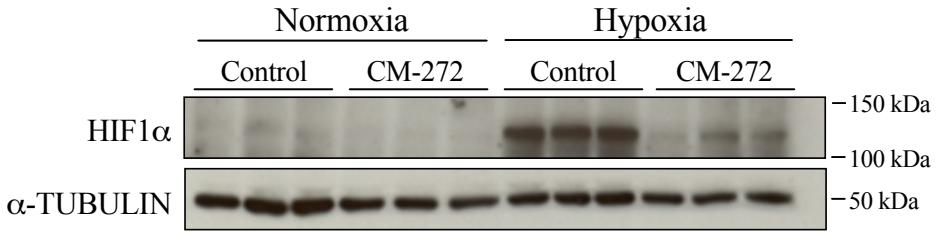

Figure 42. Impairment of hypoxia-mediated stabilization of HIF1α in HCC cells upon CM-272 treatment. Western blot of HIF1α of HepG2 cells after CM-272 treatment (GI_{50}; 400 nM) for 24 h prior to being kept in normoxic or hypoxic conditions (1% O_2) for another 24 h. α-TUBULIN western blot is a loading control.

5. CM-272 inhibits the proliferation and activation of human hepatic stellate cells and induces a more quiescent phenotype

Epigenetic enzymes play a critical role in the transformation from a quiescent to an activated state of HSCs upon fibrogenic stimuli. As was described in the introduction, the fibrotic stroma plays a critical role in HCC development. We observed that CM-272 mediates the inhibition of *TGFβ1* and *VEGF* expression in HCC cells (Fig. 41). The impairment of the up-regulation of these genes suggested an anti-tumoral mechanism targeting the tumor stroma crosstalk and prompted us to examine CM-272 effects on HSCs. We found that CM-272 dose-dependently inhibited the proliferation of the human hepatic stellate cell line LX2, showing a GI_{50} of 400 nM (Fig. 43A). Moreover, we observed that CM-272 induced apoptosis in these cells upon CM-272 treatment at its GI_{50} dose (Fig. 43B).

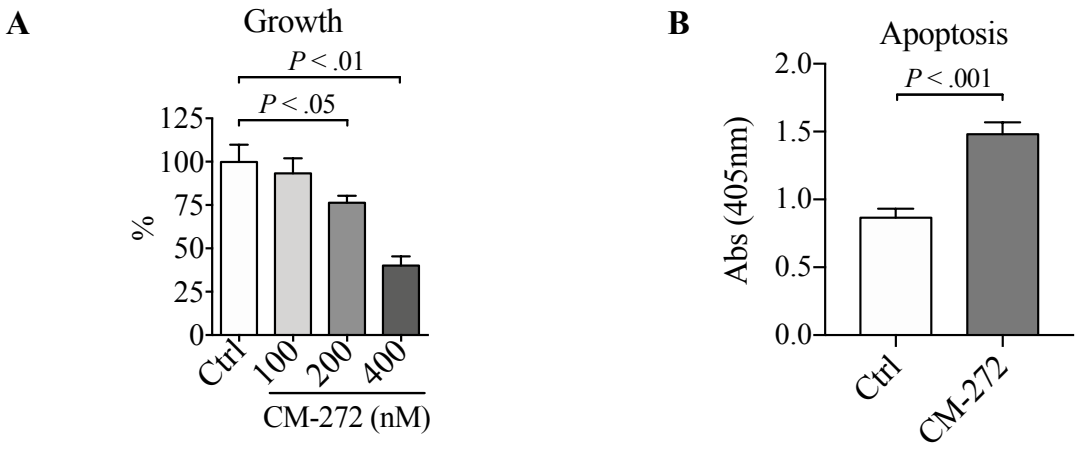

Figure 43. CM-272 reduces LX2 proliferation in a dose-dependently manner and induces apoptosis. **A)** Dose-dependently effect on LX2 cells viability after CM-272 treatment at 100, 200 and 400 nM during 48 h. **B)** ELISA apoptosis assay of LX2 cells treated at 24 h with CM-272 at its GI_{50} (400 nM).

To better understand the effects of CM-272 in liver fibrogenic cells we performed a microarray analysis of gene expression in LX2 cells. We detected 1549 upregulated and 1702 downregulated genes (P<0.01) (Fig. 44A), and GO functional classification fundamentally identified categories related to HSC metabolic differentiation ("response to vitamin A" and "response to retinoic acid") and their response to activating stimuli, and microenvironment ("response to wounding", "cell activation", "response to

decreased oxygen levels", "signaling", "response to extracellular stimulus", "regulation of kinase activity" and "response to nutrient") (Fig. 44B). Accordingly, when we applied GSEA we found significant enrichment in categories associated with metabolic functions, signal transduction and cell proliferation (Table 9). Particularly interesting was the positive enrichment in genes of the KEGG Retinol Metabolism gene-set, and the negative enrichment in genes from the Signaling by TGFβ Receptor Complex Reactome gene-set (Fig. 44C), that suggested that CM-272 treatment induces cells to maintain a more quiescent state, less responsive to external stimuli.

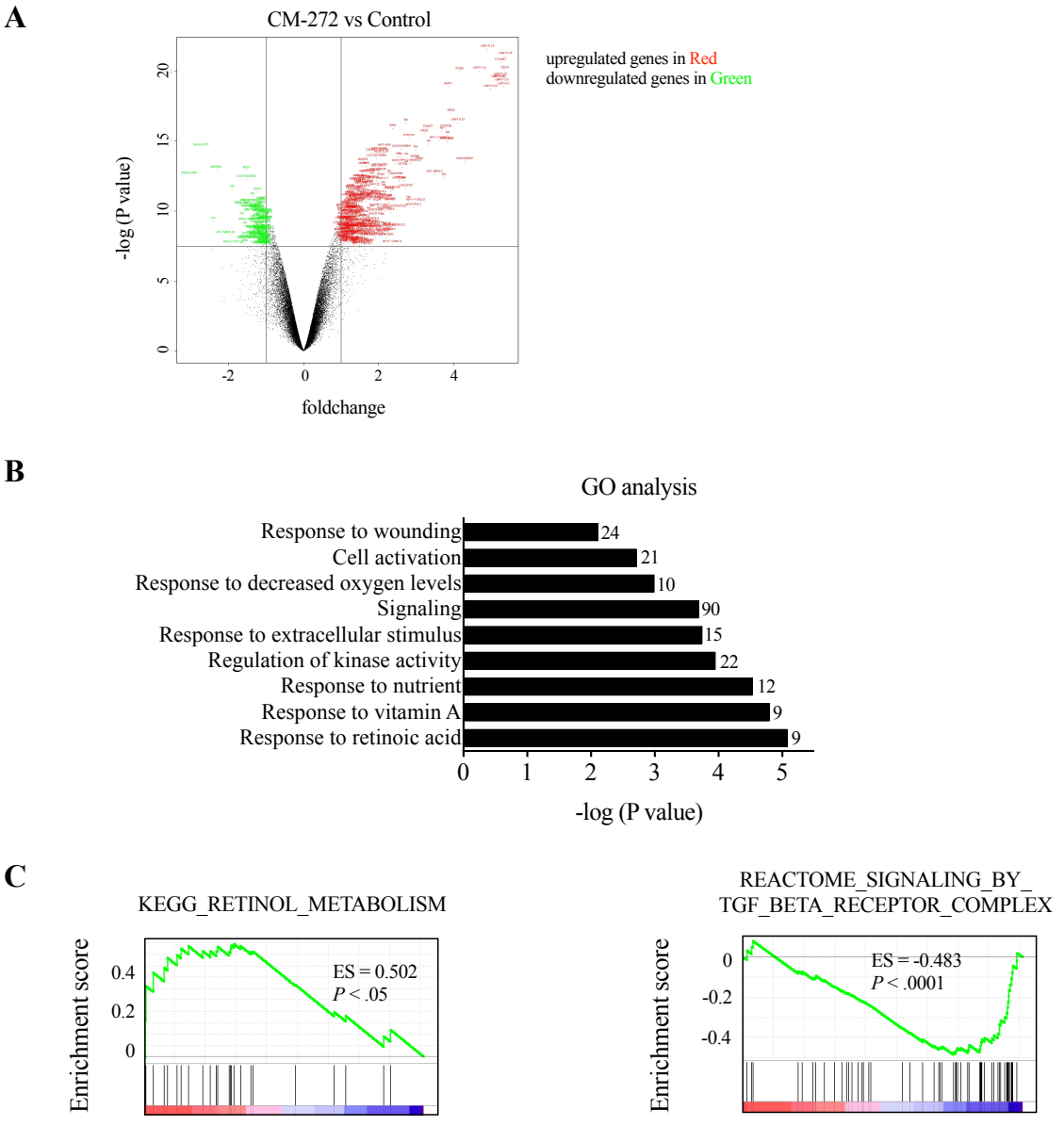

Figure 44. Microarray analysis of gene expression in LX2 cells treated with CM-272. A) Volcano-plot representation showing the differentially expressed genes after 48 h of CM-272 (GI_{50}: 400 nM) treatment in LX2. **B)** Representative graph of most relevant GO categories of genes undergoing changes in mRNA

expression. **C))** Representative gene-set enrichment plots: positive enriched gene-set plot (genes defined in retinol metabolism KEGG dataset) and negative enriched gene-set plot (genes defined in signaling by TGFβ receptor complex Reactome dataset) upon CM-272 treatment.

Table 9. GSEA of target gene-sets regulated by CM-272 in LX2 cells.

Enrichment in phenotype: na_POS		
Lipid and retinol metabolism		
GSEA	**Systematic name**	**NOM p-val**
KEGG_ARACHIDONIC_ACID_METABOLISM	M5410	0.000
PID_NFAT_TFPATHWAY	M60	0.001
BIOCARTA_RARRXR_PATHWAY	M6907	0.002
KEGG_LINOLEIC_ACID_METABOLISM	M2920	0.007
PID_ATF2_PATHWAY	M166	0.004
REACTOME_NUCLEAR_RECEPTOR_TRANSCRIPTION_PATHWAY	M8276	0.022
KEGG_RETINOL_METABOLISM	M9488	0.045
Enrichment in phenotype: na_NEG		
Growth factor signaling and cell proliferation		
GSEA	**Systematic name**	**NOM p-val**
REACTOME_DOWNREGULATION_OF_SMAD2_3_SMAD4_TRANSCRIPTIONAL_ACTIVITY	M669	0.000
REACTOME_TGF_BETA_RECEPTOR_SIGNALING_ACTIVATES_SMADS	M646	0.005
REACTOME_G1_S_TRANSITION	M17283	0.000
PID_PDGFRB_PATHWAY	M186	0.000
REACTOME_SIGNALING_BY_TGF_BETA_RECEPTOR_COMPLEX	M1041	0.000
PID_NFKAPPAB_CANONICAL_PATHWAY	M37	0.005
REACTOME_DOWNREGULATION_OF_TGF_BETA_RECEPTOR_SIGNALING	M628	0.006
REACTOME_SIGNALING_BY_HIPPO	M591	0.002
REACTOME_SIGNALING_BY_HIPPO	M665	0.005
REACTOME_REGULATION_OF_AMPK_ACTIVITY_VIA_LKB1	M19104	0.014
BIOCARTA_HIF_PATHWAY	M13324	0.020
BIOCARTA_IGF1MTOR_PATHWAY	M16991	0.027
PID_WNT_CANONICAL_PATHWAY	M90	0.017
REACTOME_SIGNALING_BY_CONSTITUTIVELY_ACTIVE_EGFR	M559	0.023
PID_TNF_PATHWAY	M128	0.014

Upregulation of genes associated with a quiescent and diferentited status of HSCs, such as *PPARγ*, BMP-activin membrane-bound inhibitor (*BAMBI*) and *LRAT* was validated in CM-272 treataed LX2 cells (Fig. 45). Moreover, we had the opportunuty to corroborate these results in primary hHSCs isolated from patients (Fig. 45).

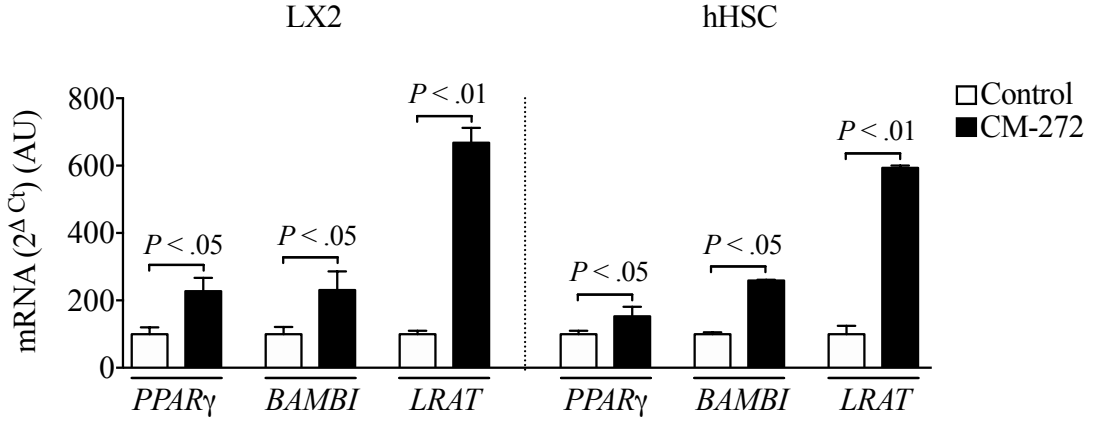

Figure 45. CM-272 strongly influences LX2 cells gene expression promoting a quiescent and differentiated phenotype. mRNA differentially expressed *PPARγ BAMBI* and *LRAT* genes after 48 h of CM-272 (400 nM) treatment in LX2 and hHSC cells. *H3F3A* was used as reference gene of constitutive expression.

As was explained in the introduction, PPARγ has a relevant role in maintaining the quiescent phenotyoe of HSCs, and its downregulation is crucial during the transdifferentation process. It was previously described that *PPARγ* expression can be negatively regulated by DNA methylation [164] and G9a HMT activity [165] in its promoter. Thereby, we postulated that CM-272 might be interfering with both epigenetic events in the promoter of these genes, leading to mRNA up-regulation. We first demonstrated that CM-272 treatment in LX2 cells was able to reduce H3K9me2 levels in a critical promoter region [165]. After that, we studied the DNA methylation status of a CpG-enriched region downstream from the sequence where we observed a fall in H3K9me2 levels (Fig. 46A). We designed MSP primers that cover that region (ANNEX 2), also coinciding with an already described hypermethylated area of the *PPARγ* promoter [164]. When we cheked the DNA methylation status after CM-272 treatment of LX2, we observed a strong demethylation of this region (Fig. 46B). Furthermore, an intense specific band apperaed after CM-272 and Decitabine treatment in the unmethylated-PCR product assay. All these

results indicated that G9a and DNMTs activities might play a role in the inhibition of the expression of genes associated with the quiescent status during the transdiferentation process. The upregulation of *PPARγ* expression by targeting G9a and DNMTs with CM-272 suggested a novel therapeutic approach to quell fibrogenic events.

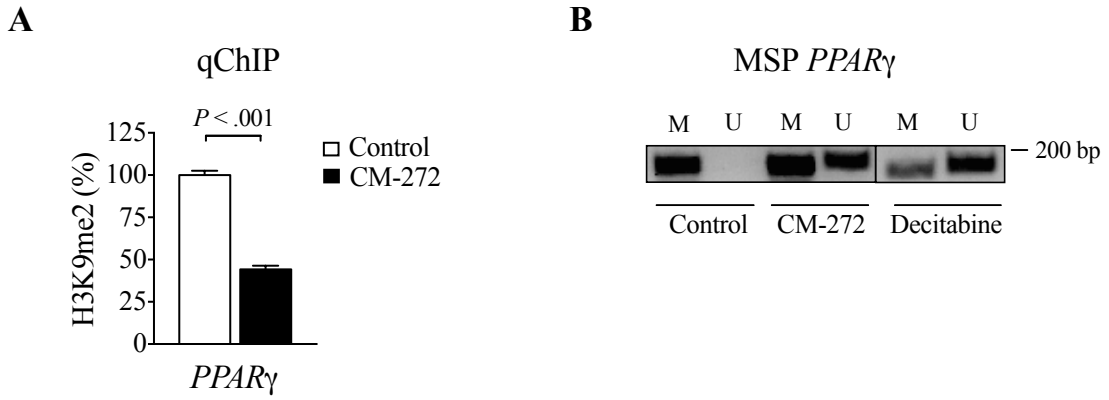

Figure 46. CM-272-mediated downregulation of H3K9me2 and DNA methylation levels of *PPARγ* promoter in LX2 cells. A) qChIP analysis reveal a fall of the epigenetic mark H3K9me2 in *PPARγ* gene promoter in LX2 cells after 48 h of CM-272 treatment (1/2 GI_{50}: 200 nM). **B)** MSP of *PPARγ* promoter region in LX2 cells after CM-272 (1/4 GI_{50}: 100 nM) treatment during 3 days. Decitabine treatment is used as a control of demethylation activity.

There are few studies on HSCs metabolic reprogramming during transdiferentation [166]. Alterations in HSC metabolism occur rapidly during their transdiferentation. Activated stellate cells become highly proliferative and show increased glycolytic activity. Significant increase in expression of glycolytic enzymes and glucose and lactate transporters with coincident downregulation of genes involved in gluconeogenesis have been reported [166]. Chen and colleagues demonstrated that *FBP1* transcripts fall by 90% during the initial 48 h in culture of primary HSC and remain extremely low at day 7. Due to our intertest in the *FBP1* gene in the context of hepatocarcinogenesis we decided tu evaluate the status of this gene in LX2 cells upon CM-272 treatment. Consistently, we observed that CM-272 strongly induced the expression of this gene (Fig. 47A) concomitantly with a reduction in the H3K9me2 (Fig. 47B) and DNA methylation levels in its promoter (Fig. 47C).

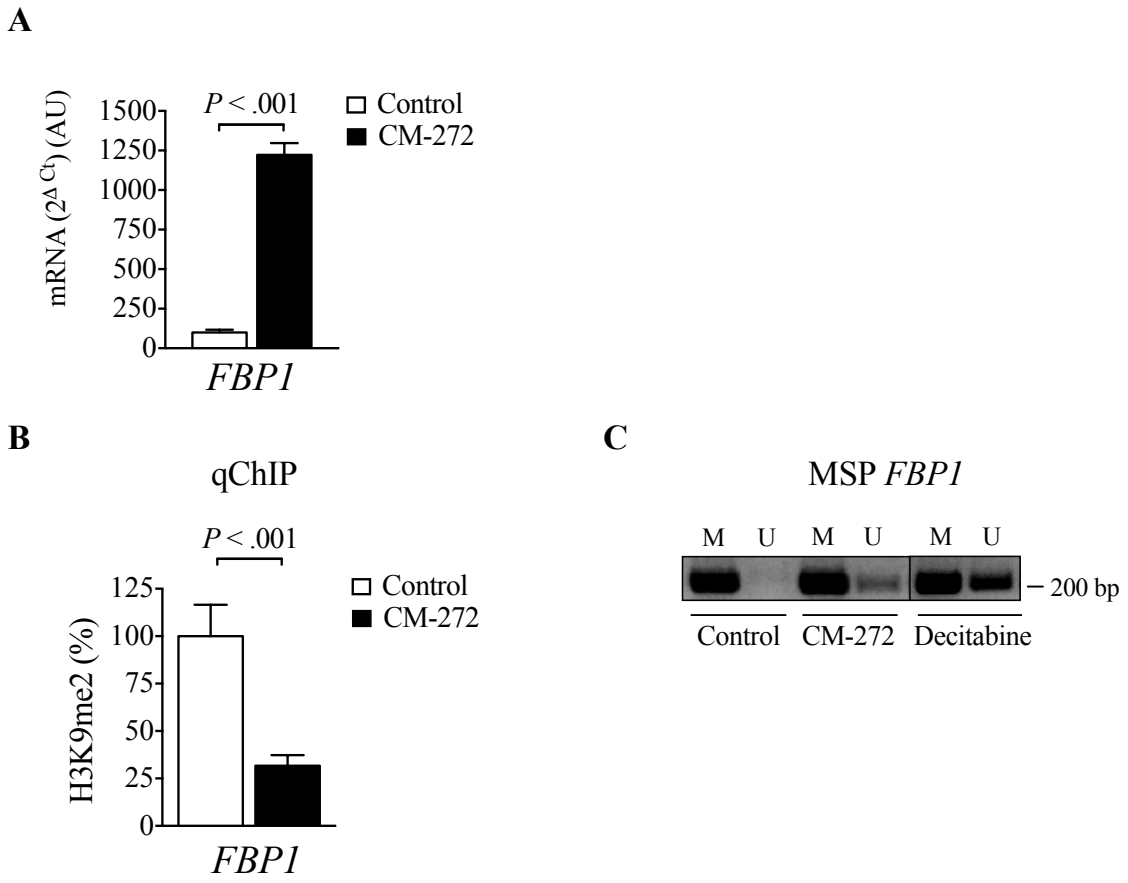

Figure 47. CM-272 strongly influences *FBP1* gene expression in LX2 cells. A) mRNA differentially expressed *FBP1* gene after 48 h of CM-272 treatment in LX2 at GI_{50} (400 nM). *H3F3A* was used as reference gene of constitutive expression. **B)** qChIP analysis reveals a fall of the epigenetic mark H3K9me2 in *FBP1* gene promoter in LX2 cells after 48 h of treatment with CM-272 (1/2 GI_{50}: 200 nM). **C)** MSP of *FBP1* promoter region in LX2 cells after CM-272 treatment (1/5 GI_{50}: 50 nM, 4 days). Decitabine treatment was used as a control of demethylation activity.

Previously we observed that CM-272 treatment is able to impair the hypoxia-mediated responses in HCC cells. Along the process of hepatocarcinogenesis the hypoxic microenvironment not only affects the parenchymal cellular compartment but also non-parenchymal cells like HSCs. HSCs exposed to hypoxia can be activated through HIF1α and its downstream target genes or signaling pathways, stimulating the release of mediators from these cells promoting fibrosis and inflammatory responses [167]. We studied the effect of CM-272 treatment in LX2 cells subjected to hypoxia. We first observed that this treatment significantly reduced the hypoxia-stimulated growth of LX2 cells (Fig. 48A). Moreover, we found a marked decrease in the expression levels of the pro-inflammatory and pro-fibrogenic genes *TGFβ1* and lysyl-oxidase (*LOX*) by CM-272

treatment (Fig. 48B). Their expression was increased in LX2 cells subjected to hypoxia, however, CM-272 treatment was able to completely inhibit this up-regulation maintaining their expression levels to those of the baseline state.

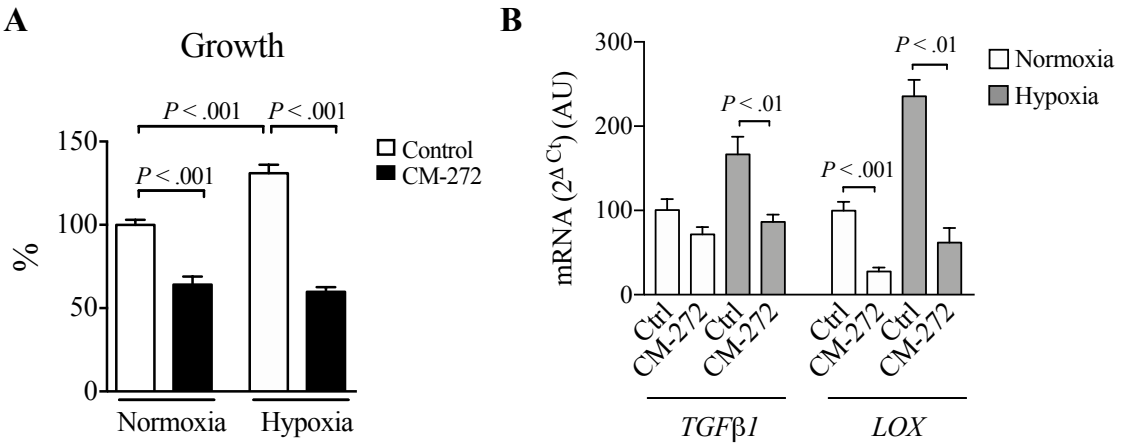

Figure 48. CM-272 impairs LX2 cells adaptation to hypoxia. A) Effect of CM-272 (GI_{50}: 400 nM) on hypoxia-induced LX2 cells growth and **B)** mRNA expression of *TGFβ1* and *LOX* genes. Cells were pre-treated with CM-272 for 24 h and then kept in normoxic or hypoxic conditions (1% O_2) for another 24 h. *H3F3A* was used as reference gene of constitutive expression.

Although hypoxia is able to mediate HSCs activation, the most classical pathway for HSCs activation is their stimulation with growth factors, being TGFβ1 the most studied. On the other hand, several studies have demonstrated that epigenetic enzymes involved in the regulation of myofibroblasts transdifferentiation are up-regulated during the activation process of HSCs. We observed that the protein levels of G9a, DNMT1 and UHRF1 in the human hepatic myofibroblast LX2 cells increased after TGFβ stimulation (Fig. 49A). This result, together with the observation that CM-272 treatment elicited a negative enrichment in gene-sets associated with TGFβ signaling (Fig. 44C, Table 9) suggested that this enzymatic complex might play a role in the TGFβ-mediated activation. In order to elucidate the possible interference of CM-272 with this pathway, we measured the expression of fibrogenic markers (*TGFβ1*; *αSMA*; *COLIA1*; *SKIL*: SKI-like protooncogene; *TAGLN*: transgelin; *LOX*) in LX2 and hHSC cells treated with the inhibitor and stimulated with recombinant TGFβ (Fig. 49B). A significant impairment in the expression of all of these genes was observed. We validated this result at the protein level measuring αSMA both in LX2 cells and hHSCs, under same conditions (Fig. 49C).

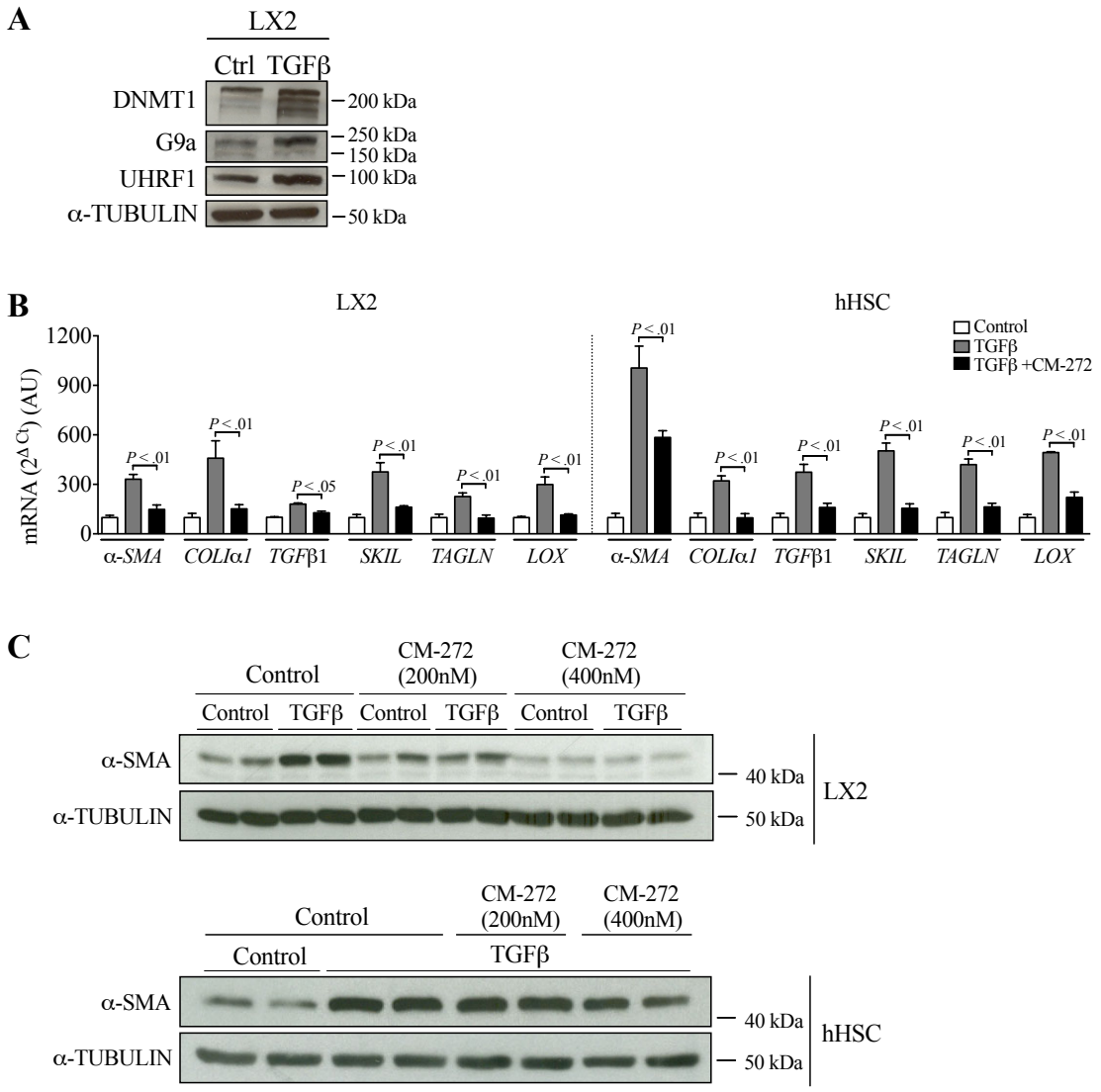

Figure 49. Inhibition of HSC fibrogenic response to TGFβ mediated by CM-272 treatment. A) Protein levels of DNMT1, G9a and UHRF1 in LX2 cells after TGFβ (5 ng/mL) stimulation during 24 h. Representative blots are shown. **B)** Panel of mRNA differentially expressed genes in LX2 and hHSCs pretreated with CM-272 (GI_{50}: 400 nM) for 24 h and then treated with TGFβ (5 ng/mL) for 24 h more. **C)** Western blot of αSMA in LX2 (up) and hHSCs (down) upon TGFβ (5 ng/mL) and CM-272 (1/2 GI_{50}: 200 nM; GI_{50}: 400 nM) treatments. α-TUBULIN western blots are loading controls.

Same qPCRs were performed in LX2 cells transfected with specific siRNA against *G9a* and stimulated with TGFβ (Fig. 50A). The results revealed the impairment of the expression of the genes by *G9a* silencing, validating the effects observed by CM-272 treatment. Specific *G9a* silencing in LX2 cells was validated at mRNA and protein level (Fig. 50B).

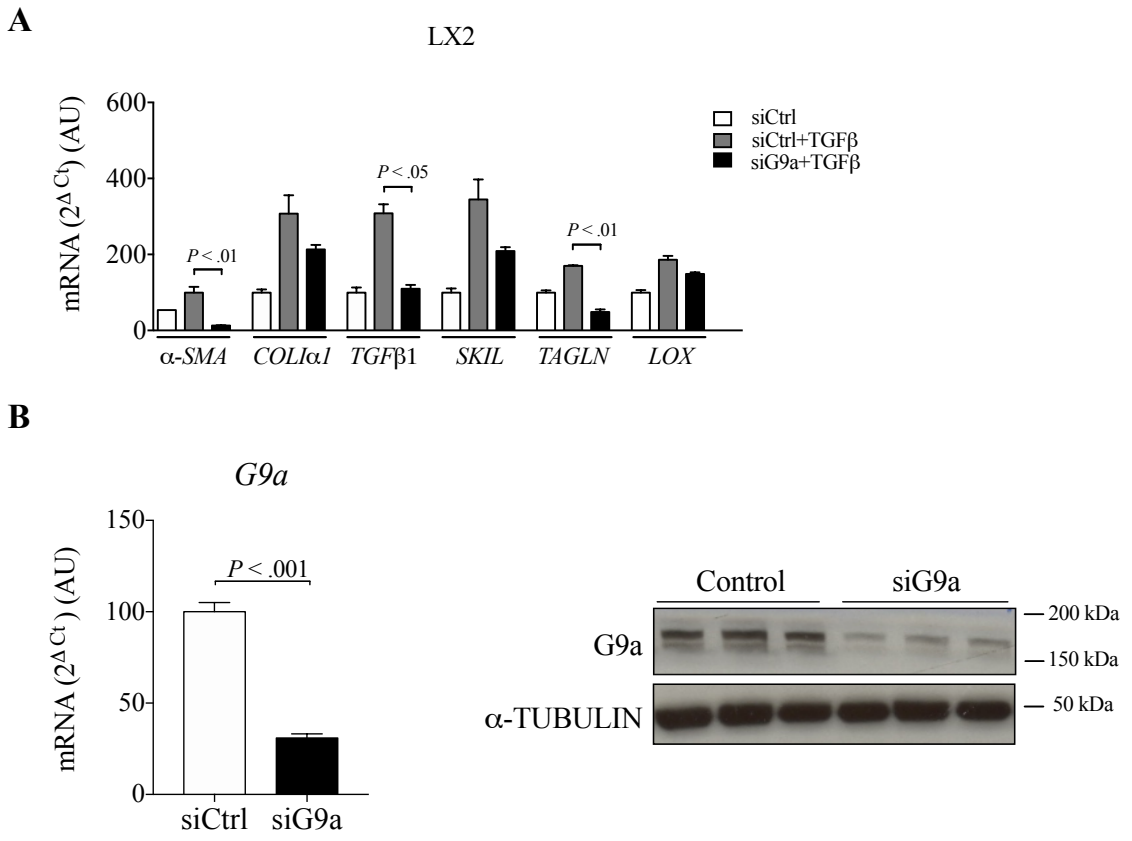

Figure 50. Inhibition of HSC fibrogenic response to TGFβ mediated by *G9a* specific silencing. A) Panel of mRNA differentially expressed genes in LX2 cells after indicated siRNA transfections for 24 h and then treated with TGFβ (5 ng/mL) for 24 h more. **B)** mRNA expression levels (left panel) and protein levels (right panel) of G9a after 48 h of indicated siRNA transfections (siCtrl: control siRNA; siG9a: *G9a* specific siRNA). *H3F3A* was used as reference gene of constitutive expression. α-TUBULIN western blot is loading control.

To better understand the mechanisms by which TGFβ signaling is impaired upon G9a/DNMTs inhibition, we studied the phosphorylation state of SMAD3 upon CM-272 treatment or siG9a transfection. We found that phosphorylation of SMAD3 in hHSC (Fig. 51A) is considerably reduced upon CM-272 treatment under TGFβ stimulation. Same was observed upon *G9a* silencing in LX2 cells (Fig. 51B). These results indicated that the inhibition of G9a was able to block TGFβ signalling in HSCs at the level of SMADs phosphorilation.

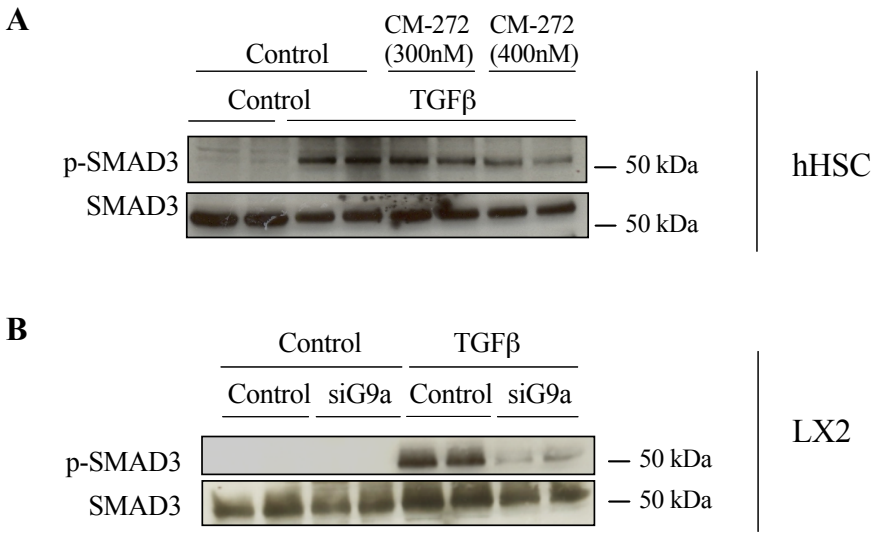

Figure 51. CM-272 and siG9a inhibits TGFβ-mediated SMAD3 phosphorylation. Western blot of p-SMAD3 and SMAD3 of **A)** hHSC upon 24 h of CM-272 treatment at the indicated doses, and **B)** LX2 cells after 48 h of transfection with the indicated siRNAs (siCtrl: control siRNA; siG9a: *G9a* specific siRNA).

Overall, we demonstrated that G9a and DNMT1 inhibition mediated by CM-272 was able to impair HSC activation. This offered an added value to CM-272 as potential anti-tumoral therapy against HCC, but also indicated its potential as anti-fibrotic therapy. Additional studies are necessary to assess this possible therapeutic application and above all to elucidate the role that epigenetic enzymes play in this context, particularly G9a.

6. Evaluation of CM-272 anti-tumoral properties *in vivo*

Based on the promising anti-tumoral properties against HCC observed *in vitro*, we decided to test the anti-tumoral efficacy of CM-272 in mouse models of HCC. PLC/PRF5 cells were subcutaneously injected into nude mice and, when tumors reached 100 mm^3, mice were treated with CM-272 or vehicle (PBS). Tumor growth was measured every 3 days, and we observed significantly reduced growth in treated mice at all times (Fig. 52A). Tumor weight at the end of the treatment was also lower (Fig. 52A). We validated these observations with other HCC cell line, HepG2 cells, and similar results were obtained (Fig. 52B). In agreement with previous studies [132] we did not appreciate any signs of CM-272 mediated toxicity in treated animals (Fig. 52C).

In order to corroborate the anti-tumoral effects observed in the subcutaneous models we decided to perform a second model using PLC/PRF5 cells orthotopically implanted in the livers of nude mice. This model also provided the additional value of tumor cells growth in their natural environment, *i. e.* the liver parenchyma. Tomours generated from human HCC cells previously grown in a subcutaneous model were implanted in the liver of nude mice, and tumor growth was followed by ultrasound (Fig. 53B). Consistently, reduced tumor growth was observed in CM-272 treated mice, and tumor weight at the end of the treatment was also lower in treated mice (Fig. 53A). Consistent with previous observations, we did not observe any weight loss nor any signs of toxicity in CM-272 treated animals (Fig. 53C).

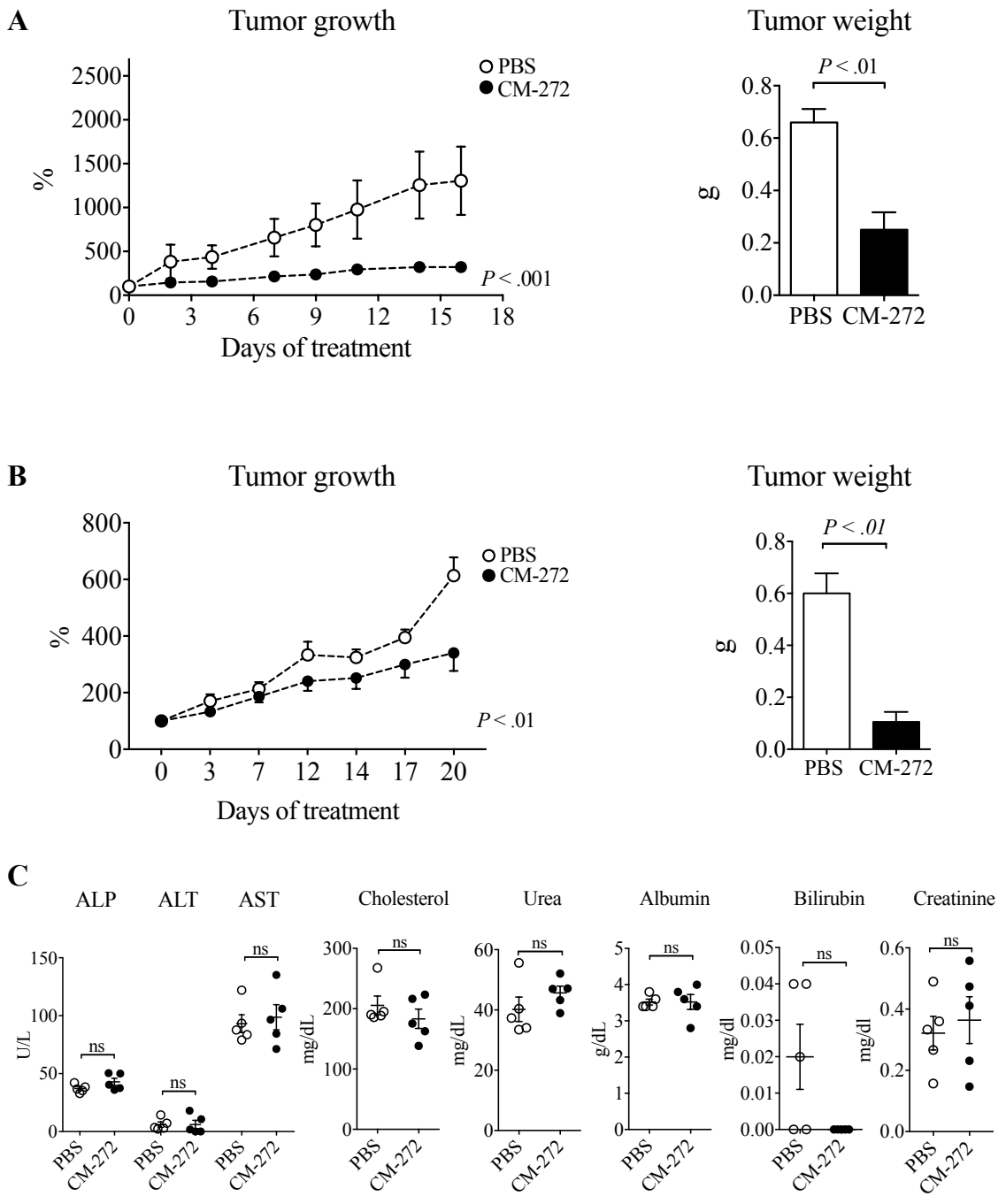

Figure 52. Anti-tumoral properties of CM-272 *in vivo* against HCC in subcutaneous xenografts of PLC/PRF5 and HepG2 cells. Effect of CM-272 on the growth of **A)** PLC/PRF5 cells or **B)** HepG2 cells in subcutaneous xenografts. Right panels: tumor weight in control (PBS, n=5) and CM-272-treated mice (5 mg/Kg mice, n=5) at the end of treatments. **C)** Analysis of liver injury and liver function serum parameters in mice treated with vehicle (PBS) or CM-272. Data from mice injected with PLC/PRF5 cells.

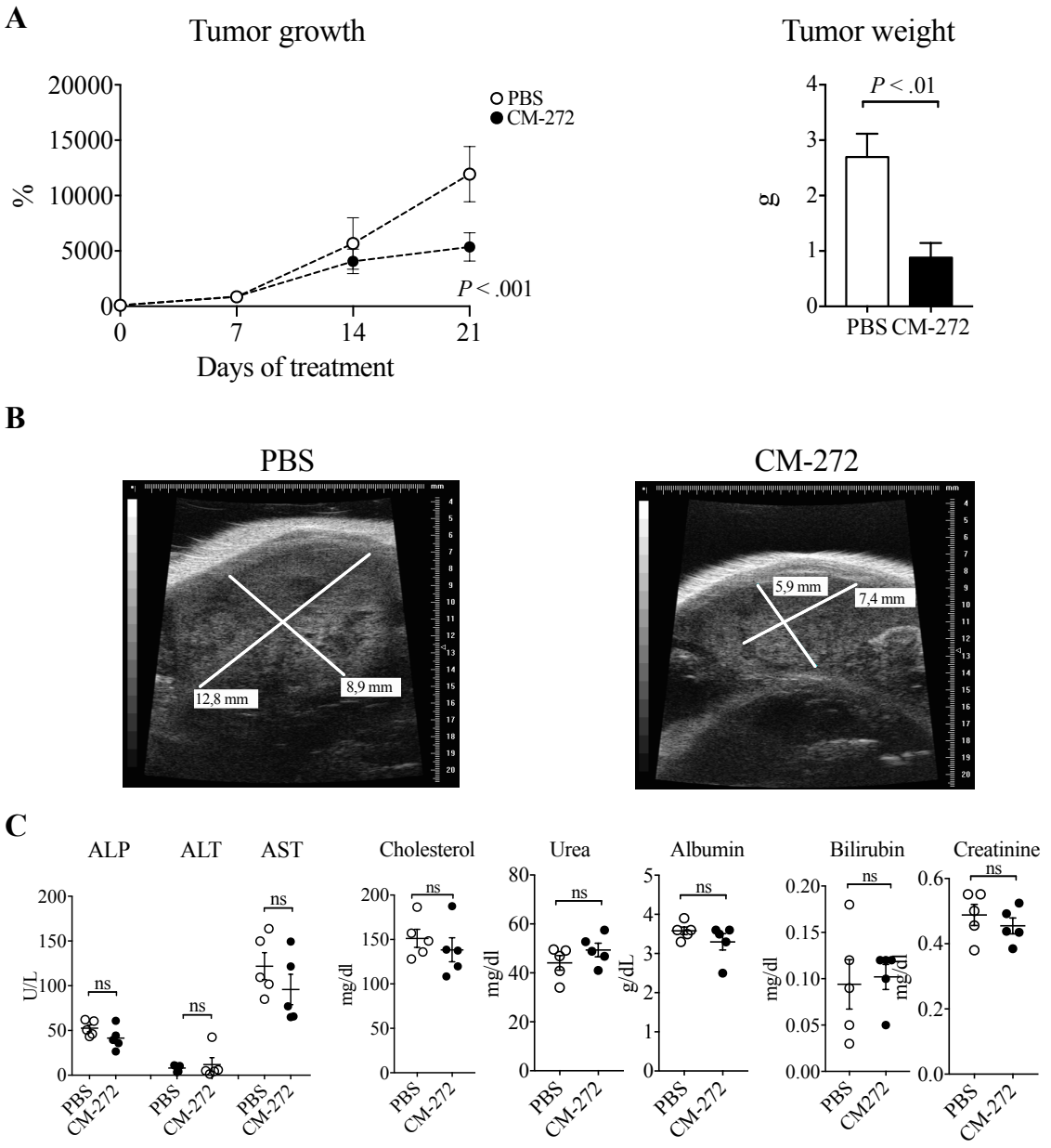

Figure 53. Anti-tumoral properties of CM-272 *in vivo* against HCC in orthotopic xenograft of PLC/PRF5 tumors. A) Effect of CM-272 on the growth of PLC/PRF5-derived tumors orthotopically implanted in the liver of nude mice. Right panels: tumor weight in control (PBS, n=5) and CM-272-treated mice (5 mg/Kg mice, n=5) at the end of treatments. **B)** Representative ultrasound images of PLC/PRF5 cells derived orthotopic tumor in the liver of mice after treatment with CM-272 or vehicle (PBS). The diameters of tumors are indicated. **C)** Analysis of liver injury and liver function serum parameters in mice treated with vehicle (PBS) or CM-272.

We measured CM-272 concentrations in serum, liver and tumor tissues from PLC/PRF5 xenograft tumor models (Table 10). Interestingly, as determined at the end of treatments serum CM-272 concentrations in treated mice were in the range of the GI_{50} found in cultured HCC cells (100-1500 nM) (Table 10). Moreover, the results obtained from liver and tumor tissue determinations in the orthotopic model demonstrated considerable accumulation of CM-272 in the tumor tissue, compared to the adjacent liver tissue (Table 10).

Table 10. Determination of CM-272 concentrations in serum, liver and tumor tissues from the indicated xenograft tumor models.

	Serum (nM)	**Liver (µmol/Kg)**	**Tumor (µmol/Kg)**
Subcutaneous PLC/PRF5	737,58 ± 243,3	30 ± 4,5	5,93± 1,81
Orthotopic PLC/PRF5	413,64 ± 73,2	35,23 ± 6,5	76,29 ± 33,62

As mentioned before, activated HSCs markedly influence HCC progression, therefore targeting the tumor-stroma crosstalk might constitute an improved therapeutic strategy. We demonstrated that CM-272 had an inhibitory effect on HSCs activation *in vitro*. Thus, we decided to perform a second mouse model of PLC/PRF5 cells in this case subcutaneously co-injected with the human hepatic stellate cell line LX2 in nude mice. As expected, growth of PLC/PRF5 tumors was significantly enhanced by LX2 cells co-implantation (Fig. 54A). CM-272 treatment had remarkable effect and tumor weights at the end of the experiment were significantly reduced (Fig. 54B). Consistently, no weight loss or any signs of toxicity were found in treated mice compared to control mice at the end of the experiments (Fig. 54C).

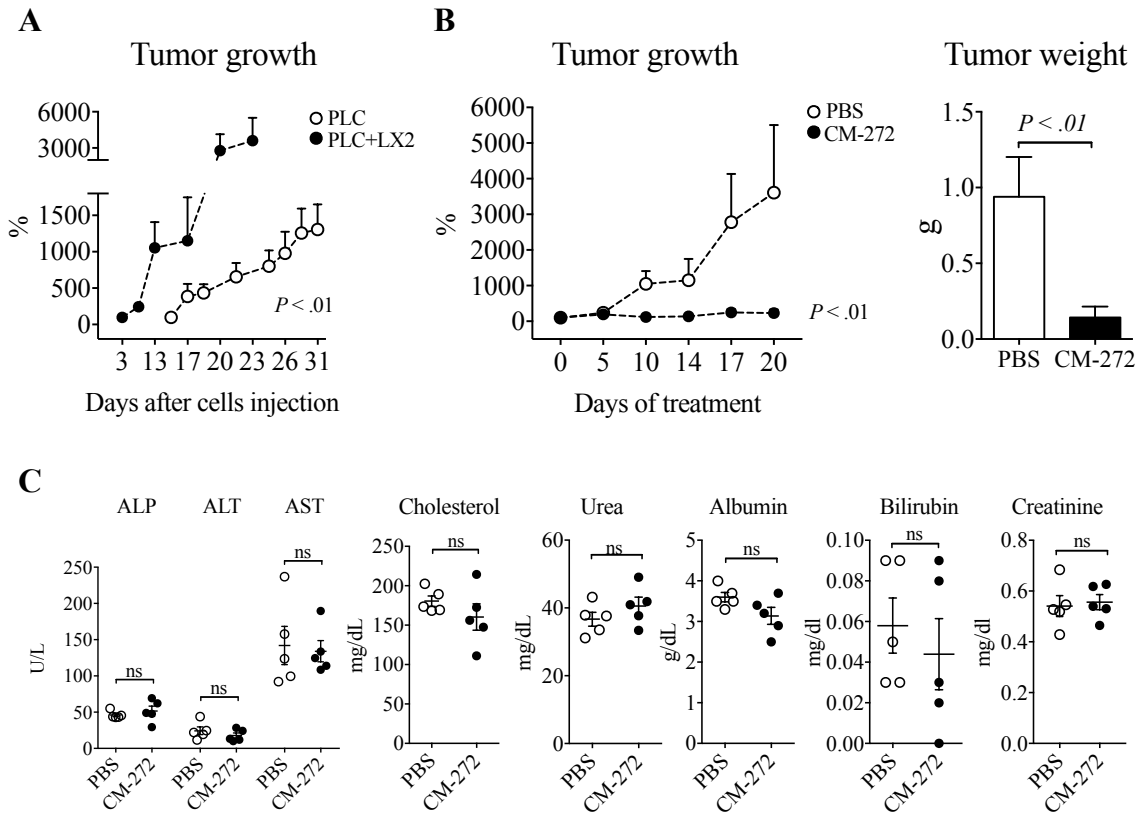

Figure 54. Anti-tumoral properties of CM-272 *in vivo* against HCC in subcutaneous xenografts of PLC/PRF5 cells combined with LX2 cells. A) Growth rate of subcutaneous tumors formed by PLC/PRF5 cells injected alone or in combination with LX2 cells in nude mice. **B)** Effect of CM-272 on the growth of PLC/PRF5 + LX2 cells in subcutaneous xenografts in nude mice. Right panels: tumor weight in control (PBS, n=5) and CM-272-treated mice (5 mg/Kg mice, n=5) at the end of treatments. **C)** Analysis of liver injury and liver function serum parameters in mice treated with vehicle (PBS) or CM-272.

The anti-tumoral properties of CM-272 were reproduced in all the *in vivo* models performed. According to our *in vitro* findings, different mechanisms could explain the anti-tumoral properties of CM-272, and we decided to explore some of these mechanisms in the tumoral tissues obtained from mice models. Consistently, we found that CM-272 downregulated G9a protein levels and strongly influenced tumor cells phenotype *in vivo* (Fig. 55A). CM-272 also inhibited the expression of the glycolysis driver HK2, while the differentiated liver markers GNMT and FBP1 were up-regulated in treated mice (Fig. 55A). These results were found in tumor samples obtained at sacrifice from the PLC/PRF5 and PLC/PRF5+LX2 subcutaneous xenograft. Moreover, tumor vascularization, assessed by CD31 staining, was reduced by CM-272 in PLC/PRF5+LX2

subcutaneous xenograft tumor samples (Fig. 55B), indicating a potential anti-angiogenic effect of CM-272 *in vivo*.

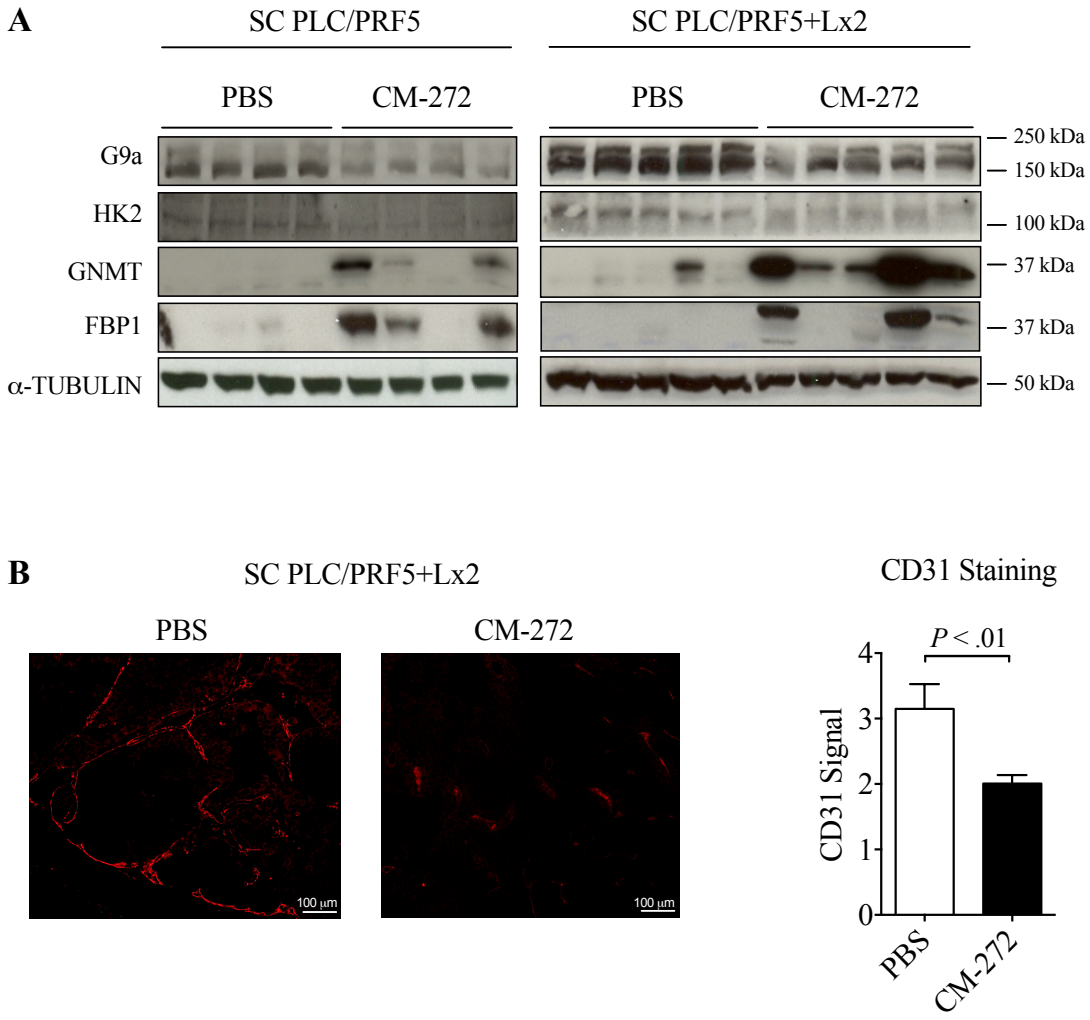

Figure 55. Anti-tumoral mechanisms of CM-272 *in vivo* against HCC in subcutaneous xenografts of PLC/PRF5 cells. A) Western blots of G9a, HK2, GNMT and FBP1 in PLC/PRF5 and PLCPRF5+LX2 xenograft tumors from control (PBS) and CM-272 treated mice. α-TUBULIN westerns blots are loading controls. **B)** Representative immunofluorescent staining for CD31 in PLC/PRF5+LX2 xenograft tumors. Right panel: quantification of vascular density assessed as CD31 immunostaining in PLC/PRF5+LX2 xenograft tumors from control (PBS) and CM-272 treated mice.

Discussion

Emerging knowledge on the importance of epigenetic mechanisms indicates that epigenetic aberrations contribute to malignant transformation at all stages of chronic liver disease and HCC development [74]. It has been found that diverse malignant phenotypes of HCC can be associated with epigenetic alterations in cancer cells, and also in other cellular populations that contribute to the underlying disease processes. These aberrations contribute to the heterogeneity of liver cancer, but also expose novel therapeutic targets. The recent approval of epigenetic drugs for the treatment of hematological malignances, together with current clinical trials testing epigenetic drugs in solid tumors, has attracted considerable interest towards the development of epigenetic-based therapies. However, in order to translate these investigations to the clinics it is necessary to better understand the functional crosstalk between epigenetic events in the disease context.

We have studied the interaction between DNA and H3K9 methylation in the context of liver cancer, providing evidences supporting the potential of combined G9a and DNMTs antagonism as a novel anti-tumoral therapy. Likewise, we have studied the biological role that this epigenetic complex plays in the process of hepatocarcionogenesis.

First, we demonstrated that *G9a*, *DNMT1* and their key adaptor *UHRF1* are overexpressed in human HCC (Fig. 11) showing a very strong positive correlation between them (Fig. 12). That already suggested a functional coordination of the epigenetic events mediated by these enzymes. As the cohort of HCC patients was perfectly characterized at the clinical, genetic and transcriptomic level, we could study a wide panel of phenotypical characteristics of these that classifies HCC samples. Very interestingly, we found that overexpression of *G9a*, *DNMT1* and *UHRF1* was associated with molecular, histological and clinical characteristics indicative of more aggressive disease and poorer prognosis (Fig. 13). These results suggested a relevant pathophysiological role of G9a-DNMT1-UHRF1 in the disease and pointed out to their involvement in the malignant phenotype of HCC.

A very recently published report by Liu and colleagues showed a synergistic anti-tumoral effect of simultaneous inhibition of G9a and DNMTs in ovarian cancer cells [168]. We demonstrated that simultaneous inhibition of G9a and DNMT1 exerted a synergistic anti-proliferative action over HCC cell lines using either molecular tools (siRNAs) (Fig. 16) or commercial inhibitors (Fig. 18). We established a rationale for the simultaneous

inhibition of G9a and DNMT1 in HCC treatment. Thereby, we decided to evaluate the potential benefits of our novel dual inhibitors of G9a and DNMT1 for HCC. Our lead compound, CM-272, demonstrated its specificity by reducing H3K9me2 and DNA methylation levels in HCC cells lines, without altering other epigenetic marks (Fig. 22). Its specificity may be explained by the fact that these compounds were mechanistically designed for a mechanism of action based on substrate-competition. Therefore, they are able to reversible compete with their substrates (DNA and K9H3), with no interference with AdoMet binding. These features may contribute to the observed absence of systemic toxicity.

We indeed found very low GI_{50} values for CM-272 against a panel of 32 HCC cell lines (Fig. 19). In all cases GI_{50} values were lower than the value found in the THLE2 hepatocyte line. However, there were differences among the HCC cell lines. Although there could be several potential explanations for this finding, we found a highly significant positive correlation between the GI_{50} values and the expression of the drug efflux pump *ABCB1* (MDR1). Indeed, we could demonstrate that CM-272 is a substrate for this membrane transporter (Fig. 21). These findings suggest that inhibition of MDR1 could further enhance the therapeutic efficacy of CM-272.

One relevant finding of our study was the downregulation of G9a protein levels in HCC cells (Fig. 23) and xenograft tumors (Fig. 55) upon CM-272 treatment. This response is coherent with previous reports describing the proteasomal degradation of other histone-methyltransferases (*e.g.* EZH2) after inhibition of their catalytic activity [153]. Reduction of G9a levels may be significant regarding to the anti-tumoral effects of CM-272. On one hand, G9a is overexpressed in HCC and thus, reduction of its levels may re-establish the normal levels found in untransformed hepatocytes. On the other hand, it might alter other G9a functions which are independently of its catalytic activity and are related to tumorigenesis, as G9a participates in the stabilization of diverse protein complexes by protein-protein interactions[130,132]. G9a has been described primarily as corepressor of gene expression by its ability to carry out H3K9 di-methylation. However, it has been observed that G9a can positively regulate gene expression as a transcriptional coactivator of cancer-related genes without involving its catalytic capacity [132]. Thus, G9a has dual and selective functions as a coregulator for target genes playing important roles in malignances. How G9a combines both activating and repressing functions may relay on

the fact that G9a is associated with multiple protein complexes that play both positive and negative roles in transcription, but also on its capacity to methylate non-histone targets [115,116,169–171]. On the other hand, post-translational modifications of G9a such as methylation and phosphorylation have been involved in controlling G9a coactivator functions [171], but the mechanisms monitoring these processes specificity are unknown.

Concomitant downregulation of DNMT1 and UHRF1 proteins upon CM-272 treatment was also found in HCC cells (Fig. 23). This finding may be explained as a consequence of G9a depletion, based on the fact that these proteins physically interact in multimeric functional complexes that condition the relative stability of each component [113,115,122,172].

The mechanisms of CM-272 anti-tumoral action are likely multifarious. However, the growth inhibitory effects of CM-272 on HCC cells were not accompanied by the induction of apoptosis or autophagy (Fig. 25, Fig. 26). Although it was previously described that G9a inhibition causes induction of both events in different cancers [173], according to our findings this is not the case for HCC. Additionally, we did not find significant effects of CM-272 on cell cycle progression in HCC cells (Fig. 27). Although we did observe some effects at higher doses of the drug, these were not sufficient to explain the potent growth inhibitory properties. In this regard, our transcriptomic analyses provided valuable mechanistic insights (Fig. 28, Table 8).

We observed that malignant markers of malignancy involved in various biological processes were down-regulated upon CM-272 treatment (Fig. 29), whereas other genes associated with anti-tumoral properties such as adhesion molecules or tumor suppressor genes (*e.g. RASSF1A*) were up-regulated (Fig. 30, Fig. 33). These results indicate that CM-272-mediated inhibition of G9a-DNMTs presents a dual anti-tumoral effect, causing either the induction or inhibition of target genes expression. Although the mechanism of this dual effect is unknown, we hypothesize that it might be related to the dual activity of G9a that as already explained can work as coactivator or corepressor [118,171]. In fact, most of the effects we observed for CM-272 were validated by specific silencing or overexpression of *G9a*.

Very interestingly, the gene sets defined by Boyault and Hosida and colleagues [16,154] that classify HCC in more aggressive phenotypes were found negatively enriched in the

samples treated by CM-272. The downregulation of these gene-sets was accompanied by a positive enrichment of genes grouped in the gene set defined by Hsiao and colleagues that encompassed liver-specific genes (Fig. 28). This led us to further investigate the induction of genes characteristic of the adult and differentiated hepatocyte upon CM-272 treatment, especially in the context of more aggressive phenotype in HCC.

On one hand, we observed the reactivation of *CDH1* expression by CM-272 (Fig. 31) that might contribute to restore an epithelial and less malignant phenotype and is consistent with G9a and DNA-mediated methylation of *CDH1* and its repression described in breast cancer cells [124]. However, perhaps more compelling was the reactivation of genes involved in central metabolic pathways, such as one-carbon metabolism and gluconeogenesis, which are specific events epigenetically repressed during hepatocarcinogenesis [31,37,148].

Methionine metabolism has been investigated in various experimental models of liver disease. The expression of several enzymes participating in this cycle are confined mainly to the liver. MAT1A converts methionine into AdoMet, and is expressed exclusively in this organ. As a consequence of this liver-specific expression, and although all tissues can synthesize and utilize AdoMet, the liver is the main place for the metabolism of this amino acid [31]. *MAT1A* is silenced during liver transformation, and its repression is mediated by DNA methylation of the gene promoter and histone deacetylation [28]. We demonstrated that CM-272 treatment is able to re-induce the expression of *MAT1A* (Fig. 31), and this effect could be attributed to the demethylating activity of the drug. Other relevant enzyme that participates in methionine metabolism is GNMT. This protein has been proposed to display tumor suppressor activity and to be frequently repressed in HCC. It has been demonstrated that its repression is mediated by DNA hypermethylation in some HCC cell lines and primary tumors, and the involvementof histone modifications in its repression has also been reported [148]. We found that CM-272 treatment reactivated its expression in association with a reduction in H3K9me2 levels (Fig. 31, Fig. 32).

CYP7A1 is a key enzyme in cholesterol homeostasis and in the regulation of bile acid synthesis, and the liver is the main organ for this metabolic function. Well differentiated hepatocytes, express large amounts of *CYP7A1* [32], whereas reduced expression of *CYP7A1* has been established in pathological stages of the liver [33,174]. Regulation of

CYP7A1 transcription is complex and involves multiple mechanisms. A regulatory mechanism leading to the repression of this gene involving G9a has been established [175]. Fang and colleagues observed that G9a expression enhanced the inhibition of *CYP7A1* transcription by a mechanism involving small heterodimer partner (SHP), a member of the nuclear receptor family but lacking DNA binding domain [175]. They further observed that catalytically inactive G9a mutant reversed the SHP-mediated inhibition of *CYP7A1* expression and demonstrated that G9a was recruited to the *CYP7A1* promoter and H3K9 were methylated in a SHP-dependent manner in bile acid-treated HepG2 cells [175]. Thus, downregulation of *CYP7A1* in transformed hepatocytes might be due to the increased levels and activity of G9a. We observed that inhibition of G9a by CM-272 reduced H3K9me2 levels in the promoter of *CYP7A1* and this was accompanied by a clear increase of its transcription (Fig. 31, Fig. 32).

Reprogramming of metabolism is a hallmark of neoplastic transformation, and this alteration is particularly extensive in a metabolic organ like the liver [176]. Rewiring of glucose metabolism, including the repression of gluconeogenic enzymes and the activation of specific glycolytic isozymes, contributes to fulfil the tumor anabolic demands particularly its hypoxic core [176]. We found that CM-272 potently counteracted these responses. In fact, the reactivation of *FBP1* expression by CM-272 may be a key mechanism in this context. FBP1 has been hypothesized to act as a tumor suppressor and some evidences support a pre-clinical rationale to develop FBP1 as a therapeutic target for HCC treatment [37]. We found that CM-272 reinduces the expression of *FBP1* in HCC cells (Fig. 31). We first observed that this transcriptional regulation was associated with decreased levels of H3K9me2 in the promoter of this gene upon treatment (Fig. 32). However, further studies revealed that this modification of histones was accompanied by DNA methylation changes (Fig. 34). By MSP and pyrosequencing analyses we demonstrated that CM-272 is able to reduce the DNA methylation in the promoter of this gene. Interestingly, reduction in DNA methylation was found in an adjacent downstream region from where the fall in H3K9me2 levels was previously observed (ANNEX 1). The proximity of these regions might be an indicative of the coordinated activity of G9a and DNMT1 forming a complex in the promoter of this gene.

We further observed that *FBP1* expression was inversely associated with those genetic subclasses and clinical signatures that we previously found positively associated with the

expression of *G9a*, *DNMT1* and *UHRF1* (Fig. 35). These results indicate that those patients with higher levels of the enzymes present greater inhibition of *FBP1* transcription. This might be a reason why this epigenetic complex is associated with more aggressive HCC phenotypes, and reinforces the potential benefit of simultaneously inhibiting G9a and DNMT1 in this pathological situation.

A loss of *FBP1* expression is linked to the activation of tumoral glycolytic program. Very recently, Yang and colleagues have observed that knockdown of *FBP1* enhances the colony formation, proliferation and metastasis of HCC cells, whereas overexpression of *FBP1* impairs the *Warburg Effect* by reducing the rate of glycolysis and glycolytic capacities [177]. Our results corroborated this effect, as CM-272 treatment was able to impair the glycolysis rate in our cells (Fig. 36).

Moreover, FBP1 has been recently reported to directly inhibit the activity of hypoxia-inducible factors in renal cancer cells in a catalytic activity-independent manner [178]. This function may be also related to the overall impairment of HCC cells adaptation to hypoxia elicited by CM-272. In this context, we observed that the proliferative inhibitory properties of CM-272 treatment on cell proliferation were exacerbated under hypoxia in HCC cells (Fig. 38). Hypoxia-stimulated overexpression of glycolytic enzymes, and also of those involved in the serine-glycine synthesis pathway, was impaired (Fig. 39, Fig. 40). Our results indicate that this defective adaptation to hypoxia can be attribute to the effect of our drug on G9a, as the results were contrasted and validated by either specific silencing or overexpression of *G9a.* This agrees with previously described findings. First, it was demonstrated that G9a protein levels are stabilized under hypoxia in various types of cancer including HCC, and we also corroborated it (Fig. 37). On the other hand, several studies have related G9a functions with hypoxia-mediated responses. Casciello and colleagues demonstrated that G9a protein stability is increased in hypoxia via reduced proline hydroxylation and subsequent inhibition of pVHL and proteasome-mediated degradation, as occurs with the master regulator of hypoxia responses HIF1α. They also demonstrate that its activity drives hypoxia-mediated gene repression in breast cancer [163]. Moreover, previous reports pointed out to G9a as a mediator of hypoxic responses in cancer cells through its non-histone catalytic activity over Reptin and Pontin, known to work as transcriptional regulators of various hypoxia responsive genes [122].

Other relevant and very recent report for this debate is the study performed of Bao and colleagues that demonstrated that G9a directly bound to HIF1α catalyzing mono- and di-methylation at lysine 674, which reduces HIF1α transactivation domain function. Consequently, HIF1α transcriptional activity and the expression of several downstream target genes is impaired by this mechanisms [179]. We observed that CM-272 treatment reduced HIF1α protein levels of in HepG2 cells under hypoxia (Fig. 42). This effect was previously found in the same cell line when treated with the G9a inhibitor BIX01294 [180]. Although it is unclear how G9a regulates the hypoxic responses in cancer, its involvement in these events seems to be critical for transformed cells. Concerning our research, further studies are necessary to establish the mechanism by which CM-272 treatment impairs these G9a-mediated functions under hypoxia. Whether these events are mediated by its catalytic inhibitory activity or not remains to be established, since as we described CM-272 can also promote the downregulation of G9a protein levels. Hypoxia is also known to foster HCC development through the stimulation of angiogenesis and liver fibrosis. We observed blunted expression of the key angiogenic mediator *VEGF* and the protumorigenic and profibrogenic marker *TGFβ1*, either by treatment with CM-272, *G9a* silencing or *G9a* overexpression (Fig. 41). All these findings encouraged us to further examine the tumor stroma crosstalk and prompted us to examine CM-272 effects of fibrogenic cells.

Epigenetic mechanisms, including coordinated DNA and histone methylation, have emerged as central events in the transcriptomic reprogramming of quiescent to activated HSCs [89]. We observed that our inhibitor was able to reduce proliferation and induce apoptosis in LX2 cell line *in vitro* (Fig. 43). More interestingly, our microarray analyses suggested that CM-272 reversed the myofibroblastic transcriptomic phenotype of HSCs towards a more differentiated and adipogenic one [181]. Gene-sets related to lipid and retinol metabolism were found positively enriched in treated LX2 cells, whereas others associated with growth factor signaling and cell proliferation were negatively enriched. Of note, some of the most statistically significant downregulated gene sets indicated a lower disposition or responsiveness to TGFβ signaling upon CM-272 treatment (Fig. 44, Table 9).

Up-regulation of quiescent genes mediated by CM-272 was validated in LX2 cells and also in primary hHSCs (Fig. 45). Although the underlying mechanisms need further elucidation, the positive effect on *PPARγ* expression can be significant. Indeed, PPARγ is a transcriptional suppressor of HSC fibrogenic activation, able to maintain quiescent and vitamin-A metabolism [89]. There are increasing evidences that PPARγ ligands have anti-fibrotic properties [182–186]. Forced expression of PPARγ in activated HSCs is able to inhibit collagen I production [186], block TGFβ signaling, reduce cell proliferation and stimulate the recovery of cytoplasmic lipid droplets driving the cells towards a quiescent phenotype [51,187,188].

Moreover, *PPARγ* expression is transcriptionally silenced during HSC activation through mechanisms involving DNA and H3K9 hypermethylation in the promoter [164,165]. We demonstrated that these epigenetic marks were reversed by CM-272 treatment (Fig. 46). Interestingly, the region of the *PPARγ* promoter where we found a reduction in the epigenetic marks followed the same scheme observed in *FBP1* promoter. DNA methylation decrease was observed in the adjacent downstream region from where a reduction in H3K9me2 levels was found (ANNEX 2).

In addition to the CM-272-mediated reinduction of quiescent genes in HSCs, we demonstrated that CM-272 is able to mediate the up-regulation of *FBP1* expression in LX2 cells (Fig. 47). This may have an effect on glucose metabolism in HSCs that although less studied has been implicated in the activation process of these cells. In fact, glucose metabolic reprogramming of HSCs is a conserved response to liver injury [166]. We also observed an impaired response of these cells to hypoxia. HSCs response to the hypoxic microenvironment stimulating the release of profibrogenic and proinflammatory mediators. It has been very recently published that histone methylation plays an important role in the HIF1α signaling cascade regulating HSC activation [167]. We observed that CM-272 was able to impair the hypoxic-mediated responses of increased proliferation and the transcriptional overexpression of *TGFβI* and *LOX* (Fig. 48).

One of the most robust effects of CM-272 that we observed in HSCs was the impairment of the TGFβ signaling. A panel of TGFβ target upregulation of key fibrogenic genes were found significantly reduced upon CM-272 treatment in LX2 cells and also in hHSCs (Fig.

49). This result was reproduced by specific silencing of *G9a* in LX2 cells (Fig. 50). Trying to elucidate the mechanisms by with G9a inhibition impairs the signaling of this pathway we found that SMAD3 phosphorylation is blunted both after CM-272 treatment and silencing *G9a* (Fig. 51). On the other hand, CM-272-mediated upregulation of *BAMBI*, a TGFβ pseudoreceptor and negative regulator of HSC activation [189], which could partially account for the blunted response to TGFβ. However, further studies are necessary to assess the mechanisms by which G9a inhibition blocks the TGFβ signaling.

The anti-tumoral properties of CM-272 we elucidated in cultured cells were translated to *in vivo* models. Tumor growth was significantly reduced upon CM-272 treatment in HCC subcutaneous xenograft models (Fig. 52). Same results were obtained in an orthotopic model (Fig. 53). We did not observe any sign of toxicity in CM-272 treated animals. However, when we measured CM-272 levels in mice at the end of the treatment, we could observe, particullary in the case of orthotopic model, how CM-272 accumulated in tumoral tissues (Table 10). This is an important aspect to be considered from a translational perspective. We further observed that HSCs markedly influence HCC progression in a third subcutaneous model in which PLC/PRF5 cells were co-injected with LX2 cells. As expected, growth of PLC/PRF5 tumors was significantly enhanced by LX2 cells. In this model we observed the most remarkable anti-tumoral effect of CM-272, as tumor growth of treated mice was drastically inhibited (Fig. 54). Consistent with our *in vitro* observations, CM-272 downregulated G9a expression and strongly influenced tumor cells phenotype *in vivo*. Indeed, CM-272 reduces the protein levels of the glycolysis driver HK2, while that of GNMT and FBP1 were increased. As an important biological consequence, tumor vascularization (CD31 staining) was also reduced by CM-272 (Fig. 55).

Summing up, we have provided evidences supporting therapeutic efficacy of dual G9a/DNMT1 targeting for the treatment of HCC with novel first-in-class reversible inhibitors. Mechanistically, our study indicates that the lead compound of this series, CM-272, can induce HCC and HSC cell differentiation and growth inhibition, underscoring the potential of differentiation therapy [190] in liver cancer, and providing a rationale for combination with other anti-cancer agents with different mechanisms of action (Fig. 56). In addition, all the findings exposed herein suggest a potent role of this enzymatic

complex in the process of fibrogenesis and HSCs activation. Resolution of fibrosis refers to pathways that either drive the stellate cells to apoptosis, or contribute to their reversion to a restoration of the quiescent phenotype [51]. As we found that CM-272 treatment induces both phenomena in HSCs an anti-fibrotic effect might be expected. Nevertheless, further studies are needed to address this issue.

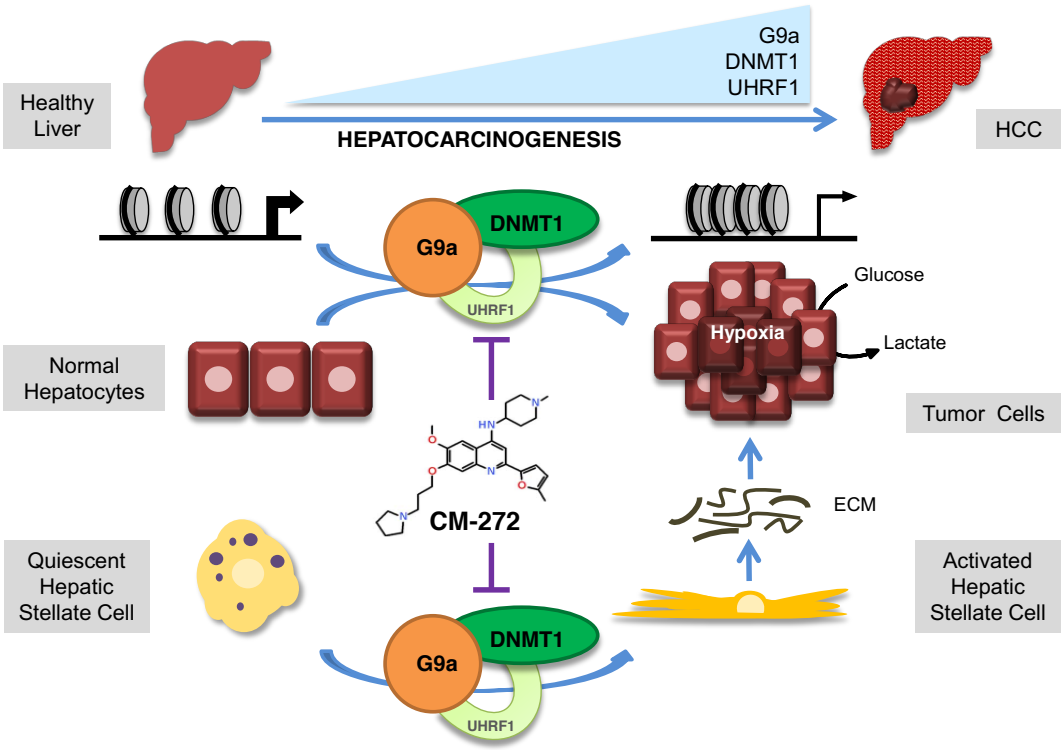

Figure 56. Dual targeting G9a and DNMT1 in HCC treatment. Schematic summary of the results.

Conclusions

1. The expression levels of the epigenetic modifiers G9a, DNMT1 and UHRF1 are significantly increased in HCC in a coordinated manner. Enhanced expression of these genes is associated with the worst molecular and clinical features of HCCs.

2. Simultaneous inhibition of G9a and DNMT1 exerts a synergistic anti-proliferative effect on HCC cells.

3. CM-272 is a novel, selective and potent dual inhibitor of G9a and DNMTs that shows strong anti-proliferative activity in a broad panel of HCC cell lines.

4. CM-272 exerts a profound reshape in the transcriptional machinery of HCC cells, downregulating the expression of malignant markers and upregulating the expression of anti-tumoral and liver-specific genes.

5. CM-272 interferes with the development of tumor microenvironment, causes apoptosis and impairs the activation of stellate cells. The dual inhibition of G9a and DNMT1 returns the myofibroblastic transcriptional phenotype of HSC cells towards a more differentiated one, making these cells less responsive to TGFβ.

6. CM-272 inhibits the growth and metabolic adaptation of HCC and HSCs to hypoxia.

7. CM-272 potently inhibits the *in vivo* growth of HCC cells, particularly when it is driven by fibrogenic (LX2) cells. Therefore this new type of drugs could simultaneously target tumor and stromal cells and might show enhanced therapeutic efficacy for the treatment of HCC.

References

1. Berasain, C. & Avila, M. A. Regulation of hepatocyte identity and quiescence. *Cell. Mol. Life Sci.* **72,** 3831–3851 (2015).
2. Michalopoulos, G. K. Liver regeneration. *J. Cell. Physiol.* **213,** 286–300 (2007).
3. Ferlay, J. *et al.* Cancer incidence and mortality worldwide: Sources, methods and major patterns in GLOBOCAN 2012. *Int. J. Cancer* **136,** E359–E386 (2015).
4. El-Serag, H. B. Hepatocellular Carcinoma. *N. Engl. J. Med.* **365,** 1118–1127 (2011).
5. Forner, A., Llovet, J. M. & Bruix, J. Hepatocellular carcinoma. *Lancet* **379,** 1245–1255 (2012).
6. Margini, C. & Dufour, J. F. The story of HCC in NAFLD: from epidemiology, across pathogenesis, to prevention and treatment. *Liver Int.* **36,** 317–324 (2016).
7. Hernandez-Gea, V., Toffanin, S., Friedman, S. L. & Llovet, J. M. Role of the microenvironment in the pathogenesis and treatment of hepatocellular carcinoma. *Gastroenterology* **144,** 512–527 (2013).
8. Bruix, J., Gores, G. J. & Mazzaferro, V. Hepatocellular carcinoma: clinical frontiers and perspectives. *Gut* **63,** 844–855 (2014).
9. Sia, D., Villanueva, A., Friedman, S. L. & Llovet, J. M. Liver cancer cell of origin, molecular class, and effects on patient prognosis. *Gastroenterology* **152,** 745–761 (2017).
10. Kouzarides, T. SnapShot: histone-modifying enzymes. *Cell* **131,** 822 (2007).
11. Tovoli, F. *et al.* Systemic treatments for hepatocellular carcinoma: challenges and future perspectives. *Hepatic Oncol.* **5,** HEP01 (2018).
12. Llovet, J. M. *et al.* Sorafenib in advanced hepatocellular carcinoma. *N. Engl. J. Med.* **359,** 378–390 (2008).
13. Villanueva, A. & Llovet, J. M. Liver Cancer in 2013: Mutational landscape of HCC—the end of the beginning. *Nat. Publ. Gr.* **11,** 73–74 (2014).
14. El-Khoueiry, A. B. *et al.* Nivolumab in patients with advanced hepatocellular carcinoma (CheckMate 040): an open-label, non-comparative, phase 1/2 dose escalation and expansion trial. *Lancet* **389,** 2492–2502 (2017).
15. Boyault, S. *et al.* Transcriptome classification of HCC is related to gene alterations and to new therapeutic targets. *Hepatology* **45,** 42–52 (2007).
16. Hoshida, Y. *et al.* Molecular classification and novel targets in hepatocellular carcinoma: recent advancements. *Semin. Liver Dis.* **30,** 35–51 (2010).
17. Hanahan, D. & Weinberg, R. A. Hallmarks of cancer: the next generation. *Cell*

144, 646–674 (2011).

18. Pavlova, N. N. & Thompson, C. B. The emerging hallmarks of cancer metabolism. *Cell Metab.* **23,** 27–47 (2016).
19. Liu, M., Jiang, L. & Guan, X. Y. The genetic and epigenetic alterations in human hepatocellular carcinoma: a recent update. *Protein Cell* **5,** 673–691 (2014).
20. Becker, D. *et al.* Genetic signatures shared in embryonic liver development and liver cancer define prognostically relevant subgroups in HCC. *Mol. Cancer* **11,** 1–11 (2012).
21. Marin, J. J. G. *et al.* Molecular bases of the poor response of liver cancer to chemotherapy. *Clin. Res. Hepatol. Gastroenterol.* **42,** 182–192 (2018).
22. Reya, T., Morrison, S. J., Clarke, M. F. & Weissman, I. L. Stem cells, cancer and cancer stem cells. *Nature* **414,** 105–111 (2001).
23. Oishi, K. *et al.* Clinicopathologic features of poorly differentiated hepatocellular carcinoma. *J. Surg. Oncol.* **95,** 311–316 (2007).
24. Voulgari, A. & Pintzas, A. Epithelial–mesenchymal transition in cancer metastasis: Mechanisms, markers and strategies to overcome drug resistance in the clinic. *Biochim. Biophys. Acta - Rev. Cancer* **1796,** 75–90 (2009).
25. Wei, Y. *et al.* Altered expression of E-cadherin in hepatocellular carcinoma: correlations with genetic alterations, beta-catenin expression, and clinical features. *Hepatology* **36,** 692–701 (2002).
26. Lamouille, S., Xu, J. & Derynck, R. Molecular mechanisms of epithelial-mesenchymal transition. *Natl. Rev. Mol. Cell Biol.* **15,** 178–196 (2014).
27. Vázquez–Chantada, M. *et al.* HuR/Methyl-HuR and AUF1 regulate the MAT expressed during liver proliferation, differentiation, and carcinogenesis. *Gastroenterology* **138,** 1943–1953 (2010).
28. Torres, L. *et al.* Liver-specific methionine adenosyltransferase MAT1A gene expression is associated with a specific pattern of promoter methylation and histone acetylation: implications for MAT1A silencing during transformation. *FASEB J.* **14,** 95–102 (2000).
29. Avila, M. A. *et al.* S-Adenosylmethionine revisited: its essential role in the regulation of liver function. *Alcohol* **27,** 163–167 (2002).
30. Martínez-Opez, N. *et al.* S-adenosylmethionine and proliferation: new pathways, new targets. *Biochem. Soc. Trans.* **36,** 848–852 (2008).
31. Avila, M. A. *et al.* Reduced mRNA abundance of the main enzymes involved in

methionine metabolism in human liver cirrhosis and hepatocellular carcinoma. *J. Hepatol.* **33,** 907–914 (2000).

32. Schrem, H., Klempnauer, J. & Borlak, J. Liver-enriched transcription factors in liver function and development. Part II: the C/EBPs and D site-binding protein in cell cycle control, carcinogenesis, circadian gene regulation, liver regeneration, apoptosis, and liver-specific gene regulation. *Pharmacol Rev* **56,** 291–330 (2004).
33. Liu, C. *et al.* Modeling hypercholesterolemia and vascular lipid accumulation in LDL receptor mutant zebrafish. *J. Lipid Res.* **59,** 391–399 (2018).
34. Yang, H. & Duan, Z. Bile acids and the potential role in primary biliary cirrhosis. *Digestion* **94,** 145–153 (2016).
35. El-Serag, H. B. Hepatocellular carcinoma: recent trends in the United States. *Gastroenterology* **127,** S27-S34 (2004).
36. Ikeda, K. *et al.* Disease progression and hepatocellular carcinogenesis in patients with chronic viral hepatitis: a prospective observation of 2215 patients. *J. Hepatol.* **28,** 930–938 (1998).
37. Hirata, H. *et al.* Decreased expression of fructose-1,6-bisphosphatase associates with glucose metabolism and tumor progression in hepatocellular carcinoma. *Cancer Res.* **76,** 3265–3276 (2016).
38. Wang, B., Hsu, S. H., Frankel, W., Ghoshal, K. & Jacob, S. T. Stat3-mediated activation of microRNA-23a suppresses gluconeogenesis in hepatocellular carcinoma by down-regulating Glucose-6-phosphatase and peroxisome proliferator-activated receptor gamma, coactivator 1 alpha. *Hepatology* **56,** 186–197 (2012).
39. Chen, M. *et al.* Promoter hypermethylation mediated downregulation of FBP1 in human hepatocellular carcinoma and colon cancer. *PLoS One* **6,** e25564 (2011).
40. Warburg, O., Wind, F. & Negelein, E. The metabolism of tumors in the body. *J. Gen. Physiol.* **8,** 519–530 (1927).
41. Beyoğlu, D. *et al.* Tissue metabolomics of hepatocellular carcinoma: Tumor energy metabolism and the role of transcriptomic classification. *Hepatology* **58,** 229–238 (2013).
42. Cairns, R. A., Harris, I. S. & Mak, T. W. Regulation of cancer cell metabolism. *Nat. Rev. Cancer* **11,** 85–95 (2011).
43. Mattaini, K. R., Sullivan, M. R. & Vander Heiden, M. G. The importance of serine metabolism in cancer. *J. Cell Biol.* **214,** 249–257 (2016).

44. Locasale, J. W. *et al.* Phosphoglycerate dehydrogenase diverts glycolytic flux and contributes to oncogenesis. *Nat. Genet.* **43,** 869–874 (2011).
45. Böhm, F., Köhler, U. A., Speicher, T. & Werner, S. Regulation of liver regeneration by growth factors and cytokines. *EMBO Mol. Med.* **2,** 294–305 (2010).
46. Bataller, R. & Brenner, D. Liver fibrosis. *J. Clin. Invest.* **115,** 209–218 (2005).
47. Page, A., Mann, D. A. & Mann, J. The mechanisms of HSC activation and epigenetic regulation of HSCs phenotypes. *Curr. Pathobiol. Rep.* **2,** 163–170 (2014).
48. Hernandez-Gea, V. & Friedman, S. L. Pathogenesis of Liver Fibrosis. *Annu. Rev. Pathol. Mech. Dis.* **6,** 425–456 (2011).
49. Friedman, S. L. Mechanisms of Hepatic Fibrogenesis. *Gastroenterology* **134,** 1655–1669 (2008).
50. Trautwein, C., Friedman, S. L., Schuppan, D. & Pinzani, M. Hepatic fibrosis: Concept to treatment. *Journal of Hepatology* **62,** S15–S24 (2015).
51. Friedman, S. L. Hepatic stellate cells: Protean, multifunctional, and enigmatic cells of the liver. *Physiol. Rev.* **88,** 125–172 (2008).
52. Puche, J. E., Saiman, Y. & Friedman, S. L. Hepatic stellate cells and liver fibrosis. *Compr. Physiol.* **3,** 1473–1492 (2013).
53. Panebianco, C., Oben, J. A., Vinciguerra, M. & Pazienza, V. Senescence in hepatic stellate cells as a mechanism of liver fibrosis reversal: a putative synergy between retinoic acid and PPAR-gamma signalings. *Clin. Exp. Med.* **17,** 269–280 (2017).
54. Mann, J. *et al.* MeCP2 controls an epigenetic pathway that promotes myofibroblast transdifferentiation and fibrosis. *Gastroenterology* **138,** 705–714 (2010).
55. Dooley, S. & Ten Dijke, P. TGF-β in progression of liver disease. *Cell Tissue Res.* **347,** 245–256 (2012).
56. Rani, B. *et al.* Role of the tissue microenvironment as a therapeutic target in hepatocellular carcinoma. *World J. Gastroenterol.* **20,** 4128–4140 (2014).
57. Giannelli, G., Villa, E. & Lahn, M. Transforming growth factor- β as a therapeutic target in hepatocellular carcinoma. *Cancer Res.* **74,** 1890–1894 (2014).
58. Inagaki, Y. & Okazaki, I. Emerging insights into transforming growth factor ?? Smad signal in hepatic fibrogenesis. *Gut* **56,** 284–292 (2007).
59. Uemura, M. *et al.* Smad2 and Smad3 play different roles in rat hepatic stellate cell function and α-smooth muscle actin organization. *Mol. Biol. Cell* **16,** 4214–4224

(2005).

60. Zavadil, J. & Böttinger, E. P. TGF-β and epithelial-to-mesenchymal transitions. *Oncogene* **24,** 5764–5774 (2005).
61. Matsuzaki, K. *et al.* Autocrine stimulatory mechanism by transforming growth factor beta in human hepatocellular carcinoma. *Cancer Res.* **60,** 1394–1402 (2000).
62. Okumoto, K. *et al.* Possible contribution of circulating transforming growth factor-beta1 to immunity and prognosis in unresectable hepatocellular carcinoma. *Liver Int.* **24,** 21–28 (2004).
63. Wu, X.Z., Xie, G.R. & Chen, D. Hypoxia and hepatocellular carcinoma: The therapeutic target for hepatocellular carcinoma. *J. Gastroenterol. Hepatol.* **22,** 1178–1182 (2007).
64. Weljie, A. M. & Jirik, F. R. Hypoxia-induced metabolic shifts in cancer cells: Moving beyond the Warburg effect. *Int. J. Biochem. Cell Biol.* **43,** 981–989 (2011).
65. Marin-Hernandez, A., Gallardo-Perez, J., Ralph, S., Rodriguez-Enriquez, S. & Moreno-Sanchez, R. HIF-1alpha modulates energy metabolism in cancer cells by inducing over-expression of specific glycolytic isoforms. *Mini Rev. Med. Chem.* **9,** 1084–1101 (2009).
66. Hamaguchi, T. *et al.* Glycolysis module activated by hypoxia-inducible factor 1alpha is related to the aggressive phenotype of hepatocellular carcinoma. *Int. J. Oncol.* **33,** 725–731 (2008).
67. Carmeliet, P. & Jain, R. K. Angiogenesis in cancer and other diseases. *Nature* **407,** 249–257 (2000).
68. Copple, B. L., Bai, S., Burgoon, L. D. & Moon, J. O. Hypoxia-inducible factor-1α regulates the expression of genes in hypoxic hepatic stellate cells important for collagen deposition and angiogenesis. *Liver Int.* **31** 230–244 (2011).
69. Copple, B. L. Hypoxia stimulates hepatocyte epithelial to mesenchymal transition by hypoxia-inducible factor and transforming growth factor-beta-dependent mechanisms. *Liver Int.* **30,** 669–682 (2010).
70. Kouzarides, T. Chromatin modifications and their function. *Cell* **128,** 693–705 (2007).
71. Albert, M. & Helin, K. Histone methyltransferases in cancer. *Seminars in Cell and Developmental Biology* **21,** 209–220 (2010).
72. Esteller, M. Molecular origins of cancer epigenetics in cancer. *N Engl J Med* **358,**

1148–1159 (2008).

73. Baxter, E., Windloch, K., Gannon, F. & Lee, J. S. Epigenetic regulation in cancer progression. *Cell Biosci.* **4,** 45(2014).
74. Pogribny, I. P. & Rusyn, I. Role of epigenetic aberrations in the development and progression of human hepatocellular carcinoma. *Cancer Lett.* **342,** 223–230 (2014).
75. Wilson, C. L., Mann, D. A. & Borthwick, L. A. Epigenetic reprogramming in liver fibrosis and cancer. *Adv. Drug Deliv. Rev.* **121,** 124–132 (2017).
76. Jones, P. A. Functions of DNA methylation: islands, start sites, gene bodies and beyond. *Nat. Rev. Genet.* **13,** 484–492 (2012).
77. Yang, X. *et al.* Gene body methylation can alter gene expression and is a therapeutic target in cancer. *Cancer Cell* **26,** 577–590 (2014).
78. McCabe, M. T., Brandes, J. C. & Vertino, P. M. Cancer DNA methylation: molecular mechanisms and clinical implications. *Clin. Cancer Res.* **15,** 3927–3937 (2009).
79. Villanueva, A. *et al.* DNA methylation-based prognosis and epidrivers in hepatocellular carcinoma. *Hepatology* **61,** 1945–1956 (2015).
80. Um, T. H. *et al.* Aberrant CpG island hypermethylation in dysplastic nodules and early HCC of hepatitis B virus-related human multistep hepatocarcinogenesis. *J. Hepatol.* **54,** 939–947 (2011).
81. Lee, S. *et al.* Aberrant CpG island hypermethylation along multistep hepatocarcinogenesis. *Am. J. Pathol.* **163,** 1371–1378 (2003).
82. Tomasi, M. L., Li, T. W., Li, M., Mato, J. M. & Lu, S. C. Inhibition of human methionine adenosyltransferase 1A transcription by coding region methylation. *J. Cell. Physiol.* **227,** 1583–1591 (2012).
83. Robertson, K. D., Keyomarsi, K., Gonzales, F. A., Velicescu, M. & Jones, P. A. Differential mRNA expression of the human DNA methyltransferases (DNMTs) 1, 3a and 3b during the G(0)/G(1) to S phase transition in normal and tumor cells. *Nucleic Acids Res.* **28,** 2108–13 (2000).
84. Roll, J. D., Rivenbark, A. G., Jones, W. D. & Coleman, W. B. DNMT3b overexpression contributes to a hypermethylator phenotype in human breast cancer cell lines. *Mol. Cancer* **7,** 15 (2008).
85. Saito, Y. *et al.* Increased protein expression of DNA methyltransferase (DNMT) 1 is significantly correlated with the malignant potential and poor prognosis of

human hepatocellular carcinomas. *Int. J. Cancer* **105,** 527–532 (2003).

86. Zhang, W. & Xu, J. DNA methyltransferases and their roles in tumorigenesis. *Biomark. Res.* **5,** 1 (2017).
87. Saito, Y. *et al.* Expression of mRNA for DNA methyltransferases and methyl-CpG-binding proteins and DNA methylation status on CpG islands and pericentromeric satellite regions during human hepatocarcinogenesis. *Hepatology* **33,** 561–568 (2001).
88. Revill, K. *et al.* Genome-wide methylation analysis and epigenetic unmasking identify tumor suppressor genes in hepatocellular carcinoma. *Gastroenterology* **145,** 1424-1435 (2013).
89. Moran-Salvador, E. & Mann, J. Epigenetics and liver fibrosis. *Cell. Mol. Gastroenterol. Hepatol.* **4,** 125–134 (2017).
90. Morgan, M. A. & Shilatifard, A. Chromatin signatures of cancer. *Genes Dev.* **29,** 238–249 (2015).
91. Hou, L., Zhang, X., Wang, D. & Baccarelli, A. Environmental chemical exposures and human epigenetics. *Int. J. Epidemiol.* **41,** 79–105 (2012).
92. Sudo, T. *et al.* Clinicopathological significance of EZH2 mRNA expression in patients with hepatocellular carcinoma. *Br. J. Cancer* **92,** 1754–1758 (2005).
93. Cai, M. Y. *et al.* EZH2 protein: a promising immunomarker for the detection of hepatocellular carcinomas in liver needle biopsies. *Gut* **60,** 967–976 (2011).
94. He, C. *et al.* High expression of trimethylated histone H3 lysine 4 is associated with poor prognosis in hepatocellular carcinoma. *Hum. Pathol.* **43,** 1425–1435 (2012).
95. Cai, M. Y. *et al.* High expression of H3K27me3 in human hepatocellular carcinomas correlates closely with vascular invasion and predicts worse prognosis in patients. *Mol. Med.* **17,** 12–20 (2011).
96. Mann, J. & Mann, D. A. Epigenetic regulation of wound healing and fibrosis. *Curr. Opin. Rheumatol.* **25,** 101–107 (2013).
97. Mann, J. & Mann, D. A. Transcriptional regulation of hepatic stellate cells. *Adv. Drug Deliv. Rev.* **61,** 497–512 (2009).
98. Page, A. *et al.* Hepatic stellate cell transdifferentiation involves genome-wide remodeling of the DNA methylation landscape. *J. Hepatol.* **64,** 661–673 (2016).
99. Carloni, V., Luong, T. V. & Rombouts, K. Hepatic stellate cells and extracellular matrix in hepatocellular carcinoma: more complicated than ever. *Liver Int.* **34,**

834–843 (2014).

100. Zhao, Q., Qin, C. Y., Zhao, Z. H., Fan, Y. C. & Wang, K. Epigenetic modifications in hepatic stellate cells contribute to liver fibrosis. *Tohoku J. Exp. Med.* **229,** 35–43 (2013).
101. Qin, L. & Han, Y. P. Epigenetic repression of matrix metalloproteinases in myofibroblastic hepatic stellate cells through histone deacetylases 4: implication in tissue fibrosis. *Am. J. Pathol.* **177,** 1915–28 (2010).
102. Pannem, R. R., Dorn, C., Hellerbrand, C. & Massoumi, R. Cylindromatosis gene CYLD regulates hepatocyte growth factor expression in hepatic stellate cells through interaction with histone deacetylase 7. *Hepatology* **60,** 1066–1081 (2014).
103. Glenisson, W., Castronovo, V. & Waltregny, D. Histone deacetylase 4 is required for TGFβ1-induced myofibroblastic differentiation. *Biochim. Biophys. Acta - Mol. Cell Res.* **1773,** 1572–1582 (2007).
104. Ding, N. *et al.* A vitamin D receptor/SMAD genomic circuit gates hepatic fibrotic response. *Cell* **153,** 601–613 (2013).
105. Mann, J. *et al.* Regulation of myofibroblast transdifferentiation by DNA methylation and MeCP2: implications for wound healing and fibrogenesis. *Cell Death Differ.* **14,** 275–285 (2007).
106. Perugorria, M. J. *et al.* Histone methyltransferase ASH1 orchestrates fibrogenic gene transcription during myofibroblast transdifferentiation. *Hepatology* **56,** 1129–1139 (2012).
107. Tachibana, M. *et al.* Histone methyltransferases G9a and GLP form heteromeric complexes and are both crucial for methylation of euchromatin at H3-K9. *Genes Dev.* **19,** 815–826 (2005).
108. Dong, K. B. *et al.* DNA methylation in ES cells requires the lysine methyltransferase G9a but not its catalytic activity. *EMBO J.* **27,** 2691–2701 (2008).
109. Estève, P.O. *et al.* Direct interaction between DNMT1 and G9a coordinates DNA and histone methylation during replication. *Genes Dev.* **20,** 3089–3103 (2006).
110. Kim, J. K., Estève, P.O., Jacobsen, S. E. & Pradhan, S. UHRF1 binds G9a and participates in p21 transcriptional regulation in mammalian cells. *Nucleic Acids Res.* **37,** 493–505 (2009).
111. McGarvey, K. M. *et al.* Silenced tumor suppressor genes reactivated by DNA demethylation do not return to a fully euchromatic chromatin state. *Cancer Res.*

66, 3541–3549 (2006).

112. Nguyen, C. T. *et al.* Histone H3-lysine 9 methylation is associated with aberrant gene silencing in cancer cells and is rapidly reversed by 5-aza-2'-deoxycytidine. *Cancer Res.* **62,** 6456–6461 (2002).
113. Wozniak, R. J., Klimecki, W. T., Lau, S. S., Feinstein, Y. & Futscher, B. W. 5-Aza-2′-deoxycytidine-mediated reductions in G9A histone methyltransferase and histone H3 K9 di-methylation levels are linked to tumor suppressor gene reactivation. *Oncogene* **26,** 77–90 (2007).
114. Collins, R. & Cheng, X. A case study in cross-talk: The histone lysine methyltransferases G9a and GLP. *Nucleic Acids Res.* **38,** 3503–3511 (2010).
115. Tachibana, M., Matsumura, Y., Fukuda, M., Kimura, H. & Shinkai, Y. G9a/GLP complexes independently mediate H3K9 and DNA methylation to silence transcription. *EMBO J.* **27,** 2681–2690 (2008).
116. Zhang, X., Huang, Y. & Shi, X. Emerging roles of lysine methylation on non-histone proteins. *Cell. Mol. Life Sci.* **72,** 4257–4272 (2015).
117. Olcina, M. *et al.* H3K9me3 facilitates hypoxia-induced p53-dependent apoptosis through repression of APAK. *Oncogene* **35,** 793–799 (2016).
118. Lee, D. Y., Northrop, J. P., Kuo, M.-H. & Stallcup, M. R. Histone H3 lysine 9 methyltransferase G9a is a transcriptional coactivator for nuclear receptors. *J. Biol. Chem.* **281,** 8476–8485 (2006).
119. Yokoyama, M. *et al.* Histone lysine methyltransferase G9a is a novel epigenetic target for the treatment of hepatocellular carcinoma. *Oncotarget* **8,** 21315–21326 (2017).
120. Bai, K. *et al.* Association of histone methyltransferase G9a and overall survival after liver resection of patients with hepatocellular carcinoma with a median observation of 40 months. *Medicine (Baltimore).* **95,** e2493 (2016).
121. Wei, L. *et al.* Histone methyltransferase G9a promotes liver cancer development by epigenetic silencing of tumor suppressor gene RARRES3. *J. Hepatol.* **67,** 758–769 (2017).
122. Casciello, F., Windloch, K., Gannon, F. & Lee, J. S. Functional role of G9a histone methyltransferase in cancer. *Front. Immunol.* **6,** 487 (2015).
123. Chen, M. W. *et al.* H3K9 histone methyltransferase G9a promotes lung cancer invasion and metastasis by silencing the cell adhesion molecule Ep-CAM. *Cancer Res.* **70,** 7830–7840 (2010).

124. Dong, C. *et al.* G9a interacts with Snail and is critical for Snail-mediated E-cadherin repression in human breast cancer. *J. Clin. Invest.* **122,** 1469–1486 (2012).

125. Chen, H., Yan, Y., Davidson, T. L., Shinkai, Y. & Costa, M. Hypoxic stress induces dimethylated histone H3 lysine 9 through histone methyltransferase G9a in mammalian cells. *Cancer Res.* **66,** 9009–9016 (2006).

126. Lee, J. S. *et al.* Negative regulation of hypoxic responses via induced Reptin methylation. *Mol. Cell* **39,** 71–85 (2010).

127. Ding, J. *et al.* The histone H3 methyltransferase G9a epigenetically activates the serine-glycine synthesis pathway to sustain cancer cell survival and proliferation. *Cell Metab.* **18,** 896–907 (2013).

128. Lachenmayer, A. *et al.* Combination therapy for hepatocellular carcinoma: Additive preclinical efficacy of the HDAC inhibitor panobinostat with sorafenib. *J. Hepatol.* **56,** 1343–1350 (2012).

129. Braun, C. J. & Hemann, M. T. Rewiring the solid tumor epigenome for cancer therapy. *Expert Rev. Anticancer Ther.* **16,** 977–987 (2016).

130. Rabal, O. *et al.* Discovery of reversible DNA methyltransferase and lysine methyltransferase G9a inhibitors with antitumoral in vivo efficacy. *J. Med. Chem.* **61,** 6518–6545 (2018).

131. Rabal, O. *et al.* Detailed exploration around 4-aminoquinolines chemical space to navigate the lysine methyltransferase G9a and DNA methyltransferase biological spaces. *J. Med. Chem.* **61,** 6546–6573 (2018).

132. San José-Enériz, E. *et al.* Discovery of first-in-class reversible dual small molecule inhibitors against G9a and DNMTs in hematological malignancies. *Nat. Commun.* **8,** 15424 (2017).

133. Chang, Y. *et al.* Structural basis for G9a-like protein lysine methyltransferase inhibition by BIX-01294. *Nat. Struct. Mol. Biol.* **16,** 312–317 (2009).

134. Liu, F. *et al.* Discovery of a 2,4-Diamino-7-aminoalkoxyquinazoline as a potent and selective inhibitor of histone lysine methyltransferase G9a. *J. Med. Chem.* **52,** 7950–7953 (2009).

135. Liu, F. *et al.* Protein lysine methyltransferase G9a inhibitors: design, synthesis, and structure activity relationships of 2,4-diamino-7-aminoalkoxy-quinazolines. *J. Med. Chem.* **53,** 5844–5857 (2010).

136. Vedadi, M. *et al.* A chemical probe selectively inhibits G9a and GLP

methyltransferase activity in cells. *Nat. Chem. Biol.* **7,** 566–574 (2011).

137. Song, J., Teplova, M., Ishibe-Murakami, S. & Patel, D. J. Structure-based mechanistic insights into DNMT1-mediated maintenance DNA methylation. *Science* **335,** 709–712 (2012).
138. Nault, J. C. *et al.* High frequency of telomerase reverse-transcriptase promoter somatic mutations in hepatocellular carcinoma and preneoplastic lesions. *Nat. Commun.* **4,** 2218 (2013).
139. Dauch, D. *et al.* A MYC-aurora kinase A protein complex represents an actionable drug target in p53-altered liver cancer. *Nat. Med.* **22,** 744–753 (2016).
140. Rebouissou, S. *et al.* Proliferation markers are associated with MET expression in hepatocellular carcinoma and predict Tivantinib sensitivity in vitro. *Clin. Cancer Res.* **23,** 4364–4375 (2017).
141. Rombouts, K. & Carloni, V. Determination and characterization of tetraspanin-associated phosphoinositide-4 kinases in primary and neoplastic liver cells. *Methods Mol. Biol.* **1376,** 203–212 (2016).
142. Chou, T.-C. Drug combination studies and their synergy quantification using the Chou-talalay method. *Cancer Res.* **70,** 440–446 (2010).
143. Irizarry, R. A. *et al.* Summaries of Affymetrix GeneChip probe level data. *Nucleic Acids Res.* **31,** e15 (2003).
144. Gentleman, R. C. *et al.* Bioconductor: open software development for computational biology and bioinformatics. *Genome Biol.* **5,** R80 (2004).
145. Smyth, G. K. Linear models and empirical bayes methods for assessing differential expression in microarray experiments. *Stat. Appl. Genet. Mol. Biol.* **3,** 1–25 (2004).
146. Rodriguez-Collazo, P., Leuba, S. H. & Zlatanova, J. Robust methods for purification of histones from cultured mammalian cells with the preservation of their native modifications. *Nucleic Acids Res.* **37,** e81 (2009).
147. Mitro, N. *et al.* Insights in the regulation of cholesterol 7α-hydroxylase gene reveal a target for modulating bile acid synthesis. *Hepatology* **46,** 885–897 (2007).
148. Huidobro, C. *et al.* A DNA methylation signature associated with the epigenetic repression of glycine N-methyltransferase in human hepatocellular carcinoma. *J. Mol. Med.* **91,** 939–950 (2013).
149. Dong, C. *et al.* Loss of FBP1 by snail-mediated repression provides metabolic advantages in basal-like breast cancer. *Cancer Cell* **23,** 316–331 (2013).
150. Jiang, Y. *et al.* Histone H3K9 demethylase JMJD1A modulates hepatic stellate

cells activation and liver fibrosis by epigenetically regulating peroxisome proliferator-activated receptor γ. *FASEB J.* **29,** 1830–1841 (2015).

151. Mudbhary, R. *et al.* UHRF1 overexpression drives DNA hypomethylation and hepatocellular carcinoma. *Cancer Cell* **25,** 196–209 (2014).
152. Nault, J. *et al.* A Hepatocellular carcinoma 5-gene score associated with survival of patients after liver resection. *Gastroenterology* **145,** 176–187 (2013).
153. Tan, J. *et al.* Pharmacologic disruption of Polycomb-repressive complex 2-mediated gene repression selectively induces apoptosis in cancer cells. *Genes Dev.* **21,** 1050–1063 (2007).
154. Hoshida, Y. *et al.* Integrative transcriptome analysis reveals common molecular subclasses of human hepatocellular carcinoma. *Cancer Res.* **69,** 7385–7392 (2009).
155. Hsiao, L.L. *et al.* A compendium of gene expression in normal human tissues. *Physiol. Genomics* **7,** 97–104 (2001).
156. Maehara, O. *et al.* A pivotal role of Krüppel-like factor 5 in regulation of cancer stem-like cells in hepatocellular carcinoma. *Cancer Biol. Ther.* **16,** 1453–1461 (2015).
157. Jin, R. *et al.* TR4 nuclear receptor suppresses HCC cell invasion via downregulating the EphA2 expression. *Cell Death Dis.* **9,** 283 (2018).
158. Oh, B.K., Chae, K. J., Park, C. & Park, Y. N. Molecular analysis of PinX1 in human hepatocellular carcinoma. *Oncol. Rep.* **12,** 861–866 (2004).
159. Cavallaro, U. & Christofori, G. Cell adhesion in tumor invasion and metastasis: loss of the glue is not enough. *Biochim. Biophys. Acta - Rev. Cancer* **1552,** 39–45 (2001).
160. Giannelli, G., Koudelkova, P., Dituri, F. & Mikulits, W. Role of epithelial to mesenchymal transition in hepatocellular carcinoma. *J. Hepatol.* **65,** 798–808 (2016).
161. Ji, Y. *et al.* Human liver methionine cycle: MAT1A and GNMT gene resequencing, functional genomics, and hepatic genotype-phenotype correlation. *Drug Metab. Dispos.* **40,** 1984–1992 (2012).
162. Qiu, X. *et al.* Upregulation of DNMT1 mediated by HBx suppresses RASSF1A expression independent of DNA methylation. *Oncol. Rep.* **31,** 202–208 (2014).
163. Casciello, F. *et al.* G9a drives hypoxia-mediated gene repression for breast cancer cell survival and tumorigenesis. *Proc. Natl. Acad. Sci. U. S. A.* **114,** 7077–7082

(2017).

164. Hardy, T. *et al.* Plasma DNA methylation: a potential biomarker for stratification of liver fibrosis in non-alcoholic fatty liver disease. *Gut* **66,** 1321–1328 (2017).
165. Wang, L. *et al.* Histone H3K9 methyltransferase G9a represses PPARγ expression and adipogenesis. *EMBO J.* **32,** 45–59 (2012).
166. Chen, Y. *et al.* Hedgehog controls hepatic stellate cell fate by regulating metabolism. *Gastroenterology* **143,** 1319–1329 (2012).
167. Hong, F. *et al.* Histone methylation regulates Hif-1 signaling cascade in activation of hepatic stellate cells. *FEBS Open Bio* **8,** 406–415 (2018).
168. Liu, M. *et al.* Dual inhibition of DNA and histone methyltransferases increases viral mimicry in ovarian cancer cells. *Cancer Res.* **17,** 3953 (2018).
169. Mozzetta, C., Pontis, J. & Ait-Si-Ali, S. Functional crosstalk between lysine methyltransferases on histone substrates: the case of G9a/GLP and Polycomb Repressive Complex 2. *Antioxid. Redox Signal* **22,** 1365–1381 (2015).
170. Chin, H. G. *et al.* Automethylation of G9a and its implication in wider substrate specificity and HP1 binding. *Nucleic Acids Res.* **35,** 7313–7323 (2007).
171. Poulard, C. *et al.* A post-translational modification switch controls coactivator function of histone methyltransferases G9a and GLP. *EMBO Rep.* **18,** 1442–1459 (2017).
172. Ferry, L. *et al.* Methylation of DNA ligase 1 by G9a/GLP recruits UHRF1 to replicating DNA and regulates DNA methylation. *Mol. Cell* **67,** 550–565 (2017).
173. Ahmad, F., Dixit, D., Joshi, S. D. & Sen, E. G9a inhibition induced PKM2 regulates autophagic responses. *Int. J. Biochem. Cell Biol.* **78,** 87–95 (2016).
174. Liu, H., Pathak, P., Boehme, S. & Chiang, J. Y. L. Cholesterol 7α-hydroxylase protects the liver from inflammation and fibrosis by maintaining cholesterol homeostasis. *J. Lipid Res.* **57,** 1831–1844 (2016).
175. Fang, S. *et al.* Coordinated recruitment of histone methyltransferase G9a and other chromatin-modifying enzymes in SHP-mediated regulation of hepatic bile acid metabolism. *Mol. Cell. Biol.* **27,** 1407–1424 (2007).
176. Hay, N. Reprogramming glucose metabolism in cancer: can it be exploited for cancer therapy? *Nat. Rev. Cancer* **16,** 635–649 (2016).
177. Yang, J. *et al.* Loss of FBP1 facilitates aggressive features of hepatocellular carcinoma cells through the Warburg effect. *Carcinogenesis* **38,** 134–143 (2017).
178. Li, B. *et al.* Fructose-1,6-bisphosphatase opposes renal carcinoma progression.

Nature **513,** 251–255 (2014).

179. Bao, L. *et al.* Methylation of hypoxia-inducible factor (HIF)-1α by G9a/GLP inhibits HIF-1 transcriptional activity and cell migration. *Nucleic Acids Res.* **46,** 6576–6591 (2018).
180. Oh, S. Y. *et al.* The histone methyltransferase inhibitor BIX01294 inhibits HIF-1D stability and angiogenesis. *Mol. Cells* **38,** 528–534 (2015).
181. De Minicis, S. *et al.* Gene expression profiles during hepatic stellate cell activation in culture and in vivo. *Gastroenterology* **132,** 1937–1946 (2007).
182. Morán-Salvador, E. *et al.* Cell-specific PPARγ deficiency establishes anti-inflammatory and anti-fibrogenic properties for this nuclear receptor in non-parenchymal liver cells. *J. Hepatol.* **59,** 1045–1053 (2013).
183. Miyahara, T. *et al.* Peroxisome proliferator-activated receptors and hepatic stellate cell activation. *J. Biol. Chem.* **275,** 35715–35722 (2000).
184. Galli, A. *et al.* Antidiabetic thiazolidinediones inhibit collagen synthesis and hepatic stellate cell activation in vivo and in vitro. *Gastroenterology* **122,** 1924–1940 (2002).
185. Tomita, K. *et al.* Pioglitazone prevents alcohol-induced fatty liver in rats through up-regulation of c-Met. *Gastroenterology* **126,** 873–885 (2004).
186. Yavrom, S. *et al.* Peroxisome proliferator-activated receptor γ suppresses proximal α1(I) collagen promoter via inhibition of p300-facilitated NF-I binding to DNA in hepatic stellate cells. *J. Biol. Chem.* **280,** 40650–40659 (2005).
187. Hazra, S. *et al.* Peroxisome proliferator-activated receptor γ induces a phenotypic switch from activated to quiescent hepatic stellate cells. *J. Biol. Chem.* **279,** 11392–11401 (2004).
188. Tsukamoto, H. Adipogenic phenotype of hepatic stellate cells. *Alcohol. Clin. Exp. Res.* **29,** 132S–133S (2005).
189. Seki, E. *et al.* TLR4 enhances TGF-β signaling and hepatic fibrosis. *Nat. Med.* **13,** 1324–1332 (2007).
190. de Thé, H. Differentiation therapy revisited. *Nat. Rev. Cancer* **18,** 117–127 (2017).

Annex

Annex 1. *FBP1* promoter sequence. Region of *FBP1* promoter sequence indicating the regions of qChip, MSP and pyrosequencing primers annealing.

>FBP1 (NM_001127628)

ttccagttggcttttccaatttatacctgcagcatggatctctcctctga
actccagatacataaatctgtctatttgacattgccttggatgtctagaa
ggcatttcaaacttagcaggtcccacacttagctcctaattgtcagtcct
gcctccagcacacgcccctctcggtgttccccatcgcagtcgaggacaac
tgcattcttctagtttctcaggcctcaaaccttagaatcatccgagactc
ctgtctctcacatatctcatctgtcaacgaatcccatcagctctaccttc
aaaatatgtccagaatccaccacctccactgctaacacctggctcactat
ctcctagtaacctggagggcactgtcttcagtctgatcttcacacagtag
ccgcagtatgaagacacagggtagaccatgcctctcttcttctccaaact
ctccagtgggttcctcctagtcaaagtcaaacctcacttggccctctaga
cctcacctctgcatcctcccgctggccttatctcctccacctctgaccct
tgctagctctatttcagctccaccggtctcctggccattccctgaacctg
aaacatggtctcctaccccagggcctgtgcactggctctcccggtgagga
aaccgctctccttcccatctccaccggcgcgttgcatccttcacctcttt
gctcacatatccctttctcagagaagcttttactgaggcctctgctcacc
ctcttctcccctccacattccgtgtcttccttttctatttcgtttctctc
tatggtacttatggcttatgtaacaaactaatctattgtttatatattta
tttttactgtttctctgtgaaaacgtacactcgaaaagggcaggagtttt
gtctgtttggatcaggctccacccctggaaggtaggacagtgttcagcac
agcaggtgctcaataggtgttgtttcgtgaatcagcacatcaattgcagc
ATTGTGGCTACCAGGGGGTCAGGATGCGGGCGGTGGAGCCCTCTGGCCTT
TGTGTGGTAGCCGAGGACTCTGTGTCAGCGACCGTTTTCCGGGAAACTTC
CGGGCGAGACTCACATCTTGGAAATTCAAATACTCAATAGCTCTCGAATT
CTAGGAATCTTGAGAAGAGGCCTGGATTAAGGATTCAGACGTGGGCCCTC
AGATGGgtgagaaacggggactctgtgtctcctagcgggGACAGAAGGGC qChiP (Fw)
caggtgacaggccaggcagagtggacggggcttgggcaggggcgggggc
aggcagccacacggggcaggagctgcagagctaaagccaggccatgtgga
ctggctgcgggtttcgctgcctagctggtggcattgagcaagttacttaa
ccttttctgaacttccgttttatgattttggaggaaaCAGTCATAGCTTTC qChiP (Rev)
tctctggcagagtccgatggcccgagtcccgctccacagtgcgggtggag
ggcacggaggggtgtgtgtgggggggcgacagcccaggaagactaggggc
ggcagggcgcgtgggggcgggggttgggagaccgcagggaggatcccCGA Pyro PCR (Fw)
ccttgtctgaagatccaagcaggcggagccgcggtctggtccgcggggta
ggcggggcgcaagagtgttcccgggggcgggggccgacccgcgtctaaa
ggtttccgcgattcacccgccggcgcctg*gcctggcccagttgcacca*cg *Pyrosequencing primer*
ag**cg**ctg**cg**gacact**cg**ggg**cg**gcagt**cg**gtctgtcagtcctcc**cg**ccag MSP (Fw)
gtcc**cgcg**gcc**cg**cacctgc**cg**cc**cg**cacctgcagctccgcacctgcggc
cagtgcctactgccctctcttgccgcccgcacctgcagccccgcacctgc Pyro PCR (Rev)
cgcttgcacctgcagCCCCGCGCTCTACCCGGTTCAAGCATGGCTGACCA
GGCGCCCTT**CG**AC**A****CG**GA**CG**TCAACACCCTGACCCGCTTCGTCATGGAGG MSP (Rev)
AGGGCAGGAAGGCCCGCGGCACGGGCGAGTTGACCCAGCTGCTCAACTCG
CTCTGCACAGCAGTCAAAGCCATCTCTTCGGCGGTGCGCAAGGCGGGCAT
CGCGCACCTgtgagtcgggccttgggcggtgggccccgtcctgtctgtct
gcctggggagcctgcccggcgggctgacgttgggccctctgagcctcctg
ccgtcagcctctgtctgtccgtctgatgtctgagcgcctctctcgctctc
tgtctggtagcccctctctccagaagctggctcagcctcactcaagtcct
catctcctcccttgaccttggaggggcccacctgggggtccgtctcacag
gtgtacacctgattccatcttgcattcctcttctctgccctgagcagcct
gcctcgtacccctctcagccggccaagtgtgggcacctggcctgcccgtc
atacccgccctagcctcagacaggaaagtgctagctcaggtgccttcctt

Annex 2. *PPARγ* promoter sequence. Region of *PPARγ* promoter sequence indicating the regions of qChip and MSP primers annealing.

>hg38_ncbiRefSeqCurated_NM_005037.5

cttttt ggagtgatgaaaatgttctaagggtagatttggtgatgatggca
caactctgtcaataaactaaaactcattgaactgtacattttatttattt
atttttgagatggagtcttgctctggggctgaagtgcagtggcgcaatct
cggcttgtaacctctgcctcccagggtcaagcgattctactgcctcagcc
ccccgagtagctgagattacaggcacgtgccaccacgcccagctaatttt
tgtatttcttagtagagatggagtttcaccatgttggccaggctggtctt
gaactcccggcctcaagtgatccacctgcctcggcctcccaaagtgctgg
gattacaggcgtgagctgccatacccggcctgaattgtacattttacttc
tatggtatttacattttagattatattaattattcctcaataaagctgtg
atttttaaaaagcaggctaggcgcagtggctggtgcctataatcccagcac
tttggaaagctgaggcaggaggatcacttgagcccaggagtttcagacta
gtctaggcaacatgtcaagacacagtctctactaaacaattaaaattaaa
aaaaaaaattagccaggcatggtggtgtgcacctgtagtcccagctactt
gggagcctggggtgggaggattccttgagcccgggaagtcgaggctgaag
tgagccgtgattgcgccacagcactccagcctgggcgacacagcaacacc
ctgtctcatggaagaaagaaagaaaagaaaggaagaaagaaaaaaaaaaa
gcagattggaactctggaattaacaagaagtaggacgcacggagcacttc qChIP(Fw)
cgcctgagtggagactgtggatccgggtcaacctgactacctaaatcaca
ggccaataaatggtctttcagtggtcagtccctgtaagatccgtggctct
cagcttcttatcttaggggctgtggaggaaggacatgattatgttgattt qChIP(Rev)
aagcgctgaatattttcccttgtgatacccatcctcgcaaaactttgctt
caaccacaaacgaggaccttctgtaccagaggggcaataaccacaatgaa
gctaggaagaaatgcagagcaccccagcatacagtccataagcttcctga
agtgggggggcctcaggcatcgctgcctccccaaagaggatcaggcccaga
acagtatgctccagaaataagactggaaaaagggaaagaggggcctcaag MSP(Fw)
tccaggagaccagcggctttctgaacgcgcacctgccaacccactttgga
caggtcacgatggacagcgtggcaggaaaagaaaaggtcactgtctaccc
aacacatgagaaactgtttctcgtgcctcacgtccccactccgtccccac MSP(Rev)
ccatgttgtctgagtccctcggtgtcagaaacactgctaagaaatttaag
aaattctgttaatgagtttaagaaatgtttttaatgattaaaagtcagtg
acttgtgaataaccatgtaacttacaaacgcaaggaactctgaaagtgtg
cagcaccaccgatcagaagagaaaaccaagggacccgaaatatgctttaa
ttaaattttcttttaaaatgtcactggaaagaacatcttgggaagacggc
ctggccgatcgccgtgtgaagggcaagccactctggccgagagggagccc
cacacctcggtctccccagaccggccctggccgggggcatccccctaaac
ttcggatccctcctcggaaatgggaccctctctgggccgcctcccagcgg
tggtggcgaggagcaaacgacaccaggtagcctgccgcggggcagagagt
ggacgcgggaaagccggtggctcccgccgtgggccctactgtgcgcgggc
ggcggccgagcccgggccgctccctcccagtcgcgcgccgccgcccccgc
ccccgcccccgcccccgcccccacccccacccccacccccacccccagcc
GGCGCCCGCGCCCGCCCCCGCGCCGGGCCCGGCTCGGCCCGACCCGGCTC
CGCCGCGGGCAGGCGGGGCCCAGCGCACTCGGAGCCCGAGCCCGAGCCGC
AGCCGCCGCCTGGGGCGCTTGGGTCGGCCTCGAGGACACCGGAGAGGGGC
GCCACGCCGCCGTGGCCGCAGgtcagagtacgggtgcccgcggcgctcgg
gaaccggctgctggctgggcggggagtgctcagggaggggcgcggaggg
ctggggccgagggtctgggggctagggccgaggaaacgggaactgacggg
gtcccagacggatgagagctggggagaaggggtctcggctgaggggtcc
ggggctgaggcagggtcatggtccggcaggacccggactgacgggtcgcg
ggcgggcggctcacgggtgaccgggtgaaggggtcttgggctgagggcac
ccgggctgagggtcgcgtctaccggagcgcgcactaggggcggagggcgc

Bárcena-Varela M, et al. Dual Targeting of Histone Methyltransferase G9a and DNA-Methyltransferase 1 for the Treatment of Experimental Hepatocellular Carcinoma. Hepatology, 2019, 69(2):587-603. https://doi.org/10.1002/hep.30168

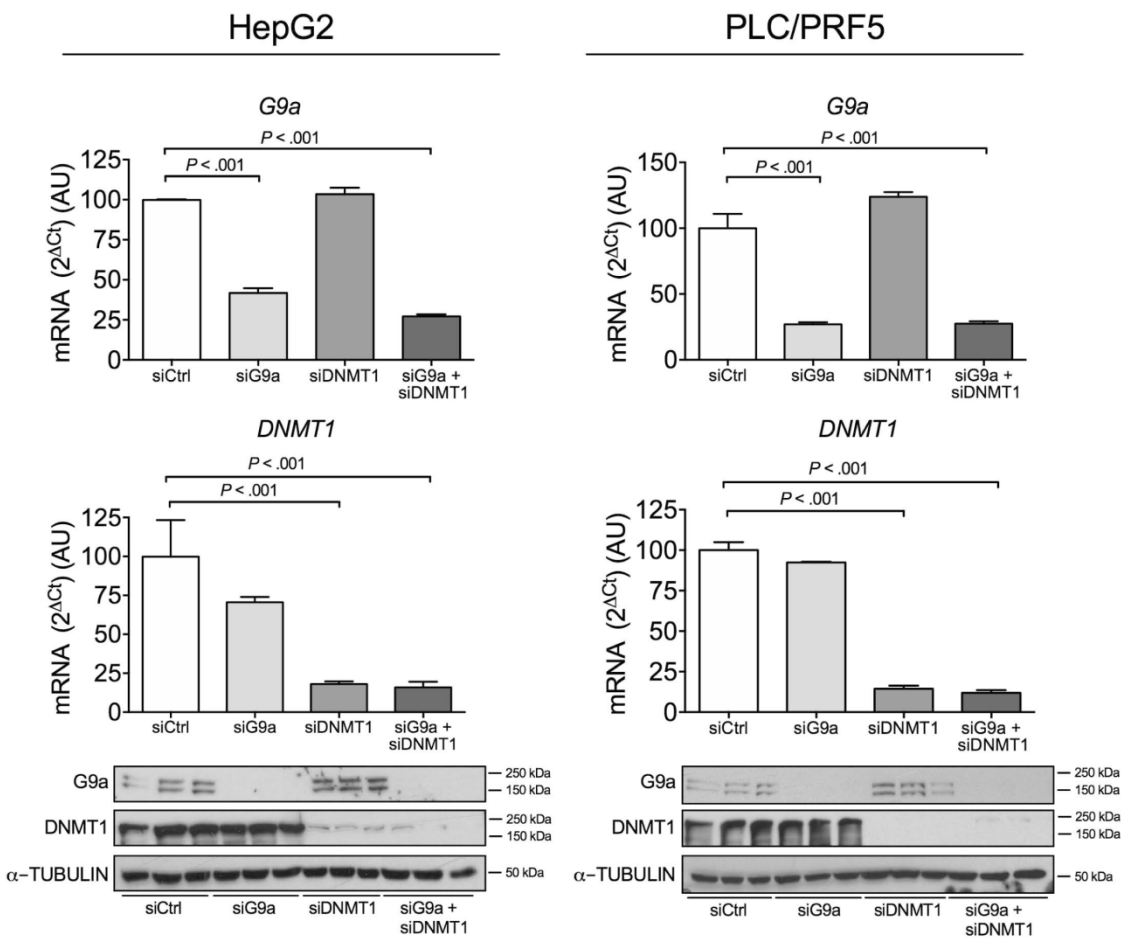

Supp. Figure 1

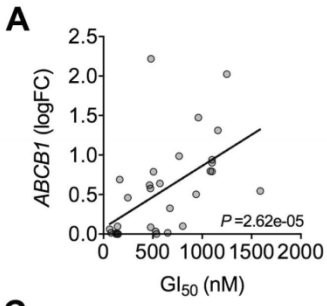

B

Compound ID	+/- GF-120 918	Cell Line	Mean Papp (10-6cm/s) A to B	Efflux Ratio	Net Efflux Ratio
Digoxin	-	MDCK II	0.79	8.84	6.73
	-	MDR1-MDCK II	0.19	59.46	
	+	MDCK II	1.97	1.73	1.35
	+	MDR1-MDCK II	1.37	2.34	
CM-272	-	MDCK II	0.40	4.02	5.35
	-	MDR1-MDCK II	0.18	21.50	
	+	MDCK II	0.37	2.16	1.36
	+	MDR1-MDCK II	0.20	2.94	

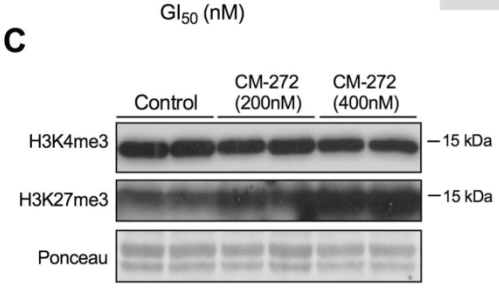

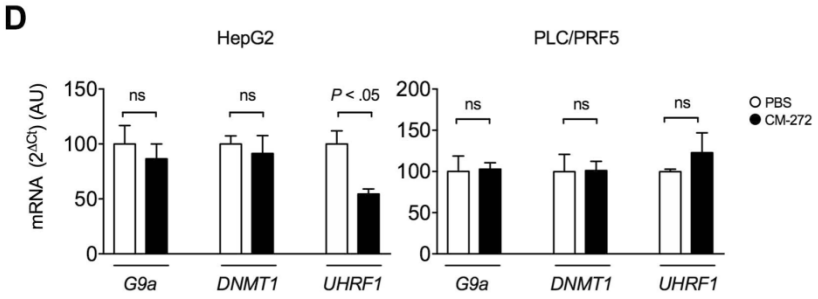

Supp. Figure 2

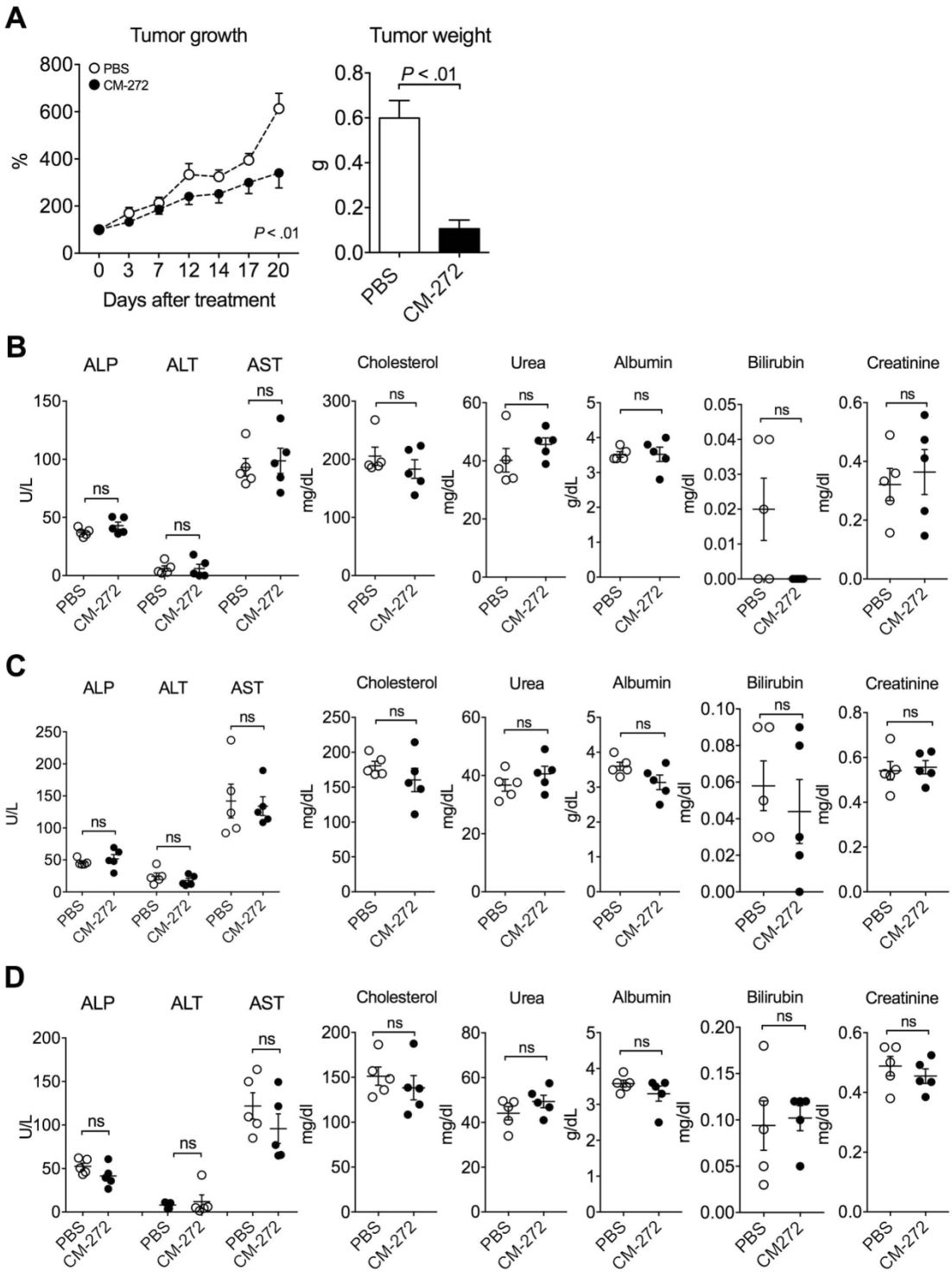

Supp. Figure 3

A

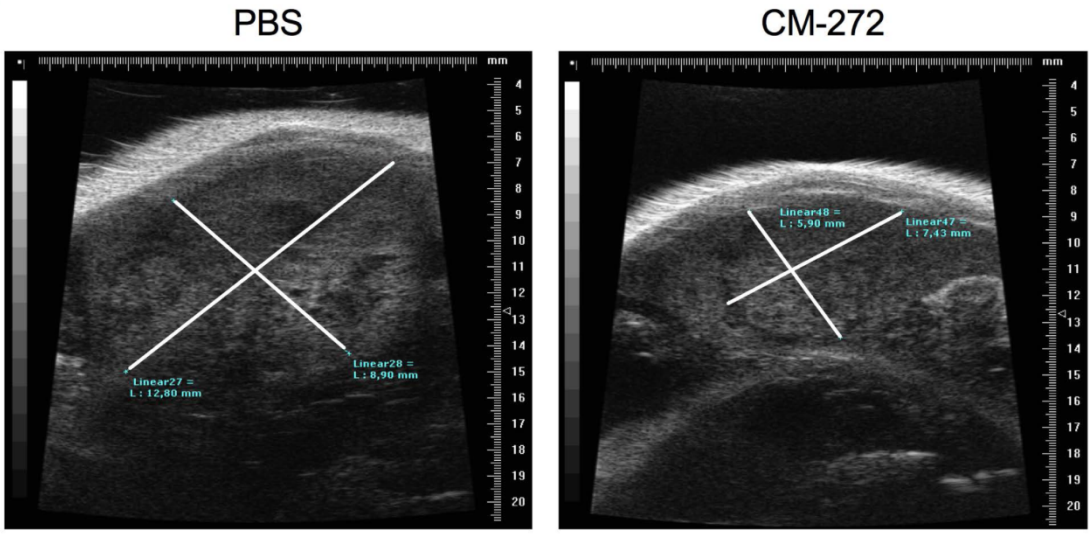

B

	Serum (µM)	Liver (µmol/kg)	Tumor (µmol/kg)
Subcutaneous PLC/PRF5	737.58 ± 243.3	30 ± 4.5	5.93 ± 1.81
Orthotopic PLC/PRF5	413.64 ± 73.2	35.23 ± 6.50	76.29 ± 33.62

Supp. Figure 4

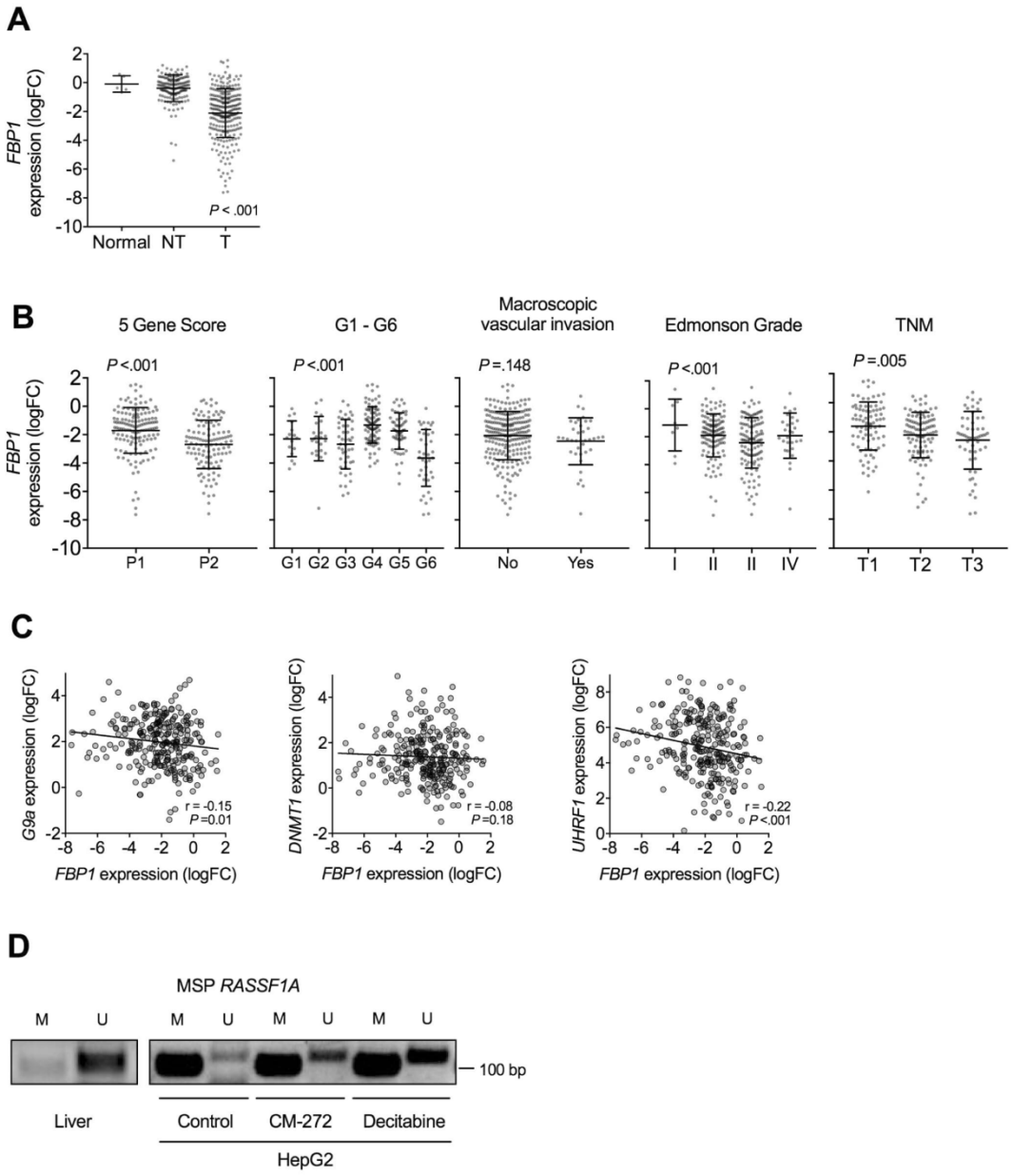

Supp. Figure 5

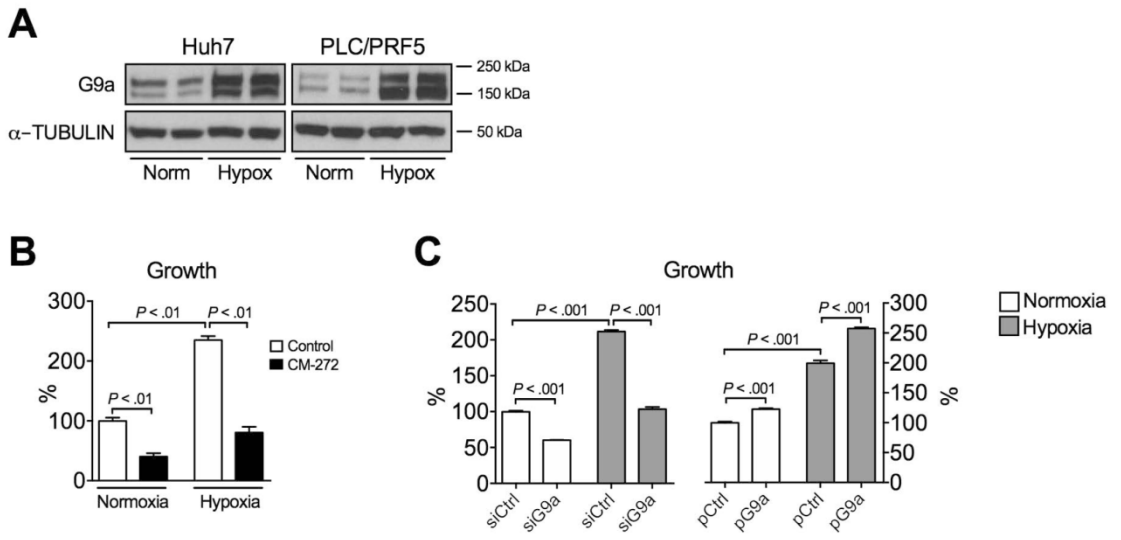

Supp. Figure 6

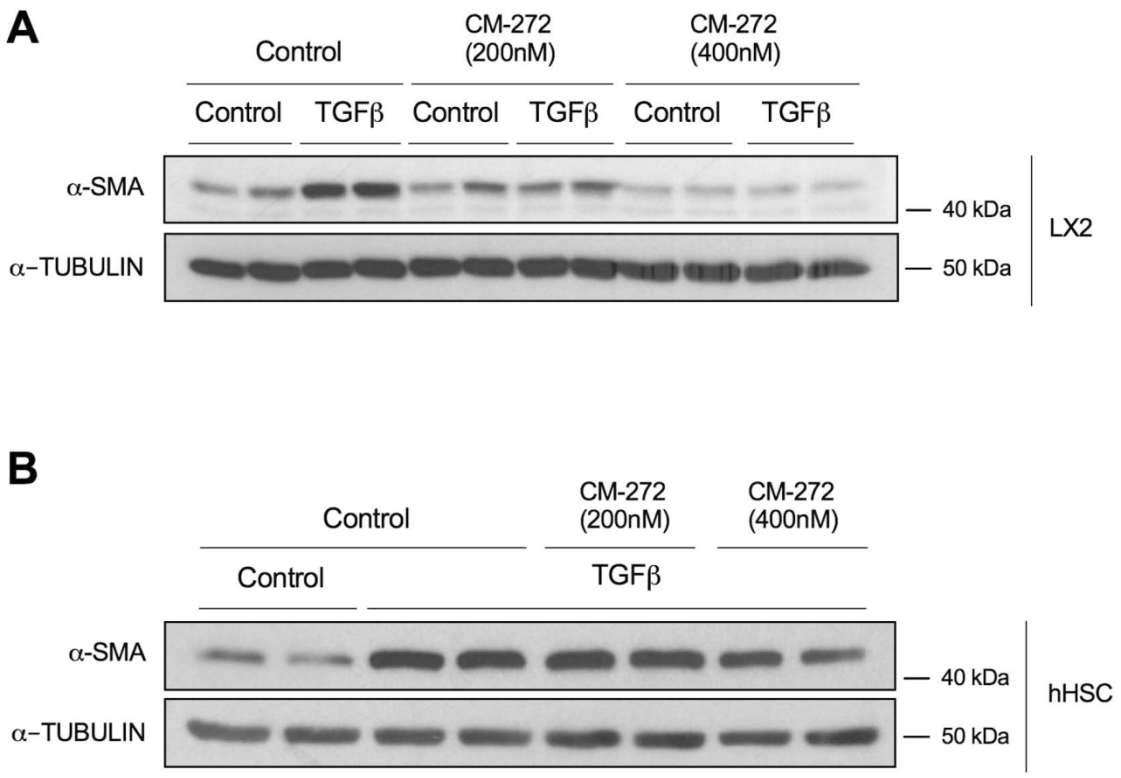

Supp. Figure 7

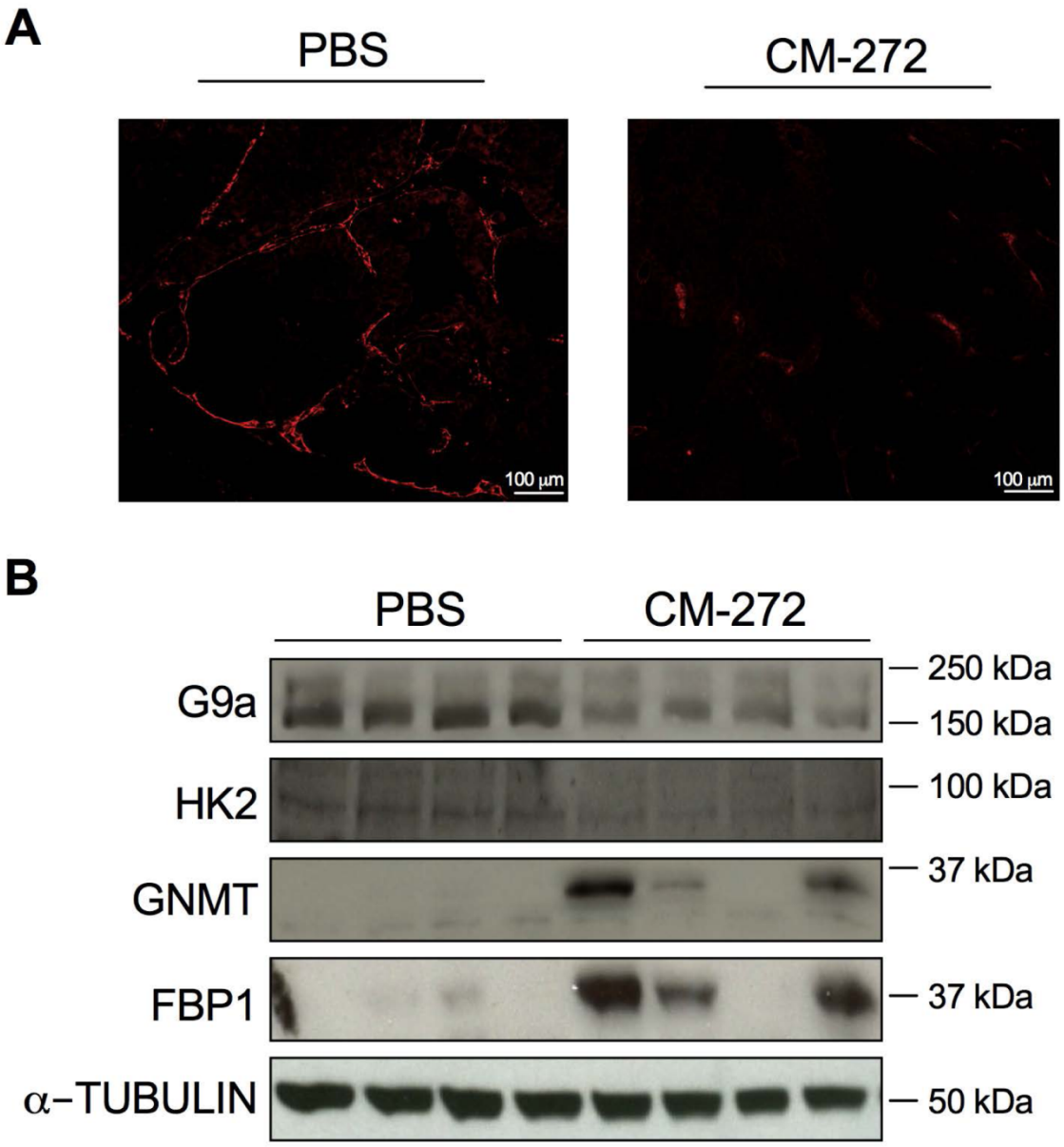

Supp. Figure 8

Supplementary Fig. 1. Validation of *G9a* and *DNMT1* expression knockdown upon specific siRNA transfections in HepG2 and PLC/PRF5 cells. mRNA levels were measured by qRT-PCR and protein levels were determined by western blotting 48h after transfections. Representative blots are shown. siCtrl: control siRNA; siG9a: G9a specific siRNA; siDNMT1: DNMT1 specific siRNA.

Supplementary Fig. 2. (A) Spearman correlation analysis of the mRNA levels of the *ABCB1* gene coding for the MDR1 drug efflux pump in our panel of HCC cell lines and their corresponding CM-272 GI_{50} values. (B) Evaluation of CM-272 as MDR1 substrate. To evaluate the MDR1 mediated efflux of CM-272 out of the cells, the efflux ratio (permeability value in the B-A direction divided by the permeability value in the A-B direction) of CM-272 was measured in MDCK cells which express human MDR1 (MDR1-MDCK II) or control MDCK cells. Compounds with an efflux ratio greater than 2 are typically considered a possible Mdr1 substrate, as for CM-272 (21.50). Further, compared to wild type MDCK II cells, the net efflux ratio is also greater than 2 (5.35). To evaluate, the Mdr1 mediated efflux, Elacridar (GF-120918), a known MDR1 inhibitor, was also included in the permeability assay. In the presence of Elacridar (10 μM), the net efflux ratio was significantly reduced (>50%; from 5.35 to 1.36) and close to unit (1.36). Digoxin, a known MDR1 substrate, was included as positive control. Nadolol and metoprolol were included as markers of low (P_{app} A to B $\leq 1.0\times10^{-6}$ cm/s) and high permeability ($\geq 5.5\times10^{-6}$ cm/s), respectively. (C) Western blot analysis of H3K4me3 and H3K27me3 levels in HepG2 cells treated with CM-272 for 48h as indicated. Representative blots are shown. (D) *G9a*, *DNMT1* and *UHRF1* mRNA levels in HepG2 and PLC/PRF5 cells treated with 400 nM of CM-272 for 48 h analyzed by qRT-PCR.

Supplementary Fig. 3. (A) Effect of CM-272 on the growth of HepG2 cells as subcutaneous xenografts in nude mice. Right panel: tumor weight in control (PBS) and CM-272-treated mice at the end of treatments. (B) Analysis of liver injury and liver function serum parameters in mice treated with vehicle (PBS) or CM-272 as indicated in the main text. Data from mice injected with PLC-PRF5 cells. (C) Analysis of liver injury and liver function serum parameters in mice treated with vehicle (PBS) or CM-272 as indicated in the main text. Data from mice injected with PLC/PRF5+LX2 cells. (D) Analysis of liver injury and liver function serum parameters in mice treated with vehicle (PBS) or CM-272 as indicated in the main text. Data from mice in which PLC/PRF5 cells derived tumors were orthotopically implanted in the livers of nude mice. Serum was analized at the end of treatments. ALP: alkaline phosphatase; ALT: alanine transaminase; AST: aspartate transaminase.

Supplementary Fig. 4. (A) Representative ultrasound images of PLC/PRF5 cells derived tumors orthotopically implanted in the liver of nude mice after treatment with CM-272 or PBS. The diameters of tumors are indicated. (B) Determination of CM-272 concentrations in serum, liver and tumor tissues from the indicated xenograft tumor models.

Supplementary Fig. 5. (A) *FBP1* mRNA levels in normal, NT and T human liver tissues. (B) *FBP1* gene expression in tumoral liver tissues from patients classified according to the 5-gene score, the G1 to G6 transcriptomic groups, the presence of macroscopic vascular invasion, the Edmonson Grade and the TNM score. (C) Spearman correlation analysis of *FBP1* expression with that of *G9a*, *DNMT1* and *UHRF1* in tumoral liver tissue samples. (D) DNA methylation analysis in *RASSF1A* promoter in control and CM-272 treated cells. Genomic DNA from normal human liver and the effect of decitabine on HepG2 cells were used as controls. Bands in lanes labeled “U” and “M” are PCR products

amplified with unmethylation- and methylation-specific primers. Images are representative of three experiments performed in duplicates.

Supplementary Fig. 6. (A) Expression of G9a in HCC cells grown under normoxic or hypoxic conditions for 24h as analyzed by western blotting. Representative blots are shown. (B) Effect of CM-272 (400nM) on hypoxia-induced PLC/PRF5 cell growth. Cells were pretreated with CM-272 for 24h and then kept in normoxic or hypoxic conditions for another 24h. (C) Effect of *G9a* knockdown or overexpression on the growth of HepG2 cells in normoxic or hypoxic conditions. Cells were transfected with siRNAs (siCtrl: control siRNA; siG9a: G9a specific siRNA) or plasmids (pCtrl: control plasmid; pG9a: G9a expression plasmid), and 24h later cells were placed under normoxic or hypoxic conditions for another 24h.

Supplementary Fig. 7. Effect of CM-272 on TGFβ induced α-SMA protein expression as analyzed by Western blotting in LX2 cells (A) and hHSCs (B). Cells were pre-tretated for 24h with CM-272 and then with TGFβ (5ng/mL) for another 24 h before proteins were analyzed. Blots were probed for α-TUBULIN to demonstrate equal loading. Representative blots are shown.

Supplementary Fig. 8. (A) Representative immunofluorescent staining for CD31 in PLC/PRF5+LX2 xenograft tumors from control (PBS) and CM-272 treated mice as described in the main text. (B) Western blot analysis of G9a, HK2, GNMT and FBP1 protein levels in xenograft tumors developed in nude mice injected with PLC/PRF5 cells treated with vehicle (PBS) or CM-272 as described in the main text.

Supplementary Table 2. Primer sequences.

	Gene	Sequence	
qRT-PCR			
	E-Cadherin	Fw	5´-CTGGTTCAGATCAAATCCAAC-3´
		Rev	5´-GAGGTTCCTGGAAGAGC-3´
	Cyp7a1	Fw	5´-TTGCTACTTCTGCGAAGGCA-3´
		Rev	5´-TCCGTGAGGGAATTCAAGGC-3´
	FBP1	Fw	5´-ACATCGATTGCCTTGTGTCC-3´
		Rev	5´-CATGAAGCAGTTGACCCCAC-3´
	GNMT	Fw	5´-AAGAGGGCTTCAGTGTGACG-3´
		Rev	5´-AGGCTTGAAGTCGCCCAGGA-3´
	MAT1A	Fw	5´-TCTTCATGTTCACATCGGAG-3´
		Rev	5´-TGCACTCCTCTGTCTCGTCG-3´
	GLUT1	Fw	5´-CCTTTGAGATGCTGATCCTG-3´
		Rev	5´-TCTTGGCCCGGTTCTCCTCG-3´
	HK2	Fw	5´-TTGACCAGTATCTCTACCACATGCG-3´
		Rev	5´-CAATGTGGTCAAACAGCTGGG-3´
	ALDOA	Fw	5´-AGTCCATTGGCACCGAGAAC-3´
		Rev	5´-AACATTGGCATTTTCCATGA-3´
	PGK-I	Fw	5´-GTTCCTATGAAGAACAACCAG-3´
		Rev	5´-CATCTTTTCCCTTCCCTTCTTCC-3´
	PKM2	Fw	5´-AGAAACAGCCAAAGGGGACT-3´
		Rev	5´-CTGCCAGACTTGGTGAGGACG-3´
	LDHA	Fw	5´-GTTGGTGCTGTTGGCATGGC-3´
		Rev	5´-GTGATAATGACCAGCTTGGAG-3´
	VEGF	Fw	5´-CTGCTGTCTTGGGTGCATTGG-3´
		Rev	5´-CACCGCCTCGGCTTGTCACA-3´
	TGFβ	Fw	5´-TGGTGGAAACCCACAACGAA-3´
		Rev	5´-GGCCATGAGAAGCAGGAAAG-3´
	PPARɣ	Fw	5´-GCTGTTATGGGTGAAACTCTG-3´
		Rev	5´-GAATAATAAGGTGGAGATGCAGG-3´
	LRAT	Fw	5´-CAGAAGGTGGTCTCCAACAA-3´
		Rev	5´-CCAAGACTGCTGAAGCAAGA-3´
	BAMBI	Fw	5´-CTCCAGCTACATCTTCATCTGG-3´
		Rev	5´-CTGCTACCATCATGCTGATACC-3´
	aSMA	Fw	5´-CCAGGGCTGTTTTCCCATCC-3´
		Rev	5´-GTCATTTTCTCCCGGTTGGCC-3´
	COLIA1	Fw	5´-GGCTCCTGCTCCTCTTAGCGG-3´
		Rev	5´-CGGGACAGCACTCGCCCTCGG-3´
	TAGLN	Fw	5´-GACCAAGAATGATGGGCACTA-3´
		Rev	5´-ATGACATGCTTTCCCTCCTG-3´
	SKIL	Fw	5´-GGAGAAAAGAGACTCTGTTTGCC-3´
		Rev	5´-CCACTTCAAAGGCACTGCC-3´
	LOX	Fw	5´-CCCCAAAGAGTGAAAAACCA-3´
		Rev	5´-CCAGGACTCAATCCCTGTGT-3´
	H3F3A	Fw	5´-AAAGCCGCTCGCAAGAGTGCG-3´
		Rev	5´-ACTTGCCTCCTGCAAAGCAC-3´
	G9a	Fw	5´-GCAGCACTGCACGTGTGTGGA-3´
		Rev	5´-ACATCAGCCTCAGCATCAGA-3´
	DNMT1	Fw	5´-GAGGCCCGAAGAAAAAGAAC-3´
		Rev	5´-TGAAGCAGGTCAGTTTGTGC-3´

	UHRF1	Fw	5´-CAAGAAGAAGGCGAAGATGG-3´
		Rev	5´-AAAAATTCCCATGGTCCACA-3´
qChIP			
	GNMT	Fw	5´-AAGGACCTAGCCCAGGATTG-3´
		Rev	5´-CCGCATTAAAGCATAAGCA-3´
	FBP1	Fw	5´-GACAGAAGGGCCAGGTGA-3´
		Rev	5´-GCCAGAGAGAAAGCTATGACTG-3´
	CYP7A1	Fw	5´-CATAATTCAGTCACCTCCTACCAGG-3´
		Rev	5´-AGGCATGGTAGTGTGACATGGTT-3´
	PPARɣ	Fw	5´-GGACGCACGGAGCACTTCCG-3´
		Rev	5´-TGTCCTTCCTCCACAGCCCCT-3´
MSP			
	M_FBP1	Fw	5´-GTTAGTTTTTTCGTTAGGTTTCGC-3´
		Rev	5-AATCAAAATATTAACGTCCGTATCG-3´
	U_ FBP1	Fw	5´-TTAGTTTTTTTGTTAGGTTTTGTGG-3´
		Rev	5´-TCAAAATATTAACATCCATATCAAA-3´
	M_RASSF1A	Fw	5´-GTGTTAACGCGTTGCGTATC-3´
		Rev	5-AACCCCGCGAACTAAAAACGA-3´
	U_RASSF1A	Fw	5´-TTTGGTTGGAGTGTGTTAATGTG-3´
		Rev	5´- CAAACCCCACAAACTAAAAACAA-3´
	M_PPARɣ	Fw	5´-GAGATTAGCGGTTTTTTGAAC-3´
		Rev	5-TAAATAAAAACGAAATAAAAACGTA-3´
	U_PPARɣ	Fw	5´-TTTAGGAGATTAGTGGTTTTTTGAAT-3´
		Rev	5´-ACAACATAAATAAAAACAAAATAAAAACAT-3´
Pyroseq			
	PYRO-PCR_FBP1	Fw	5´-GATTTTGTTTGAAGATTTAAGTAGG-3´
		Rev	5-ACAAAAAAAAACAATAAACACTAAC-3´
	PYRO-SEQ_FBP1	Fw	5´-GTTTGGTTTGGTTTAGTTGTATTA-3´

Supplementary Table 3. Gene Set Enrichment Analysis of target gene-sets regulated by CM-272 treatment in HepG2 cells.

Enrichment in phenotype: na_POS		
Liver healthy & Liver cancer		
GSEA	**Systematic name**	**NOM p-val**
HSIAO_LIVER_SPECIFIC_GENES	M13283	0.020
OHGUCHI_LIVER_HNF4A_TARGETS_UP	M2193	0.024
SERVITJA_LIVER_HNF1A_TARGETS_DN	M2398	0.012
CHIANG_LIVER_CANCER_SUBCLASS_UNANNOTATED_UP	M19610	0.034
CHIANG_LIVER_CANCER_SUBCLASS_INTERFERON_DN	M14353	0.017
LEE_LIVER_CANCER	M3879	0.063
LEE_LIVER_CANCER_DENA_UP	M16524	0.05
CHIANG_LIVER_CANCER_SUBCLASS_INTERFERON_UP	M16141	0.061
CHIANG_LIVER_CANCER_SUBCLASS_CTNNB1_DN	M8689	0.053
ACEVEDO_LIVER_TUMOR_VS_NORMAL_ADJACENT_TISSUE_DN	M13014	0.002
YAMASHITA_LIVER_CANCER_STEM_CELL_DN	M9206	0.016
Down regulation of cancer-associated genes		
GSEA	**Systematic name**	**NOM p-val**
ZUCCHI_METASTASIS_DN	M16826	0.009
JAEGER_METASTASIS_DN	M10702	0.004
BOQUEST_STEM_CELL_DN	M1578	0.0
JECHLINGER_EPITHELIAL_TO_MESENCHYMAL_TRANSITION_DN	M1417	0.0
AMIT_DELAYED_EARLY_GENES	M10550	0.006
ENGELMANN_CANCER_PROGENITORS_DN	M9246	0.002
AZARE_NEOPLASTIC_TRANSFORMATION_BY_STAT3_DN	M2311	0.020
SARRIO_EPITHELIAL_MESENCHYMAL_TRANSITION_DN	M11513	0.0
GRAHAM_NORMAL_QUIESCENT_VS_NORMAL_DIVIDING_UP	M4406	0.008
RAFFEL_VEGFA_TARGETS_DN	M2358	0.025
LOPEZ_MESOTELIOMA_SURVIVAL_TIME_DN	M5899	0.014
MCBRYAN_PUBERTAL_TGFB1_TARGETS_DN	M1125	0.028
LABBE_TARGETS_OF_TGFB1_AND_WNT3A_DN	M1843	0.008
Adhesion & Thigh junctions		

GSEA	Systematic name	NOM p-val
ONDER_CDH1_TARGETS_3_DN	M11790	0.010
ONDER_CDH1_TARGETS_2_DN	M4306	0.0
KEGG_CELL_ADHESION_MOLECULES_CAMS	M16476	0.023
Metabolism		
	Systematic name	NOM p-val
REACTOME_GLUCONEOGENESIS	M13748	0.83
KEGG_FOLATE_BIOSYNTHESIS	M2220	0.783
KEGG_GLYCINE_SERINE_AND_THREONINE_METABOLISM	M766	0.211
Enrichment in phenotype: na_NEG		
Cell Cycle and Proliferation		
GSEA	**Systematic name**	**NOM p-val**
CHIANG_LIVER_CANCER_SUBCLASS_PROLIFERATION_UP	M3268	0.0
BENPORATH_PROLIFERATION	M2114	0.0
REACTOME_CELL_CYCLE_CHECKPOINTS	M16647	0.0
REACTOME_DNA_REPLICATION	M1017	0.0
KEGG_CELL_CYCLE	M7963	0.001
LEE_LIVER_CANCER_SURVIVAL_DN	M7987	0.0
SCIAN_CELL_CYCLE_TARGETS_OF_TP53_AND_TP73_DN	M9402	0.011
GRAHAM_NORMAL_QUIESCENT_VS_NORMAL_DIVIDING_DN	M5198	0.00
ZHANG_PROLIFERATING_VS_QUIESCENT	M16992	0.057
FIRESTEIN_PROLIFERATION	M5354	0.022
REACTOME_CELL_CYCLE_MITOTIC	M5336	0.0
EGUCHI_CELL_CYCLE_RB1_TARGETS	M4455	0.001
TGFβ signaling		
GSEA	**Systematic name**	**NOM p-val**
REACTOME_DOWNREGULATION_OF_SMAD2_3_SMAD4_TRANSCRIPTIONAL_ACTIVITY	M669	0.0
REACTOME_TGF_BETA_RECEPTOR_SIGNALING_ACTIVATES_SMADS	M646	0.001
REACTOME_DOWNREGULATION_OF_TGF_BETA_RECEPTOR_SIGNALING	M628	0.001
REACTOME_SIGNALING_BY_TGF_BETA_RECEPTOR_COMPLEX	M1041	0.0
SARRIO_EPITHELIAL_MESENCHYMAL_TRANSITION_UP	M4288	0.0
KARAKAS_TGFB1_SIGNALING	M17300	0.007
KOINUMA_TARGETS_OF_SMAD2_OR_SMAD3	M2356	0.0
REACTOME_TRANSCRIPTIONAL_ACTIVITY_OF_SMAD2_SMAD3_SMAD4_HETEROTRIMER	M665	0.005

PID_SMAD2_3PATHWAY	M228	0.016
BIOCARTA_TGFB_PATHWAY	M18933	0.029
CHANG_CORE_SERUM_RESPONSE_DN	M5793	0.007
PID_TGFBR_PATHWAY	M286	0.029
KARLSSON_TGFB1_TARGETS_DN	M2081	0.007
Metastasis, EMT & Cell adhesion		
GSEA	**Systematic name**	**NOM p-val**
ROESSLER_LIVER_CANCER_METASTASIS_DN	M2545	0.011
GOTZMANN_EPITHELIAL_TO_MESENCHYMAL_TRANSITION_DN	M1376	0.0
SUNG_METASTASIS_STROMA_UP	M9483	0.006
CHANDRAN_METASTASIS_UP	M16036	0.0
TOMLINS_METASTASIS_DN	M7090	0.048
ZUCCHI_METASTASIS_UP	M14951	0.05
PID_ECADHERIN_NASCENT_AJ_PATHWAY	M156	0.01
Differentiation & Cancer signature		
GSEA	**Systematic name**	**NOM p-val**
RICKMAN_TUMOR_DIFFERENTIATED_WELL_VS_MODERATELY_UP	M7141	0.012
RICKMAN_TUMOR_DIFFERENTIATED_MODERATELY_VS_POORLY_UP	M15672	0.038
LIU_COMMON_CANCER_GENES	M18694	0.002
Liver cancer subclass		
GSEA	**Systematic name**	**NOM p-val**
BOYAULT_LIVER_CANCER_SUBCLASS_G123_UP	M13831	0.0
BOYAULT_LIVER_CANCER_SUBCLASS_G3_UP	M18436	0.0
CHIANG_LIVER_CANCER_SUBCLASS_UNANNOTATED_DN	M10986	0.0
IIZUKA_LIVER_CANCER_PROGRESSION_G1_G2_DN	M16374	0.0
HOSHIDA_LIVER_CANCER_SUBCLASS_S2	M7995	0.001
YAMASHITA_LIVER_CANCER_WITH_EPCAM_UP	M16542	0.0
WANG_RECURRENT_LIVER_CANCER_UP	M10922	0.001
CAIRO_HEPATOBLASTOMA_CLASSES_UP	M4772	0.0
PATIL_LIVER_CANCER	M1195	0.0
ACEVEDO_LIVER_CANCER_UP	M15709	0.0
KUROKAWA_LIVER_CANCER_CHEMOTHERAPY_DN	M11545	0.001
CAIRO_HEPATOBLASTOMA_UP	M14601	0.0
BOYAULT_LIVER_CANCER_SUBCLASS_G1_UP	M14146	0.005
MIDORIKAWA_AMPLIFIED_IN_LIVER_CANCER	M1065	0.027
SMITH_LIVER_CANCER	M18761	0.031

ACEVEDO_LIVER_TUMOR_VS_NORMAL_ADJACENT_TISSUE_UP	M4950	0.0
Hypoxia		
GSEA	**Systematic name**	**NOM p-val**
MANALO_HYPOXIA_DN	M18562	0.0
JIANG_HYPOXIA_CANCER	M7547	0.025
KRIEG_HYPOXIA_NOT_VIA_KDM3A	M2469	0.0
JIANG_HYPOXIA_VIA_VHL	M2522	0.039
JIANG_HYPOXIA_NORMAL	M3996	0.0
GROSS_HYPOXIA_VIA_ELK3_UP	M1303	0.017
BIOCARTA_HIF_PATHWAY	M13324	0.013
KRIEG_HYPOXIA_NOT_VIA_KDM3A	M2469	0.0
JIANG_HYPOXIA_VIA_VHL	M2522	0.039
JIANG_VHL_TARGETS	M18850	0.002
GROSS_HYPOXIA_VIA_ELK3_UP	M1303	0.017
MIKHAYLOVA_OXIDATIVE_STRESS_RESPONSE_VIA_VHL_UP	M2263	0.141
Angiogenesis		
GSEA	**Systematic name**	**NOM p-val**
HU_ANGIOGENESIS_DN	M18833	0.015
PID_VEGFR1_2_PATHWAY	M237	0.030
WESTON_VEGFA_TARGETS_6HR	M1521	0.074
Metabolism		
GSEA	**Systematic name**	**NOM p-val**
KEGG_PYRUVATE_METABOLISM	M7934	0.003
CHEN_LIVER_METABOLISM_QTL_CIS	M1947	0.030
PENG_GLUCOSE_DEPRIVATION_DN	M7970	0.028
REACTOME_REGULATION_OF_PYRUVATE_DEHYDROGENASE_PDH_COMPLEX	M716	0.213
REACTOME_SIGNALING_BY_INSULIN_RECEPTOR	M1021	0.043
Growth factor signaling & microenvironment		
GSEA	**Systematic name**	**NOM p-val**
NAKAMURA_CANCER_MICROENVIRONMENT_DN ST_INTEGRIN_SIGNALING_PATHWAY	M2427	0.002
PID_ERBB1_INTERNALIZATION_PATHWAY	M214	0.0
PID_IL2_PI3K_PATHWAY	M143	0.004
PID_IL1_PATHWAY	M110	0.0

STEIN_ESRRA_TARGETS_RESPONSIVE_TO_ESTROGEN_DN	M19002	0.007
REACTOME_SIGNALING_BY_EGFR_IN_CANCER	M563	0.016
REACTOME_SIGNALING_BY_PDGF	M2049	0.040
REACTOME_PLATELET_ADHESION_TO_EXPOSED_COLLAGEN	M9450	0.031
Histone/DNA remodeling		
GSEA	**Systematic name**	**NOM p-val**
KAMMINGA_EZH2_TARGETS	M1486	0.0
NUYTTEN_EZH2_TARGETS_DN	M17122	0.0
NUYTTEN_NIPP1_TARGETS_DN	M18090	0.0
MISSIAGLIA_REGULATED_BY_METHYLATION_DN	M6866	0.0
ZHONG_RESPONSE_TO_AZACITIDINE_AND_TSA_DN	M3988	0.001
LIANG_SILENCED_BY_METHYLATION_DN	M6302	0.007
MARIADASON_REGULATED_BY_HISTONE_ACETYLATION_DN	M1552	0.032
NUYTTEN_EZH2_TARGETS_UP	M4196	0.0

Supplementary Table 4. Gene Set Enrichment Analysis of target gene-sets regulated by CM-272 treatment in LX2 cells.

Enrichment in phenotype: na_POS		
Lipid and retinol metabolism		
GSEA	**Systematic name**	**NOM p-val**
KEGG_ARACHIDONIC_ACID_METABOLISM	M5410	0.000
PID_NFAT_TFPATHWAY	M60	0.001
BIOCARTA_RARRXR_PATHWAY	M6907	0.002
KEGG_LINOLEIC_ACID_METABOLISM	M2920	0.007
PID_ATF2_PATHWAY	M166	0.004
REACTOME_NUCLEAR_RECEPTOR_TRANSCRIPTION_PATHWAY	M8276	0.022
KEGG_RETINOL_METABOLISM	M9488	0.045
Enrichment in phenotype: na_NEG		
Growth factor signaling and cell proliferation		
GSEA	**Systematic name**	**NOM p-val**
REACTOME_DOWNREGULATION_OF_SMAD2_3_SMAD4_TRANSCRIPTIONAL_ACTIVITY	M669	0.000
REACTOME_TGF_BETA_RECEPTOR_SIGNALING_ACTIVATES_SMADS	M646	0.005
REACTOME_G1_S_TRANSITION	M17283	0.000
PID_PDGFRB_PATHWAY	M186	0.000
REACTOME_SIGNALING_BY_TGF_BETA_RECEPTOR_COMPLEX	M1041	0.000
PID_NFKAPPAB_CANONICAL_PATHWAY	M37	0.005
REACTOME_DOWNREGULATION_OF_TGF_BETA_RECEPTOR_SIGNALING	M628	0.006
REACTOME_SIGNALING_BY_HIPPO	M591	0.002
REACTOME_SIGNALING_BY_HIPPO	M665	0.005
REACTOME_REGULATION_OF_AMPK_ACTIVITY_VIA_LKB1	M19104	0.014
BIOCARTA_HIF_PATHWAY	M13324	0.020
BIOCARTA_IGF1MTOR_PATHWAY	M16991	0.027
PID_WNT_CANONICAL_PATHWAY	M90	0.017
REACTOME_SIGNALING_BY_CONSTITUTIVELY_ACTIVE_EGFR	M559	0.023
PID_TNF_PATHWAY	M128	0.014

Supplementary Materials and Methods

Mouse models, ethical statement.

All animal used received humane care according to the criteria outlined in the "Guide for the care and Use of Laboratory Animals" prepared by the National Academy of Sicences and published by the National Institutes of Health (NIH publication 86-23 revised 1985). Protocols were also approved and performed according to the guidelines of the Animal Care Committee of the University of Navarra (#R-CP001-15GN).

Orthotopic tumor xenograft model.

Subcutaneous xenograft tumors were generated with PLC/PRF5 cells in nude mice as described previously (1). When tumors reached approximately 1 cm in diameter, animals were sacrificed and tumor tissue was sliced into equal fragments of ~1mm^3. These fragments were implanted orthotopically by laparotomy in the left lobe of the liver of a second group of nude mice. The orthotopic xenograft model provides additional information, as tumors grow in the natural environment of its cells of origin, the liver parenchyma. Tumor engraftment was monitored by ultrasound scan (US) using Vevo 770 High-Resolution Imaging System (Visualsonics, Toronto, Canada) enabling *in vivo* visualization, assessment, and measurement of tumors, and when lesions reached ~2mm^3 mice (n=5 per group) were randomized into control and treatment groups. Mice received 5 mg/kg (*i.p.*) of CM-272 or same volume of vehicle (phosphate-buffered saline, PBS), for the indicated period of time and mice were sacrified and tumors extracted.

Serum biochemistry determinations.

Serum levels of alanine aminotransferase (ALT), aspartate aminotransferase (AST), alkaline phosphatase (ALP), cholesterol, urea, albumin, bilirubin and creatinine were measured as previously reported using a C311 Cobas Analyzer (Roche Diagnostics)(2).

Analysis of gene expression.

Human tissue RNA was extracted as described(3-5). Quantitative reverse transcription PCR (qRT-PCR) was performed using Fluidigm 96.96 Dynamic Arrays and specific TaqMan pre-designed assays for G9A (Hs00198710_m1), DNMT1 (Hs02558036_s1), UHRF1 (Hs00273589_m1), FBP1 (Hs00166829_m1) and ABCB1 (Hs00184491_m1). Gene expression was normalized with the RNA ribosomal 18S, and the level of expression of T and NT samples was compared with the mean level of gene expression in normal liver tissues, being expressed as an n-fold ratio. The relative amount of RNA was calculated with the -ΔΔCT method[37]. Total RNA from cell lines was extracted using the automated Maxwell system from Promega (Madison, WI). qRT-PCR was performed as described(6). Primer sequences are described in **Supplementary Table 2.**

siRNAs and plasmid transfections

Human *G9a* and *DNMT1*-specific siRNAs and control siRNA (siC) were from Santa Cruz Biotechnology (Santa Cruz, CA). Transfections were performed with 75 nM of each siRNA using Lipofectamine RNAiMAX reagent (Invitrogen, Grand Island, NY) as previously described(7) and following the manufacturer's instructions. In those cases where combined siRNAs transfections were performed, each specific siRNA was used

at 32.5 nM. For overexpression experiments, 1.8 µg of pEGFP-G9a or control pEGFP plasmids (Cat. Nos 33025 and 86775, Addgene, Cambridge, MA) were transfected in PLC/PRF5 cell ($2x10^5$) using Lipofectamine 2000 (Invitrogen, Carlsbad, CA) according to the manufacturer's instructions. In each set of experiments, equal amounts of plasmid were used by adding empty vector. Cells were harvested 48 h after transfection. Gene expression was confirmed by qPCR and western blot after transfections.

Histone extraction

Histones were isolated as previously described(8). Briefly, cells were lysed in a buffer containing 10mM Tris-HCl pH 7.4, 10mM NaCl and 3mM $MgCl_2$. Afer centrifugation at 2500 rpm for 10 min at 4°C supernatants were removed and pellets were lysed in the previous buffer but containing 0.5% NP40 on ice for 10 min with gentle stirring. Nuclei were pelleted by centrifugation at 2500 rpm for 10 min at 4°C and resuspended in 5mM $MgCl_2$ and 0.8M HCl. Nuclei were incubated in this buffer during 30 min at 4ºC to extract the histones. Samples were then centrifuged at 14000 rpm for 10 min at 4°C to pellet debris and supernatants were transfered to a clean tube where TCA 50% was added to precipitate the histones. After washing the pellets with acetone they were air-dried and resuspended in 100mM Tris-HCl pH 7.5, 1mM EDTA and 1% SDS. The histone concentration in the extract was measured using the BCA assay (Pierce Technologies, Rockford, IL) according to manufacturer's specifications.

Western blot

Cells and tissues were lysed in RIPA buffer. Samples of human primary hepatocytes used for protein analyses have been described previously(7). Histone extracts, as well as homogenates form cells and tissues, were subjected to western blot analysis as reported(6,9). Antibodies used were: anti-H3K9me2 (07-212, Millipore-Merck,

Darmstadt, Germany), anti-total H3 (07-690, Millipore-Merck, Darmstadt, Germany), anti-G9a (3306S, Cell Signalling Technology, Leiden, The Netherlands), anti-DNMT1 (5032S, Cell Signalling Technology), anti-UHRF1(ab57083, Abcam), anti-HK2 (sc28889, Santa Cruz Biotechnology, Santa Cruz, CA), anti-FBP1 (HPA005857, Sigma Aldrich, St. Louis, MO), anti-GNMT (kindly provided by Dr M. Martinez-Chantar, CIC-BioGune, Bilbao, Spain), anti-α-Smooth Muscle Actin (A2547, Sigma Aldrich, St. Louis, MO) . Blots were probed with anti-alpha-tubulin (Cell Signalling Technology), or stained with Ponceau S solution (Sigma) as described(10) to demonstrate equal loading. Representative images are shown throughout the study.

Immunofluorescence

Immunofluorescent staining of 3- to 5-μM thick formalin-fixed paraffin embedded tissues was performed following standard protocols. The paraffin was removed and the tissues rehydrated using a slide wash/incubation sequence with Histoclear II (Nottingham, UK), ethanol 10%, 90%, 70% and ddH20. Antigen retrieval was performed with Citrate Buffer (pH 6.0) (Dako, Glostrup, Denmark) and sections were blocked in 1% BSA in PBS and incubated with primary antibodies diluted in blocking solution for 1 hour at room temperature. After washing, sections were incubated with secondary antibodies diluted in 1% BSA in PBS for another 1 hour at room temperature and then washed and counterstained with DAPI. The primary antibody for CD31 detection was diluted 1:100 (77699S, Cell Signalling) and the secondary antibody, Alexa Fluor conjugate (594, A21207 Invitrogen- Life technologies), was diluted 1:400. Images were obtained using an Axoimagen M1 microscope (Zeiss, Oberkochen, Germany). Controls were performed using only secondary antibody. Images from

multiple fields (at least 5) and tissue samples from each mouse xenograft were taken, processed and signal was quantitated with a Zen 2.1 Zeiss Image Analysis System.

Slot blot assay of DNA methylation

After the corresponding treatments genomic DNA was extracted from cells using a the Nucleo Spin Tissue kit (74095250, Macherey-Nagel, Düren, Germany) following the manufacturer's instructions. DNA purity and concentration was measured using a NanoDrop spectrophotometer (Thermo Fisher Scientific, Waltham, MA). 500 ng of genomic DNA were loaded onto a nitrocellulose membrane (Amersham Hybond_N+, RPN203B, GE Healthcare, Little Chalfont, UK), pre-wetted in 6X SSC for 10 min, using the Bio-Dot microfiltration apparatus (170-6545, BioRad, Hercules, CA). Then the membrane was incubated with 2X SSC for 5 min and was cross-linked for 2 h at 80 ºC. The membrane, after being blocked with Tropix I- block blocking reagent (AI300, Tropix-Thermo Fisher Scientific) in PBS with 0.1 % of Tween-20 and 0.02 NaN_3, was incubated overnight at 4 ºC with an antibody against 5-methylcytosine (1:500 dilution) (BI-MECY-1000, Eurogentec, Liege, Belgium), and then with an alkaline phosphatase-conjugated secondary antibody. Blots were developed with a chemiluminescent reagent (ECL Prime Western Blotting Detection, GE Healthcare) and detected using HyperfilmTM enhanced chemiluminescence as previously described(11). Equal DNA loading in membranes was assessed by Methylene-blue staining (Sigma).

Measurement of glucose uptake in cultured cells

Prior to assay, HCC cells in the different conditions were cultured for 90 minutes in regular media without glucose. The medium was then replaced with media containing 1

μCi/mL [14C]-2-deoxyglucose (Perkin Elmer, Waltham, MA). After 15 minutes, cells were quenched and washed in ice-cold PBS and lysed in 1M NaOH and Triton-X100. 80% of each lysate was subjected to liquid scintillation counting using a Beckman Coulter (Brea, CA) LS6500 scintillation counter. Protein content in the remaining lysate was quantified with the dye-binding assay of Bradford (Bio-Rad, Hercules, CA). Uptake was normalized for protein content.

Measurement of lactate production

Lactate production was measured with the Lactate Colorimetric Assay Kit from Biovision (Milpitas, CA) according to manufacturer´s instructions.

Colony formation assays

Colony formation assays were performed with HepG2 and PLC/PRF5 cells essentially as described(12). Five thousand cells were seeded in complete medium in six-well plates and treated (CM-272 50nM) the next day. Media was changed every two days and cultures maintained until differences between treatment conditions were noticeable (2-3 weeks). Plates were washed with PBS, fixed with 4% formaldehyde (Sigma) in PBS for 10 minutes and stained with crystal violet. Representative pictures were taken. At least two biological replicates with three technical replicates were performed.

Microarray hybridization and gene expression analysis

HepG2 or LX2 cells were treated with CM-272 at 400 nM for 48h. RNA was extracted using the automated Maxwell system from Promega (Madison, WI) according to the manufacturer's instructions. Before cDNA synthesis, RNA integrity from each sample was confirmed on Agilent RNA Nano LabChips (Agilent Technologies, Santa Clara, CA). The sense cDNA was prepared from 200 ng of total RNA and then fragmented

and biotinylated using Affymetrix GeneChip® WT PLUS Reagent Kit. Labeled sense cDNA was hybridized to the Affymetrix Human Gene 2.0 ST microarray according to the manufacturer protocols and using GeneChip® Hybridization, Wash and Stain Kit. Genechips were scanned with the Affymetrix GeneChip® Scanner 3000.
Both background correction and normalization were done using RMA (Robust Multichip Average) algorithm(13). After quality assessment, a filtering process was performed to eliminate low expression probe sets. Applying the criterion of an expression value greater than 16 in 2 samples for each experimental condition (control and CM-272 treatment), 26432 probe sets for experiments performed in HepG2 cells, and 29762 probe sets for those performed in LX2 cells were selected for statistical analysis. R and Bioconductor(14) were used for preprocessing and statistical analysis. LIMMA (Linear Models for Microarray Data) was used to find out the probe sets that showed significant differential expression between experimental conditions(15). Genes were selected as significant using a criterion of $B>0$ and $|logFC|>1$ in the case of LX2 cells and $p<0.01$ and $|logFC|>0.56$ for HepG2 cells.

Functional enrichment analysis of Gene Ontology (GO) categories(16) was carried out using standard hypergeometric test and the gene list ranked by logFC was also analyzed with Gene Set Enrichment Analysis (GSEA)(17). The biological knowledge extraction was complemented through the use of Ingenuity Pathway Analysis (Ingenuity Systems, www.ingenuity.com), which database includes manually curated and fully traceable data derived from literature sources. Microarray data can be downloaded from Gene Expression Omnibus (GEO) public functional genomics data repository under the accession number GSE110418.

Quantitative chromatin immunoprecipitation (Q-ChIP)

Q-ChIP assays were performed in HepG2 cells treated with vehicle or CM272 (48 h treatment at 400 nM), as previously described(11). Briefly, for crosslinking of DNA and proteins cells were treated with 1% formaldehyde for 10 min before quenching with 0.125 M glycine. Cells were harvested in ice-cold PBS with proteases inhibitors. Cells were incubated with lysis buffer (10 mM EDTA, 50 mM Tris-HCl pH 8.1, 1 % SDS and proteases inhibitor mixture) and sonicated on ice to yield 200-800 bp DNA fragments. After centrifugation at 14000 rpm for 10 min, supernatant was collected and frozen at -80°C to obtain the chromatin. Fifty micrograms of DNA were used per immunoprecipitation (IP). Chromatin was pre-cleared with protein A-agarose/salmon sperm DNA (Upstate Biotechnology, Merck, Darmstadt, Germany), then diluted 1/4 in IP dilution buffer (0.01 % SDS, 1.1 % Triton-X100, 1.2 mM EDTA, 16.7 mM Tris-HCl pH 8.1, 167 mM NaCl) and incubated overnight at 4°C with 5µg of anti-H3K9me2 antibodies (ab1220, Abcam) or 5µg nonspecific IgGs (2729, Cell Signalling Technology). Immuno-complexes were precipitated by incubation for 1 hour with protein A-agarose/salmon sperm DNA. Bound DNA-protein complexes were eluted and cross-links were reversed after a series of washes. Purified DNA was resuspended in TE buffer for PCR. The specific primers used were described previously by Mitro et al. for *CYP7A1*(18), by Huidobro et al. for *GNMT*(19), by Dong et al. for *FBP1*(20), and by Jiang et al for *PPARγ*(21) and their sequences are listed in **Supplementary Table 2**. Independent ChIP assays were performed at least twice in duplicates. The proportion of H3K9me2 of each gene was quantified calculating [($2^{(-\Delta\Delta Ct)}$ CM-272 sample / $2^{(-\Delta\Delta Ct)}$ control)*100].

DNA methylation analysis

DNA methylation status of the *FBP1, RASSF1A* and *PPARγ* promoters was analyzed

by methylation-specific PCR (MSP). HepG2 cells were treated with vehicle (0.1% DMSO), decitabine (5 μM) or CM-272 (100nM or 200nM as appropriate) for the times indicated, with daily medium change. At the end of treatment cells were washed twice with PBS and genomic DNA was extracted using a DNA kit (Maxwell 16 LEV Blood DNA Kit, Promega, Madison, WI) following the manufacturer's instructions. DNA purity and concentration was measured using a NanoDrop spectrophotometer (Thermo Fisher Scientific). One μg of genomic DNA was treated and modified using the CpGenome DNA modification Kit (S7820, Chemicon International, Fisher Scientific) following the manufacturer's instructions.

MSP was performed on bisulfite-modified DNA using a set of primers for *FBP1, RASSF1A* and *PPARγ* designed with MethPrimer software (The Li Lab, www.urogene.org) and listed in **Supplementary Table 2**. The positive control for the methylated reaction was *in vitro*-methylated DNA (CpGenome Universal Methylated DNA, S7821, Chemicon International). MSP reaction was performed using Phusion U Hot Start DNA Polymerase kit (F-555S, Thermo Fisher Scientific) and PCR products were electrophoresed and visualized in GelRed Nucleic Acid (41003, Biotium, Fremont, CA) stained gels (2% agarose) under UV light.

For pyrosequencing, "hot start" PCR (PyroMark PCR Kit, 978703, Qiagen, Hilden, Germany) was performed with a denaturalization at 95°C for 15 minutes and for 45 cycles consisting of denaturation at 94°C for 1min, annealing at 55ºC for 1min, and extension at 72°C for 1min, followed by a final 10 min extension. This PCR was performed using 2μl of modified DNA, 12.5μl of 2X Buffer, 1μl of 10μM of each specific *PPARγ* primer (specific sequences listed in **Supplementary Table 2**) in a final volume of 25μl. The resulting biotinylated PCR products were immobilized to

streptaviding Sepharose High Performance beads (GE Healthcare, Little Chalfont, UK) and processed to yield high quality ssDNA using the PyroMark Vacuum Prep Workstation (Biotage, Uppsala, Sweden), according to the manufacturer's instructions. The pyrosequencing reactions were performed using the PyromarkTM ID (Biotage) with a specific primer for *PPARγ* listed in **Supplementary Table 2**, and sequence analysis was performed using the PyroQ-CpG analysis software (Biotage).

Compound synthesis

CM-272 was prepared according to the synthetic protocol recently reported(11). Purity, for utilized compound, is >95%.

Evaluation of CM-272 as MDR1 substrate.

The assay was performed by Wuxi (http://www.wuxi.com/). Briefly, test and reference compounds were diluted with transport buffer (HBSS with 10mM Hepes, with and without GF120918, pH7.4) from stock solutions to a concentration of 2 μM (10 μM for digoxin)(DMSO<1%) and applied to the apical or basolateral side of the cell monolayer. Wild type MDCK II cells, and MDCK II cells overexpressing MDR1 (MDR1-MDCK II) obtained from Dr. Piet Borst (Netherlands Cancer Institute, Amsterdam, The Netherlands) were used. Permeation of the test compounds from A to B direction or B to A direction was determined in duplicate with/without MDR1 inhibitor (Elacridar, 10 μM) over a 150-minute incubation at 37°C and 5% CO_2 with a relative humidity of 95%. Test and reference compounds were quantified by LC-MS/MS analysis (Waters Aquity UPLC, API4000) based on the peak area ratio of analyte/internal standard (tolbutamide). Results were interpreted according to the FDA guideline 2012 (Guidance for Industry Drug Interaction Studies — Study Design, Data Analysis, Implications for Dosing, and Labeling Recommendations;

https://www.fda.gov/downloads/drugs/guidances/ucm292362.pdf). Lucifer yellow rejection assays were applied to determine the cell monolayer integrity.

CM-272 determination in mice serum, liver and tumor tissue samples.

CM-272 was measured in serum, liver and tumor tissues using a Xevo-TQ MS triple quadrupole mass spectrometer with an electrospray ionization (ESI) source and Acquity UPLC (Waters, Manchester, UK) as previously described (11).

References

1. Urtasun R, Latasa MU, Demartis MI, Balzani S, Goñi S, Garcia-Irigoyen O, et al. Connective tissue growth factor autocriny in human hepatocellular carcinoma: oncogenic role and regulation by epidermal growth factor receptor/yes-associated protein-mediated activation. Hepatology. 2011;54:2149–2158.

2. Uriarte I, Fernandez-Barrena MG, Monte MJ, Latasa MU, Chang HCY, Carotti S, et al. Identification of fibroblast growth factor 15 as a novel mediator of liver regeneration and its application in the prevention of post-resection liver failure in mice. Gut. 2013;62:899–910.

3. Nault J-C, Mallet M, Pilati C, Calderaro J, Bioulac-Sage P, Laurent C, et al. High frequency of telomerase reverse-transcriptase promoter somatic mutations in hepatocellular carcinoma and preneoplastic lesions. Nature Communications. 2013;4.2218.

4. Schulze K, Imbeaud S, Letouzé E, Alexandrov LB, Calderaro J, Rebouissou S, et al. Exome sequencing of hepatocellular carcinomas identifies new mutational signatures and potential therapeutic targets. Nat. Genet. 2015;47:505–511.

5. Dauch D, Rudalska R, Cossa G, Nault J-C, Kang T-W, Wuestefeld T, et al. A MYC-aurora kinase A protein complex represents an actionable drug target in p53-altered liver cancer. Nature Medicine. 2016;22:744–753.

6. Elizalde M, Urtasun R, Azkona M, Latasa MU, Goñi S, Garcia-Irigoyen O, et al. Splicing regulator SLU7 is essential for maintaining liver homeostasis. J. Clin. Invest. 2014;124:2909-2920.

7. Urtasun R, Elizalde M, Azkona M, Latasa MU, García-Irigoyen O, Uriarte I, et al. Splicing regulator SLU7 preserves survival of hepatocellular carcinoma cells and other solid tumors via oncogenic miR-17-92 cluster expression. Oncogene. 2016;35:4719-4729.

8. Rodriguez-Collazo P, Leuba SH, Zlatanova J. Robust methods for purification of histones from cultured mammalian cells with the preservation of their native modifications. Nucleic Acids Research. 2009;37:e81–e81.

9. Alvarez-Sola G, Uriarte I, Latasa MU, Fernandez-Barrena MG, Urtasun R, Elizalde M, et al. Fibroblast growth factor 15/19 (FGF15/19) protects from diet-induced hepatic steatosis: development of an FGF19-based chimeric molecule to promote fatty liver regeneration. Gut. 2017;66:1818-1828.

10. Garcia-Irigoyen O, Carotti S, Latasa MU, Uriarte I, Fernandez-Barrena MG, Elizalde M, et al. Matrix metalloproteinase-10 expression is induced during hepatic injury and plays a fundamental role in liver tissue repair. Liver Int. 2014;34:e257-e270.

11. San José-Enériz E, Agirre X, Rabal O, Vilas-Zornoza A, Sanchez-Arias JA, Miranda E, et al. Discovery of first-in-class reversible dual small molecule

inhibitors against G9a and DNMTs in hematological malignancies. Nature Communications. 2017;8:15424.

12. Andreu-Pérez P, Hernandez-Losa J, Moliné T, Gil R, Grueso J, Pujol A, et al. Methylthioadenosine (MTA) inhibits melanoma cell proliferation and in vivo tumor growth. BMC Cancer. 2010;10:265.

13. Irizarry RA, Bolstad BM, Collin F, Cope LM, Hobbs B, Speed TP. Summaries of Affymetrix GeneChip probe level data. Nucleic Acids Research. 2003;31:e15.

14. Gentleman RC, Carey VJ, Bates DM, Bolstad B, Dettling M, Dudoit S, et al. Bioconductor: open software development for computational biology and bioinformatics. Genome Biol. 2004;5:R80.

15. Smyth GK. Linear models and empirical bayes methods for assessing differential expression in microarray experiments. Stat Appl Genet Mol Biol. 2004;3:Article3–25.

16. Gene Ontology Consortium, Blake JA, Dolan M, Drabkin H, Hill DP, Li N, et al. Gene Ontology annotations and resources. Nucleic Acids Research. 2013;41:D530–5.

17. Subramanian A, Tamayo P, Mootha VK, Mukherjee S, Ebert BL, Gillette MA, et al. Gene set enrichment analysis: a knowledge-based approach for interpreting genome-wide expression profiles. Proceedings of the National Academy of Sciences. 2005;102:15545–15550.

18. Mitro N, Godio C, De Fabiani E, Scotti E, Galmozzi A, Gilardi F, et al. Insights in the regulation of cholesterol 7alpha-hydroxylase gene reveal a target for modulating bile acid synthesis. Hepatology. 2007;46:885–897.

19. Huidobro C, Toraño EG, Fernández AF, Urdinguio RG, Rodríguez RM, Ferrero C, et al. A DNA methylation signature associated with the epigenetic repression of glycine N-methyltransferase in human hepatocellular carcinoma. J. Mol. Med. 2013;91:939–950.

20. Dong C, Yuan T, Wu Y, Wang Y, Fan TWM, Miriyala S, et al. Loss of FBP1 by Snail-mediated repression provides metabolic advantages in basal-like breast cancer. Cancer Cell. 2013;23:316–331.

21. Jiang Y, Wang S, Zhao Y, Lin C, Zhong F, Jin L, et al. Histone H3K9 demethylase JMJD1A modulates hepatic stellate cells activation and liver fibrosis by epigenetically regulating peroxisome proliferator-activated receptor γ. FASEB J. 2015;29:1830–1841.